

**A Novel Biodegradable Poly( $\epsilon$ -caprolactone  
urea)urethane Incorporating Polyhedral Oligomeric  
Silsesquioxane Nanocomposite and Applications for  
Skin Tissue Engineering**

**Submitted in partial fulfilment of the  
requirements for the degree of**

**Doctor of Philosophy (Ph.D.)**

**March 2014**

**by**

**Lara Yildirimer**

**UNIVERSITY COLLEGE LONDON**



'I, Lara Yildirimer, confirm that the work presented in this thesis is my own. Where information has been derived from other sources, I confirm that this has been indicated in the thesis.'





## **DEDICATION**

*Für meine Eltern,  
meinen Bruder Simon, und Tom*



## ABBREVIATIONS

a/bFGF	Acidic/basic fibroblast growth factor	KGF	Keratinocyte growth factor
AFM	Atomic force microscopy	LBL	Layer-by-layer
ALI	Air-liquid interface	LMW	Low molecular weight
ALP	Alkaline phosphatase	MDA	4,4'-methylene dianiline
ATR-FTIR	Attenuated total reflectance-Fourier transform infrared	MDI	4,4'-methylenebis(phenyl isocyanate)
BSA	Bovine serum albumin	MMP	Matrix metalloproteinases
CE	Cholesterol esterase	$M_n$	Number average molecular weight
CoCl <sub>2</sub>	Cobalt chloride	$M_w$	Molecular weight
DAPI	4',6-diamidino-2-phenylindole	NaHCO <sub>3</sub>	Sodium bicarbonate
DMAC	N,N'-Dimethylacetamide	PBS	Phosphate buffered saline
DMEM	Dulbecco's modified Eagle medium	PCLU	Poly( $\epsilon$ -caprolactone urea)urethane
DMF <sub>d</sub>	Deuterated dimethylformamide	PCU	Poly(carbonate urea)urethane
DMSO	Dimethylsulfoxide	PDGF	Platelet-derived growth factor
DSC	Differential scanning calorimetry	PDMS	Polydimethylsiloxane
ECM	Extracellular matrix	PEG-DA	Poly ethylene glycol-diacrylate
EGF	Epidermal growth factor	PFA	paraformaldehyde
EtO	Ethylene oxide	PGA	Polyglycolic acid
FBGC	Foreign body giant cell	PI	Propidium iodide
FBS	Foetal bovine serum	PIP	Poly Implant Prosthèse
FDA	Food and Drug Administration	PLA	Poly(lactic acid)
FGF-2	Fibroblast growth factor-2	PLGA	Poly(lactic co-glycolic) acid
FITC	Fluorescein isothiocyanate	POSS	Polyhedral oligomeric silsesquioxane
GelMA	Gelatin methacrylate	PU	Polyurethane
GPC	Gel permeation chromatography	RGD	Arginine-Glycine-Aspartic acid
<sup>1</sup> H NMR	<sup>1</sup> H nuclear magnetic resonance	RhB	Rhodamine blue
H & E	Haematoxylin & eosin	SEM	Scanning electron microscopy
H <sub>2</sub> O <sub>2</sub>	Hydrogen peroxide	TCP	Tissue culture plastic
HA	Hyaluronic acid	TDA	2,4-toluene diamine
HaCaT	Immortalized human keratinocytes	TDI	2,4-toluene diisocyanate
HDFa	Adult human dermal fibroblast	$T_g$	Glass transition temperature
HDI	Hexamethylene diisocyanate	TGF- $\beta$	Transforming growth factor- $\beta$
HMDI	4,4'-methylenebis(cyclohexylisocyanate)	$T_m$	Melting temperature
hMSC	Human bone marrow-derived mesenchymal stem cells	TMSPMA	(Trimethoxysilyl) propyl methacrylate
IGF	Insulin-like growth factor	VEGF	Vascular endothelial growth factor
		XRD	X-ray diffraction



# TABLE OF CONTENTS

---

<b>TITLE</b> .....	<b>1</b>
<b>DECLARATION</b> .....	<b>3</b>
<b>DEDICATION</b> .....	<b>5</b>
<b>ABBREVIATIONS</b> .....	<b>7</b>
<b>LIST OF FIGURES</b> .....	<b>15</b>
<b>LIST OF TABLES</b> .....	<b>31</b>
<b>ACKNOWLEDGEMENTS</b> .....	<b>35</b>
<b>ABSTRACT</b> .....	<b>37</b>
<b>ABOUT ME</b> .....	<b>39</b>
<b>1 INTRODUCTION TO BIODEGRADABLE SCAFFOLDS FOR TISSUE ENGINEERING APPLICATIONS</b> .....	<b>41</b>
<b>1.1 Introduction</b> .....	<b>41</b>
<b>1.2 Degradable Polyurethanes for Biomedical Applications</b> .....	<b>43</b>
1.2.1 Hard Segment Isocyanates .....	44
1.2.2 Soft Segment Polyols .....	45
1.2.3 Polyurethane Structure .....	46
<b>1.3 Polymer Degradation and Biocompatibility</b> .....	<b>52</b>
1.3.1 Polyester-based Polyurethane Degradation .....	52
1.3.2 Biological Response to Implants .....	58
<b>1.4 Organization of Thesis</b> .....	<b>60</b>
<b>1.5 Hypothesis</b> .....	<b>62</b>
<b>1.6 Aims of Thesis</b> .....	<b>62</b>
<b>2 3-DIMENSIONAL BIOMATERIAL DEGRADATION – QUITE LITERALLY TAKING A LEAF OUT OF NATURE’S BOOK</b> .....	<b>71</b>
<b>2.1 Synopsis</b> .....	<b>71</b>
<b>2.2 Introduction</b> .....	<b>73</b>
<b>2.3 Tissue Engineering Scaffolds as Carbon Copies of Nature</b> .....	<b>74</b>
<b>2.4 Determinants of Scaffold Degradation Kinetics</b> .....	<b>78</b>
<b>2.5 Scaffold Design Influences Biomaterial Degradation and Tissue Regeneration</b> .....	<b>81</b>
<b>2.6 Biodegradable Materials as Self-Propagating Delivery Vehicles – an Interactive Platform</b> .....	<b>86</b>

2.7	<b>Single and Dual Growth Factor Delivery .....</b>	<b>87</b>
2.8	<b>Stem Cell Delivery.....</b>	<b>89</b>
2.9	<b>The Design Challenge – Leafing through the Past to Uncover the Next Generation Delivery Vehicle .....</b>	<b>91</b>
2.10	<b>Biomaterial Degradation Products and Toxicity.....</b>	<b>94</b>
2.11	<b>Conclusion and Future Perspective .....</b>	<b>100</b>
3	<b>INTRODUCTION TO SKIN TISSUE ENGINEERING .....</b>	<b>121</b>
3.1	<b>Synopsis .....</b>	<b>121</b>
3.2	<b>Introduction – A Multimodal Cocktail for Skin regeneration.....</b>	<b>122</b>
3.2.1	The Structure of Normal Skin.....	123
3.2.2	Normal Wound Healing.....	124
3.2.3	Foetal Wound Healing.....	126
3.2.4	Management of Thermal Wounds .....	127
3.3	<b>Current State of Tissue Engineered Skin Substitutes.....</b>	<b>128</b>
3.4	<b>Bioengineering ‘Smart’ Scaffolds for Skin Regeneration: A Bottom-Up Approach .....</b>	<b>129</b>
3.5	<b>Growth Factor Functionalized Skin Regeneration Scaffolds .....</b>	<b>131</b>
3.5.1	Epidermal Growth Factor (EGF) .....	131
3.5.2	Basic Fibroblast Growth Factor (bFGF).....	132
3.5.3	Keratinocyte Growth Factor (KGF).....	133
3.5.4	Vascular Endothelial Growth Factor (VEGF) .....	134
3.5.5	Insulin-Like Growth Factor (IGF) .....	135
3.5.6	Platelet-Derived Growth Factor (PDGF) .....	136
3.5.7	Transforming Growth Factor- $\beta$ (TGF- $\beta$ ).....	137
3.6	<b>Stem Cell-Seeded Skin Regeneration Scaffolds .....</b>	<b>139</b>
3.7	<b>Nano-Engineered Scaffolds for a Bottom-Up Approach to Wound Regeneration .....</b>	<b>140</b>
3.8	<b>Conclusion and Future Perspective .....</b>	<b>142</b>
4	<b>SYNTHESIS AND CHARACTERIZATION OF BIODEGRADABLE POSS NANOCOMPOSITE POLY(E-CAPROLACTONE UREA)URETHANE (POSS-PCLU).....</b>	<b>155</b>
4.1	<b>Synopsis .....</b>	<b>155</b>
4.2	<b>Introduction .....</b>	<b>157</b>
4.3	<b>Materials and Methods.....</b>	<b>162</b>

4.3.1	Polymer Synthesis .....	162
4.3.2	Scaffold Fabrication .....	164
4.3.3	Scaffold Surface Modification .....	165
4.3.4	Scaffold Characterization .....	165
4.3.5	Scaffold Cytocompatibility .....	169
4.3.6	Statistical Analysis .....	172
<b>4.4</b>	<b>Results and Discussion.....</b>	<b>172</b>
4.4.1	Synthesis and Molecular Characterization of POSS-PCLU Scaffolds .....	172
4.4.2	Thermal Properties of POSS-PCLU Polyurethanes.....	175
4.4.3	Microstructure and Surface Properties of POSS-PCLU Scaffolds .....	176
4.4.4	Mechanical Properties of POSS-PCLU Scaffolds .....	179
4.4.5	<i>In Vitro</i> Cytocompatibility .....	181
<b>4.5</b>	<b>Conclusion.....</b>	<b>186</b>
<b>5</b>	<b>AN OPTIMIZED STERILIZATION METHOD FOR BIODEGRADABLE POSS-PCLU .....</b>	<b>191</b>
<b>5.1</b>	<b>Synopsis .....</b>	<b>191</b>
<b>5.2</b>	<b>Introduction .....</b>	<b>192</b>
<b>5.3</b>	<b>Materials and Methods.....</b>	<b>194</b>
5.3.1	Polymer Synthesis .....	194
5.3.2	Manufacturing of Scaffolds .....	194
5.3.3	Scaffold Sterilization Techniques .....	194
5.3.4	Sterilization Efficiency .....	195
5.3.5	Scaffold Characterization .....	195
5.3.6	Cell Behaviour on Sterilized Surfaces.....	196
5.3.7	Statistics.....	197
<b>5.4</b>	<b>Results and Discussion.....</b>	<b>197</b>
5.4.1	Effectiveness of Different Sterilization Techniques by Immersion in Culture Medium .....	199
5.4.2	Sterilization Induced Microscopic Changes in Scaffold Architecture and Topography.....	201
5.4.3	Chemical Bond Scission Demonstrated by ATR-FTIR .....	203
5.4.4	Surface Roughness Changed Significantly as Demonstrated with Contact Angle and AFM.....	205
5.4.5	Mechanical Characteristics of Sterilized Scaffolds .....	211

5.4.6	<i>In Vitro</i> Cell Viability and Proliferation .....	212
5.4.7	Cell Morphology and Attachment.....	215
5.4.8	POSS-PCLU Scaffolds as Tissue Engineering Platforms.....	217
<b>5.5</b>	<b>Conclusion.....</b>	<b>219</b>
<b>6</b>	<b>EFFECT OF HARD SEGMENT CHEMISTRY ON LONG-TERM <i>IN VITRO</i> OXIDATIVE AND HYDROLYTIC STABILITY OF POSS-PCLU SCAFFOLDS .....</b>	<b>229</b>
<b>6.1</b>	<b>Synopsis .....</b>	<b>229</b>
<b>6.2</b>	<b>Introduction .....</b>	<b>231</b>
6.2.1	Oxidative degradation.....	233
6.2.2	Hydrolytic degradation .....	233
6.2.3	Enzymatic degradation.....	234
<b>6.3</b>	<b>Materials and Methods.....</b>	<b>234</b>
6.3.1	Polymer Synthesis .....	234
6.3.2	Scaffold Fabrication .....	234
6.3.3	<i>In Vitro</i> Degradation .....	234
6.3.4	Evaluation of <i>In Vitro</i> Degraded Films .....	235
6.3.5	Cell Viability.....	236
6.3.6	Animals.....	237
6.3.7	Statistics.....	238
<b>6.4</b>	<b>Results and Discussion.....</b>	<b>238</b>
6.4.1	Synthesis and Molecular Characterization of Degraded POSS-PCLU Films .....	238
6.4.2	Thermal Properties of Degraded POSS-PCLU.....	243
6.4.3	Degradation-Induced Changes in Mechanical Properties .....	249
6.4.4	Contact Angle Measurements.....	253
6.4.5	Surface Changes Induced by Degradation.....	254
6.4.6	Cytocompatibility of Degradation Products.....	256
6.4.7	<i>In Vivo</i> Blood Flow and Oxygenation .....	261
6.4.8	Histological and Immunohistochemical Analysis of Explanted Samples .....	262
<b>6.5</b>	<b>Conclusion.....</b>	<b>265</b>
<b>7</b>	<b>PHOTO-POLYMERIZABLE GELATIN AS SKIN TISSUE ENGINEERING SCAFFOLDS: MECHANICAL, DEGRADATION AND BIOLOGICAL CONSIDERATIONS .....</b>	<b>273</b>
<b>7.1</b>	<b>Synopsis .....</b>	<b>273</b>



<b>7.2</b>	<b>Introduction .....</b>	<b>275</b>
<b>7.3</b>	<b>Materials and Methods.....</b>	<b>277</b>
7.3.1	Materials.....	277
7.3.2	Synthesis of Gelatin Methacrylate (GelMA).....	278
7.3.3	Preparation of GelMA Hydrogels with Varying Degrees of Methacrylation	278
7.3.4	Characterization of GelMA Hydrogels.....	279
7.3.5	Culture of Human Keratinocytes (HaCaT) .....	280
7.3.6	Statistics.....	282
<b>7.4</b>	<b>Results and Discussion.....</b>	<b>283</b>
7.4.1	Effects of Methacrylation Degree, PEG and Surface Modifications on GelMA Hydrogel Properties.....	283
7.4.2	Reconstructed Human Epidermis .....	292
<b>7.5</b>	<b>Conclusion.....</b>	<b>293</b>
<b>8</b>	<b>OVERALL CONCLUSIONS AND FUTURE OUTLOOK .....</b>	<b>299</b>
<b>8.1</b>	<b>Limitations of Synthetic Polyurethanes and Collagen-Based Hydrogels and a Proposal for a Future Bio-Synthetic Composite Material .....</b>	<b>299</b>
8.1.1	Advantages and Disadvantages of Polyurethanes as Tissue Engineering Platforms .....	299
8.1.2	Advantages and Disadvantages of Collagen/Gelatin Hydrogels as Tissue Engineering Platforms .....	300
<b>8.2</b>	<b>Conclusions .....</b>	<b>301</b>
<b>8.3</b>	<b>Closing Remarks and Future Outlook .....</b>	<b>305</b>
<b>APPENDIX .....</b>		<b>309</b>
<b>9</b>	<b>SURFACE AND MECHANICAL ANALYSIS OF EXPLANTED POLY IMPLANT PROSTHÈSE SILICONE BREAST IMPLANTS .....</b>	<b>309</b>
<b>9.1</b>	<b>Synopsis .....</b>	<b>309</b>
<b>9.2</b>	<b>Introduction .....</b>	<b>311</b>
<b>9.3</b>	<b>Materials and Methods.....</b>	<b>312</b>
9.3.1	Mechanical and Viscoelastic Properties of Implanted Silicone Shells .....	312
9.3.2	Surface Characterization of Silicone Shells and Gels .....	312
9.3.3	Statistical Analysis .....	312
<b>9.4</b>	<b>Results and Discussion.....</b>	<b>313</b>
9.4.1	Mechanical Testing of Silicone Shells .....	314
9.4.2	Surface Characterization of Silicone Shells and Gels .....	316

<b>9.5</b>	<b>Conclusion.....</b>	<b>321</b>
------------	------------------------	------------

## LIST OF FIGURES

- Figure 1.1.** Different structures of silsesquioxanes.
- Figure 1.2.** Schematic illustration of soft segment hydrolysis.
- Figure 1.3.** Schematic illustration of material degradation.
- Figure 2.1.** Leaf degradation is the breakdown of leaf starch into simple sugars which are utilised in the growth and development of the plant.
- Figure 2.2.** Scaffold porosity, particle dimensionality and bulk to fluid ratio play critical roles in regulating the degradation process.
- Figure 2.3.** Schematic illustration of the two main scaffold fabrication techniques to modulate release kinetics of incorporated molecules. (B) Microscopic image of a porous polymer surface incorporating bioactive molecules. (C, D) Different manufacturing processes yield different release kinetics.
- Figure 2.4.** Schematic illustration of a variety of scaffold shapes.
- Figure 2.5.** Optimum model of mechanical properties of a scaffold as new tissue develops.
- Figure 2.6.** Chemical structures of the major biodegradable polyesters used in tissue engineering applications.
- Figure 2.7.** Photograph of the left shoulder of a 25-year-old man with aneurysmal dilatation.
- Figure 3.1.** An illustration of human skin showing the three constituting layers and skin adnexae.
- Figure 3.2.** A schematic representation of the normal wound healing process incorporating various cell-signalling molecules.

- Figure 3.3.** Schematic representation of the ideal scaffold to promote skin regeneration.
- Figure 4.1.** Diagrammatic illustration of the evaluation pathway for novel tissue engineering biomaterials.
- Figure 4.2.** Synthesis of prepolymer.
- Figure 4.3.** Chain extension reaction of the poly( $\epsilon$ -caprolactone urea)urethane prepolymer with ethylenediamine and integration of POSS nanoparticles as endcapped pendant chains.
- Figure 4.4.**  $^1\text{H}$  nuclear magnetic resonance (NMR) spectrum of a representative POSS-PCLU polyurethane.
- Figure 4.5.** Overlaid attenuated total reflectance (ATR)-Fourier transform infrared (FTIR) spectrograph of cast PCLU-24, POSS-PCLU-24, POSS-PCLU-28 and POSS-PCLU-33 samples.
- Figure 4.6.** Representative molecular weight distribution curve of PCLU and POSS-PCLU polymer samples.
- Figure 4.7.** DSC heating curve of PCLU-24, POSS-PCLU-24, POSS-PCLU-28 and POSS-PCLU-33.
- Figure 4.8.** XRD pattern of non-degraded polyurethane samples of varying hard segment contents.
- Figure 4.9.** (A) Scanning electron microscopy image of a salt-leached POSS-PCLU scaffold edge. (B) Top down view of a cast POSS-PCLU scaffold.
- Figure 4.10.** (A) Contact angle measurement of a cast POSS-PCLU disc demonstrates relative surface hydrophobicity ( $\theta > 90^\circ$ ). (B)

Comparison of contact angle between cast discs of the 4 different polymer compositions.

**Figure 4.11.** Atomic force microscopy (AFM) image illustrating a textured nanotopography of cast POSS-PCLU scaffolds.

**Figure 4.12.** Overlaid stress versus strain and Young's modulus versus strain curves of PCLU and POSS-PCLU polyurethanes at room temperature.

**Figure 4.13.** Light microscopy image of adult human dermal fibroblasts growing on tissue culture plastic.

**Figure 4.14.** Scratch test qualitatively assessing cellular proliferation.

**Figure 4.15.** Evaluation of optimal cell seeding density on tissue culture plastic using 3 different cell seeding concentrations.

**Figure 4.16.** Top panel: Confocal laser scanning microscopy images of human dermal fibroblasts cultured on cast POSS-PCLU discs Bottom panel: Human dermal fibroblasts stained with Live/Dead<sup>®</sup> stain.

**Figure 4.17.** Confocal laser scanning microscopy image of human dermal fibroblasts seeded onto porous POSS-PCL scaffolds after 7 days of culture.

**Figure 4.18.** Cell cytocompatibility on tissue culture plastic (TCP), cast non-porous PCLU films, cast non-porous POSS-PCLU films and porous POSS-PCLU scaffolds over a period of 7 days as measured using AlamarBlue<sup>®</sup>.

**Figure 5.1.** Representative SEM images of coagulated sterilized (A-D) and control (E) scaffold surfaces.

**Figure 5.2.** Representative SEM images of cut scaffold edges.

- Figure 5.3.** Overlaid attenuated total reflectance-Fourier transform infrared spectrum of cast sterilized and control samples.
- Figure 5.4.** Contact angle ( $\theta$ ) measurements on cast sterilized (A-D) and control (E) POSS-PCL samples.
- Figure 5.5.** (I) Representative AFM images of cast sterilized (A-D) and non-sterilized control (E) POSS-PCL sheets.
- Figure 5.6.** (I) Water drop on a hydrophilic surface forms a low internal contact angle. (II) Superhydrophobic non-wetting surfaces form a quasi-drop with a high internal contact angle. (III) A drop on a solid surface decorated with pillars with air filling the interpillar spaces.
- Figure 5.7.** (I) A representative stress-strain curve of a cast POSS-PCLU sample. (II) A comparison of stress-strain curves of cast (top) and coagulated (bottom) scaffolds. (III) Treatment of cast samples using antibiotic solution reduced maximal stress values significantly compared to unsterilized controls (C;  $p < 0.05$ ). (IV) Young's modulus was not significantly affected by any sterilization method; however, a negative trend could be observed in antibiotic soaked scaffolds (C).
- Figure 5.8.** Percentage viability of HDFa grown on sterilized cast discs compared to cells grown on tissue culture plastic over a 7 day period assessed using AlamarBlue® cell viability assay.
- Figure 5.9.** Representative laser scanning confocal microscopy images of HDFa cells grown on cast sterilized POSS-PCLU discs stained with Live/Dead® stain.

- Figure 5.10.** (I) Representative confocal images of HDFa cultured on sterilized cast POSS-PCLU films for 7 days. (II) Planar surface area calculations support the hypothesis that different sterilization methods induce changes in surface topographies which can influence cell spreading and alignment.
- Figure 5.11.** (I) Analysis of % cell viability on porous POSS-PCL scaffolds compared to cells grown on tissue culture plastic. (II) Z-stack of a porous POSS-PCLU scaffold and (III) Integra® dermal regeneration template seeded with HDFa and cultured for 7 days.
- Figure 6.1.** Mass loss of (A) PCLU-24 and (B) POSS-PCLU-24 over time after degradation in PBS, lipase, collagenase, cholesterol esterase and hydrogen peroxide buffers.
- Figure 6.2.** Overlaid attenuated total reflectance (ATR)-Fourier transform infrared (FTIR) spectra of films after 6 months in (A) PBS, (B) lipase buffer, (C) collagenase buffer, (D) cholesterol esterase buffer and (E) hydrogen peroxide + CoCl<sub>2</sub> buffer.
- Figure 6.3.** Differential scanning calorimetry graphs of (A) PCLU-24, (B) POSS-PCLU-24, (C) POSS-PCLU-28 and (D) POSS-PCLU-33 films.
- Figure 6.4.** Soft segment glass transition temperatures ( $T_g(s)$ ) as a function of percentage crystallinity of control and degraded polymers.
- Figure 6.5.** The normalized step height of the specific heat at  $T_g$  as a function of crystallinity.
- Figure 6.6.** XRD patterns of control and degraded polymer.

- Figure 6.7.** Stress-strain curves overlaid against Young's moduli for (A) PCLU-24, (B) POSS-PCLU-24, (C) POSS-PCLU-28 and (D) POSS-PCLU-33.
- Figure 6.8.** Water contact angles of (A) PCLU-24, (B) POSS-PCLU-24, (C) POSS-PCLU-28 and (D) POSS-PCLU-33 at 4 weeks (TP1), 12 weeks (TP2) and 24 weeks (TP3).
- Figure 6.9.** Macroscopic image of polymer films after 6 months in degradative media.
- Figure 6.10.** Scanning electron microscopy images of (A) PCLU-24, (B) POSS-PCLU-24, (C) POSS-PCLU-28 and (D) POSS-PCLU-33: (i) control, (ii) in PBS, (iii) in lipase, (iv) in collagenase, (v) in cholesterol esterase and (vi) in hydrogen peroxide + CoCl<sub>2</sub>.
- Figure 6.11.** Media containing filter-sterilized leachables from degraded polymers at 10 % v/v, 50 % v/v and 70 % v/v.
- Figure 6.12.** AlamarBlue® cell viability assay over a period of 7 days. (PBS)
- Figure 6.13.** AlamarBlue® cell viability assay over a period of 7 days. (Lipase)
- Figure 6.14.** AlamarBlue® cell viability assay over a period of 7 days.  
(Collagenase)
- Figure 6.15.** AlamarBlue® cell viability assay over a period of 7 days. (Cholesterol esterase)
- Figure 6.16.** AlamarBlue® cell viability assay over a period of 7 days. (hydrogen peroxide + CoCl<sub>2</sub>)
- Figure 6.17.** Macroscopic view of subcutaneously implanted scaffolds at (A) 4 weeks and (B) 12 weeks. (C) Laser Doppler calibration using full fat milk and (D) analysis of vascularized scaffolds prior to explantation.



(E-G) Monitoring of oxygen transfer from scaffolds through an oxygen sensor film as a measure of scaffold vascularization.

**Figure 6.18.** Histological haematoxylin & eosin stain of (A) non-implanted control scaffold and (B) implanted scaffold.

**Figure 6.19.** Histological comparison of the extent of connective tissue regeneration and in vivo degradation of scaffold groups.

**Figure 6.20.** Haematoxylin & eosin stained images of PCLU-24 after 4 weeks (A) and 8 weeks (C) and corresponding MSB stained images (B and D).

**Figure 6.21.** MSB stained POSS-PCLU-24 (A) and POSS-PCLU-33 (B) at 4 weeks demonstrating increased degradation of scaffolds of lower hard segment. (C) Vascular infiltration visible at 4 weeks post-implantation.

**Figure 6.22.** Representative haematoxylin & eosin stains of in vivo response to PCLU and POSS-PCLU scaffolds.

**Figure 7.1.** Schematic illustration of the synthesis steps involved in creating an artificial epidermis on gelatin methacrylate (GelMA) hydrogels.

**Figure 7.2.** Compressive moduli of hydrogels of different GelMA concentrations with or without PEG-DA supplementation.

**Figure 7.3.** Macroscopic view of GelMA hydrogels of increasing methacrylation degree.

**Figure 7.4.** (I) Diffusion study on 5 % and 20 % GelMA using Fluorescein isothiocyanate (FITC)-labelled bovine serum albumin (BSA). (A) GelMA 5 % at 0 h, (B) GelMA 5 % at 24 h, (C) GelMA 20 % at 0 h and (D) GelMA 20 % at 24 h. (II) Water content analysis as a function of

GelMA concentration. (III) Hydrogel swelling capacity as a function of GelMA concentration.

**Figure 7.5.** Remaining mass as a function of time for (A) GelMA hydrogels of different methacrylation degrees and (B) GelMA PEG-DA composite hydrogels.

**Figure 7.6.** (I) Cell proliferation on GelMA hydrogels of (A) 5 %, (B) 10 % and (C) 20 % GelMA concentration. (II) Cell counts per mm<sup>2</sup> as a function of GelMA concentration. (III) Influence of GelMA concentration and resultant compressive moduli on cell proliferation over a period of seven days.

**Figure 7.7.** Fluorescent images of HaCaTs grown on GelMA hydrogels of different compositions or surface coatings.

**Figure 7.8.** (A) Haematoxylin and eosin (H&E) histological section of human skin and (B) fluorescent image human skin stained for Ki61 and involucrin. (C and D) Corresponding images of HaCaTs cultured on GelMA hydrogels at the air-liquid interface for 4 weeks.

**Figure 9.1.** (A) Ruptured Poly Implant Prosthèse (PIP) breast implant (arrow) revealing yellow discoloration of the industrial-grade silicone gel within. (B) Direct comparison between silicone gels removed from ruptured (yellow) and intact (white) implants. (C) Yellowing and calcifications can be seen on the surface of an explanted, non-ruptured PIP implants.

**Figure 9.2.** (A-C) Spearman rank correlation between duration of implantation and mechanical parameters of Poly Implant Prosthèse (PIP) silicone

shells: (A) tensile strength, (B) elongation at break, and (C) tear strength. (D-F) Box plots comparing tensile strength (D), elongation at break (E), and tear strength (F) between medical-grade silicone control implants and intact and ruptured PIP shells.

**Figure 9.3.** Overlaid attenuated total reflectance-Fourier transform infrared spectra of silicone gels and shells from explanted Poly Implant Prosthèse (PIP) implants (A), (C) and comparison with medical-grade silicone control implants (B), (D).



## List of Tables

- Table 2.1.** In vitro and in vivo degradation outcomes of a selection of natural, synthetic and composite polymers.
- Table 2.2.** Schematic representation of selected delivery strategies and their representative release profiles.
- Table 3.1.** Characteristics of the 'ideal' skin substitute.
- Table 4.1.** Composition of the 4 different polyurethanes.
- Table 4.2.** Composition, number average molecular weight ( $M_n$ ) and polydispersity indices (PDI) of PCLU and POSS-PCLU polyurethanes.
- Table 4.3.** Thermal properties of POSS-PCLU polyurethanes.
- Table 4.4.** Mechanical properties of PCLU and POSS-PCLU polyurethanes.
- Table 5.1.** Sterility testing of cast and coagulated samples by immersion in culture medium for 7 days post-sterilization.
- Table 5.2.** Surface topographical properties of cast sterilized POSS-PCLU samples.
- Table 5.3.** Morphological and mechanical characteristics of differently sterilized POSS-PCLU scaffolds compared to human skin.
- Table 6.1.** Composition, percentage crystallinity, number average molecular weight ( $M_n$ ) and polydispersity indices (PDI) of control non-degraded polyurethane films and films degraded in various buffers for a period of 6 months.
- Table 6.2.** Material properties of (A) PCLU-24, (B) POSS-PCLU-24, (C) POSS-PCLU-28 and (D) POSS-PCLU-33 polyurethanes.
- Table 7.1.** Differences in mechanical properties, water content and degradation rate with incrementally increasing GelMA content.

**Table 9.1.** Patient age, duration of implantation and reasons for removal of implants.

## ACKNOWLEDGEMENTS

I am forever grateful to my supervisor, Professor Seifalian, who has believed in and supported me from the very beginning. Thank you for guiding me through the past three years, for the numerous opportunities and discussions which have challenged me on a scientific as well as personal level, enabling me to achieve my best. This work could not have been possible without your help and guidance and for that I am thankful.

My sincerest thanks to Professor Butler whose refreshingly insightful and thought-provoking comments really pushed my scientific thought boundaries, helping me become a more critically-thinking person.

My most heartfelt thanks go to all my friends and colleagues at the Centre for Nanotechnology & Regenerative Medicine. In particular, I am deeply grateful to Mr Arnold Darbyshire, our polymer chemist, who really is the heart of our lab and Dr Brian Cousins whose genuine and inexhaustible help has seen me through many a challenge. I am grateful to Dr Marilena Loizidou who instantly lights up whichever room she enters. Thank you to Dr Bala Ramesh – what would I have done without your curious ability to tame our temperamental confocal microscope! I really want to thank Tina Sedaghati for supporting me while I was in Boston.

Speaking of which – I am deeply grateful to Associate Professor Ali Khademhosseini at Harvard-MIT for giving me a most superb experience at his labs. I'd like to express my sincerest gratitude to Dr Xin Zhao, the most hard-working, honest and humorous person I have come across so far.

I'd like to thank Mr Naiem Moiemmen and Dr Gary Reynolds for helping me with histology, Dr Simon Gaisford and Dr Asma Buanz for their kind help with the DSC and XRD and Dr Remzi Becer, Ed and Resat for their help with GPC and NMR. I am very grateful to the MRC DTG and the Rosetrees Trust for their financial support which made life inconceivably less stressful than it could have been!

I am indebted to my parents and my brother Simon for their life-long support and firm believe in me. Thank you always.

Last, but certainly not least, I want to thank you, Tom, for being truly inspirational. I love you.





## ABSTRACT

Skin protects our bodies for a lifetime and extensive loss of this barrier renders the individual susceptible to infections and death. Clinically available treatment options, however, are limited in establishing both functional and cosmetic satisfaction. The work described in this thesis is therefore concerned with the development and characterization of a novel biodegradable nanocomposite system displaying suitable properties as skin tissue engineering scaffolds. A novel family of segmented polyurethanes (PU) with increasing hard segment content based on a poly( $\epsilon$ -caprolactone urea)urethane backbone incorporating POSS nanoparticles was synthesized and analysed in terms of material characteristics and biocompatibility. Incorporation of POSS nanoparticles into the PU backbone yielded mostly amorphous materials as corroborated by distinct glass transitions visible on differential scanning calorimetry spectra. With incrementally increasing hard segment content, ultimate tensile strength increased from  $\sim 10$  to 21 MPa accompanied by increased values for elastic moduli from 0.03 to 0.06 MPa. Number average molecular weights ( $M_n$ ) decreased with increasing hard segment content due to a corresponding decrease in the proportion of PCL. Sterilization studies raised fundamental concerns regarding the suitability of conventionally available techniques since hydrolytically and temperature labile polymers are susceptible to degradation. The results obtained suggest 70 % ethanol to be a suitable laboratory-based disinfectant which was further demonstrated to have favourable effects on skin cell compatibility. Degradation studies revealed hard segment-dependent modulation of the degradation rate and the materials' viscoelasticity. *In vivo* implantation studies of porous scaffolds demonstrated firm integration with the subcutaneous tissue and extensive vascularization. The results obtained in this work highlight (i) the ability to control scaffold degradation rates and mechanical properties

and (ii) cellular as well as *in vivo* biocompatibility, all of which fundamental in the development of a versatile skin tissue engineering scaffold.

## **About me**

Being an MBPhD student, I have a keen interest not only in the systematic elucidation of scientific conundrums, but am also curious as to their clinical translatability. Being particularly interested in the plastic and reconstructive surgical aspects of clinical medicine, a scientific enthusiasm for skin tissue engineering appears a natural choice. This is reflected not only in my doctoral work at the Centre for Nanotechnology and Regenerative Medicine (which is generously funded by the MRC Doctoral Training Grant and the Rosetrees Trust) but also in the six months I spent at the Khademhosseini labs at Harvard-MIT (funded by the MRC Centenary Award) where hydrogel-based scaffolds for skin regeneration were a major focus (see Chapter 7).

My aspirations to embark on a path in academic surgery are additionally reflected in the work carried out on silicone breast implants of the now infamous manufacturer Poly Implant Prosthèse (see Appendix).

I believe that close-knit relationships between scientists of various backgrounds and clinical surgeons (or the medical community in general) are of fundamental importance in developing and advancing patient care. Working at the interface of science and medicine has been tremendously rewarding for me so far and is very much anticipated to be continued in the future.



# 1 INTRODUCTION TO BIODEGRADABLE SCAFFOLDS FOR TISSUE ENGINEERING APPLICATIONS

---

## 1.1 INTRODUCTION

Scientific research is forever inspired by the quest for knowledge and the endless possibilities of sculpting our ideas and actions. The term ‘tissue engineering’ first emerged during a congregation of the National Science Foundation in 1987 and was subsequently further coined by Langer and Vacanti who provided an internationally accredited definition of this concept summarized as “an interdisciplinary field that applies the principles of engineering and life sciences toward the development of biological substitutes that restore, maintain, or improve tissue function” (Langer and Vacanti, 1993). The pivotal strategies underlying tissue engineering have been identified as (i) the use of isolated cells or cell substitutes, (ii) the use of tissue-inducing substances and (iii) the use of cells placed on or within matrices (Bell et al., 1981). These fundamental mechanisms have, over decades, evolved into the field today known as regenerative medicine which combines living cellular components with sophisticated biomaterials to create tissues and organs of physiologically satisfactory size and function. Dramatic deficiencies in organ and tissue donations co-existing with the ever increasing demand for such organs are determining factors for the exponentially rising interest and rapid development within the fields of tissue engineering and regenerative medicine. The emergence of nanotechnology and its integration into the medical arena carries the field above and beyond former limitations, thereby igniting a wave of interest for the exploration of research into biotechnological systems at the nanometer scale. One nanometer, or a billionth of a meter ( $1 \times 10^{-9}$  m) is to a football what a football is to the Earth. With regards

to tissue engineering, the emergence of nanotechnology ('nano-engineering') has revolutionized the approach to fabricating tissues and organs since the manufacture of novel biosynthetic scaffolds with enhanced material properties enables scientists to develop controllable and application-specific biomatrices. Novel biomaterials synthesized within nanometer dimensions are particularly attractive as they can closely mimic the molecular structure of tissues and organs, thus providing an ideal environment for cellular interactions and tissue regeneration. Skin is the largest organ of the body and its outermost covering which provides a protective interface between internal organs and the external environment. Being subject to continuous environmental strain, its physical integrity is of pivotal importance. Extensive breaches (e.g. due to large burn injuries) of this external layer render the affected individual prone to invading pathogens and subsequent, potentially lethal infections. Currently available and widely used skin substitutes such as harvested autologous and cadaveric skin play a major role in the immediate coverage of such wounds and undoubtedly have saved many lives. However, limitations in terms of availability, mechanical properties as well as durability within the wound due to immunological rejection prevent permanent graft integration into the wound bed. The development of various polymeric biomaterials for tissue engineering skin constructs has advanced the development of new skin grafts. One property fundamental to the idea of tissue engineering scaffolds is their controlled biodegradability concurring with the simultaneous regeneration of new tissues and vasculature within such scaffolds. Biodegradation rates should ideally be tunable to suit individual applications, with relatively fast degradation rates potentially being more applicable to scaffolds placed, for example, into cutaneous wound beds, whereas longer biostability may be required for tissue engineered vascular grafts or heart valves (Bettinger et al., 2009). Several important principles underlie the concept of tunable biodegradation of

tissue engineered scaffolds; (i) suitable polymer materials, (ii) scaffold fabrication methods and (iii) incorporation of cell-signaling morphogens or drugs into the scaffold matrix which may, over time, stimulate cell recruitment and tissue regeneration as well as influence biomaterial degradation. Multiple advantages of engineered synthetic over natural biological scaffolds exist; (i) their known production techniques, (ii) their controllable chemical and physical structures, (iii) their rate-tunable biodegradation, and (iv) biocompatibility of the scaffold material and its degradation products (Kannan et al., 2005b).

Nanotechnology has provided new impetus for research into biodegradable scaffolds composed of biologically safe natural, synthetic or composite polymers. Nano-engineering of such scaffolds could enhance scaffold characteristics even further by exploiting the fundamental changes in material properties once transition from micro- to nanoscale has taken place, thereby opening up new avenues for the field of regenerative medicine.

## **1.2 DEGRADABLE POLYURETHANES FOR BIOMEDICAL APPLICATIONS**

Segmented polyurethanes (PUs) are amongst the most favoured synthetic polymers used in the manufacture of biomedical devices due to their superior biomechanical properties and a unique combination of toughness, durability, flexibility and biocompatibility. Generally, PUs are synthesized by reacting a polyol, often from the polyester family, with a diisocyanate which is followed by chain extension with a diamine. Since their discovery by Otto Bayer in 1937, the PU family has become the most versatile of any families of plastic materials, gaining considerable popularity in the biomedical field as pacemaker leads, catheters, vascular grafts and prosthetic heart valves (Chawla et al., 1988, Izci et al., 2009, Rahmani et al., 2012, Desai et al., 2012). Whilst such applications

tend to favour the use of non-degradable materials, regenerative strategies involving organs such as the skin and bone as well as cases involving paediatric patients frequently require resorbable scaffolds to allow for unobstructed new tissue formation. In biodegradable systems, the ratio of the hard segment, soft polyols and chain extender significantly influences the rate and mode of degradation such that scaffold breakdown may be fine-tuned to suit individual applications.

### **1.2.1 Hard Segment Isocyanates**

Isocyanates can be divided into two broad categories comprising of the relatively more stable aromatic isocyanates (e.g. 2,4-Toluene diisocyanate (TDI), methylene-*bis*-diphenyl diisocyanate (MDI)) and the more labile aliphatic isocyanates (e.g. 4,4'-methylenebis(cyclohexylisocyanate)). Aromatic groups are stabilised by resonance involving the sharing of  $\pi$ -electrons by adjacent atoms. This strengthens the linkages between atoms and results in higher bond strengths than those found in the equivalent aliphatic linkages, rendering aromatic PUs less susceptible to degradation (Lamba et al., 1998). Whilst potentially useful for applications requiring long-term resistance to degradation, aromatic hard segments are unsuitable isocyanates for temporary PU scaffolds. Additionally, ongoing controversies pertaining to the potential carcinogenicity of breakdown products of heat-sterilized PUs containing aromatic isocyanates further discouraged their usage in biomedical implantable devices (Gogolewski, 1987, Bolognesi et al., 2001). Cleavage of the urethane linkage of PUs containing aromatic isocyanates results in the formation of either 2,4-toluene diamine (TDA) (Amin et al., 1993, Szycher and Siciliano, 1991) or 4-4'-methylene dianiline (MDA) (Mazzu and Smith, 1984) – both considered carcinogenic (Lamba et al., 1998, Darby et al., 1978). Aliphatic isocyanates such as 4,4'-methylenebis(cyclohexylisocyanate) (also referred to as hydrogenated MDI, or HMDI) on the other hand, have demonstrated to render degradation products which



are less toxic (Tang et al., 2003). Additionally, HMDI demonstrates beneficial mechanical properties including stronger elastomers with low elastic modulus and high strength due to rendering highly amorphous segmented PUs at relatively low hard segment content (Solis-Correa et al., 2007).

### **1.2.2 Soft Segment Polyols**

The second building block of PUs is the polyol. The immense variety within polyol types accounts for the ability of PUs to adapt a material versatility unparalleled by other plastics. In terms of biomedical uses, polyols such as polyethylene glycol (PEG) are incorporated to confer critical material characteristics including bio- and cytocompatibility, haemocompatibility, biodegradability or degradability producing non-toxic degradation products. Polyols can be classified into polyethers or polyesters which are manufactured by the reaction of epoxides with active hydrogen compounds or via the polycondensation of multifunctional carboxylic acids (-COOH) and hydroxyl (-OH) compounds, respectively. While polyether polyols are extensively used for industrial purposes, biomedical applications preferably utilize polyesters which, when in their degradable form, break down into non-toxic end-products. Poly( $\epsilon$ -caprolactone) (PCL), a polyester, has attracted particular attention within the biomedical arena, especially in the field of tissue-engineering, due to its ability to fine-tune degradation rates by varying its starting molecular weight. Degradation under physiological conditions (e.g. 37 °C in the presence of body fluids, enzymes or free radicals) via hydrolysis of its ester linkages results in non-toxic by-products, rendering it suitable for the development of implantable devices and tissue engineered scaffolds. Furthermore, additives including catalysts, surfactants and cross-linkers exert additional control over the reaction process and final characteristics of the PU.

### 1.2.3 Polyurethane Structure

PUs may have a phase separated structure or a highly cross-linked glassy amorphous arrangement. Phase separation occurs at room temperature as the highly polar hard segments of the PU which confer material stability are incompatible with the less polar soft segments which confer elasticity. The hard segments crystallize into microphases via hydrogen bonding which, in turn, link together via the flexible soft segments to produce flexible foams, thermoplastic PUs or elastomers. The ratio between the hard segment and soft segment determines the final elasticity and toughness of the polymer. PU rigidity is achieved via non-reversible covalent bond formation, yielding highly cross-linked glassy amorphous materials. The level of cross-linking and therefore the degree of rigidity depends on the functionality and the molecular weight of the starting material. A higher level of cross-linking is achieved with more available functional groups and lower molecular weights.

In terms of biomedical applications of PUs, certain materials properties such as non-immunogenicity, adequate mechanical strength, biodegradability and non-toxicity prove indispensable – some more and some less depending on each individual application. Biocompatibility certainly is a basic prerequisite for all materials intended for use in the human body. Increasing the soft segment in PUs has been demonstrated to enhance biocompatibility by reducing protein adsorption onto the polymer, thereby reducing harmful interference with cellular attachment and function (Braatz et al., 1992). Steric hindrance secondary to PU surface modification with chains of soft segment as well as repulsion of incoming proteins are the grounds for a reduction in surface protein adsorption with adsorption being inversely proportional to the chain length (Noishiki et al., 1987). In terms of soft tissue-engineering, material porosity is a further determining

factor (Stenhamre et al., 2011, McBane et al., 2011b, McBane et al., 2011a) as is haemocompatibility, particularly in vascular applications. Thrombosis and intimal hyperplasia are major causes for early and long-term vascular graft failure. Graft material hydrophobicity and positive charge contribute to the activation of the clotting cascade and subsequent inflammatory response via factor XII (Hageman factor) activation and platelet adherence (Sarkar et al., 2007). Therefore, synthetic graft materials with a hydrophilic interface and a negatively charged surface are required to exclude platelet aggregation. However, fibrinogen has both hydrophobic and hydrophilic binding sites, necessitating an amphiphilic material. The integration of nanosized silica particles into polymer materials has been demonstrated to confer such favourable surface qualities (Miyake et al., 2009)

#### ***1.2.3.1 Polyhedral Oligomeric Silsesquioxane Nanoparticle***

First introduced into the biomedical field as an alternative, more biocompatible breast implant material in the 1960s, polyhedral oligomeric silsesquioxane (POSS) has risen considerably in global popularity ever since (K.Pielichowski et al., 2006, M.Joshi and B.S.Butola, 2004). This is because of its unique 3-dimensional (3D) cage structure consisting of silanol (Si-OH) and silicon carbide (Si-C) bonds which can serve as nanosized building blocks in the manufacture of unique and precisely controlled organic-inorganic hybrid materials (E.Markovic et al., 2011, C.Sanchez et al., 2001). Hybrid, or composite materials are frequently considered superior in both functionality and processability conferred by the organic phase as well as heat/chemical stability and enhanced elastic modulus provided by the inorganic phase. POSS being a member of the silsesquioxane family, has the basic stoichiometric formula  $(RSiO_{1.5})_{2n}$  where  $n = 4$  and R (the vertex group) = hydrogen, alkyl, aryl or halogen amongst others. These 3D oligomeric structures are formed by complete hydrolytic condensation of their

trifunctional monomers,  $\text{Si}_4\text{O}_6$ . Figure 1.1 illustrates the versatility of the compound's molecular architecture with ladder structures, cage and partial cage structures known so far.

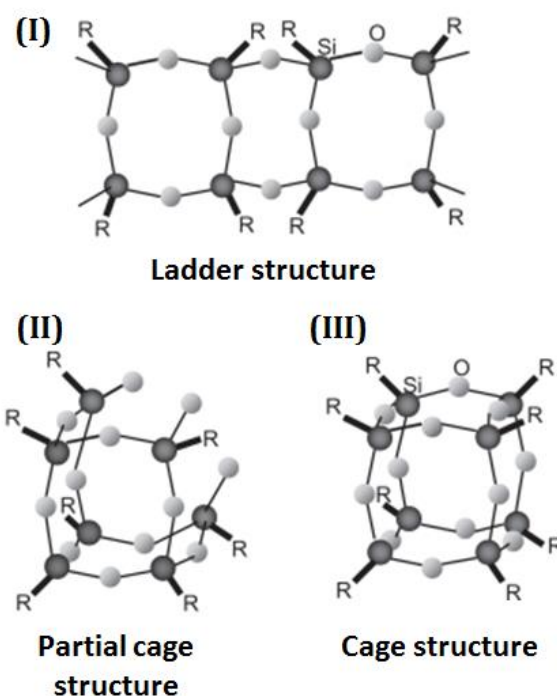


**Figure 1.1.** Different structures of silsesquioxanes: (I) ladder structure, (II) partial cage structure, and (III) cage structure. The stoichiometric formula of the silsesquioxane family is  $R_n\text{Si}_n\text{O}_{1.5n}$  yielding a structure consisting of an inner organic framework of Si and O atoms and external organic groups (R) which may either be hydrogen, alkyl, alkene, aryl, and arylene group.

Nanocomposite materials incorporating silica are particularly well suited for biomedical applications due to their biostability and degradative resistance which is due to shorter bond lengths (Si-Si distance = 0.5 nm) and strong intermolecular forces leading to a strong framework (Voronkov and Lavrent'yev, 1982). The POSS molecule may exist as a pendant cage, be integrated into a polymeric backbone or be cross-linked, depending on the number of side groups (Kannan et al., 2005b).

In 1995, the octameric closed caged silsesquioxane structure (POSS) based on Si-O linkages with one silicon atom at each of the eight vertices (R groups) was developed (Fig. 1.1 (III)) (Lee and Lichtenhan, 1998a). The organic R groups assemble to form a tetrahedral structure around the inorganic silica core and play a fundamental role in determining the unique physical properties encountered with the POSS molecule (Suresh et al., 2004). POSS is regarded the smallest possible silica particle with an inner cage diameter of approximately 0.5 nm (Waddon and Coughlin, 2003) and an overall diameter of 1.5 nm including the R groups (Ghanbari et al., 2011a). POSS has an extraordinary potential to succeed both in scientific, biomedical and commercial terms due to several synergizing factors; (1) POSS is inherently versatile, thus customizable, due to the ability to attach any chemical moieties to the organic vertex groups (R) and its ability to be incorporated into many polymer matrices (Hong et al., 1997, Lee and Lichtenhan, 1998b, Mantz et al., 1996, Tsuchida et al., 1997, Zhao and Schiraldi, 2005, Lichtenhan et al., 1995, Romo-Uribe et al., 1998, Mather et al., 1999), (2) the manufacturing process with yields of up to 90% is straight-forward, facilitating large scale production, (3) the raw materials are inexpensive, thereby making commercialization economically beneficial with a multitude of possible applications ranging from packaging over inert material coatings to biomedical system enhancements (Bakhshi et al., 2011, Kidane et al., 2009, Kannan et al., 2005b), and (4) its rigid inorganic core renders the POSS molecule chemically and thermally stable (Zheng et al., 2002). On oxidation of the organic R-groups, a SiO<sub>2</sub> layer is formed which acts as a protective barrier to further oxidative damage of the silica-like core (Deng et al., 2002). This 'self-protection' property of POSS is increasingly exploited for biomedical purposes to create an ideal and dually active biosynthetic interface combining both antithrombogenicity and amphiphilicity (Kidane et al., 2004, J. Armstrong et al., 2004). Amphiphilicity, i.e. the state of being simultaneously hydrophilic and

lipophilic, is postulated to be of great exploitable significance within the field of regenerative medicine by rendering the material highly versatile and enhancing vascular graft endothelialisation by providing an interface for cellular attachment (Rosler et al., 2001, Rimmer et al., 2005). During the manufacturing process, POSS nanoparticles are extruded onto the polymeric surface, creating an amphiphilic, antithrombogenic blood-polymer interface with increased material durability and mechanical strength (Ghanbari et al., 2011a). Antithrombogenicity is a principally important feature of cardiovascular graft materials as thrombo-occlusive events with subsequent early graft failure represent the main limiting factors for successful vascular bypass procedures.

#### ***1.2.3.2 POSS-Containing Nanocomposite Polymers***

In principle, composite materials are a combination of two or more materials where each individual material retains their own distinctive properties. The resulting composite displays synergistic material characteristics superior to those demonstrated by each individual component alone. Nanocomposite polymers are materials which are physically reinforced with inorganic particles at the nanometer level where at least one of the particle dimensions is less than 100 nm. Nanoparticulates come in various different shapes including fibers, platelets or spheres to serve as nano-bridges between individual molecules within the polymer. Nanoparticles are incorporated into the polymeric backbone and become chemically integrated into a polymer network. This incorporation into a polymeric host amalgamates the processibility of thermoplastic polymers with the properties of the filler, resulting in superior material characteristics including increased conductivity, higher optical activity, high use temperature and oxidation resistance as well as higher mechanical strength compared to their individual components (Wu and Mather, 2009, Zhang et al., 2004, Merkel et al., 2002).

POSS integration into polymers either in the form of nanoparticulate fillers or as pendant structures confined to the polymer backbone is known to form nanocrystalline aggregates (Zheng et al., 2002). Fu *et al.* demonstrated this with POSS-containing PUs where POSS was sequestered in the hard segment and enhanced microphase separation between hard and soft segments (Fu et al., 2001, Fu et al., 2000). This has been corroborated in the present study. Despite extensive knowledge on the favourable materials characteristics obtained by POSS-integration into polymers, comparatively little focus has been placed on the development of tissue engineered biomaterials incorporating POSS.

Our group has synthesized and patented a family of novel biomaterials incorporating POSS, yielding nanocomposites of excellent biocompatibility and vast clinical potential (Kannan et al., 2007b, Kidane et al., 2009, Ghanbari et al., 2010). POSS-incorporating poly(carbonate-urea)urethane (POSS-PCU), now commercially available as UCL-Nano<sup>TM</sup>, has emerged as a clinically applicable non-resorbable biomaterial used for the fabrication of tissue engineering scaffolds with first-in-man transplantations of artificial tracheal replacements, vascular conduits, and lacrimal drainage systems (Chaloupka et al., 2011, Jungebluth et al., 2011a, Kannan et al., 2006d, Kannan et al., 2006c, Kannan et al., 2006a, Kannan et al., 2006b). Whilst non-resorbable scaffolds are adequately suited for certain applications, their lack of degradation limits their use to the adult population and potentially necessitates revision surgeries to replace or remove such scaffolds. Bioresorbable scaffolds, on the other hand, must maintain temporary structural integrity within relatively harsh wound environments and degrade in a controllable fashion surrounded by enzymes and free radicals, pH as well as temperature

fluctuations. Whilst POSS-PCU is regarded for its exceptional biostability, this thesis will discuss a novel degradable nanocomposite derivative based on PCL (POSS-PCLU).

### **1.3 POLYMER DEGRADATION AND BIOCOMPATIBILITY**

While bio-durability may well be of fundamental importance in certain implantable medical devices, biodegradability is a defining characteristic of tissue-engineered materials. Use of degradable materials requires rigorous assessments of cellular behaviour in response to (i) products released as a results of material degradation, and (ii) material surface changes induced by degradation. Reports on the degradative behaviour of PUs frequently are of qualitative nature only, documenting visual changes of the degraded polymer surfaces. It is, however, of fundamental importance to appreciate quantitative changes induced by degradation in order to understand and predict the *in vivo* behaviour of the material. Changes in molecular weight and crystallinity throughout the degradation process provide more reliable information regarding rates and modes of material breakdown. These combined with additional tests relating to the analysis of breakdown products can then be correlated with *in vitro* cellular behaviour and *in vivo* tissue responses.

#### **1.3.1 Polyester-based Polyurethane Degradation**

Upon implantation into the body, devices are exposed to a range of degradative environments, most notably hydrolysis and enzymatic attack and to a lesser extent oxidation. For this work, all three mechanisms will be discussed. In subsequent work, samples will be exposed to representative media *in vitro* in order to comprehensively assess degradation patterns.



Degradation is influenced by both chemical and physical properties of a material; surface properties (e.g. surface area and wettability), first order structures (chemical structure, molecular weight and molecular weight distribution) as well as higher order structures (glass transition temperature, melting temperature, degree of crystallinity and elastic modulus) of polymers play fundamental roles in the biodegradation process (Tokiwa et al., 2009). It is well known that higher molecular weight PCL ( $M_n > 4000$ ) is more slowly degraded by *Rhizopus delemar* lipase than PCL of lower molecular weight (Tokiwa and Suzuki, 1978). Similarly, polymer morphology, and by extension, their crystallinity affects degradation. Crystalline domains consist of tightly packed molecules which are more resistant than the loosely packed amorphous regions where hydrolytic or enzymatic attack mainly occurs. Thus, with increasing crystallinity, the rate of degradation decreases (Tsuji and Miyauchi, 2001, Iwata and Doi, 1998). Tokiwa *et al.* further showed in several experiments that the melting temperature ( $T_m$ ) has strong effects on the enzymatic degradation of polymers; the higher the  $T_m$ , the lower the polymer degradation (Tokiwa et al., 1979, Tokiwa and Suzuki, 1978, Tokiwa and Suzuki, 1981). Such protection towards enzymatic or hydrolytic degradation can be related to the hard segment's extensive hydrogen bonding network which physically protects labile bonds from scission (Shibayama et al., 1986). Such structural inhibition is further amplified as hard and soft segments within PU materials tend to phase separate and form domains containing many PU hard segments imbedded in a matrix of soft segment (Lelah and Cooper, 1986). The combined effect of phase separation and the ability to hydrogen bond significantly increases the formation of highly ordered structures among the hard segment components (Sung and Schneider, 1978). Additionally, it has been observed by Ratner and colleagues that the degree of phase separation in polymers influences the concentration of hard segment chemistry found at the surface of PUs (Ratner, 1983). All

of these factors influence the rate of material degradation by enzymes adsorbing to the surface of a PU.

### 1.3.1.1 Hydrolysis

Hydrolytic degradation of polyester-based PUs occurs as the chemical bonds within the polymer backbone, most often the ester bonds, are attacked by water molecules (Fig. 1.2).

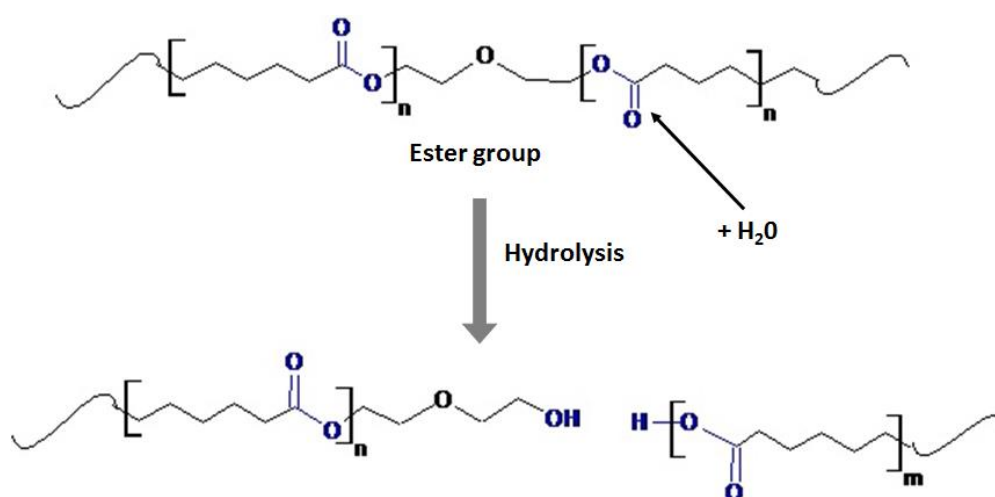


**Figure 1.2.** Schematic illustration of soft segment hydrolysis.

Initially, water contacts the water-labile bonds, resulting in the electrons from the negatively charged hydroxyl attacking the electron-deficient carbon of the ester carbonyl group, thereby breaking the  $\pi$ -bond and creating a tetrahedral intermediate. Once the intermediate collapses, the carbonyl reforms after severing the bond between the carbonyl and oxygen from the original ester group. This results in the carbonyl group now attaching to the hydroxyl group from the water, re-forming a carboxylic acid group. The previously negatively charged oxygen gains the remaining proton and forms a new hydroxyl group. Progressive loss of ester bonds results in the formation of low-molecular

weight products which dissolve in the surrounding medium, as well as in a mass loss of the bulk PU.

Degradation rates and mechanisms are primarily influenced by matrix dimensionality, manner of assembly and consequent water penetration efficiency. If water molecules penetrate the 3D architecture at a higher rate than natural hydrolysis takes place, e.g. potentially influenced by scaffold porosity, thickness and exposed surface area, degradation proceeds throughout the entire polymer matrix resulting in uniform or 'bulk' degradation. On the contrary, if water permeation is slow, hydrolytic erosion will mainly occur on the exterior surface (Fig. 1.3).

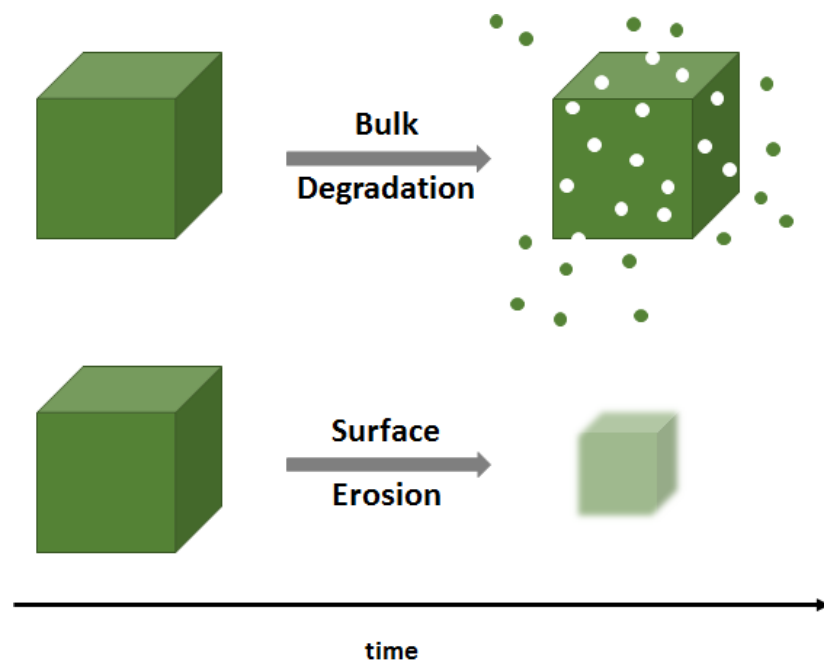


**Figure 1.3.** Schematic illustration of (I) bulk degradation and (II) surface erosion over time.

The internal matrix remains largely unchanged thus allowing for temporary shielding of any core-integrated trophic factors. Modes of degradation, however, do not solely depend on external conditions or material assembly but are further influenced by

the type of polymer material used. Hydrolytically unstable materials including polylactic acid (PLA) and polyglycolic acid (PGA) are known to degrade within days to weeks whereas polycaprolactone (PCL) takes relatively long to fully break down.

Several *in vitro* studies have investigated the effect of various enzymes on biodegradable polymers. Such investigations are crucial for two reasons; (i) in order to study the effects of different micro-environments found within the body on implanted polymers, and (ii) to assess potential cytotoxic effects of any degradation products released from the polymer.

### **1.3.1.2 Enzyme-Mediated Degradation**

Enzymes are essential macromolecules which work at the interface of the body's metabolic pathways and are known to accelerate breakdown of many chemical bonds found in natural as well as artificial biomaterials (Ratner et al., 1986, Smith et al., 1987, Marchant et al., 1987). Hydrolase enzymes including esterases, proteases, glycosidases and phosphatases can all accelerate hydrolytic breakdown as well as several other reactions within the body in order to facilitate absorption of nutrients and solutes (Azevedo and Reis, 2005). Depending on the wound site, however, other enzymes become more prevalent as described in the following sections.

#### 1.3.1.2.1 Collagenase

Collagenase is a highly specific enzyme that breaks the peptide bonds in collagen. It is produced and released during wound healing by macrophages and other immune cells surrounding any implantable device.

#### 1.3.1.2.2 Lipase

Lipase is an enzyme that is able to catalyse the hydrolysis of ester bonds in polyesters when in the presence of an aqueous media (Liu et al., 2000). It was found that

certain lipases enhance the degradation of PCL when compared with incubation in phosphate buffered solution only (Gan et al., 1997). The enzymatic hydrolysis of PCL occurs mainly at the polymer surface since it is difficult for a hydrophilic enzyme to diffuse into a hydrophobic polymer like PCL (Lakhani et al., 2013).

#### 1.3.1.2.3 Cholesterol Esterase

Earlier studies have shown that esterolytic activity is the most degradative enzymatic activity to a variety of PUs (Labow et al., 1999, Labow et al., 1994). Polyester- PUs (Santerre et al., 1994) were much more degradable by CE than polyether PUs (Santerre and Labow, 1997) as would be expected, since the soft segment of the polyester PU was readily hydrolysed (Wang et al., 1997). It has further been shown that the degree of biodegradation of PUs, in the presence of cholesterol esterase enzyme, is about 10 times higher than in the presence of buffer alone (Santerre et al., 1994). Our observations match those obtained by Santerre with a difference in degradation of up to 36 % by weight when PU films were exposed to esterase compared to phosphate buffered saline (PBS) alone (see chapter 6).

#### **1.3.1.3 Oxidative Degradation**

Oxidation-induced surface cracking has been proposed to be a major reason for premature failure of implantable devices based on PUs (Stachelek et al., 2006). This is thought to be due to the interaction between the body's inflammatory cells and the PU implant (Schubert et al., 1995) which primarily targets the ester bonds of the PU soft segments (Lee and Chu, 2000). Modifications of both soft and hard segments (Takahara et al., 1991a, Takahara et al., 1991b, Wiggins et al., 2004) – whilst successful in preventing stress cracking – also resulted in inferior mechanical properties of the PU (Jorge-Herrero et al., 1999, Pinchuk, 1994).

### 1.3.2 Biological Response to Implants

Prior to introduction into the human body, degradable implants require vigorous evaluation for their biocompatibility. However, it should be noted that cytotoxicity may be induced by numerous factors besides the pure biomaterial and its degradation products; various parameters ranging from material processing, sterilization and additives may influence host-material interactions. Whilst *in vitro* compatibility studies are a recognized means of screening material toxicities (Chiellini et al., 2006), the extrapolation of such results into an *in vivo* animal or even clinical setting remains problematic (Yildirimer et al., 2011). Such discrepancies will be discussed in chapter 3.

Sterilization of polymeric implantable devices is an essential step in order to prevent host infection and implant rejection. Several disinfectant or sterilization methods are conventionally available including autoclaving (high temperature steam sterilization), gamma-irradiation, exposure to toxic ethylene oxide (EtO) vapour, soaking in hydrogen peroxide, ethanol or antibiotic solutions. Due to the labile nature of degradable polymers, autoclaving is frequently not possible. Common choices are thus EtO exposure and gamma-irradiation. However, both have significant disadvantages; gamma rays can potentially induce polymer cross-linking which influences mechanical and degradation profiles while exposure to EtO vapour requires prolonged degassing to prevent residual EtO toxicity.

After sterilization, implantation of the polymeric device creates a host immune response regardless of the material's biocompatibility due to host tissue injuries created by the surgical intervention. Once within the body, the biomaterial is exposed to a plethora of conditions created by tissue-specific and resident immune cells which immediately populate the material upon tissue contact. Thus, in order to predict the

material's degradation behaviour as much as possible prior to implantation studies, *in vitro* experiments should attempt to closely mimic the conditions found *in vivo* which include a range of enzymatic, oxidative and purely hydrolytic environments.

The inevitable foreign body response may be divided into several stages which culminate in a timely resolution of inflammation in the case of biocompatible materials. Initially, chemotactic factors released by cells within the wound bed attract neutrophils which enter the wound via the damaged vasculature. These are succeeded by the monocyte-macrophages which can reside within the implantation site for months and are commonly referred to as the hallmark cells in an acute inflammatory response. These cells along with resident tissue cells release enzymes and free radicals which break down the foreign material and engulf or phagocytose smaller particles. These particles are then further degraded within the cell by subjecting them to a battery of toxic chemicals contained within phagolysosomes. However, if a phagocyte fails to completely engulf a particle some toxic chemicals may be released into the extracellular space, potentially damaging both host cells and the implanted material. Chronic inflammation is characterised by the persistence of macrophages, monocytes and lymphocytes along with the formation of new vasculatures. Several material-adherent macrophages may fuse together to form foreign-body giant cells (FBGCs) which further act to degrade the material. Whilst even chronic inflammation should resolve within several weeks, FBGCs usually remain adherent to the implanted device and continue degradation. As part of the foreign-body response, a tough fibrous capsule consisting of Type III collagen produced by fibroblasts forms around the material, shielding it from its surrounding tissues in an attempt to prevent further interaction between the host's immune cells and the foreign material. Despite that, cells continue to pass through the capsule to degrade the material.

Whilst the quest for developing an immune-tolerant biomaterial continues to keep the scientific community on their toes, it is evident that in the meantime, the analysis of biomaterial degradation and the interaction of material and breakdown products in cells and tissues is of principal importance in the evaluation of material biocompatibility.

#### **1.4 ORGANIZATION OF THESIS**

The following work describes the synthesis and characterization of a novel biodegradable nanocomposite material based on a poly( $\epsilon$ -caprolactone urea)urethane backbone with integrated POSS nanoparticles (POSS-PCLU) for the development of tissue engineering scaffolds. The integration of POSS nanoparticles is hypothesized to not only enhance cell adherence to the inherently hydrophobic synthetic PU but also confer a degree of immune tolerance to the material. The effects of varying the hard segment content of POSS-PCLU polymers on their *in vitro* and *in vivo* degradation profiles and subsequent material properties are analysed.

**Chapter 2** provides a comprehensive introduction into biodegradable materials used within the realms of tissue engineering and regenerative medicine. The potential of exploiting biodegradable systems as drug and cell delivery vehicles will be discussed and emphasis will be placed on the importance of scaffold designs to enable tunable degradation rates which enhances versatility in terms of scaffold application.

**Chapter 3** introduces the ideas of skin tissue engineering, critically appraising the current state-of-the-art skin substitutes and subsequently focussing on the determination of what might constitute the ideal 'smart' tissue engineering strategy to regenerate lost skin.



**Chapter 4** discusses the synthesis of POSS-PCLU polymer of increasing hard segment content and polymer processing into cast or porous scaffolds. Different methods of scaffold surface modifications to prevent skin formation and increase overall porosity are presented. For initial material characterization, structural, surface and mechanical properties of POSS-PCLU scaffolds are discussed.

**Chapter 5** continues to discuss the problem of effectively sterilizing biodegradable polymer systems. Sterilization-induced changes in polymer chemistry, scaffold architecture and mechanical properties will be discussed, followed by the effects of changes in surface micro- and nanotopographies on cell adherence, proliferation and morphology.

**Chapter 6** begins the discussion on the degradable nature of POSS-PCLU and the effects of hard segment chemistries on the degradation and crystallization rates. Polymer films are subjected to both *in vitro* and *in vivo* degradation. Different conditions artificially created *in vitro* attempt to mimic bodily environments, as suggested above. Changes in material properties post-degradation *in vitro* and the extent of *in vivo* vascularization and tissue integration are subsequently analysed and discussed.

**Chapter 7** introduces a different tissue engineering concept, namely the use of naturally-derived polymers such as collagen and gelatin fashioned into a hydrogel as opposed to a synthetic polymer system prepared using a salt-leaching process. In a collaboration with the Khademhosseini laboratories at Harvard-MIT in Boston, photopolymerized gelatin methacrylate (GelMA) hydrogels were synthesized and their mechanical and degradation profiles were fine-tuned by varying parameters including the GelMA and PEG content. The ability of GelMA hydrogels to support keratinocyte growth in order to form a reconstructed neo-epidermis is discussed.

**Chapter 8** briefly outlines the advantages and disadvantages of using either synthetic or natural polymers as base materials for tissue engineering platforms. It is suggested that the elucidation of the optimal combination of both natural and synthetic materials in order to create composite scaffolds may lead to the development of a 'super-platform' with optimal mechanical properties and natural biocompatibility.

**Appendix.** Due to the relatively recent scandal involving the French breast implant manufacturers Poly Implant Prosthèse (PIP), we investigated the mechanical and surface characteristics of explanted PIP silicone implants and compared the results to control, medical-grade ones. The strength and degrees of chemical degradation of both sets of implant shells and gels are discussed.

## **1.5 HYPOTHESIS**

Poly( $\epsilon$ -caprolactone urea)urethane incorporating polyhedral oligomeric silsesquioxane (POSS-PCLU) is a novel biodegradable polymer suitable for skin tissue engineering purposes due to their optimal mechanical properties, biocompatibility and the ability to fine-tune the degradation rate.

## **1.6 AIMS OF THESIS**

The primary aim of this thesis was to introduce a novel bioresorbable nanocomposite polymer for skin tissue engineering purposes. To this end, several different polymer formulations were studied in order to analyse the rate and mode of degradation. The selected nanocomposite polymers should be cyto- and biocompatible and display excellent elasticity.

The secondary aim was to establish a method for efficient sterilization of this novel degradable nanocomposite. The optimal technique should reliably remove all

microorganisms, endotoxins and endospores whilst having no or minimal effects on the material's chemical composition, surface topography and 3D structure.

## References

- AMIN, P., WILLE, J., SHAH, K. & KYDONIEUS, A. 1993. Analysis of the extractive and hydrolytic behavior of microthane poly(ester-urethane) foam by high pressure liquid chromatography. *J Biomed Mater Res*, 27, 655-66.
- AZEVEDO, H. S. & REIS, R. L. 2005. *Biodegradable Systems in Tissue Engineering and Regenerative Medicine.*, CRC Press.
- BAKHSHI, R., DARBYSHIRE, A., EVANS, J. E., YOU, Z., LU, J. & SEIFALIAN, A. M. 2011. Polymeric coating of surface modified nitinol stent with POSS-nanocomposite polymer. *Colloids Surf.B Biointerfaces.*, 86, 93-105.
- BELL, E., EHRLICH, H. P., BUTTLE, D. J. & NAKATSUJI, T. 1981. Living tissue formed in vitro and accepted as skin-equivalent tissue of full thickness. *Science (New York, N.Y.)*, 211, 1052-4.
- BETTINGER, C. J., BRUGGEMAN, J. P., BORENSTEIN, J. T. & LANGER, R. 2009. In vitro and in vivo degradation of poly(1,3-diamino-2-hydroxypropane-co-polyol sebacate) elastomers. *J.Biomed.Mater.Res.A*, 91, 1077-88.
- BIOSCIENCES, O. Z. 2013. *RE: 3D-Fect TM*.
- BOLOGNESI, C., BAUR, X., MARCZYNSKI, B., NORPPA, H., SEPAI, O. & SABBIONI, G. 2001. Carcinogenic risk of toluene diisocyanate and 4,4'-methylenediphenyl diisocyanate: epidemiological and experimental evidence. *Critical reviews in toxicology*, 31, 737-72.
- BRAATZ, J. A., HEIFETZ, A. H. & KEHR, C. L. 1992. A new hydrophilic polymer for biomaterial coatings with low protein adsorption. *J Biomater.Sci Polym Ed*, 3, 451-62.
- C.SANCHEZ, A.A.SOLER-ILLIA, G. J. D., F.RIBOT, T.LALOT, C.R.MAYER & V.CABUIL 2001. Designed Hybrid Organic-Inorganic Nanocomposites from Functional Nanobuilding Blocks. *Chem.Mater*, 13, 3061-83.
- CHALOUPKA, K., MOTWANI, M. & SEIFALIAN, A. M. 2011. Development of a new lacrimal drainage conduit using POSS nanocomposite. *Biotechnology and applied biochemistry*, 58, 363-70.
- CHAWLA, A. S., BLAIS, P., HINBERG, I. & JOHNSON, D. 1988. Degradation of explanted polyurethane cardiac pacing leads and of polyurethane. *Biomaterials, artificial cells, and artificial organs*, 16, 785-800.
- CHEN, F. M., AN, Y., ZHANG, R. & ZHANG, M. 2011. New insights into and novel applications of release technology for periodontal reconstructive therapies. *Journal of controlled release : official journal of the Controlled Release Society*, 149, 92-110.
- CHEN, F. M., ZHANG, M. & WU, Z. F. 2010. Toward delivery of multiple growth factors in tissue engineering. *Biomaterials*, 31, 6279-308.
- CHIELLINI, E. E., CHIELLINI, F. & SOLARO, R. 2006. Bioerodible polymeric nanoparticles for targeted delivery of proteic drugs. *J Nanosci Nanotechnol*, 6, 3040-7.
- DARBY, T. D., JOHNSON, H. J. & NORTHUP, S. J. 1978. An evaluation of a polyurethane for use as a medical grade plastic. *Toxicol Appl Pharmacol*, 46, 449-53.
- DENG, J., POLIDAN, J. T., HOTTLE, J. R., FARMER-CREELY, C. E., VIERS, B. D. & ESKER, A. R. 2002. Polyhedral oligomeric silsesquioxanes: a new class of amphiphiles at the air/water interface. *J Am.Chem.Soc.*, 124, 15194-5.
- DESAI, M., BAKHSHI, R., ZHOU, X., ODLYHA, M., YOU, Z., SEIFALIAN, A. M. & HAMILTON, G. 2012. A sutureless aortic stent-graft based on a nitinol scaffold bonded to a compliant nanocomposite polymer is durable for 10 years in a simulated in vitro model. *Journal of endovascular therapy : an official journal of the International Society of Endovascular Specialists*, 19, 415-27.

E.MARKOVIC, K.CONSTANTOPOLOUS & J.G.MATISONS 2011. Polyhedral Oligomeric Silsesquioxanes: From Early and Strategic Development through to Materials Application. *In: J.MATISONS & THOMPSON, C. H. (eds.). Springer.*

FU, B. X., HSIAO, B. S., WHITE, H., RAFAILOVICH, M., MATHER, P. T., JEON, H. G., PHILLIPS, S., LICHTENHAN, J. D. & SCHWAB, J. 2000. Nanoscale reinforcement of polyhedral oligomeric silsesquioxane (POSS) in polyurethaneelastomer. . *Polymer international*, 49, 437-40.

FU, B. X., YANG, L., SOMANI, R. H., ZONG, S. X., HSIAO, B. S., PHILLIPS, S., BLANSKI, R. & RUTH, P. 2001. Crystallization studies of isotactic polypropylene containing nanostructured polyhedral oligomeric silsesquioxane molecules under quiescent and shear conditions. *Journal of Polymer Science: Part B: Polymer Physics*, 39, 2727-39.

GHANBARI, H., COUSINS, B. G. & SEIFALIAN, A. M. 2011. A nanocage for nanomedicine: polyhedral oligomeric silsesquioxane (POSS). *Macromolecular rapid communications*, 32, 1032-46.

GOGOLEWSKI, S. 1987. Implantable segmented polyurethanes: controversies and uncertainties. *Life support systems : the journal of the European Society for Artificial Organs*, 5, 41-6.

GUNATILLAKE, P. A. & ADHIKARI, R. 2003. Biodegradable synthetic polymers for tissue engineering. *European cells & materials*, 5, 1-16; discussion

HONG, B., THOMS, T. P. S., MURFEE, H. J. & LEBRUN, M. J. 1997. Highly Branched Dendritic Macromolecules with Core Polyhedral Silsesquioxane Functionalities. . *Inorganic Chemistry*, 36, 6146-7.

IWATA, T. & DOI, Y. 1998. Morphology and enzymatic degradation of poly(L-lactic acid) single crystals. *Macromolecules*, 31, 2461-7.

IZCI, Y., SECER, H., AKAY, C. & GONUL, E. 2009. Initial experience with silver-impregnated polyurethane ventricular catheter for shunting of cerebrospinal fluid in patients with infected hydrocephalus. *Neurological research*, 31, 234-7.

J.ARMSTRONG, H.J.SALACINSKI, Q.MU, A.M.SEIFALIAN, L.PEEL, N.FREEMAN, C.M.HOLT & J.R.LU 2004. Interfacial adsorption of fibrinogen and its inhibition by RGD peptide: a combined physical study. *J Phys Condens Matter*, 16.

JORGE-HERRERO, E., FERNANDEZ, P., TURNAY, J., OLMO, N., CALERO, P., GARCIA, R., FREILE, I. & CASTILLO-OLIVARES, J. L. 1999. Influence of different chemical cross-linking treatments on the properties of bovine pericardium and collagen. *Biomaterials*, 20, 539-45.

JUNGEBLUTH, P., ALICI, E., BAIGUERA, S., LE, B. K., BLOMBERG, P., BOZOKY, B., CROWLEY, C., EINARSSON, O., GRINNEMO, K. H., GUDBJARTSSON, T., LE, G. S., HENRIKSSON, G., HERMANSON, O., JUTO, J. E., LEIDNER, B., LILJA, T., LISKA, J., LUEDDE, T., LUNDIN, V., MOLL, G., NILSSON, B., RODERBURG, C., STROMBLAD, S., SUTLU, T., TEIXEIRA, A. I., WATZ, E., SEIFALIAN, A. & MACCHIARINI, P. 2011. Tracheobronchial transplantation with a stem-cell-seeded bioartificial nanocomposite: a proof-of-concept study. *Lancet*, 378, 1997-2004.

K.PIELICHOWSKI, L.NJUGUNA, B. J. & J.PIELICHOWSKI 2006. Polyhedral oligomeric silsesquioxane (POSS)-containing nanohybrid polymers. *In: B.DONNIO, D.GUILLON, HARADA, A., A.HASHIDZUME, W.JAEGER, JANOWSKI, B., S.KUDAIBERGENOV, A.LASCHEWSKY, J.NJUGUNA, J.PIELICHOWSKI, K.PIELICHOWSKI & Y.TAKASHIMA (eds.). Berlin: Springer.*

KANNAN, R. Y., SALACINSKI, H. J., BUTLER, P. E. & SEIFALIAN, A. M. 2005. Polyhedral oligomeric silsesquioxane nanocomposites: the next generation material for biomedical applications. *Acc.Chem.Res.*, 38, 879-84.

KANNAN, R. Y., SALACINSKI, H. J., DE GROOT, J., CLATWORTHY, I., BOZEC, L., HORTON, M., BUTLER, P. E. & SEIFALIAN, A. M. 2006a. The antithrombogenic potential of a polyhedral oligomeric silsesquioxane (POSS) nanocomposite. *Biomacromolecules*, 7, 215-23.

KANNAN, R. Y., SALACINSKI, H. J., EDIRISINGHE, M. J., HAMILTON, G. & SEIFALIAN, A. M. 2006b. Polyhedral oligomeric silsesquioxane-polyurethane nanocomposite microvessels for an artificial capillary bed. *Biomaterials*, 27, 4618-26.

KANNAN, R. Y., SALACINSKI, H. J., GHANAVI, J. E., NARULA, A., ODLYHA, M., PEIROVI, H., BUTLER, P. E. & SEIFALIAN, A. M. 2007. Silsesquioxane nanocomposites as tissue implants. *Plast.Reconstr.Surg.*, 119, 1653-62.

KANNAN, R. Y., SALACINSKI, H. J., ODLYHA, M., BUTLER, P. E. & SEIFALIAN, A. M. 2006c. The degradative resistance of polyhedral oligomeric silsesquioxane nanocomposite integrated polyurethanes: an in vitro study. *Biomaterials*, 27, 1971-9.

KANNAN, R. Y., SALACINSKI, H. J., SALES, K. M., BUTLER, P. E. & SEIFALIAN, A. M. 2006d. The endothelialization of polyhedral oligomeric silsesquioxane nanocomposites: an in vitro study. *Cell Biochem.Biophys.*, 45, 129-36.

KIDANE, A. G., BURRIESCI, G., EDIRISINGHE, M., GHANBARI, H., BONHOEFFER, P. & SEIFALIAN, A. M. 2009. A novel nanocomposite polymer for development of synthetic heart valve leaflets. *Acta Biomater.*, 5, 2409-17.

KIDANE, A. G., SALACINSKI, H., TIWARI, A., BRUCKDORFER, K. R. & SEIFALIAN, A. M. 2004. Anticoagulant and antiplatelet agents: their clinical and device application(s) together with usages to engineer surfaces. *Biomacromolecules.*, 5, 798-813.

LABOW, R. S., DUGUAY, D. G. & SANTERRE, J. P. 1994. The enzymatic hydrolysis of a synthetic biomembrane: a new substrate for cholesterol and carboxyl esterases. *Journal of biomaterials science. Polymer edition*, 6, 169-79.

LABOW, R. S., MEEK, E. & SANTERRE, J. P. 1999. The biodegradation of poly(urethane)s by the esterolytic activity of serine proteases and oxidative enzyme systems. *Journal of biomaterials science. Polymer edition*, 10, 699-713.

LAKHANI, H. A., DE MEL, A. & SEIFALIAN, A. M. 2013. The effect of TGF-beta1 and BMP-4 on bone marrow-derived stem cell morphology on a novel bioabsorbable nanocomposite material. *Artificial cells, nanomedicine, and biotechnology (Print)*.

LAMBA, N. M. K., VOODHOUSE, K. A. & COOPER, S. L. 1998. *Polyurethanes in Biomedical Applications*, Boca Raton, FL, CRC Press.

LANGER, R. & VACANTI, J. P. 1993. Tissue engineering. *Science*, 260, 920-6.

LEE, A. & LICHTENHAN, J. D. 1998a. Viscoelastic Responses of Polyhedral Oligosilsesquioxane Reinforced Epoxy Systems. *Macromolecules*, 31, 4970-4.

LEE, K. H. & CHU, C. C. 2000. The role of superoxide ions in the degradation of synthetic absorbable sutures. *Journal of biomedical materials research*, 49, 25-35.

LELAH, M. D. & COOPER, S. L. 1986. *Polyurethanes in Medicine*, Boca Raton, Florida, CRC Press.

LICHTENHAN, J. D., OTONARI, Y. A. & CARR, M. J. 1995. Linear Hybrid Polymer Building Blocks: Methacrylate-Functionalized Polyhedral Oligomeric Silsesquioxane Monomers and Polymers. *Macromolecules* 28, 8435-7.

LIU, L., LI, S., GARREAU, H. & VERT, M. 2000. Selective enzymatic degradations of poly(L-lactide) and poly(epsilon-caprolactone) blend films. *Biomacromolecules*, 1, 350-9.

M.JOSHI & B.S.BUTOLA 2004. Polymeric nanocomposites - Polyhedral oligomeric silsesquioxane (POSS) as hybrid nanofiller. *J Macromol Sci Part C Polym Rev*, C44, 389-410.

MANTZ, R. A., JONES, P. F., CHAFFEE, K. P., LICHTENHAN, J. D., GILMAN, J. W., ISMAIL, I. M. K. & BURMEISTER, M. J. 1996. Thermolysis of Polyhedral Oligomeric Silsesquioxane (POSS) Macromers and POSS-Siloxane Copolymers. *Chemistry of Materials*, 8, 1250-9.

MARCHANT, R. E., ZHAO, Q., ANDERSON, J. M. & HILTNER, A. 1987. Degradation of a poly(ether urethane urea) elastomer: infra-red and XPS studies. *Polymer*, 2023-9.

MATHER, P. T., JEON, H. G. & ROMO-URIBE, A. 1999. Mechanical Relaxation and Microstructure of Poly(norbornyl-POSS) Copolymers. *Macromolecules* 1194-203.

MAZZU, A. L. & SMITH, C. P. 1984. Determination of extractable methylene dianiline in thermoplastic polyurethanes by HPLC. *J Biomed Mater Res*, 18, 961-8.

MCBANE, J. E., BATTISTON, K. G., WADHWANI, A., SHARIFPOOR, S., LABOW, R. S. & SANTERRE, J. P. 2011a. The effect of degradable polymer surfaces on co-cultures of monocytes and smooth muscle cells. *Biomaterials*, 32, 3584-95.

MCBANE, J. E., SHARIFPOOR, S., CAI, K., LABOW, R. S. & SANTERRE, J. P. 2011b. Biodegradation and in vivo biocompatibility of a degradable, polar/hydrophobic/ionic polyurethane for tissue engineering applications. *Biomaterials*, 32, 6034-44.

MEINEL, A. J., GERMERSHAUS, O., LUHMANN, T., MERKLE, H. P. & MEINEL, L. 2012. Electrospun matrices for localized drug delivery: current technologies and selected biomedical applications. *European journal of pharmaceutics and biopharmaceutics : official journal of Arbeitsgemeinschaft für Pharmazeutische Verfahrenstechnik e.V*, 81, 1-13.

MERKEL, T. C., FREEMAN, B. D., SPONTAK, R. J., HE, Z., PINNAU, I., MEAKIN, P. & HILL, A. J. 2002. Ultrapermeable, reverse-selective nanocomposite membranes. *Science*, 296, 519-22.

MIYAKE, J., SAWAMURA, T., KOKADO, K. & CHUJO, Y. 2009. Amphiphilic Hybrid pi-Conjugated Polymers Containing Polyhedral Oligomeric Silsesquioxanes. *Macromol Rapid Commun*, 30, 1559-63.

NOISHIKI, Y., YAMANE, Y., TAKAHASHI, M., KAWANAMI, O., FUTAMI, Y., NISHIKAWA, T., NOGUCHI, N., NAGAOKA, S. & MORI, Y. 1987. Prevention of thrombosis-related complications in cardiac catheterization and angiography using a heparinized catheter (Anthon). *ASAIO Trans.*, 33, 359-65.

PINCHUK, L. 1994. A review of the biostability and carcinogenicity of polyurethanes in medicine and the new generation of 'biostable' polyurethanes. *Journal of biomaterials science. Polymer edition*, 6, 225-67.

QUÉRÉ, D. 2002. Surface chemistry: Fakir droplets. *Nature materials*, 1, 14-5.

RAGHUNATH, J., ROLLO, J., SALES, K. M., BUTLER, P. E. & SEIFALIAN, A. M. 2007. Biomaterials and scaffold design: key to tissue-engineering cartilage. *Biotechnol Appl Biochem*, 46, 73-84.

RAHMANI, B., TZAMTZIS, S., GHANBARI, H., BURRIESCI, G. & SEIFALIAN, A. M. 2012. Manufacturing and hydrodynamic assessment of a novel aortic valve made of a new nanocomposite polymer. *Journal of biomechanics*, 45, 1205-11.

RATNER, B. D. 1983. Surface characterization of biomaterials by electron spectroscopy for chemical analysis. *Annals of biomedical engineering*, 11, 313-36.

RATNER, B. D., GLADHILL, K. W. & HORBETT, T. A. In vitro studies of the enzymatic biodegradation of polyurethanes. Transactions of the 12th Annual Meeting of the Society for Biomaterials, 1986 Minneapolis-St. Paul, Minnesota, USA.

RICHARDSON, T. P., PETERS, M. C., ENNETT, A. B. & MOONEY, D. J. 2001. Polymeric system for dual growth factor delivery. *Nature biotechnology*, 19, 1029-34.

RIMMER, S., GERMAN, M. J., MAUGHAN, J., SUN, Y., FULLWOOD, N., EBDON, J. & MACNEIL, S. 2005. Synthesis and properties of amphiphilic networks 3: preparation and

characterization of block conetworks of poly(butyl methacrylate-block-(2,3 propandiol-1-methacrylate-stat-ethandiol dimethacrylate)). *Biomaterials*, 26, 2219-30.

ROMO-URIBE, A., MATHER, P. T., HADDAD, T. S. & LICHTENHAN, J. D. 1998. Viscoelastic and morphological behavior of hybrid styryl-based polyhedral oligomeric silsesquioxane (POSS) copolymers. *Journal of Polymer Science: Part B: Polymer Physics*, 36, 1857-72.

ROSLER, A., VANDERMEULEN, G. W. & KLOK, H. A. 2001. Advanced drug delivery devices via self-assembly of amphiphilic block copolymers. *Adv. Drug Deliv. Rev.*, 53, 95-108.

SANTERRE, J. P. & LABOW, R. S. 1997. The effect of hard segment size on the hydrolytic stability of polyether-urea-urethanes when exposed to cholesterol esterase. *Journal of biomedical materials research*, 36, 223-32.

SANTERRE, J. P., LABOW, R. S., DUGUAY, D. G., ERFLE, D. & ADAMS, G. A. 1994. Biodegradation evaluation of polyether and polyester-urethanes with oxidative and hydrolytic enzymes. *Journal of biomedical materials research*, 28, 1187-99.

SARKAR, S., SALES, K. M., HAMILTON, G. & SEIFALIAN, A. M. 2007. Addressing thrombogenicity in vascular graft construction. *Journal of biomedical materials research. Part B, Applied biomaterials*, 82, 100-8.

SCHÄFER, M. & WERNER, S. 2008. Cancer as an overhealing wound: an old hypothesis revisited. *Nature reviews. Molecular cell biology*, 9, 628-38.

SCHUBERT, M. A., WIGGINS, M. J., SCHAEFER, M. P., HILTNER, A. & ANDERSON, J. M. 1995. Oxidative biodegradation mechanisms of biaxially strained poly(etherurethane urea) elastomers. *J Biomed Mater Res*, 29, 337-47.

SHIBAYAMA, M., KAWAUCHI, T., KOTANI, T., NOMURA, S. & MATSUDA, T. 1986. *Structure and properties of fatigued segmented poly(urethaneurea)s I. Segment orientation mechanism due to fatigue.*

SMITH, R., WILLIAMS, D. F. & OLIVER, C. 1987. The biodegradation of poly(ether urethanes). *J Biomed. Mater Res.*, 21, 1149-66.

SOLIS-CORREA, R. E., VARGAS-CORONADO, R., AGUILAR-VEGA, M., CAUICH-RODRIGUEZ, J. V., ROMAN, J. S. & MARCOS, A. 2007. Synthesis of HMDI-based segmented polyurethanes and their use in the manufacture of elastomeric composites for cardiovascular applications. *J Biomater Sci Polym Ed*, 18, 561-78.

SPARK, J. I., YELURI, S., DERHAM, C., WONG, Y. T. & LEITCH, D. 2008. Incomplete cellular depopulation may explain the high failure rate of bovine ureteric grafts. *Br J Surg*, 95, 582-5.

STACHELEK, S. J., ALFERIEV, I., CHOI, H., CHAN, C. W., ZUBIATE, B., SACKS, M., COMPOSTO, R., CHEN, I. W. & LEVY, R. J. 2006. Prevention of oxidative degradation of polyurethane by covalent attachment of di-tert-butylphenol residues. *J Biomed Mater Res A*, 78, 653-61.

STENHAMRE, H., NANNMARK, U., LINDAHL, A., GATENHOLM, P. & BRITTBURG, M. 2011. Influence of pore size on the redifferentiation potential of human articular chondrocytes in poly(urethane urea) scaffolds. *J Tissue Eng Regen. Med.*, 5, 578-88.

SUNG, C. S. P. & SCHNEIDER, N. S. 1978. Structure-property relationships of polyurethanes based on toluene diisocyanate. *J Mater Sci*, 13, 1689-99.

SURESH, S., ZHOU, W., SPRAUL, B., LAINE, R. M., BALLATO, J. & SMITH JR, D. W. 2004. Novel fluoropolymer functionalized silsesquioxanes for nanoscale architecture of hybrid composites. *J Nanosci. Nanotechnol.*, 4, 250-3.

SZYCHER, M. & SICILIANO, A. A. 1991. An assessment of 2,4 TDA formation from Surgitek polyurethane foam under simulated physiological conditions. *Journal of biomaterials applications*, 5, 323-36.



- TAKAHARA, A., COURY, A. J., HERGENROTHER, R. W. & COOPER, S. L. 1991a. Effect of soft segment chemistry on the biostability of segmented polyurethanes. I. In vitro oxidation. *J Biomed Mater Res*, 25, 341-56.
- TAKAHARA, A., OKKEMA, A. Z., WABERS, H. & COOPER, S. L. 1991b. Effect of hydrophilic soft segment side chains on the surface properties and blood compatibility of segmented poly(urethaneureas). *J Biomed Mater Res*, 25, 1095-118.
- TANG, Y. W., LABOW, R. S. & SANTERRE, J. P. 2003. Isolation of methylene dianiline and aqueous-soluble biodegradation products from polycarbonate-polyurethanes. *Biomaterials*, 24, 2805-19.
- TOKIWA, Y., CALABIA, B. P., UGWU, C. U. & AIBA, S. 2009. Biodegradability of plastics. *International journal of molecular sciences*, 10, 3722-42.
- TOKIWA, Y. & SUZUKI, T. 1978. Hydrolysis of polyesters by *Rhizopus delemar* lipase. *Agric. Biol. Chem.*, 42, 1071-2.
- TOKIWA, Y. & SUZUKI, T. 1981. Hydrolysis of copolyesters containing aromatic and aliphatic ester blocks by lipase. *J Appl Polymer Science*, 26, 441-8.
- TOKIWA, Y., SUZUKI, T. & ANDO, T. 1979. Synthesis of copolyamide-esters and some aspects involved in their hydrolysis by lipase. *J Appl Polymer Science*, 24, 1701-11.
- TSUCHIDA, A., BOLLN, C., SERNETZ, F. G., FREY, H. & MUELHAUPT, R. 1997. Ethene and propene copolymers containing silsesquioxane side groups. *Macromolecules*, 30, 2818-24.
- TSUJI, H. & MIYAUCHI, S. 2001. Poly(L-lactide) VI. Effects of crystallinity on enzymatic hydrolysis of poly(l-lactide) without free amorphous region. *Polym Degrad Stab*, 71, 415-24.
- VORONKOV, M. & LAVRENT'YEV, V. 1982. Polyhedral oligosilsesquioxanes and their homo derivatives Inorganic Ring Systems. Springer Berlin / Heidelberg.
- WADDON, A. J. & COUGHLIN, E. B. 2003. Crystal Structure of Polyhedral Oligomeric Silsesquioxane (POSS) Nano-materials: A Study by X-ray Diffraction and Electron Microscopy. *Chemistry of Materials* 15, 4555-61.
- WANG, G. B., LABOW, R. S. & SANTERRE, J. P. 1997. Biodegradation of a poly(ester)urea-urethane by cholesterol esterase: isolation and identification of principal biodegradation products. *Journal of biomedical materials research*, 36, 407-17.
- WIGGINS, M. J., MACEWAN, M., ANDERSON, J. M. & HILTNER, A. 2004. Effect of soft-segment chemistry on polyurethane biostability during in vitro fatigue loading. *J Biomed Mater Res A*, 68, 668-83.
- WU, J. & MATHER, P. T. 2009. POSS Polymers: Physical Properties and Biomaterials Applications. *Polymer Reviews*, 49, 25-63.
- YILDIRIMER, L., THANH, N. T. K., LOIZIDOU, M. & SEIFALIAN, A. M. 2011. Toxicology and clinical potential of nanoparticles. *Nano Today*, 6, 585-607.
- YOSHIMITSU, Z., NAKAJIMA, A., WATANABE, T. & HASHIMOTO, K. 2002. Effects of Surface Structure on the Hydrophobicity and Sliding Behavior of Water Droplets. *Langmuir*, 18, 5818-22.
- Z.GAN, Q.LIANG, J.ZHANG & X.JING 1997. Enzymatic degradation of poly(e-caprolactone) film in phosphate buffer solution containing lipases. *Polym Degrad Stab*, 56, 209-13.
- ZHANG, Y., SUN, H. & CHEN, C. 2004. Superhard cubic BC<sub>2</sub>N compared to diamond. *Physical review letters*, 93, 195504.
- ZHAO, Y. & SCHIRALDI, D. A. 2005. Thermal and mechanical properties of polyhedral oligomeric silsesquioxane (POSS)/polycarbonate composites. *Polymer*, 46, 11640-7.

ZHENG, L., WADDON, A. J., FARRIS, R. J. & COUGHLIN, E. B. 2002. X-ray Characterizations of Polyethylene Polyhedral Oligomeric Silsesquioxane Copolymers. *Macromolecules*, 35, 2375-9.

# **2 3-DIMENSIONAL BIOMATERIAL DEGRADATION – QUITE LITERALLY TAKING A LEAF OUT OF NATURE’S BOOK<sup>1</sup>**

---

## **2.1 SYNOPSIS**

The apparent difficulty to precisely control fine-tuning of biomaterial degradation has initiated the recent paradigm shift from conventional top-down fabrication methods to more nature-inspired bottom-up assemblies. Sophistication of material fabrication techniques allows today’s scientists to reach beyond conventional natural materials in order to synthesize tomorrow’s ‘designer material’. Material degradation into smaller components and subsequent release of encapsulated cells or cell-signalling agents have opened medically exploitable avenues, transforming the area of regenerative medicine into a dynamic and self-propagating branch of modern medicine. The race to create complex and ever more refined scaffolding structures seems to have assumed a life of its own and represents an ever growing niche in the materials sciences. Recently, we have developed and conducted the world’s first in-human tracheal transplantation using a non-degradable completely synthetic biomaterial. Fuelled by such clinical potential, we are currently developing a biodegradable version suitable for skin tissue engineering and paediatric applications. However, despite enormous efforts, current, as yet insurmountable challenges include precise biomaterial degradation within pre-determined spatial and temporal confines in an effort to release bio-signalling agents in such orchestrated fashion as to fully regenerate functioning tissues. In this chapter, the readers, almost anticlimactically, are asked to step out of the artificially over-constructed

---

<sup>1</sup> A modified version of the following chapter has been accepted for publication in *Biotechnology Advances*.

spiral of ever more convoluted scaffold fabrication techniques and consider nature's tried and tested approach to material degradation – the leaf. It will further be investigated how scaffold designs and fabrication methods may influence degradation and subsequent release of incorporated elements. A focus will be placed on the delivery of growth factors, stem cells and therapeutic agents alone or in parallel. The difficulties of designing a delivery vehicle capable of delivering multiple factors whilst maintaining distinct release kinetics will be highlighted. Finally, this chapter will be rounded off with an insight into current literature addressing the recurring issues of degradation product toxicities and suggest means of overcoming those.

## **2.2 INTRODUCTION**

Biodegradable materials have undergone extensive research and represent a popular platform for tissue engineering bone (Cui et al., 2012), skin (Yildirimer et al., 2012), cardiovascular tissues (Salacinski et al., 2003, Ghanbari et al., 2009, de Mel et al., 2008, Ahmed et al., 2011a) and nerves (Sedaghati et al., 2011, Pabari et al., 2011, Kannan et al., 2005a, Tan et al., 2012) amongst many other organs and tissues. Conceptually, degradation is defined as a molecular change due to chemical chain scission within a polymer matrix. The subsequent breakdown into smaller material components and potential release of encapsulated cells or cell-signalling agents have opened medically exploitable avenues, transforming the area of regenerative medicine into a dynamic and self-propagating branch of modern medicine. The race to create complex and ever more refined scaffolding structures in order to dazzle even the most complacent tissue engineers seems to have assumed a life of its own and appears to represent an ever growing niche in the materials sciences. Despite enormous efforts, current, as yet insurmountable challenges include precise biomaterial degradation within pre-determined spatial and temporal confines in an effort to release bio-signalling agents in such orchestrated fashion as to fully regenerate functioning tissues. It thus appears almost anti-climactic to be asked to step out of the artificially over-constructed spiral of ever more convoluted scaffold fabrication techniques and consider nature's tried and tested approach to material degradation.

## **2.3 TISSUE ENGINEERING SCAFFOLDS AS CARBON COPIES OF NATURE**

Taking a tree's leaf as an example, one soon discovers the relatively simplistic mechanism leading to repeated blossoming over several decades if not centuries. The soft

matter of leaves is composed of an array of straight, chain-like cellulose molecules which tend to degrade first leaving behind a scaffold made of lignin (Fig. 2.1).

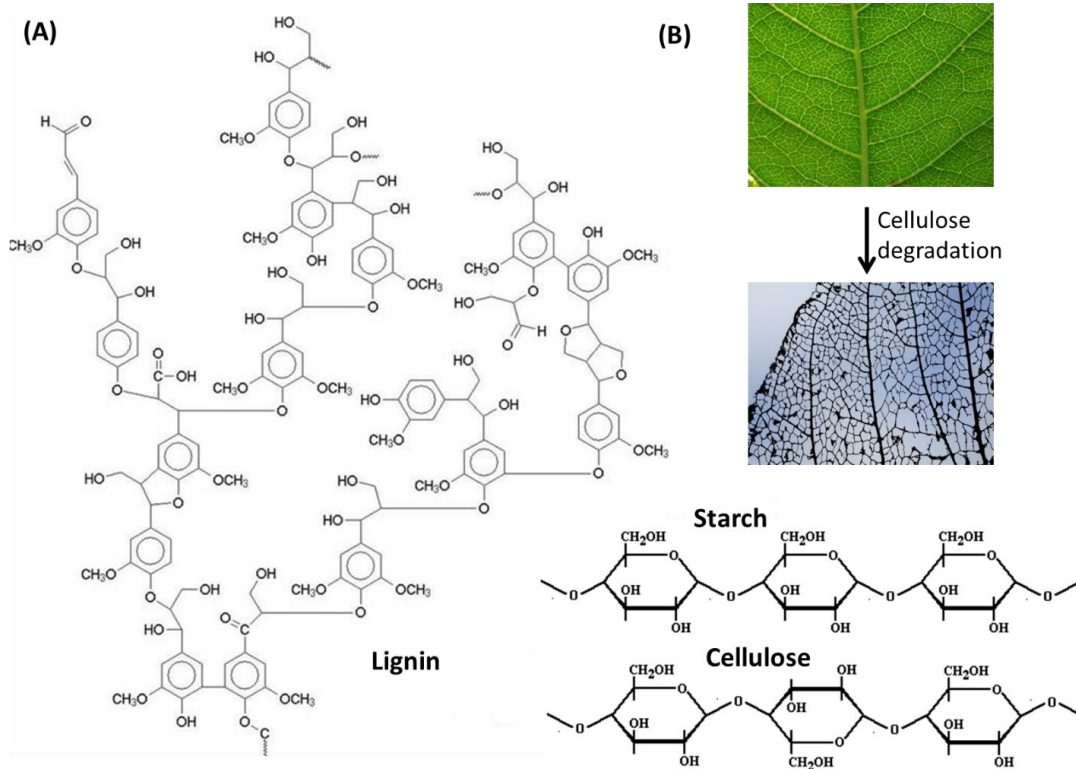


**Figure 2.1.** (A) Lignin being a more complex folded structure than cellulose, it is more difficult to break down. (B) The soft matter of a leaf is made of cellulose which degrades first, leaving behind a 3D scaffold made of lignin. Leaf degradation is the breakdown of leaf starch into simple sugars which are utilised in the growth and development of the plant. Images taken from (University of Waikato, 2014) (A), (Ridge, 2009, Decelles, 2006) (B).

Lignin, being a more complex folded structure, delays enzymatic breakdown due to steric hindrance thereby sustaining structural integrity for longer. A second growth-enhancing corollary of leaf degradation is the breakdown of leaf starch into simple sugars which are utilised in the growth and development of the plant (Wang et al., 2013c).

This simple and elegant combination of staggered material breakdown resulting in the controlled release of regenerative cues such as growth factors, cells or genes has found particular resonance in the field of regenerative medicine and controlled particle

delivery where breakdown of the delivery vehicle permits particle release and action whilst maintaining a structurally intact 3D scaffold for tissue ingrowth (Fig. 2.2) (Shmueli et al., 2013, Seras-Franzoso et al., 2013, Chen et al., 2011c, Biosciences, 2013).

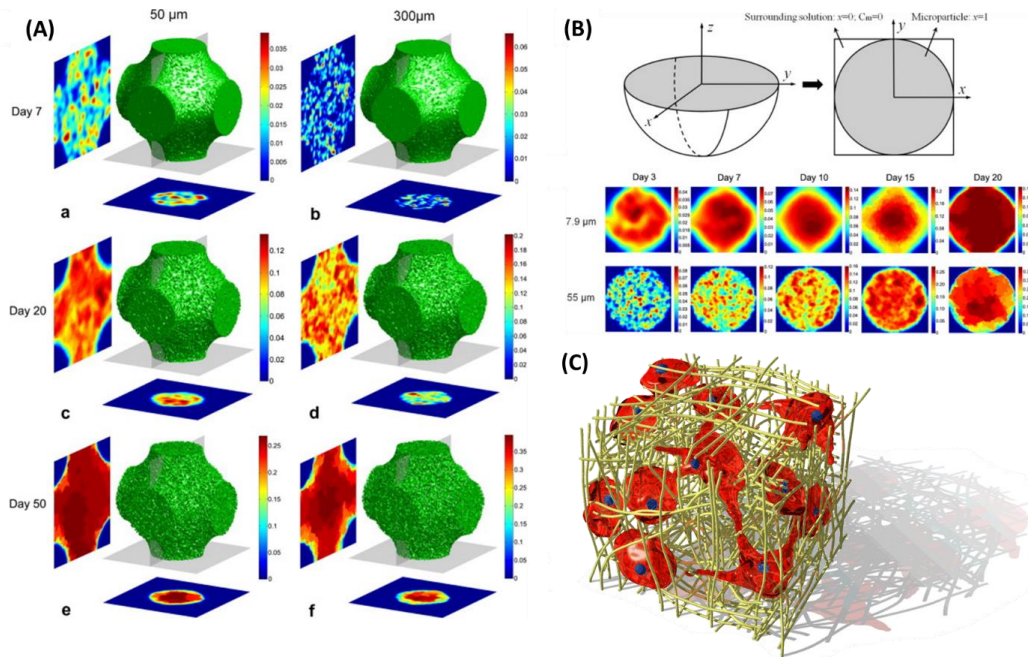


**Figure 2.2.** Scaffold porosity, particle dimensionality and bulk to fluid ratio play critical roles in regulating the degradation process. Staggered material breakdown results in the controlled release of incorporated factors (A, B). Images taken from (Chen et al., 2011b). (C) A structurally intact scaffold is maintained while incorporated cells break down the surrounding biomaterial matrix to make space for cell migration, proliferation and own matrix deposition. Images taken from (Biosciences, 2013).

During unassisted wound healing, cells and cell components release a myriad of trophic factors including growth factors (GF), cytokines and other molecules to minimize wound dimensions and induce spontaneous healing (Yildirimer et al., 2012). However, natural healing is frequently accompanied by scar formation, functional and cosmetic compromise. Accelerated *in situ* tissue regeneration using scaffold structures supplemented with tissue-specific trophic factors is hoped to be able to induce complete scar-free tissue regeneration with preservation or restoration of function. The major

determinants in elucidating the complicated molecular cascade required for true regeneration are (a) finding the correct cocktail of GFs capable of stimulating suitable cellular differentiation and (b) unlocking the correct sequence of GF release. To date, the delivery of multiple bioactive factors with distinct kinetics to mirror physiological processes remains a challenge (Weissman, 2000, Chapanian and Amsden, 2010, Cheng and Sefton, 2009, Yan et al., 2009, Richardson et al., 2001). Initial studies demonstrated the use of a multi-protein delivery system for accelerated vascularisation and tissue formation in an effort to mimic the synergistic action of cell-signalling molecules (Richardson et al., 2001). Poly(lactide-co-glycolic acid) (PLGA) microspheres encapsulating both vascular endothelial growth factor (VEGF) and platelet derived growth factor (PDGF) were processed into porous scaffolds which were implanted into a murine hindlimb ischaemia model. Dual delivery of GFs resulted in both a high blood vessel density and the formation of thicker and more mature vessels exhibiting typically multilayered structures when compared to vessels exposed to single GFs. Further, the ability to modulate release kinetics for sustained or successive release of bioactive molecules has been found to be of fundamental importance for functional tissue formation (Chen et al., 2011b). It is generally accepted that in order for regenerative cues to function precisely, their release and activity are subject to a critical window. If release kinetics are timed correctly, natural regeneration of tissues ensues; if released outside this window, previously incorporated biological agents may potentially have antagonistic actions rendering localised factor delivery futile or even harmful.

Richardson's study exemplifies the two main modes of release kinetics of biological molecules incorporated into delivery vehicles (Fig. 2.3) (Richardson et al., 2001).



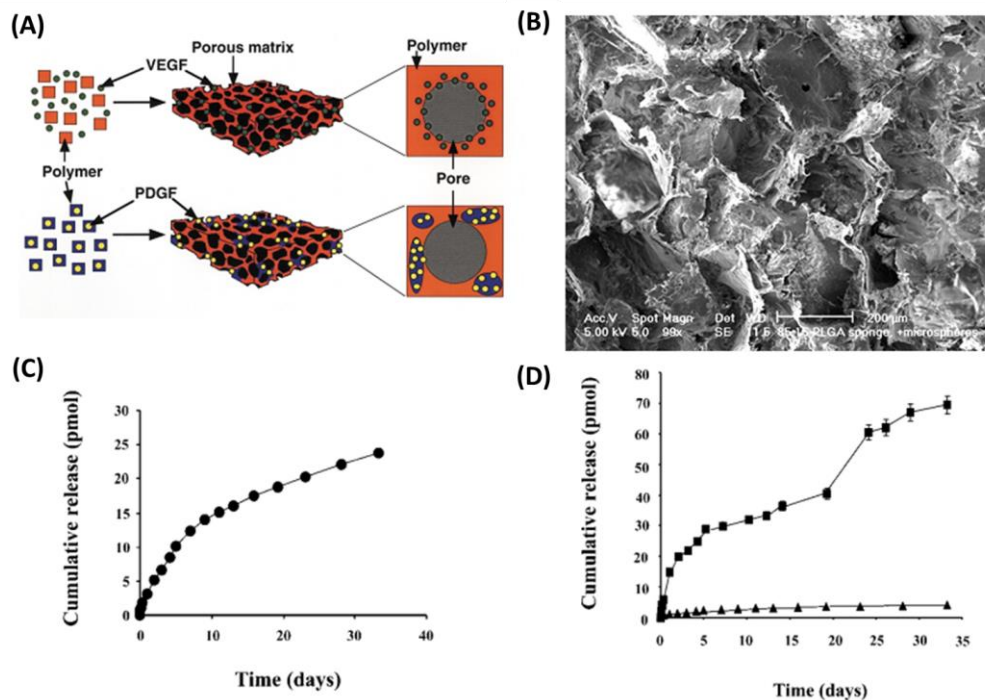


**Figure 2.3.** (A) A schematic illustration of the two main scaffold fabrication techniques to modulate release kinetics of incorporated molecules. Mixing of bioactive agents with the polymer solution prior to processing into a scaffold results in their molecular adhesion mainly to scaffold surfaces and subsequent burst release. Pre-encapsulation of molecular agents into microspheres and subsequent mixing and casting into a scaffold results in a more even distribution of molecules. (B) Microscopic image of a porous polymer surface incorporating bioactive molecules. (C, D) Different manufacturing processes yield different release kinetics enabling distinctly multiphasal release profiles. Images taken from (Richardson et al., 2001).

Mixing of molecular agents with the material before processing into a 3D scaffold results in the factors being largely associated with the material surface and are thus subject to rapid release. In contrast, pre-encapsulation of molecular agents into polymeric microspheres and subsequent mixing and casting into a scaffold are thought to yield a more even distribution of agents throughout the scaffold with release regulated by material degradation kinetics. A combination of both methods can predictably result in a distinctly multiphasal release profile of more than one factor.

## 2.4 DETERMINANTS OF SCAFFOLD DEGRADATION KINETICS

Release kinetics may further be influenced by external conditions including temperature (Esteban et al., 1990), presence of a degradative environment (e.g. hydrolytic or oxidative), pH of fluid environment and fluid dynamics surrounding the delivery vehicle (Agrawal et al., 2000). It has further been demonstrated that scaffold degradation kinetics and potential release of adsorbed bioactive molecules can be affected by scaffold-intrinsic features such as porosity, pore size and shape and overall design. It was further suggested that scaffold hydrophilicity may actively influence the extent to which water can diffuse through the scaffold, thereby directly affecting the release kinetic of any molecules adsorbed to the scaffolds (Xu et al., 2013). Precise molecular bottom-up assemblies warrant further and more varied modes of degradation ranging from bulk degradation or surface erosion to more specific and complex designer scaffolds capable of degrading within precise temporo-spatial confines. Degradation rates and mechanisms are primarily influenced by matrix dimensionality, manner of assembly and consequent water penetration efficiency. If water molecules penetrate the 3D architecture at a higher rate than natural hydrolysis takes place, e.g. potentially influenced by scaffold porosity, thickness and exposed surface area, degradation proceeds throughout the entire material matrix resulting in uniform or 'bulk' degradation. On the contrary, if water permeation is slow, hydrolytic erosion will mainly occur on the exterior surface. The internal matrix remains largely unchanged thus allowing for temporary shielding of any core-integrated trophic factors. The conceptual integration of rapidly and slowly degrading entities within the same scaffold assembly, again, draws from the idea of creating longer lasting structural support structures whilst accelerating tissue regeneration using rapid, though constant, growth-stimulating factor release. Modes of degradation, however, do not solely depend on external conditions or material

assembly but are further influenced by the type of material used. Hydrolytically unstable materials including polylactide (PLA) and polyglycolide (PGA) are known to degrade within weeks whereas PCL may take up to two years to fully break down (Raghunath et al., 2009). Several *in vitro* studies have investigated the effect of various enzymes on biodegradable materials in an effort to synthesize scaffolds responsive to specific enzymes found at the wound site. This would then result in accelerated material breakdown and release of incorporated factors as well as enhanced cell migration and spreading (Kim et al., 2008, Galler et al., 2010, He and Jabbari, 2007). Enzymes, essential macromolecules working at the interface of the body's metabolic pathways, are known to accelerate breakdown of many chemical bonds found in natural as well as artificial biomaterials. A recent study investigating bone regeneration in a rat bone defect model utilized a hydrogel scaffold incorporating peptide crosslinkers which are cleaved by naturally occurring matrix metalloproteinases (MMPs) to release entrapped bone morphogenic protein (BMP) (Mariner et al., 2013). Precise cleavage and degradation of the delivery vehicle allowed for the incorporation of significantly reduced BMP levels for equally therapeutic effects. Whilst targeting susceptible bonds with naturally occurring enzymes is one step closer to precisely controlled scaffold breakdown, the amount of natural enzymes within a specific wound site is often unpredictable. Consequently, a synthetic hydrogel containing hydrophobic diepoxyoctane crosslinks which could only be broken down by endosialidases not found in the human body was developed (Berski et al., 2008).

The synergistic union of enzymes and degradable biomaterials to release regenerative cues is comparable to the symbiosis between ants and leaves in nature – the breakdown of plant materials to sustain the growth of the ant population simultaneously

releases basic sugars required for plant development. Enzymatic degradation, however, is not solely responsible for scaffold breakdown and subsequent release of biomolecules; hydrolytically labile materials initiate degradation as soon as contact with water molecules is established. This has recently been exploited in a study demonstrating that targeted incorporation of hydrolytically labile structures within a scaffold network enables the precise engineering of appropriate degradation profiles (Parlato et al., 2013). Whilst scaffold degradation and subsequent release of an entrapped biomolecular agent is highly desirable, such scaffolds simultaneously lose their mechanical integrity which may have detrimental consequences in terms of tissue dimensionality. It has therefore been suggested that drug release mechanisms needed to be decoupled from the intrinsic scaffold degradation kinetics (Mouriño et al., 2013). Several studies thereupon investigated the potential of biomolecular adsorption on the scaffold surface in an effort to separate the two entities. However, the pattern of molecule release was found to frequently involve an initial burst release followed by a very slow release rate which may be clinically unsuitable (Fig. 2.3). Such drawbacks may be advanced upon by biomolecular entrapment through multilayered polymer coatings onto a slowly degrading scaffold surface or by loaded nano- or microspheres which are incorporated into the scaffold matrix (Kim et al., 2005). An excellent review has recently highlighted the possibility of entrapping multiple biomolecular agents within different layers of a nano- or microsphere that have different degradation profiles in order to release active agents in sequential manners (Mouriño et al., 2013). Such mixed-mode degradation profiles, again reminiscent of the degradation pattern of leaves, may serve as an attractive option for emerging tissue engineering, drug delivery and gene delivery applications.

The following sections will aim to investigate how scaffold designs and fabrication methods may influence degradation and subsequent release of incorporated elements. A

focus will be placed on the delivery of GFs, stem cells and therapeutic agents alone or in parallel. The difficulties of designing a delivery vehicle capable of delivering multiple factors whilst maintaining distinct release kinetics will be highlighted. Finally, this chapter will conclude with an insight into current literature addressing the recurring problems of unwanted side effects including degradation product toxicity and suggested solutions of overcoming those.

## 2.5 SCAFFOLD DESIGN INFLUENCES BIOMATERIAL DEGRADATION AND TISSUE REGENERATION

Just as nature designed leaves of different shapes and patterns to face different challenges, biomaterial scaffolds may also be built to serve a specific purpose. Depending on their functional requirements, scaffolds may be designed into various morphologies (Fig. 2.4) using a range of biodegradable materials allowing for a precise problem-solving approach (Meinel et al., 2012).

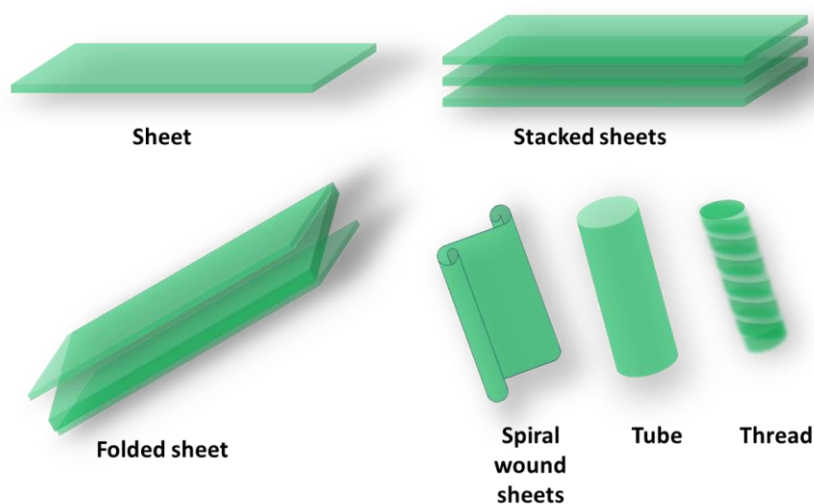


**Figure 2.4.** Schematic illustration of a variety of scaffold shapes. Different scaffold morphologies influence degradation behaviour. Images inspired by (Meinel et al., 2012).

Flat sheets may serve as dermal/epidermal regeneration platforms (van der Veen et al., 2011), whereas cell seeding on sheets and subsequent stacking or folding prior to implantation may improve cell distribution and accelerate wound healing by providing not a naked scaffold but a preconditioned cell-laden environment (Ng et al., 2005, Agarwal et al., 2012). Scaffolds wound into a spiral have demonstrated significant efficacy in bone regeneration due to macrochannels formed by spiral-wound matrices that enhance cell migration from the periphery to the centre (Pişkin et al., 2009). Spiral-wound channels have further been shown to better support nerve regeneration compared to tubular or hydrogel-based cylindrical scaffolds (Valmikinathan et al., 2008). Superior results were demonstrated to be due to enhanced surface areas combined with good mechanical properties and porosities of spiral scaffolds to support higher cell attachments and proliferation. Additionally, macrochannels formed by spiral-wound scaffolds impart an open architecture that permeates the scaffold evenly thereby leaving sufficient volume for media influx and deeper cell penetration into the scaffold. A different approach towards achieving tissue engineered scaffolds with high cell- or drug-loading capacity is to electrospin threaded fibres made of suspensions containing cells or bioactive molecules. This enables the fabrication of 'living' or biologically active threads which may be used to fabricate medical agent-loaded fibrous threads for tissue suturing and regenerative applications (He et al., 2009).

Such differences in scaffold conformations often go hand in hand with different surface areas exposed to potentially degradative conditions and subsequently different degradation modes and rates. Flat porous sheets, ideally suited for dermal regeneration (Wang et al., 2013a), degrade relatively fast which is likely to be related to the fact that thin porous films have a large surface area to volume ratio and thus a greater water

uptake (Lu et al., 1999b). This area-dependence was confirmed in a more recent study demonstrating accelerated scaffold degradation by modulating porogen size and shapes (Liebschner and Wettergreen, 2012). Further investigations of the impact of scaffold geometry on its rate of degradation and bioactive molecule release profile linked differences in scaffold geometries to their surface area exposed to water which directly impacted on the degradation (Lee et al., 2012). In this study, the descending order of the relative surface area was found to be honeycomb > grid > ring > circle which indicated that scaffolds with complex structures and inner holes (or pores) had large surface areas and were therefore more easily degradable. Furthermore, nanoscaled architectures on material surfaces predictably increase surface area and allow for significantly more rapid biodegradation (Sun and Downes, 2009).

Tissue engineered scaffolds should ideally have a degradation rate synchronized with their replacement by regenerating tissues (Fig. 2.5) (Raghunath et al., 2007).

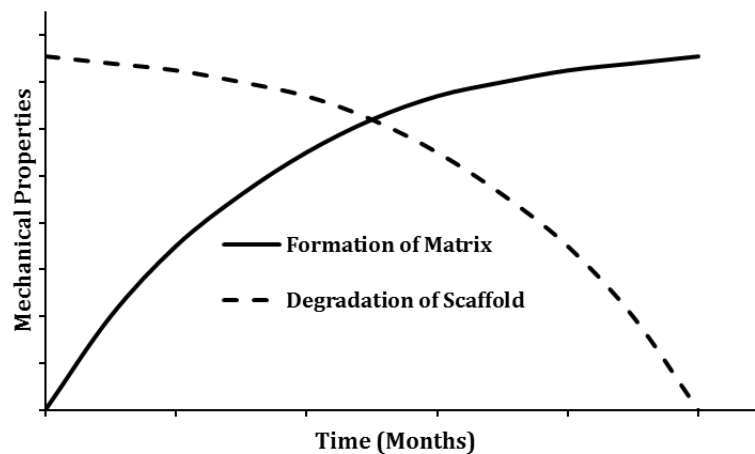


**Figure 2.5.** Optimum model of mechanical properties of a scaffold as new tissue develops. Image taken from (Raghunath et al., 2007).

It thus is of utmost importance to ensure that degradation properties and breakdown products of scaffolds do not interfere with cell attachment and tissue

regeneration. It has previously been shown that the degradation rate of scaffolds may affect cellular interactions including cell proliferation, tissue synthesis and host response (Lewandrowski et al., 2000, Mikos et al., 1998). Cell viability was found to be inversely related to degradation rate with slowly degrading PCL better able to support cell growth compared to PLGA (Sung et al., 2004). PLGA being more hydrophilic and of lower molecular weight compared to PCL predictably experienced accelerated material degradation both *in vitro* and *in vivo* conditions, thus providing progressively less surface area for cell integration and proliferation (Giunchedi et al., 1998). Several studies highlighted the importance of high surface area for sufficient cell attachment as well as a requirement for a 3D scaffolding structure for cell guidance and subsequent extracellular matrix (ECM) deposition. Yu *et al.* demonstrated the successful combination of large surface area with sufficient structural support and guidance in an *in vivo* nerve regeneration model (Yu et al., 2011). Electrospun PCL conduits were functionalized with a collagen layer for superior biocompatibility whilst exploiting the load-bearing abilities and good flexibility of PCL electrospun fibres (Wang et al., 2008). Structural support was provided until cells deposited sufficient ECM for scaffold-independent sustenance. It has been shown that certain cell types are unable to produce and correctly assemble sufficient ECM and form cell-cell junctions when grown without the guidance and signalling provided by a scaffold (Nichol and Khademhosseini, 2009). Cellular functions including their biosynthetic activities may be affected by cell-material interactions as well as scaffold degradation rate (Guaccio et al., 2008). Clearly, a balance needs to be struck between de novo synthesis of ECM, its deposition and maturation and the scaffold's mechanical integrity (Shreiber et al., 2003). Thus, scaffold degradation kinetics play a crucial role in the process of tissue regeneration by influencing the final ECM composition and assembly (Imparato et al., 2013).



Degradation of synthetic materials such as the aliphatic polyesters PCL and PLGA proceeds via the hydrolysis of ester bonds (Schmitt et al., 1994, Grizzi et al., 1995, Li, 1999, Li and McCarthy, 1999). Breakage of these bonds by water molecules results in smaller and smaller chains (chain scission) eventually leading to the formation of short fragments of chains with exposed water soluble carboxyl (-COOH) end groups. As the hydrogen ions (H<sup>+</sup>) dissociate from the carboxyl (-COOH) groups the local pH value decreases. The acidic pH catalyses the hydrolysis of yet other ester bonds thus speeding up degradation. This mechanism is called autocatalysis (Lu et al., 1999b, Grizzi et al., 1995, Li and McCarthy, 1999, Li, 1999). Several studies have demonstrated the detrimental effect of acidic environments on cellular viability (Wu et al., Razaq et al., 2003, Oh et al., 2006). However, the static *in vitro* setting is a poor representation of the more dynamic *in vivo* environment where localised acidity is more likely to become effluxed via the vasculature and lymphatic system (Göpferich, 1996, Yellowley et al., 1997).

Degradation of biological scaffolding materials such as collagen or hydroxyapatite usually proceeds significantly faster than synthetic materials with degradation products considered safe. Rapid and more unpredictable degradation kinetics, however, render biological scaffolds unsuitable for long-term structural support and sustained particle delivery. Such materials may be structurally reinforced by carefully choosing suitable fabrication methods or creating bio-synthetic composite materials. It has been shown that changing of crosslinking densities using increasing concentrations of glutaraldehyde increases stability of gelatine microscaffolds, thereby enabling sufficient cell guidance and subsequent collagen deposition and assembly within the extracellular space provided by the scaffold (Imparato et al., 2013). Degradation was thus found to match collagen maturation and tissue regeneration. The use of crosslinking agents such as

glyceraldehydes or glutaraldehyde represents a convenient alternative to maintain collagen matrix stability by bridging amine groups between two adjacent polypeptide chains (Khor, 1997). However, high degrees of crosslinking have been shown to have cytotoxic effects *in vitro* as well as *in vivo* (Sisson et al., 2009, Maranto and Schoen, 1988, Dahm et al., 1990). Other, more biocompatible alternative crosslinking agents such as 1-ethyl-3-(3- dimethyl aminopropyl)carbodiimide (EDC), polyepoxidic and polyglycidyl have been developed and are currently under investigation (Khor, 1997, Sung et al., 1996, Courtman et al., 2001). Tables 2.1 and 2.2 summarise the degradation kinetics of a selection of synthetic, natural and composite materials and discusses methods of fine-tuning rates of material degradation.

**Table 2.1.** *In vitro* degradation outcomes of a selection of natural, synthetic and composite polymers.

Scaffold material	Scaffold fabrication method	Degradation Condition	<i>In vitro</i> degradation outcome	Reference	
Natural	Collagen	Double-emulsion technique	Collagenase	Rate of collagen degradation was strictly a function of percentage glycer-aldehyde crosslinking with higher crosslinking corresponding to stiffer substrates.	(Imparato et al., 2013)
	Gelatin	Air sprayed microbeads	Collagenase/ dispase	Rate of gelatin microbead degradation was inversely proportional to degree of carbodiimide crosslinking.	(Serban et al., 2013)
	Chitosan /gelatin	Freeze dried and cross-linked with WSC.  Ratio of chitosan to gelatin was: 5:0 (C); 4:1 (C4G1); 3:2 (C3G2); 1:1 (C1G1); 2:3 (C2G3); 1:4 (C1G4); 0:5 (G)	pH 7.4 PBS, 37°C	Non-crosslinked gelatin degraded quickly in PBS in absence of enzymes. Chitosan degradation proceeded significantly more slowly due to strong hydrogen bonds and crystallinity. The chitosan in chitosan /gelatin composites promoted stabilization of the scaffold likely due to static electric forces created between chitosan and gelatin.	(Whu et al., 2013)
	Chitosan	Phase separation	pH 7.4 PBS, 37°C, lysozyme	Porous chitosan scaffolds degraded significantly faster than non-porous scaffolds. Further, degradation rate was accelerated in scaffolds with bigger pores or higher porosities. These results are due to higher surface areas provided in porous sponges which enable lysozymes to cleave chitosan molecules more efficiently.	(Wan et al., 2005)

Synthetic	PCL	Electrospun fibres of different thicknesses	pH 7.4 Ringer solution, 37°C	Rate of PCL degradation was dependent on electrospun fibre diameter. Thinner fibres degraded faster than thicker fibres which is likely due to a greater surface area to volume ratio. Electrospun matrices exhibited slower degradation rate compared to scaffolds obtained via solvent casting method.	(Bölgén et al., 2005)
	PLGA	Solvent casting/ particulate leaching  Ratio of PGA to PLA was:  70:30 (A); 75:25 (B); 80:20 (C)	SBF 1-5 formulations	Degradation rate was fastest with sample C, possibly due to a relatively higher PGA content which is hydrophilic. However, degradation rate was not even which makes this combination unsuitable for clinical applications. Sample B had optimum and stable degradation rates and A had low degradation rates. These results indicate that increasing PLA content resulted in increasingly hydrophobic scaffolds which, in turn, results in slower degradation.	(Mekala et al., 2013)
	PLA/PCL	Electrospinning  PLA to PCL ratios were:  3:1; 2:1; 1:1	pH 7.4 PBS, 37°C	Rate of scaffold degradation was a function of PLA concentration. Higher PLA contents corresponded to faster degradation rates which was consistent with previous findings that PLA was highly degradable.	(Chen et al., 2013)
Bio-synthetic composite	PGSU	Solvent casting	CE	Rate of scaffold degradation was a function of degree of crosslinking. The ester groups in the polymer backbone are highly sensitive to enzymatic degradation; however, a higher HDI content resulted in free hydroxyl groups being replaced by urethane groups. With increased urethane content the accessibility to ester bonds is hindered resulting in slower degradation rates.	(Pereira et al., 2013)
	PGSU-S	Spincoating			
	PGSU-SF	CO <sub>2</sub> foaming (porous scaffolds)  PGSU to HDI ratio was:  1:1; 1:0.5; 1:0.3			
Bio-synthetic composite	PCL/collagen/elastin	Electrospun vascular grafts  Crosslinked with EDC or GEN  PCL to elastin to collagen ratio was:  45:45:10; 55:35:10; 65:25:10	DMEM/F12 + 10% FBS + 1% P/S	Biodegradation rate of EDC crosslinked vascular grafts progressed more slowly than GEN crosslinked grafts. Additionally, degradation rate depended on the elastin content within the composite grafts with higher elastin corresponding to a faster degradation rate.	(McClure et al., 2012)
	Chitosan/PLGA	Sintering to obtain micro-spheres	pH 7.4 PBS, 37°C, lysozyme	The chitosan/PLGA scaffold demonstrated slower degradation compared to PLGA alone after 12 weeks. This may be due to chitosan/PLGA microspheres exhibiting a porous microstructure whilst PLGA microspheres are solid. This enables acidic degradation products of PLGA (which lead to accelerated autocatalysis) to escape more easily from the chitosan/PLGA scaffold.	(Jiang et al., 2010)
	mβ-TCP nβ-TCP	Wet grinding method  PLA to mβ-TCP to nβ-TCP ratio was:  100:0:0 (PLA); 90:0:10 (PLA/10 nβ-TCP); 70:30:0 (PLA/	pH 7.4 PBS, 37°C	Porosity and average pore size decreased in the order of PLA/50 nβ-TCP, PLA/30 nβ-TCP, and PLA/10 nβ-TCP. However, the size of β-TCP did not seem to affect scaffold porosity. The porosity of PLA/50 nβ-TCP scaffolds increased faster than PLA/10 nβ-TCP, PLA/30 nβ-TCP, or PLA/50 nβ-TCP scaffolds beyond 7 weeks. But no significant differences in porosity were observed between PLA/30 nβ-TCP and PLA/30 mβ-	(Cao et al., 2012)

	30 m $\beta$ -TCP);70:0:30 (PLA/30 n $\beta$ -TCP); 50:0:50 (PLA/50 n $\beta$ -TCP)		TCP scaffolds. Weight loss of PLA/30 n $\beta$ -TCP scaffolds was significantly faster than PLA/30m $\beta$ -TCP scaffolds and weight loss of PLA/50 n $\beta$ -TCP scaffolds was significantly faster than PLA/10 n $\beta$ -TCP or PLA/30 n $\beta$ -TCP scaffolds.  $\beta$ -TCP has been employed as a filler in order to offset acid degradation products of PLA scaffolds. It was demonstrated that the buffering effect of n $\beta$ -TCP was not only stronger than that of m $\beta$ -TCP but was also concentration dependent with higher n $\beta$ -TCP content inducing a higher buffering effect.
PLA	Melt blending technique	Non-carbonated basal mineral medium	Biodegradation was in order of PLA-GA > PLA-TPS > PLA > PLA-MC > PLA-PEG > PLA-PHB. (Nair et al., 2012)
PLA blends	Blends of PLA were prepared as 1:1 ratios:  PLA+PHB; PLA+TPS; PLA+GA; PLA+MC; PLA+PEG		PLA-GA and PLA-TPS started disintegrating after the first 24 h while all other blends and virgin PLA retained original nature of scaffold for 48 h.  The results demonstrated that PLA degradation could be tuned by the addition of gradually more hydrolytically resistant factors.

**Key:** DMEM, Dulbecco's modified Eagle medium; EDC, 1-ethyl-3-(3-dimethylaminopropyl)-carbodiimide; FBS, fetal bovine serum; GA, gum arabic; GEN, genipin; HDI, hexamethylene diisocyanate; m $\beta$ -TCP, micro-sized  $\beta$ -tricalcium phosphate; MC, microcrystalline cellulose;  $M_w$ , molecular weight; n $\beta$ -TCP, nano-sized  $\beta$ -tricalcium phosphate; PBS, phosphate buffered saline; PCL, polycaprolactone; PDI, polydispersity index; PEG, polyethylene glycol; PGA, polyglycolic acid; PGSU, poly(glycerol sebacate urethane); PGSU-S, solvent-based synthesis of PGSU; PGSU-SF, solvent-free synthesis of PGSU; PHB, polyhydroxybutyrate; PLA, polylactic acid; PLGA, poly(lactic-co-glycolic acid); P/S, penicillin/streptomycin; SBF, simulated body fluids; TPS, thermoplastic starch; WSC, water-soluble carbodiimide.

**Table 2.2.** *In vivo* degradation outcomes of a selection of natural and synthetic polymers.

Scaffold material	Scaffold fabrication method	Animal model	<i>In vivo</i> degradation outcome	Reference
Natural	Gelatin	Air sprayed microbeads	Lewis rats	Cell-laden microbeads were injected into the renal parenchyma of rats. Degradation patterns observed <i>in vivo</i> correlated well with <i>in vitro</i> data.. (Serban et al., 2013)
	Collagen	BioGide (NCL) BioMend Extend (GCL) Ossix (RCL)	Wistar rats	3 calvarial defects of 5 mm $\emptyset$ each were created and subsequently covered with one of each membrane. Results demonstrate tunable degradation characteristics of collagen membranes using different crosslinking agents. These differences in degradation pattern may have clinical implications and membranes should be chosen according to the clinical demand. Glutaraldehyde is generally considered a poor agent due to low biocompatibility (Matsumoto et al. 1993, Speer et al., 1980, Wiebe et al., 1988).
	Chitosan	Phase separation	Wistar rats	Subcutaneously implantation revealed slower <i>in vivo</i> degradation compared to <i>in vitro</i> which may be ascribed to the fact that concentrations of lysozyme in rats may be lower than that used for <i>in vitro</i> enzymatic degradation, resulting in a lesser (Wan et al., 2005)

				amount of weight loss in <i>in vivo</i> implanted scaffolds.	
Synthetic	PCL	Electrospun fibres of different thicknesses	Wistar-Albino rats	Subcutaneously implanted scaffolds demonstrated faster <i>in vivo</i> degradation rates compared to <i>in vitro</i> . This may be due to factors including foreign body response which results in inflammatory cell accumulation around the implant. The combination of free radicals, acidic products and enzymes has been suggested to accelerate degradation (Tracy et al. , 1999). In particular, various lipases have been implicated in the degradation of PCL (Li et al. , 2003).	(Bölgén et al. , 2005)
	PLGA	Electrospinning into random or aligned fibres	Wistar rats	Subcutaneously implanted scaffolds of randomly aligned fibres demonstrated faster degradation rates compared to parallel fibres. This may be due to a larger exposed total surface area for hydrolytic degradation in random fibres compared with parallel ones.	(Subramanian et al. , 2013)
	PGA/ $\beta$ -TCP	Solvent casting/particulate leaching  Ratio of PGA to $\beta$ -TCP was:  1:1; 1:3	Sprague-Dawley rats	Critical bone defects of 3 mm $\varnothing$ each were created in femoral medial epicondyles and subsequently covered with PGA/ $\beta$ -TCP scaffolds (1:1 and 1:3), 100% HAP, or left blank (control).  After 90 days, PGA/ $\beta$ -TCP (1:1) scaffolds exhibited fastest degradation rates (99.0 $\pm$ 1.0 %) compared to PGA/ $\beta$ -TCP (1:3) (96.2 $\pm$ 3.3 %) or HAP (35.1 $\pm$ 5.5 %) scaffolds. The biodegradation rates of PGA/ $\beta$ -TCP further matched the osteogenesis rate, whereas the slowly degrading HAP prevented ingrowth of bone cells. The results indicate that the rate of biodegradation of PGA/ $\beta$ -TCP scaffolds allowed a more rapid replacement and osteogenesis than HAP.	(Cao and Kuboyama, 2010)

**Key:** GCL, glutaraldehyde crosslinked; HAP, hydroxylapatite;  $M_w$ , molecular weight; NCL, not crosslinked; PCL, polycaprolactone; PGA/ $\beta$ -TCP, polyglycolic acid/ $\beta$ -tricalcium phosphate; PLGA, poly(lactic-co-glycolic acid); RCL, ribose crosslinked.

One soon realizes that such multiplicity of options and parameters in the design and fabrication of biodegradable regeneration platforms offers incredible possibilities in terms of synthesizing materials for individualised scaffolds.

## 2.6 BIODEGRADABLE MATERIALS AS SELF-PROPAGATING DELIVERY VEHICLES – AN INTERACTIVE PLATFORM

Biodegradable materials have undergone intensive evaluation as particle delivery systems (Song et al., 2012, Ben-David et al., 2013, Son et al., 2011, Wang et al., 2013b,

Ueng et al., 2011). A prerequisite for controlled particle release after the incorporation into a matrix involves diffusion into and contact of water molecules with the material (Wischke et al., 2010). This may suggest an inherently passive nature of particle release which is true for many commercialised drug delivery platforms (Thakral et al., 2013, Rujivipat and Bodmeier, 2010). Despite decades of research, the ideal material for use as a delivery vehicle has not, as yet, been realized into clinical practice. A model delivery vehicle would allow for tailored clinical efficacy which entails potentially longer-lasting therapeutic effects and delivery of multiple factors in sequential fashion. Such materials require tunable degradation rates to subsequently enable controlled delivery of incorporated elements. In order for the biomaterial to achieve such independent 'activeness' which according to the perspective of Materials Science is obtained by 'changes of its physical properties in response to external stimuli', factors including water penetration efficiency, types of material and their degradation kinetics as well as temperature sensitivity are of fundamental importance.

## **2.7 SINGLE AND DUAL GROWTH FACTOR DELIVERY**

In recent years, biodegradable delivery systems for localised transportation of GFs have received considerable attention. For example, delivery of active keratinocyte growth factor (KGF) was shown to be most successful using a ternary formulation based on PLA, PGA and sodium bis(ethylhexyl)sulfosuccinate (Aerosol-OT, AOT) (Cho et al., 2003). It was demonstrated the KGF release kinetics were tunable by adjusting the molecular weight, and by extension the degradation rate of PLA. Several studies highlighted the association between increasing molecular weights, reduced water penetration efficiency and decreased degradation rates, enabling fine-tuning of release kinetics of any entrapped molecular agents or cells (Fu and Kao, 2009, Gu et al., 2007). In order to

demonstrate the relationship between exposed surface area and biomaterial degradation rate, the sustained release kinetics of BMP-2 from micro- and nanosphere carrier gels was investigated (Wang et al., 2012). As expected, nanospheres with larger surface area to volume ratio were found to have significantly accelerated release kinetics compared to larger carrier spheres. A different approach to molecular delivery involves layer-by-layer (LBL) assembly where sequential deposition of positively and negatively charged polyelectrolytes onto material surfaces can be utilized to construct drug delivery depots by incorporating drugs of interest into self-assembled nanoscale thin films (Mao et al., 2005, Saurer et al., 2011, Ma et al., 2007, Macdonald et al., 2008, Macdonald et al., 2011). LBL technique benefits from mild fabrication conditions which given the fragile nature of incorporated elements including biomolecules or cells, render more aggressive incorporation techniques (e.g. ones using organic solvents) obsolete. LBL incorporating proteins or GFs have experienced successful applications in experimental bone growth models amongst several others (Liebschner and Wettergreen, 2012, Go et al., 2011, Park et al., 2012a, Shah et al., 2011). However, clinical translatability of this technique remains difficult due to uncontrollable degradation kinetics and subsequent burst release rates of incorporated agents. Recently, an LBL technique with tunable release kinetics was successfully developed by varying material chemistry (Keeney et al., 2013). Increasing hydrophobicity has been shown to prolong the degradation profile of the resultant LBL films, enabling gradual release of GFs over a period of 14 days as opposed to 50 h (Zhang et al., 2006).

Biodegradable delivery platforms including LBL method have sparked intensive interest in multiple factor delivery as well as distinct release kinetics of each incorporated element. For example, one study demonstrated the dual release of BMP-2 and VEGF from

the surfaces of PCL-based scaffolds (Shah et al., 2011). VEGF was released over the first 8 days whereas BMP-2 was continually released for over 2 weeks. Such a multiphase release profile enables blood vessel formation with subsequent bone formation which mimics natural bone development. Further, *in vivo* implantation of this dual delivery system showed greater bone formation compared to groups receiving single GFs. Such staggered material breakdown, again reminiscent of a degrading plant leaf, aims to maintain a 3D structural framework throughout a pre-defined period of time whilst providing gradually enlarging gaps for ingrowing tissues. Other formulations capable of dual/multiple drug release include composite scaffolds as shown by Numata *et al.* (Numata et al., 2012). Rhodamine Blue (RhB) was added to the molecular network of silk hydrogels, whilst fluorescent isothiocyanate (FITC) was incorporated into silk nanoparticles within the hydrogels. Degradation of hydrogels by proteases resulted in an initial burst release of RhB within the first hour. Nanoparticle-incorporated FITC, however, exhibited a slower and more constant release over 5 days demonstrating the feasibility of dual drug release using composite matrices. Fine-tuning of degradation rates has been suggested to be regulated by physical properties including material crystallinity and size (Numata and Kaplan, 2010, Numata et al., 2011).

## **2.8 STEM CELL DELIVERY**

Biodegradable delivery platforms have not only garnered significant interest in GF and drug delivery but have also been applied to the delivery of stem cells (SCs). Tentative early attempts of injecting SC precursors directly into an injury have yielded limited success (Harting et al., 2009). Poor cell engraftment is thought to stem from a combination of harsh, non-permissive conditions created by the injury site which lacks nutrients, survival factors and a supportive matrix. It thus is plausible to incorporate cells



into a scaffold which effectively provides structural support, shields fragile cells and simultaneously supplies environmental cues for cellular adhesion and proliferation (Yap et al., 2013, Peng et al., 2013, Di Felice et al., 2013, Tate et al., 2009). Thus, a multispherical chitosan-heparin complex capable of dual incorporation and targeted delivery of FGF-2 and viable neural precursors was developed for brain tissue regeneration (Skop et al., 2013). Degradation and subsequent release of factors were successfully controlled by the degree of crosslinking demonstrating both tunable degradation kinetics and controllable microsphere swelling. The crucial importance of supportive scaffolds in the delivery of regeneration cues has further been corroborated in an experimental traumatic brain injury (TBI) model (Guan et al., 2013). Rats with experimental TBI were transplanted with human bone marrow-derived mesenchymal stem cells (hMSCs) in conjunction with or without a supportive collagen matrix. Cells delivered inside the collagen scaffolds exhibited significantly higher hMSC retention at the lesion site and localised distribution at the transplanted region indicating a supportive and shielding effect of the scaffold. Additionally, cells showed better neurite outgrowth resulting in superior neuronal functional recovery. Collagen, being a relatively quickly degrading biomaterial, provided early retention of hMSCs within the lesion site without spatially hindering ingrowing neuronal tissue. Depending on the clinical scenario, delivery vehicles may only need to provide structural support for limited periods of time. In fact, slowly degrading scaffolds may either obstruct regenerating tissue or fail to release factors or cells in time to replicate the natural healing cascade. Bone regeneration by distraction osteogenesis is one such example where the prime concern lies in accelerating bone formation through providing regenerative cues rather than offering structural support. In a recent study, Gelfoam<sup>®</sup>, a gelatine-based soft scaffold, was loaded with bone marrow-derived MSCs with or without FGF-2 and transplanted into a porcine mandibular distraction site (Sun

et al., 2013). MSCs successfully engrafted while the scaffold completely degraded within a relatively fast time frame without causing local inflammation. Furthermore, scaffold-incorporated FGF-2 induced MSC osteogenic differentiation as evidenced by dose-dependent increases in alkaline phosphatase (ALP) expression. Such mutually beneficial, even synergistic interactions between scaffold matrix and incorporated factors are prime examples of self-sufficient, self-propagating scaffolds. Independence from surrounding tissues is obtained when a delivery platform transports all necessary components required for functional tissue regeneration whilst protecting said components from harsh environmental conditions generated by injuries. Composite scaffold designs are then able to mimic the ingenious reciprocity observed in natural plant leaf metabolism – the degradation of individual leaf components liberate growth-stimulating breakdown products which may then be used for newly growing leaves.

Unlike natural leaf degradation, breakdown of synthetically generated scaffolds requires careful evaluation of potentially harmful, even toxic, by-products which may negatively affect tissues in immediate vicinity as well as downstream target organs.

## **2.9 THE DESIGN CHALLENGE – LEAFING THROUGH THE PAST TO UNCOVER THE NEXT GENERATION DELIVERY VEHICLE**

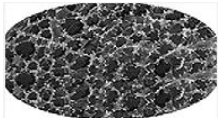
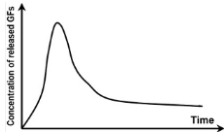
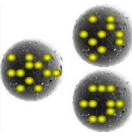
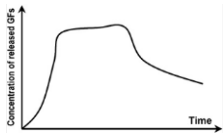


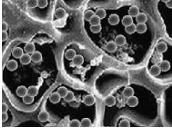
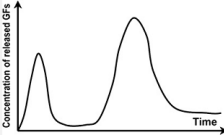
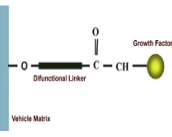
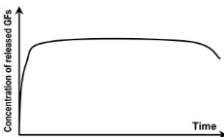
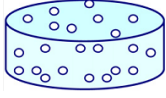
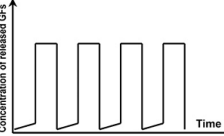
Functional tissue regeneration continues to be a major, as yet unresolved challenge for biomedical scientists, materials engineers, and the medico-surgical community, not to mention the affected individuals in need for tissue replacements (Chen and Jin, 2010, Williams, 2006, Khan et al., 2008). Decades have passed with significant developments in material selection, scaffold design and successively more intricate composite structures. In spite of this, optimal tissue regeneration using tissue engineered scaffolds remains elusive, rendering clinically accepted restorative therapies reliant on organ/tissue

transplantations, GF therapies and synthetic devices (Chen and Jin, 2010, Williams, 2006, Khan et al., 2008, Varkey et al., 2004). Pivotal challenges hindering progression of tissue engineered scaffolds into the clinical arena include (1) the elucidation of the complex biomolecular cascade of cells, cell-signalling factors and structural components required for complete tissue restoration, and (2) identifying the ideal 3D scaffold design capable of providing an integrated platform which consistently mimics the natural microenvironment and regulates cell fates. In recent years, it has become widely accepted that the body's self-healing capacities can be supported by accelerating migration, proliferation and differentiation of implanted cells via the integration of appropriate GFs and other trophic molecules (Vasita and Katti, 2006, Andreadis and Geer, 2006, Kobsa and Saltzman, 2008). Advanced understanding of the pathways involved in the development of tissues theoretically enables a more sophisticated approach to the development of delivery vehicles to facilitate spatio-temporal release of required factors (Uebersax et al., 2009). However, in order to be effective, cell-signalling agents have to reach their target site without degrading and remain in place for long enough to exert the desired actions (Chen et al., 2009b). Delivery of GFs dissolved in solution has been deemed ineffective due to non-specific diffusion away from the target and enzymatic degradation resulting in low availability or toxicity due to excess concentrations (Chen et al., 2009b, Tayalia and Mooney, 2009, Guldborg, 2009). It has therefore been deemed necessary to develop targeted release technologies capable of providing spatio-temporal delivery of cell-signalling factors whilst avoiding local or systemic side effects. While single GF delivery has been studied relatively extensively, strategies involving the delivery of two or more factors require further optimization. Developments in the field of biodegradable materials technology are being harnessed to generate the next

generation medical devices to stimulate endogenous repair mechanisms by means of an integrated and self-sufficient platform technology.

Table 2.3 schematically illustrates a selection of available strategies for factor delivery and their respective release profiles.

**Table 2.3.** Schematic representation of selected delivery strategies and their representative release profiles. Adapted from (Chen et al., 2010).

Strategies	Images	Release profiles	Delivery models (Examples)
Incorporation (bolus injection or growth factors directly adsorbed in vehicles)			Burst release (frequently investigated, porous scaffolds, hydrogels etc.)
Non-covalent immobilisation (growth factors encapsulated into low cross-linked microspheres)			Sustained release (frequently investigated, microspheres, nanoparticles, etc.)
Non-covalent immobilisation (growth factors encapsulated into high cross-linked microspheres)			Delayed release (well-designed microspheres, core-shell vehicles, etc.)
Non-covalent immobilisation (growth factors delivered by both scaffolds and microspheres)			Pulse-like release (well-designed composites, multifunctional vehicles, etc.)
Covalent immobilisation (growth factors chemically cross-linked via di-functional linkers)			Continuous release (fibrillar collagen, alginate gel, etc.)
Covalent immobilisation or chemical modification (Environment-sensitive materials)			Pulsatile release (Intelligent hydrogels, on-off delivery systems, etc.)

With the fact in mind that the ideal delivery system provides a large degree of control over the type(s) of molecule(s) delivered, the rate at which delivery takes place

in addition to providing protection for a bioactive agent to achieve prolonged availability, two delivery methods appear optimal; continuous delivery and pulsatile delivery. Both designs, alone or in conjunction with each other, are hoped to advance the development of delivery systems capable of sequential and spatio-temporally controlled delivery of multiple GFs (Tayalia and Mooney, 2009, Biondi et al., 2008).

Several studies using combinatorial approaches have already demonstrated results using biodegradable materials which simultaneously provide physical scaffolding, a reservoir for sustained and/or multiple factor delivery and which act as cell encapsulating devices (Macaya and Spector, 2012, Syková et al., 2006). Using this integrative approach, Kanczler *et al.* developed an independent hybrid platform for bone repair and regeneration (Kanczler et al., 2010). Supercritical CO<sub>2</sub> and alginate entrapment technique was applied to synthesize scaffolds consisting of alginate and poly(D,L-lactic acid) (PLA) to allow for different biodegradation and subsequent release rates of incorporated factors (Ginty et al., 2008). Human bone marrow stromal cells were seeded onto a VEGF/ BMP-2 releasing composite scaffold and implanted into a murine critical sized femur defect. Different degradation kinetics of alginate and PLA resulted in distinct release profiles of GFs which resulted in significant new bone formation. Similarly, Chen *et al.* successfully incorporated BMP-2 loaded basic gelatin and IGF-1 loaded acidic gelatin microparticles into a glycidyl methacrylated dextran (Dex-GMA) hydrogel scaffold (Chen et al., 2009a). Chemical crosslinking agents such as Dex-GMA have previously been shown to reduce rapid solubilisation of gelatin to avoid burst release of GFs and are therefore preferably used for gelatin-based delivery vehicles (Chen et al., 2009b, Young et al., 2005, Chen et al., 2006, Chen et al., 2007a et al. 2007). In addition, Dex-GMA/gelatine hybrid hydrogel cannot be hydrolytically degraded but

requires the presence of enzymes (Chen et al., 2009b, Chen et al., 2007a et al. 2007, Chen et al., 2007b et al. 2007) such as dextranase which enables selective delivery of their cargo to sites where such enzymes are present. Alternatively, dextranase may be directly incorporated into the hybrid hydrogel structure, making the composite truly self-sufficient.

Functional tissue regeneration involves the precise regulation of GF concentrations and spatio-temporal gradients as these key parameters are thought to significantly influence the final outcome of regenerative therapies (Guldberg, 2009). It thus is of considerable importance to develop sophisticated delivery systems with multiple functionalities and tunable delivery patterns. The first step in the identification of an appropriate biomaterial or combination of biomaterials for delivery involves an assessment of the required properties, followed by a scan of available materials which eventually results in the selection of the best possible material or a combination of materials which are predicted to perform reliably (Vasita and Katti, 2006). Past efforts have taught that it will likely be a combination of several materials which may offer the best compromise for positive clinical outcomes. Composite materials may draw from each individual benefit as well as act synergistically to eventually create the next generation of 'super-materials'.

## **2.10 BIOMATERIAL DEGRADATION PRODUCTS AND TOXICITY**

Biodegradable materials intended to be used as implantable drug-eluting scaffolds must fulfil several requirements in order to be considered for clinical integration. They must not elicit abnormal responses in local tissues and should neither produce local nor systemic toxic or carcinogenic side-effects. First and foremost, biodegradable platforms should serve their intended scaffolding and cell-signalling functions whilst degrading into

non-toxic metabolites (Athanasίου et al., 1996, Lotz et al., 2009). As opposed to natural leaf degradation, breakdown of artificially manufactured scaffolds requires rigorous toxicological evaluation of each constituent component. Particularly when ambitious strategies involving the use of composite materials with integrated trophic factors is concerned, the importance of material biocompatibility evaluation rises significantly. The desired notion of effecting synergistic actions of GF and other incorporated component requires careful consideration of factor concentrations and release mechanisms in order to avoid potentially harmful overdosing. It therefore remains a priority to conduct systematic and rigorous toxicological studies – both *in vitro* and *in vivo* – to (1) eliminate grossly ineffective or toxic delivery platforms in order to (2) narrow down on potentially suitable candidate technologies as well as (3) ascertain any dose or time-dependencies which may influence the materials' biocompatibilities. Biocompatibility refers to the ability of a material to perform with an appropriate host response in a specific situation. This means that depending on the area within the body, the implantable materials require different properties to obtain biocompatibility.

Currently, there is discord between those postulating the use of naturally derived materials, synthetic materials or a combination of both – not least due to a lack of consistent proof of one's superiority above the other. Naturally derived biomaterials such as collagen or hyaluronic acid are frequently selected for their benefits including similarity to native ECM, thus favouring natural cell-cell and cell-matrix interactions. Numerous studies have demonstrated both the *in vitro* and *in vivo* beneficial potential of natural scaffolds in wound healing (Lee and Chu, 2000, Chlapanidas et al., 2013, Park et al., 2012b). Using a genetically diabetic mouse model, the biocompatibility and wound healing properties of a fibrin-based scaffold incorporating both VEGF and bFGF was

demonstrated (Losi et al., 2013). Degradation of the fibrin scaffold over a 7 day period ensured timely release of GFs and accelerated wound healing compared to wounds not exposed to GFs. As previously mentioned, degradation rates of biological scaffolds may be fine-tuned using crosslinking agents (Zeugolis et al., 2009), but several crosslinking agents such as glutaraldehyde have demonstrated cytotoxicities (Duan and Sheardown, 2006). Substitution with other, more biocompatible crosslinking agents is beginning to show tentative success and has to be researched further in terms of their long-term stability and biocompatibility (Park et al., 2002). High purification costs, relative unavailability and unsuitability for large scale processing as well as batch to batch variations and an immunogenic potential of naturally derived materials, however, have encouraged scientists to search for realistically applicable synthetic alternatives. Synthetic materials are thought to overcome the aforementioned disadvantages of natural materials and provide additional key benefits including the ability to tailor mechanical properties and degradation kinetics to suit individual applications. As seen in previous sections of this chapter, synthetic materials may be fabricated into various shapes with desired pore morphological features conducive and individually tailorable for tissue ingrowth.

The majority of synthetic biodegradable materials studied for tissue engineering applications belong to the polyester family which include polyglycolides, polylactides and their various co-polymers (Fig. 2.6) (Gunatillake and Adhikari, 2003). They have long been used in a number of clinical applications ranging from biodegradable sutures (Cutright et al., 1971) to orthopaedic plates and fixture devices (Mayer and Hollinger, 1995) and are also intensively studied as scaffold materials for cell transplantation and tissue regeneration (Thomson et al., 1995).



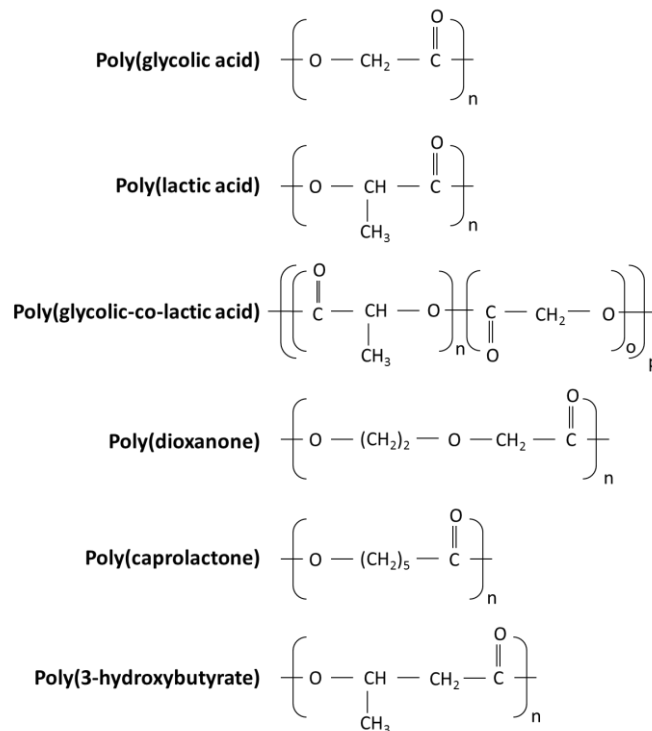


**Figure 2.6.** Chemical structures of the major biodegradable polyesters used in tissue engineering applications including polyglycolides, polylactides and their various co-polymers. Image taken from (Gunatillake and Adhikari, 2003).

Polyesters mainly degrade in two stages; at first the amorphous region degrades via hydrolytic chain scission of ester bonds. The second stage involves mainly the degradation of the crystalline areas of the material. Degradation of polyesters releases lactic acid and glycolic acid which are resorbable even at high concentrations. However, concerns regarding their toxicity have been raised; several studies have highlighted the formation of local aseptic sinuses and osteolytic changes in conjunction with intermittent joint swellings in animals and patients treated with rods, screws and other fixation devices made of degradable PGA or PLA implants (Bergsma et al., 1993, Böstman, 1991, Böstman et al., 1989). Since infections were excluded, it was deemed likely that the observed adverse effects were related to the biodegradation of the PLA-PGA implants. Solazzo *et al.* studied the effects of PLA/PGA composite plates on osteoblastic

differentiation and proliferation of mesenchymal stem cells (MSCs) (Sollazzo et al., 2011). Initial results demonstrated strong influences on MSCs by enhancing proliferation, differentiation and matrix deposition but long-term effects of degradation products were not studied. Previous studies, on the other hand, already demonstrated long-term dramatic reductions of biocompatibility, likely due to degradation products causing bone resorption in and around the implant site (Spivak et al., 1990). Many *in vitro* studies previously determined that both PLA and PGA produced cytotoxic degradation products but did not consider the buffering effects of physiological solutions present *in vivo*. On the other hand, systemic distribution may result in potentially harmful degradation products becoming trapped in end-organs such as liver, kidney and spleen where they pose an inflammatory risk (Yildirimer et al., 2011, Tang et al., 2003). Implantation of larger PLA-PGA materials as well as placement in anatomical region without access to sufficient quantities of body fluids may overwhelm the body's capacity to provide adequate buffering. These issues were successfully addressed by incorporating basic salts within PLA-PGA implants which offset the pH decrease observed in the vicinity of degrading implants (Agrawal and Athanasiou, 1997).

Other synthetic materials frequently used in tissue engineering applications include polycarbonates which possess 3 hydrolysable bonds: (1) amide, (2) carbonate, and (3) ester. The hydrolysis of carbonate groups yields two alcohols and CO<sub>2</sub> thus eliminating the problem of the acid burst seen in polyesters. Varying the structure of the pendant R groups allows for tuning of mechanical properties, degradation rates and subsequent cellular responses to the material.

PUs are a major class of synthetic elastomers which are usually used in the manufacture of non-degradable medical implants such as cardiac pacemakers and

vascular grafts (Ahmed et al., 2011b, Kannan et al., 2006a et al. 2006, Xie et al., 2010, Kannan et al., 2006c et al. 2006). Biodegradable versions of PU, obtained by incorporating degradable chemical linkages into the backbone, are of increasing interest due to excellent mechanical properties, biocompatibility and versatile degradation kinetics. However, a major problem has been the toxicity of degradation products, especially those from diisocyanate components such as 4,4'-methylenediphenyl diisocyanate (MDI) and toluene diisocyanate (TDI) (McGill and Motto, 1974). Due to the advantages of precise control over material characteristics, it is possible to design non-toxic degradable PUs using diisocyanates such as lysine diisocyanate (LDI) (2,6-diisocyanatohexanoate) and other aliphatic diisocyanates like hexamethylene diisocyanate (HDI).

Despite excellent and controllable physical properties of synthetic biomaterials, the apparent lack of innate cell recognition entities has led to the fabrication of composite bio-artificial scaffolds which aim to harness the distinct benefits of both material classes whilst simultaneously compensating for each other's weaknesses. A good idea in theory, biosynthetic composite scaffolds however retain their individual drawbacks which, in the case of synthetic materials, are more predictable and therefore more easily rectifiable. For instance, natural biomaterials pose an innate risk of eliciting an immunological graft rejection which could be detrimental in cases of vital placements of grafts, e.g. vascular interpositional implants (Fig. 2.7) (Spark et al., 2008).

With ever advancing material processing techniques, however, synthetic scaffold designs incorporating artificial cell-recognition entities may replace immunogenic cell surface epitopes with synthetic mimics which enhances biocompatibility of synthetic materials (Chen et al., 2011a). Additionally, synthetic materials may be designed with

chemical functional groups which can enhance cell attachment, proliferation and induce tissue ingrowth.



**Figure 2.7.** Photograph of the left shoulder of a 25-year-old man with aneurysmal dilatation of a bovine ureteric axillary-innominate arteriovenous graft 2 months after operation. Image taken from (Spark et al., 2008).

## 2.11 CONCLUSION AND FUTURE PERSPECTIVE

Biomaterials scientists currently pursue 3 main avenues for the optimization of tissue engineering scaffold materials – (1) purely natural scaffolds, (2) synthetic alternatives, and (3) biosynthetic composites. The authors believe that rather than attempting an overcomplicated top down approach by aiming to modify natural materials with inherent material properties which may or may not be suitable, scientists would be better advised to adhere to the bottom-up fabrication of synthetic materials which may be strictly controlled throughout the fabrication process. Whilst we suggest developing nature-inspired materials by copying natural material structures, we postulate using

man-made materials for greater control and flexibility during the manufacturing process.

This would ideally enable utilization of the best concepts of both worlds.

## References

- AGARWAL, A., NELSON, T. B., KIERSKI, P. R., SCHURR, M. J., MURPHY, C. J., CZUPRYNSKI, C. J., MCANULTY, J. F. & ABBOTT, N. L. 2012. Polymeric multilayers that localize the release of chlorhexidine from biologic wound dressings. *Biomaterials*, 33, 6783-92.
- AGRAWAL, C. M. & ATHANASIOU, K. A. 1997. Technique to control pH in vicinity of biodegrading PLA-PGA implants. *Journal of biomedical materials research*, 38, 105-14.
- AGRAWAL, C. M., MCKINNEY, J. S., LANCTOT, D. & ATHANASIOU, K. A. 2000. Effects of fluid flow on the in vitro degradation kinetics of biodegradable scaffolds for tissue engineering. *Biomaterials*, 21, 2443-52.
- AHMED, M., GHANBARI, H., COUSINS, B. G., HAMILTON, G. & SEIFALIAN, A. M. 2011a. Small calibre polyhedral oligomeric silsesquioxane nanocomposite cardiovascular grafts: influence of porosity on the structure, haemocompatibility and mechanical properties. *Acta biomaterialia*, 7, 3857-67.
- ANDREADIS, S. T. & GEER, D. J. 2006. Biomimetic approaches to protein and gene delivery for tissue regeneration. *Trends in biotechnology*, 24, 331-7.
- ATHANASIOU, K. A., NIEDERAUER, G. G. & AGRAWAL, C. M. 1996. Sterilization, toxicity, biocompatibility and clinical applications of polylactic acid/polyglycolic acid copolymers. *Biomaterials*, 17, 93-102.
- BEN-DAVID, D., SROUJI, S., SHAPIRA-SCHWEITZER, K., KOSOVER, O., IVANIR, E., KUHN, G., MÜLLER, R., SELIKTAR, D. & LIVNE, E. 2013. Low dose BMP-2 treatment for bone repair using a PEGylated fibrinogen hydrogel matrix. *Biomaterials*, 34, 2902-10.
- BERGSMA, E. J., ROZEMA, F. R., BOS, R. R. & DE BRUIJN, W. C. 1993. Foreign body reactions to resorbable poly(L-lactide) bone plates and screws used for the fixation of unstable zygomatic fractures. *Journal of oral and maxillofacial surgery : official journal of the American Association of Oral and Maxillofacial Surgeons*, 51, 666-70.
- BERSKI, S., VAN BERGEIJK, J., SCHWARZER, D., STARK, Y., KASPER, C., SCHEPER, T., GROTHE, C., GERARDY-SCHAHN, R., KIRSCHNING, A. & DRÄGER, G. 2008. Synthesis and biological evaluation of a polysialic acid-based hydrogel as enzymatically degradable scaffold material for tissue engineering. *Biomacromolecules*, 9, 2353-9.
- BIONDI, M., UNGARO, F., QUAGLIA, F. & NETTI, P. A. 2008. Controlled drug delivery in tissue engineering. *Advanced drug delivery reviews*, 60, 229-42.
- BIOSCIENCES, O. Z. 2013. RE: 3D-Fect TM.
- BÖLGEN, N., MENCELOĞLU, Y. Z., ACATAY, K., VARGEL, I. & PIŞKIN, E. 2005. In vitro and in vivo degradation of non-woven materials made of poly(epsilon-caprolactone) nanofibers prepared by electrospinning under different conditions. *Journal of biomaterials science. Polymer edition*, 16, 1537-55.
- BÖSTMAN, O., HIRVENSALO, E., VAINIONPÄÄ, S., MÄKELÄ, A., VIHTONEN, K., TÖRMÄLÄ, P. & ROKKANEN, P. 1989. Ankle fractures treated using biodegradable internal fixation. *Clinical orthopaedics and related research*, 195-203.
- BÖSTMAN, O. M. 1991. Osteolytic changes accompanying degradation of absorbable fracture fixation implants. *The Journal of bone and joint surgery. British volume*, 73, 679-82.
- BURG, K. J., PORTER, S. & KELLAM, J. F. 2000. Biomaterial developments for bone tissue engineering. *Biomaterials*, 21, 2347-59.

CAO, H. & KUBOYAMA, N. 2010. A biodegradable porous composite scaffold of PGA/beta-TCP for bone tissue engineering. *Bone*, 46, 386-95.

CAO, L., DUAN, P.-G., WANG, H.-R., LI, X.-L., YUAN, F.-L., FAN, Z.-Y., LI, S.-M. & DONG, J. 2012. Degradation and osteogenic potential of a novel poly(lactic acid)/nano-sized  $\beta$ -tricalcium phosphate scaffold. *International journal of nanomedicine*, 7, 5881-8.

CHAPANIAN, R. & AMSDEN, B. G. 2010. Combined and sequential delivery of bioactive VEGF165 and HGF from poly(trimethylene carbonate) based photo-cross-linked elastomers. *Journal of controlled release : official journal of the Controlled Release Society*, 143, 53-63.

CHEN, C., CONSTANTINO, A. & DEONARAIN, M. 2011a. Modulating antibody pharmacokinetics using hydrophilic polymers. *Expert opinion on drug delivery*, 8, 1221-36.

CHEN, F. M., AN, Y., ZHANG, R. & ZHANG, M. 2011b. New insights into and novel applications of release technology for periodontal reconstructive therapies. *Journal of controlled release : official journal of the Controlled Release Society*, 149, 92-110.

CHEN, F. M., CHEN, R., WANG, X. J., SUN, H. H. & WU, Z. F. 2009a. In vitro cellular responses to scaffolds containing two microencapsulated growth factors. *Biomaterials*, 30, 5215-24.

CHEN, F. M. & JIN, Y. 2010. Periodontal tissue engineering and regeneration: current approaches and expanding opportunities. *Tissue engineering. Part B, Reviews*, 16, 219-55.

CHEN, F. M., SHELTON, R. M., JIN, Y. & CHAPPLE, I. L. C. 2009b. Localized delivery of growth factors for periodontal tissue regeneration: role, strategies, and perspectives. *Medicinal research reviews*, 29, 472-513.

CHEN, F. M., ZHANG, M. & WU, Z. F. 2010. Toward delivery of multiple growth factors in tissue engineering. *Biomaterials*, 31, 6279-308.

CHEN, F. M., ZHAO, Y. M., SUN, H. H., JIN, T., WANG, Q. T., ZHOU, W., WU, Z. F. & JIN, Y. 2007a. Novel glycidyl methacrylated dextran (Dex-GMA)/gelatin hydrogel scaffolds containing microspheres loaded with bone morphogenetic proteins: formulation and characteristics. *Journal of controlled release : official journal of the Controlled Release Society*, 118, 65-77.

CHEN, F. M., ZHAO, Y. M., WU, H., DENG, Z. H., WANG, Q. T., ZHOU, W., LIU, Q., DONG, G. Y., LI, K., WU, Z. F. & JIN, Y. 2006. Enhancement of periodontal tissue regeneration by locally controlled delivery of insulin-like growth factor-I from dextran-co-gelatin microspheres. *Journal of controlled release : official journal of the Controlled Release Society*, 114, 209-22.

CHEN, F. M., ZHAO, Y. M., ZHANG, R., JIN, T., SUN, H. H., WU, Z. F. & JIN, Y. 2007b. Periodontal regeneration using novel glycidyl methacrylated dextran (Dex-GMA)/gelatin scaffolds containing microspheres loaded with bone morphogenetic proteins. *Journal of controlled release : official journal of the Controlled Release Society*, 121, 81-90.

CHEN, L., BAI, Y., LIAO, G., PENG, E., WU, B., WANG, Y., ZENG, X. & XIE, X. 2013. Electrospun Poly(L-lactide)/Poly( $\epsilon$ -caprolactone) Blend Nanofibrous Scaffold: Characterization and Biocompatibility with Human Adipose-Derived Stem Cells. *PloS one*, 8, e71265-e.

CHEN, Y., ZHOU, S. & LI, Q. 2011c. Mathematical modeling of degradation for bulk-erosive polymers: applications in tissue engineering scaffolds and drug delivery systems. *Acta biomaterialia*, 7, 1140-9.

CHENG, D. & SEFTON, M. V. 2009. Dual delivery of placental growth factor and vascular endothelial growth factor from poly(hydroxyethyl methacrylate-co-methyl methacrylate) microcapsules containing doubly transfected luciferase-expressing L929 cells. *Tissue engineering. Part A*, 15, 1929-39.

CHLAPANIDAS, T., TOSCA, M. C., FARAGÒ, S., PERTEGHELLA, S., GALUZZI, M., LUCCONI, G., ANTONIOLI, B., CIANCIO, F., RAPISARDA, V., VIGO, D., MARAZZI, M., FAUSTINI, M. & TORRE, M. L. 2013. Formulation and characterization of silk fibroin films as a scaffold for adipose-derived stem cells in skin tissue engineering. *International journal of immunopathology and pharmacology*, 26, 43-9.

CHO, E. J., TAO, Z., TANG, Y., TEHAN, E. C., BRIGHT, F. V., HICKS, W. L., GARDELLA, J. A. & HARD, R. 2003. Tailored delivery of active keratinocyte growth factor from biodegradable polymer formulations. *Journal of biomedical materials research. Part A*, 66, 417-24.

COURTMAN, D. W., ERRETT, B. F. & WILSON, G. J. 2001. The role of crosslinking in modification of the immune response elicited against xenogenic vascular acellular matrices. *Journal of biomedical materials research*, 55, 576-86.

CUI, H., LIU, Y., DENG, M., PANG, X., ZHANG, P., WANG, X., CHEN, X. & WEI, Y. 2012. Synthesis of biodegradable and electroactive tetraaniline grafted poly(ester amide) copolymers for bone tissue engineering. *Biomacromolecules*, 13, 2881-9.

CUTRIGHT, D. E., BEASLEY, J. D. & PEREZ, B. 1971. Histologic comparison of polylactic and polyglycolic acid sutures. *Oral surgery, oral medicine, and oral pathology*, 32, 165-73.

DAHM, M., LYMAN, W. D., SCHWELL, A. B., FACTOR, S. M. & FRATER, R. W. 1990. Immunogenicity of glutaraldehyde-tanned bovine pericardium. *The Journal of thoracic and cardiovascular surgery*, 99, 1082-90.

DE MEL, A., BOLVIN, C., EDIRISINGHE, M., HAMILTON, G. & SEIFALIAN, A. M. 2008. Development of cardiovascular bypass grafts: endothelialization and applications of nanotechnology. *Expert.Rev Cardiovasc.Ther.*, 6, 1259-77.

DECELLES, P. 2006. Carbohydrates.

DI FELICE, V., SERRADIFALCO, C., RIZZUTO, L., DE LUCA, A., RAPPA, F., BARONE, R., DI MARCO, P., CASSATA, G., PULEIO, R., VERIN, L., MOTTA, A., MIGLIARESI, C., GUERCIO, A. & ZUMMO, G. 2013. Silk fibroin scaffolds enhance cell commitment of adult rat cardiac progenitor cells. *Journal of tissue engineering and regenerative medicine*.

DUAN, X. & SHEARDOWN, H. 2006. Dendrimer crosslinked collagen as a corneal tissue engineering scaffold: Mechanical properties and corneal epithelial cell interactions. *Biomaterials*, 27, 4608-17.

ESTEBAN, M. J., CANTÓN, E. & RIUS, F. 1990. Influence of temperature on degradation kinetics of ceftriaxone in diluted and undiluted human serum. *Antimicrobial agents and chemotherapy*, 34, 1268-70.

FU, Y. & KAO, W. J. 2009. Drug release kinetics and transport mechanisms from semi-interpenetrating networks of gelatin and poly(ethylene glycol) diacrylate. *Pharmaceutical research*, 26, 2115-24.

GALLER, K. M., AULISA, L., REGAN, K. R., D'SOUZA, R. N. & HARTGERINK, J. D. 2010. Self-assembling multidomain peptide hydrogels: designed susceptibility to enzymatic cleavage allows enhanced cell migration and spreading. *Journal of the American Chemical Society*, 132, 3217-23.



- GHANBARI, H., VIATGE, H., KIDANE, A. G., BURRIESCI, G., TAVAKOLI, M. & SEIFALIAN, A. M. 2009. Polymeric heart valves: new materials, emerging hopes. *Trends Biotechnol.*, 27, 359-67.
- GINTY, P. J., BARRY, J. J. A., WHITE, L. J., HOWDLE, S. M. & SHAKESHEFF, K. M. 2008. Controlling protein release from scaffolds using polymer blends and composites. *European journal of pharmaceutics and biopharmaceutics : official journal of Arbeitsgemeinschaft für Pharmazeutische Verfahrenstechnik e.V.*, 68, 82-9.
- GIUNCHEDI, P., CONTI, B., SCALIA, S. & CONTE, U. 1998. In vitro degradation study of polyester microspheres by a new HPLC method for monomer release determination. *Journal of controlled release : official journal of the Controlled Release Society*, 56, 53-62.
- GO, D. P., GRAS, S. L., MITRA, D., NGUYEN, T. H., STEVENS, G. W., COOPER-WHITE, J. J. & O'CONNOR, A. J. 2011. Multilayered microspheres for the controlled release of growth factors in tissue engineering. *Biomacromolecules*, 12, 1494-503.
- GÖPFERICH, A. 1996. Mechanisms of polymer degradation and erosion. *Biomaterials*, 17, 103-14.
- GRIZZI, I., GARREAU, H., LI, S. & VERT, M. 1995. Hydrolytic degradation of devices based on poly(DL-lactic acid) size-dependence. *Biomaterials*, 16, 305-11.
- GU, F., NEUFELD, R. & AMSDEN, B. 2007. Sustained release of bioactive therapeutic proteins from a biodegradable elastomeric device. *Journal of controlled release : official journal of the Controlled Release Society*, 117, 80-9.
- GUACCIO, A., BORSELLI, C., OLIVIERO, O. & NETTI, P. A. 2008. Oxygen consumption of chondrocytes in agarose and collagen gels: a comparative analysis. *Biomaterials*, 29, 1484-93.
- GUAN, J., ZHU, Z., ZHAO, R. C., XIAO, Z., WU, C., HAN, Q., CHEN, L., TONG, W., ZHANG, J., HAN, Q., GAO, J., FENG, M., BAO, X., DAI, J. & WANG, R. 2013. Transplantation of human mesenchymal stem cells loaded on collagen scaffolds for the treatment of traumatic brain injury in rats. *Biomaterials*, 34, 5937-46.
- GULDBERG, R. E. 2009. Spatiotemporal delivery strategies for promoting musculoskeletal tissue regeneration. *Journal of bone and mineral research : the official journal of the American Society for Bone and Mineral Research*, 24, 1507-11.
- GUNATILLAKE, P. A. & ADHIKARI, R. 2003. Biodegradable synthetic polymers for tissue engineering. *European cells & materials*, 5, 1-16; discussion
- HARTING, M. T., SLOAN, L. E., JIMENEZ, F., BAUMGARTNER, J. & COX, C. S. 2009. Subacute neural stem cell therapy for traumatic brain injury. *The Journal of surgical research*, 153, 188-94.
- HE, C. L., HUANG, Z. M. & HAN, X. J. 2009. Fabrication of drug-loaded electrospun aligned fibrous threads for suture applications. *Journal of biomedical materials research. Part A*, 89, 80-95.
- HE, X. & JABBARI, E. 2007. Material properties and cytocompatibility of injectable MMP degradable poly(lactide ethylene oxide fumarate) hydrogel as a carrier for marrow stromal cells. *Biomacromolecules*, 8, 780-92.
- IMPARATO, G., URCIUOLO, F., CASALE, C. & NETTI, P. A. 2013. The role of micro scaffold properties in controlling the collagen assembly in 3D dermis equivalent using modular tissue engineering. *Biomaterials*, 34, 7851-61.
- JIANG, T., NUKAVARAPU, S. P., DENG, M., JABBARZADEH, E., KOFRON, M. D., DOTY, S. B., ABDEL-FATTAH, W. I. & LAURENCIN, C. T. 2010. Chitosan-poly(lactide-co-glycolide)

microsphere-based scaffolds for bone tissue engineering: in vitro degradation and in vivo bone regeneration studies. *Acta biomaterialia*, 6, 3457-70.

KANCZLER, J. M., GINTY, P. J., WHITE, L., CLARKE, N. M. P., HOWDLE, S. M., SHAKESHEFF, K. M. & OREFFO, R. O. C. 2010. The effect of the delivery of vascular endothelial growth factor and bone morphogenic protein-2 to osteoprogenitor cell populations on bone formation. *Biomaterials*, 31, 1242-50.

KANNAN, R. Y., SALACINSKI, H. J., BUTLER, P. E. & SEIFALIAN, A. M. 2005. Artificial nerve conduits in peripheral-nerve repair. *Biotechnol Appl Biochem*, 41, 193-200.

KANNAN, R. Y., SALACINSKI, H. J., DE GROOT, J., CLATWORTHY, I., BOZEC, L., HORTON, M., BUTLER, P. E. & SEIFALIAN, A. M. 2006a. The antithrombogenic potential of a polyhedral oligomeric silsesquioxane (POSS) nanocomposite. *Biomacromolecules*, 7, 215-23.

KANNAN, R. Y., SALACINSKI, H. J., ODLYHA, M., BUTLER, P. E. & SEIFALIAN, A. M. 2006b. The degradative resistance of polyhedral oligomeric silsesquioxane nanocore integrated polyurethanes: an in vitro study. *Biomaterials*, 27, 1971-9.

KEENEY, M., MATHUR, M., CHENG, E., TONG, X. & YANG, F. 2013. Effects of polymer end-group chemistry and order of deposition on controlled protein delivery from layer-by-layer assembly. *Biomacromolecules*, 14, 794-800.

KHAN, I. M., GILBERT, S. J., SINGHRAO, S. K., DUANCE, V. C. & ARCHER, C. W. 2008. Cartilage integration: evaluation of the reasons for failure of integration during cartilage repair. A review. *European cells & materials*, 16, 26-39.

KHOR, E. 1997. Methods for the treatment of collagenous tissues for bioprotheses. *Biomaterials*, 18, 95-105.

KIM, H.-W., KNOWLES, J. C. & KIM, H.-E. 2005. Hydroxyapatite porous scaffold engineered with biological polymer hybrid coating for antibiotic Vancomycin release. *Journal of materials science. Materials in medicine*, 16, 189-95.

KIM, J., PARK, Y., TAE, G., LEE, K. B., HWANG, S. J., KIM, I. S., NOH, I. & SUN, K. 2008. Synthesis and characterization of matrix metalloprotease sensitive-low molecular weight hyaluronic acid based hydrogels. *Journal of materials science. Materials in medicine*, 19, 3311-8.

KIM, K., YU, M., ZONG, X., CHIU, J., FANG, D., SEO, Y.-S., HSIAO, B. S., CHU, B. & HADJIARGYROU, M. 2003. Control of degradation rate and hydrophilicity in electrospun non-woven poly(D,L-lactide) nanofiber scaffolds for biomedical applications. *Biomaterials*, 24, 4977-85.

KOBSA, S. & SALTZMAN, W. M. 2008. Bioengineering approaches to controlled protein delivery. *Pediatric research*, 63, 513-9.

LEE, B. K., YUN, Y. H., CHOI, J. S., CHOI, Y. C., KIM, J. D. & CHO, Y. W. 2012. Fabrication of drug-loaded polymer microparticles with arbitrary geometries using a piezoelectric inkjet printing system. *International journal of pharmaceutics*, 427, 305-10.

LEE, K. H. & CHU, C. C. 2000. The role of superoxide ions in the degradation of synthetic absorbable sutures. *Journal of biomedical materials research*, 49, 25-35.

LEWANDROWSKI, K. U., GRESSER, J. D., WISE, D. L., TRANTOLO, D. J. & HASIRCI, V. 2000. Tissue responses to molecularly reinforced polylactide-co-glycolide implants. *Journal of biomaterials science. Polymer edition*, 11, 401-14.

LI, S. 1999. Hydrolytic degradation characteristics of aliphatic polyesters derived from lactic and glycolic acids. *Journal of biomedical materials research*, 48, 342-53.

- LI, S., LIU, L., GARREAU, H. & VERT, M. 2003. Lipase-catalyzed biodegradation of poly(epsilon-caprolactone) blended with various polylactide-based polymers. *Biomacromolecules*, 4, 372-7.
- LI, S. & MCCARTHY, S. 1999. Further investigations on the hydrolytic degradation of poly(DL-lactide). *Biomaterials*, 20, 35-44.
- LIEBSCHNER, M. A. K. & WETTERGREEN, M. 2012. Scaffold pore space modulation through intelligent design of dissolvable microparticles. *Methods in molecular biology* (Clifton, N.J.), 868, 71-89.
- LOSI, P., BRIGANTI, E., ERRICO, C., LISELLA, A., SANGUINETTI, E., CHIELLINI, F. & SOLDANI, G. 2013. Fibrin-based scaffold incorporating VEGF- and bFGF-loaded nanoparticles stimulates wound healing in diabetic mice. *Acta biomaterialia*, 9, 7814-21.
- LOTZ, A. S., HAVLA, J. B., RICHTER, E., FROLICH, K., STAUDENMAIER, R., HAGEN, R. & KLEINSASSER, N. H. 2009. Cytotoxic and genotoxic effects of matrices for cartilage tissue engineering. *Toxicology letters*, 190, 128-33.
- LU, L., GARCIA, C. A. & MIKOS, A. G. 1999a. In vitro degradation of thin poly(DL-lactic-co-glycolic acid) films. *Journal of biomedical materials research*, 46, 236-44.
- MA, L., ZHOU, J., GAO, C. & SHEN, J. 2007. Incorporation of basic fibroblast growth factor by a layer-by-layer assembly technique to produce bioactive substrates. *Journal of biomedical materials research. Part B, Applied biomaterials*, 83, 285-92.
- MACAYA, D. & SPECTOR, M. 2012. Injectable hydrogel materials for spinal cord regeneration: a review. *Biomedical materials* (Bristol, England), 7, 012001-.
- MACDONALD, M., RODRIGUEZ, N. M., SMITH, R. & HAMMOND, P. T. 2008. Release of a model protein from biodegradable self assembled films for surface delivery applications. *Journal of controlled release : official journal of the Controlled Release Society*, 131, 228-34.
- MACDONALD, M. L., SAMUEL, R. E., SHAH, N. J., PADERA, R. F., BEBEN, Y. M. & HAMMOND, P. T. 2011. Tissue integration of growth factor-eluting layer-by-layer polyelectrolyte multilayer coated implants. *Biomaterials*, 32, 1446-53.
- MAO, Z., MA, L., ZHOU, J., GAO, C. & SHEN, J. 2005. Bioactive thin film of acidic fibroblast growth factor fabricated by layer-by-layer assembly. *Bioconjugate chemistry*, 16, 1316-22.
- MARANTO, A. R. & SCHOEN, F. J. 1988. Alkaline phosphatase activity of glutaraldehyde-treated bovine pericardium used in bioprosthetic cardiac valves. *Circulation research*, 63, 844-8.
- MARINER, P. D., WUDEL, J. M., MILLER, D. E., GENOVA, E. E., STREUBEL, S.-O. & ANSETH, K. S. 2013. Synthetic hydrogel scaffold is an effective vehicle for delivery of INFUSE (rhBMP2) to critical-sized calvaria bone defects in rats. *Journal of orthopaedic research : official publication of the Orthopaedic Research Society*, 31, 401-6.
- MATSUMOTO, T., KAWAI, M. & MASUDA, T. 1993. Rheological properties and fractal structure of concentrated polyion complexes of chitosan and alginate. *Biorheology*, 30, 435-41.
- MAYER, M. H. & HOLLINGER, J. O. 1995. Biodegradable bone fixation devices. In: HOLLINGER, J. O. (ed.). Boca Raton, FL: CRC Press.
- MCCLURE, M. J., SIMPSON, D. G. & BOWLIN, G. L. 2012. Tri-layered vascular grafts composed of polycaprolactone, elastin, collagen, and silk: Optimization of graft properties. *Journal of the mechanical behavior of biomedical materials*, 10, 48-61.

MCGILL, D. B. & MOTTO, J. D. 1974. An industrial outbreak of toxic hepatitis due to methylenedianiline. *The New England journal of medicine*, 291, 278-82.

MEINEL, A. J., GERMERSHAUS, O., LUHMANN, T., MERKLE, H. P. & MEINEL, L. 2012. Electrospun matrices for localized drug delivery: current technologies and selected biomedical applications. *European journal of pharmaceutics and biopharmaceutics : official journal of Arbeitsgemeinschaft für Pharmazeutische Verfahrenstechnik e.V*, 81, 1-13.

MEKALA, N. K., BAADHE, R. R., PARCHA, S. R. & YALAVARTHY, P. D. 2013. Physical and degradation properties of PLGA scaffolds fabricated by salt fusion technique. *Journal of biomedical research*, 27, 318-25.

MIKOS, A. G., MCINTIRE, L. V., ANDERSON, J. M. & BABENSEE, J. E. 1998. Host response to tissue engineered devices. *Adv. Drug Deliv. Rev.*, 33, 111-39.

MOSES, O., VITRIAL, D., ABOODI, G., SCULEAN, A., TAL, H., KOZLOVSKY, A., ARTZI, Z., WEINREB, M. & NEMCOVSKY, C. E. 2008. Biodegradation of three different collagen membranes in the rat calvarium: a comparative study. *Journal of periodontology*, 79, 905-11.

MOURIÑO, V., CATTALINI, J. P., ROETHER, J. A., DUBEY, P., ROY, I. & BOCCACCINI, A. R. 2013. Composite polymer-bioceramic scaffolds with drug delivery capability for bone tissue engineering. *Expert opinion on drug delivery*.

NAIR, N. R., NAMPOOTHIRI, K. M. & PANDEY, A. 2012. Preparation of poly(L-lactide) blends and biodegradation by *Lentzea waywayandensis*. *Biotechnology letters*, 34, 2031-5.

NG, K. W., THAM, W., LIM, T. C. & WERNER HUTMACHER, D. 2005. Assimilating cell sheets and hybrid scaffolds for dermal tissue engineering. *Journal of biomedical materials research. Part A*, 75, 425-38.

NICHOL, J. W. & KHADEMOSSEINI, A. 2009. Modular Tissue Engineering: Engineering Biological Tissues from the Bottom Up. *Soft matter*, 5, 1312-9.

NUMATA, K. & KAPLAN, D. L. 2010. Silk-Based Gene Carriers with Cell Membrane Destabilizing Peptides. *Biomacromolecules*.

NUMATA, K., KATASHIMA, T. & SAKAI, T. 2011. State of water, molecular structure, and cytotoxicity of silk hydrogels. *Biomacromolecules*, 12, 2137-44.

NUMATA, K., YAMAZAKI, S. & NAGA, N. 2012. Biocompatible and biodegradable dual-drug release system based on silk hydrogel containing silk nanoparticles. *Biomacromolecules*, 13, 1383-9.

OH, S. H., KANG, S. G. & LEE, J. H. 2006. Degradation behavior of hydrophilized PLGA scaffolds prepared by melt-molding particulate-leaching method: comparison with control hydrophobic one. *Journal of materials science. Materials in medicine*, 17, 131-7.

PABARI, A., YANG, S. Y., MOSAHEBI, A. & SEIFALIAN, A. M. 2011. Recent advances in artificial nerve conduit design: strategies for the delivery of luminal fillers. *J Control Release*, 156, 2-10.

PARK, J. S., YANG, H. N., WOO, D. G., JEON, S. Y. & PARK, K.-H. 2012a. SOX9 gene plus heparinized TGF- $\beta$  3 coated dexamethasone loaded PLGA microspheres for inducement of chondrogenesis of hMSCs. *Biomaterials*, 33, 7151-63.

PARK, S. N., PARK, J. C., KIM, H. O., SONG, M. J. & SUH, H. 2002. Characterization of porous collagen/hyaluronic acid scaffold modified by 1-ethyl-3-(3-dimethylaminopropyl)carbodiimide cross-linking. *Biomaterials*, 23, 1205-12.

PARK, S. U., LEE, B. K., KIM, M. S., PARK, K. K., SUNG, W. J., KIM, H. Y., HAN, D. G., SHIM, J. S., LEE, Y. J., KIM, S. H., KIM, I. H. & PARK, D. H. 2012b. The possibility of microbial cellulose for dressing and scaffold materials. *International wound journal*.

PARLATO, M., JOHNSON, A., HUDALLA, G. A. & MURPHY, W. L. 2013. Adaptable poly(ethylene glycol) microspheres capable of mixed-mode degradation. *Acta biomaterialia*.

PENG, L. H., MAO, Z. Y., QI, X. T., CHEN, X., LI, N., TABATA, Y. & GAO, J. Q. 2013. Transplantation of bone-marrow-derived mesenchymal and epidermal stem cells contribute to wound healing with different regenerative features. *Cell and tissue research*, 352, 573-83.

PEREIRA, M. J. N., OUYANG, B., SUNDBACK, C. A., LANG, N., FRIEHS, I., MURELI, S., POMERANTSEVA, I., MCFADDEN, J., MOCHEL, M. C., MWIZERWA, O., DEL NIDO, P., SARKAR, D., MASIAKOS, P. T., LANGER, R., FERREIRA, L. S. & KARP, J. M. 2013. A highly tunable biocompatible and multifunctional biodegradable elastomer. *Advanced materials (Deerfield Beach, Fla.)*, 25, 1209-15.

PIŞKIN, E., IŞOĞLU, I. A., BÖLGEN, N., VARGEL, I., GRIFFITHS, S., CAVUŞOĞLU, T., KORKUSUZ, P., GÜZEL, E. & CARTMELL, S. 2009. In vivo performance of simvastatin-loaded electrospun spiral-wound polycaprolactone scaffolds in reconstruction of cranial bone defects in the rat model. *Journal of biomedical materials research. Part A*, 90, 1137-51.

RAGHUNATH, J., GEORGIU, G., ARMITAGE, D., NAZHAT, S. N., SALES, K. M., BUTLER, P. E. & SEIFALIAN, A. M. 2009. Degradation studies on biodegradable nanocomposite based on polycaprolactone/polycarbonate (80:20%) polyhedral oligomeric silsesquioxane. *J Biomed.Mater Res.A*, 91, 834-44.

RAGHUNATH, J., ROLLO, J., SALES, K. M., BUTLER, P. E. & SEIFALIAN, A. M. 2007. Biomaterials and scaffold design: key to tissue-engineering cartilage. *Biotechnol Appl Biochem*, 46, 73-84.

RAZAQ, S., WILKINS, R. J. & URBAN, J. P. G. 2003. The effect of extracellular pH on matrix turnover by cells of the bovine nucleus pulposus. *European spine journal : official publication of the European Spine Society, the European Spinal Deformity Society, and the European Section of the Cervical Spine Research Society*, 12, 341-9.

RICHARDSON, T. P., PETERS, M. C., ENNETT, A. B. & MOONEY, D. J. 2001. Polymeric system for dual growth factor delivery. *Nature biotechnology*, 19, 1029-34.

RIDGE, J. 2009. Biodiversity.

RUJIVIPAT, S. & BODMEIER, R. 2010a. Modified release from hydroxypropyl methylcellulose compression-coated tablets. *International journal of pharmaceutics*, 402, 72-7.

RUJIVIPAT, S. & BODMEIER, R. 2010b. Modified release from hydroxypropyl methylcellulose compression-coated tablets. *International Journal of Pharmaceutics*, 402, 72-7.

SALACINSKI, H. J., HAMILTON, G. & SEIFALIAN, A. M. 2003. Surface functionalization and grafting of heparin and/or RGD by an aqueous-based process to a poly(carbonate-urea)urethane cardiovascular graft for cellular engineering applications. *Journal of biomedical materials research. Part A*, 66, 688-97.

SAURER, E. M., YAMANOUCHI, D., LIU, B. & LYNN, D. M. 2011. Delivery of plasmid DNA to vascular tissue in vivo using catheter balloons coated with polyelectrolyte multilayers. *Biomaterials*, 32, 610-8.

SCHMITT, E. A., FLANAGAN, D. R. & LINHARDT, R. J. 1994. Importance of distinct water environments in the hydrolysis of poly(DL-lactide-co-glycolide). *Macromolecules*, 27, 743-8.

SEDAGHATI, T., YANG, S. Y., MOSAHEBI, A., ALAVIJEH, M. S. & SEIFALIAN, A. M. 2011. Nerve regeneration with aid of nanotechnology and cellular engineering. *Biotechnol Appl Biochem*, 58, 288-300.

SERAS-FRANZOSO, J., STEUER, C., ROLDÁN, M., VENDRELL, M., VIDAURRE-AGUT, C., TARRUELLA, A., SALDAÑA, L., VILABOIA, N., PARERA, M., ELIZONDO, E., RATERA, I., VENTOSA, N., VECIANA, J., CAMPILLO-FERNÁNDEZ, A. J., GARCÍA-FRUITÓS, E., VÁZQUEZ, E. & VILLAVERDE, A. 2013. Functionalization of 3D scaffolds with protein-releasing biomaterials for intracellular delivery. *Journal of Controlled Release*.

SERBAN, M. A., KNIGHT, T., PAYNE, R. G., BASU, J., RIVERA, E. A., ROBBINS, N., MCCOY, D., HALBERSTADT, C., JAIN, D. & BERTRAM, T. A. 2013. Crosslinked Gelatin Microspheres with Continuously Tunable Degradation Profiles for Renal Tissue Regeneration. *Biotechnology and applied biochemistry*.

SHAH, N. J., MACDONALD, M. L., BEBEN, Y. M., PADERA, R. F., SAMUEL, R. E. & HAMMOND, P. T. 2011. Tunable dual growth factor delivery from polyelectrolyte multilayer films. *Biomaterials*, 32, 6183-93.

SHMUELI, R. B., OHNAKA, M., MIKI, A., PANDEY, N. B., LIMA E SILVA, R., KOSKIMAKI, J. E., KIM, J., POPEL, A. S., CAMPOCHIARO, P. A. & GREEN, J. J. 2013. Long-term suppression of ocular neovascularization by intraocular injection of biodegradable polymeric particles containing a serpin-derived peptide. *Biomaterials*, 34, 7544-51.

SHREIBER, D. I., BAROCAS, V. H. & TRANQUILLO, R. T. 2003. Temporal variations in cell migration and traction during fibroblast-mediated gel compaction. *Biophysical journal*, 84, 4102-14.

SISSON, K., ZHANG, C., FARACH-CARSON, M. C., CHASE, D. B. & RABOLT, J. F. 2009. Evaluation of cross-linking methods for electrospun gelatin on cell growth and viability. *Biomacromolecules*, 10, 1675-80.

SKOP, N. B., CALDERON, F., LEVISON, S. W., GANDHI, C. D. & CHO, C. H. 2013. Heparin crosslinked chitosan microspheres for the delivery of neural stem cells and growth factors for central nervous system repair. *Acta biomaterialia*, 9, 6834-43.

SOLLAZZO, V., LUCHESE, A., PALMIERI, A., ZOLLINO, I., IACCARINO, C., CARNEVALI, G., PEZZETTI, F., BRUNELLI, G. & CARINCI, F. 2011. Polylactide-polyglycolide resorbable plates stimulates adipose tissue-derived stem cells towards osteoblasts differentiation. *International journal of immunopathology and pharmacology*, 24, 59-64.

SON, J. S., APPLEFORD, M., ONG, J. L., WENKE, J. C., KIM, J. M., CHOI, S. H. & OH, D. S. 2011. Porous hydroxyapatite scaffold with three-dimensional localized drug delivery system using biodegradable microspheres. *Journal of controlled release : official journal of the Controlled Release Society*, 153, 133-40.

SONG, S.-H., LEE, S. J. & RHEE, S.-H. 2012. Synthesis of biodegradable poly( $\epsilon$ -caprolactone)-organosiloxane hybrid with carboxylate groups. *Journal of biomedical materials research. Part B, Applied biomaterials*, 100, 1289-97.

SPARK, J. I., YELURI, S., DERHAM, C., WONG, Y. T. & LEITCH, D. 2008. Incomplete cellular depopulation may explain the high failure rate of bovine ureteric grafts. *Br J Surg*, 95, 582-5.

SPEER, D. P., CHVAPIL, M., ESKELSON, C. D. & ULREICH, J. 1980. Biological effects of residual glutaraldehyde in glutaraldehyde-tanned collagen biomaterials. *Journal of biomedical materials research*, 14, 753-64.

SPIVAK, J. M., RICCI, J. L., BLUMENTHAL, N. C. & ALEXANDER, H. 1990. A new canine model to evaluate the biological response of intramedullary bone to implant materials and surfaces. *Journal of biomedical materials research*, 24, 1121-49.

SUBRAMANIAN, A., KRISHNAN, U. M. & SETHURAMAN, S. 2013. In Vivo Biocompatibility of PLGA-Polyhexylthiophene Nanofiber Scaffolds in a Rat Model. *BioMed research international*, 2013, 390518-.

SUN, M. & DOWNES, S. 2009. Physicochemical characterisation of novel ultra-thin biodegradable scaffolds for peripheral nerve repair. *J Mater Sci Mater Med*, 20, 1181-92.

SUN, Z., TEE, B. C., KENNEDY, K. S., KENNEDY, P. M., KIM, D.-G., MALLERY, S. R. & FIELDS, H. W. 2013. Scaffold-based delivery of autologous mesenchymal stem cells for mandibular distraction osteogenesis: preliminary studies in a porcine model. *PloS one*, 8, e74672-e.

SUNG, H. J., MEREDITH, C., JOHNSON, C. & GALIS, Z. S. 2004. The effect of scaffold degradation rate on three-dimensional cell growth and angiogenesis. *Biomaterials*, 25, 5735-42.

SUNG, H. W., HSU, H. L., SHIH, C. C. & LIN, D. S. 1996. Cross-linking characteristics of biological tissues fixed with monofunctional or multifunctional epoxy compounds. *Biomaterials*, 17, 1405-10.

SYKOVÁ, E., JENDELOVÁ, P., URDZÍKOVÁ, L., LESNÝ, P. & HEJCL, A. 2006. Bone marrow stem cells and polymer hydrogels--two strategies for spinal cord injury repair. *Cellular and molecular neurobiology*, 26, 1113-29.

TAN, A., RAJADAS, J. & SEIFALIAN, A. M. 2012. Biochemical engineering nerve conduits using peptide amphiphiles. *J Control Release*, 163, 342-52.

TANG, Y. W., LABOW, R. S. & SANTERRE, J. P. 2003. Isolation of methylene dianiline and aqueous-soluble biodegradation products from polycarbonate-polyurethanes. *Biomaterials*, 24, 2805-19.

TATE, C. C., SHEAR, D. A., TATE, M. C., ARCHER, D. R., STEIN, D. G. & LAPLACA, M. C. 2009. Laminin and fibronectin scaffolds enhance neural stem cell transplantation into the injured brain. *Journal of tissue engineering and regenerative medicine*, 3, 208-17.

TAYALIA, P. & MOONEY, D. J. 2009. Controlled growth factor delivery for tissue engineering. *Advanced materials (Deerfield Beach, Fla.)*, 21, 3269-85.

THAKRAL, S., THAKRAL, N. K. & MAJUMDAR, D. K. 2013. Eudragit: a technology evaluation. *Expert opinion on drug delivery*, 10, 131-49.

THOMSON, R. C., YASZEMSKI, M. J., POWERS, J. M. & MIKOS, A. G. 1995. Fabrication of biodegradable polymer scaffolds to engineer trabecular bone. *Journal of biomaterials science. Polymer edition*, 7, 23-38.

TRACY, M. A., WARD, K. L., FIROUZABADIAN, L., WANG, Y., DONG, N., QIAN, R. & ZHANG, Y. 1999. Factors affecting the degradation rate of poly(lactide-co-glycolide) microspheres in vivo and in vitro. *Biomaterials*, 20, 1057-62.

UEBERSAX, L., MERKLE, H. P. & MEINEL, L. 2009. Biopolymer-based growth factor delivery for tissue repair: from natural concepts to engineered systems. *Tissue engineering. Part B, Reviews*, 15, 263-89.

UENG, S. W. N., YUAN, L.-J., LIN, S.-S., LIU, S.-J., CHAN, E.-C., CHEN, K.-T. & LEE, M. S. 2011. In vitro and in vivo analysis of a biodegradable poly(lactide-co-glycolide) copolymer capsule and collagen composite system for antibiotics and bone cells delivery. *The Journal of trauma*, 70, 1503-9.

UNIVERSITY OF WAIKATO. 2014. *Plant Structure & Function. Cellulose & Lignin*.

VALMIKINATHAN, C. M., TIAN, J., WANG, J. & YU, X. 2008. Novel nanofibrous spiral scaffolds for neural tissue engineering. *Journal of neural engineering*, 5, 422-32.

VAN DER VEEN, V. C., BOEKEMA, B. K. H. L., ULRICH, M. M. W. & MIDDELKOOP, E. 2011. New dermal substitutes. *Wound repair and regeneration : official publication of the Wound Healing Society [and] the European Tissue Repair Society*, 19 Suppl 1, s59-65.

VARKEY, M., GITTENS, S. A. & ULUDAG, H. 2004. Growth factor delivery for bone tissue repair: an update. *Expert opinion on drug delivery*, 1, 19-36.

VASITA, R. & KATTI, D. S. 2006. Growth factor-delivery systems for tissue engineering: a materials perspective. *Expert review of medical devices*, 3, 29-47.

WAN, Y., YU, A., WU, H., WANG, Z. & WEN, D. 2005. Porous-conductive chitosan scaffolds for tissue engineering II. in vitro and in vivo degradation. *Journal of materials science. Materials in medicine*, 16, 1017-28.

WANG, H., BOERMAN, O. C., SARIIBRAHIMOGLU, K., LI, Y., JANSEN, J. A. & LEEUWENBURGH, S. C. G. 2012. Comparison of micro- vs. nanostructured colloidal gelatin gels for sustained delivery of osteogenic proteins: Bone morphogenetic protein-2 and alkaline phosphatase. *Biomaterials*, 33, 8695-703.

WANG, H. M., CHOU, Y. T., WEN, Z. H., WANG, Z. R., CHEN, C. H. & HO, M. L. 2013a. Novel biodegradable porous scaffold applied to skin regeneration. *PloS one*, 8, e56330-e.

WANG, W., ITOH, S., MATSUDA, A., ICHINOSE, S., SHINOMIYA, K., HATA, Y. & TANAKA, J. 2008. Influences of mechanical properties and permeability on chitosan nano/microfiber mesh tubes as a scaffold for nerve regeneration. *Journal of biomedical materials research. Part A*, 84, 557-66.

WANG, Y., NIE, J., CHANG, B., SUN, Y. & YANG, W. 2013b. Poly(vinylcaprolactam)-Based Biodegradable Multiresponsive Microgels for Drug Delivery. *Biomacromolecules*, 14, 3034-46.

WANG, Y., YU, B., ZHAO, J., GUO, J., LI, Y., HAN, S., HUANG, L., DU, Y., HONG, Y., TANG, D. & LIU, Y. 2013c. Autophagy Contributes to Leaf Starch Degradation. *The Plant cell*, 25, 1383-99.

WEISSMAN, I. L. 2000. Translating stem and progenitor cell biology to the clinic: barriers and opportunities. *Science (New York, N.Y.)*, 287, 1442-6.

WHU, S. W., HUNG, K.-C., HSIEH, K.-H., CHEN, C.-H., TSAI, C.-L. & HSU, S.-H. 2013. In vitro and in vivo evaluation of chitosan-gelatin scaffolds for cartilage tissue engineering. *Materials science & engineering. C, Materials for biological applications*, 33, 2855-63.

WIEBE, D., MEGERMAN, J., L'ITALIEN, G. J. & ABBOTT, W. M. 1988. Glutaraldehyde release from vascular prostheses of biologic origin. *Surgery*, 104, 26-33.

WILLIAMS, D. F. 2006. To engineer is to create: the link between engineering and regeneration. *Trends in biotechnology*, 24, 4-8.



WISCHKE, C., ZHANG, Y., MITTAL, S. & SCHWENDEMAN, S. P. 2010. Development of PLGA-based injectable delivery systems for hydrophobic fenretinide. *Pharmaceutical research*, 27, 2063-74.

WU, M. H., URBAN, J. P. G., CUI, Z. F., CUI, Z. & XU, X. Effect of extracellular pH on matrix synthesis by chondrocytes in 3D agarose gel. *Biotechnology progress*, 23, 430-4.

XIE, X., EBERHART, A., GUIDOIN, R., MAROIS, Y., DOUVILLE, Y. & ZHANG, Z. 2010. Five types of polyurethane vascular grafts in dogs: the importance of structural design and material selection. *Journal of biomaterials science. Polymer edition*, 21, 1239-64.

XU, Q., CHIN, S. E., WANG, C.-H. & PACK, D. W. 2013. Mechanism of drug release from double-walled PDLGA(PLGA) microspheres. *Biomaterials*, 34, 3902-11.

YAN, S., XIAOQIANG, L., SHUIPING, L., XIUMEI, M. & RAMAKRISHNA, S. 2009. Controlled release of dual drugs from emulsion electrospun nanofibrous mats. *Colloids and surfaces. B, Biointerfaces*, 73, 376-81.

YAP, K. K., DINGLE, A. M., PALMER, J. A., DHILLON, R. S., LOKMIC, Z., PENINGTON, A. J., YEOH, G. C., MORRISON, W. A. & MITCHELL, G. M. 2013. Enhanced liver progenitor cell survival and differentiation in vivo by spheroid implantation in a vascularized tissue engineering chamber. *Biomaterials*, 34, 3992-4001.

YELLOWLEY, C. E., JACOBS, C. R., LI, Z., ZHOU, Z. & DONAHUE, H. J. 1997. Effects of fluid flow on intracellular calcium in bovine articular chondrocytes. *The American journal of physiology*, 273, C30-6.

YILDIRIMER, L., THANH, N. T. K., LOIZIDOU, M. & SEIFALIAN, A. M. 2011. Toxicology and clinical potential of nanoparticles. *Nano Today*, 6, 585-607.

YILDIRIMER, L., THANH, N. T. K. & SEIFALIAN, A. M. 2012. Skin regeneration scaffolds: a multimodal bottom-up approach. *Trends in biotechnology*.

YOUNG, S., WONG, M., TABATA, Y. & MIKOS, A. G. 2005. Gelatin as a delivery vehicle for the controlled release of bioactive molecules. *Journal of controlled release : official journal of the Controlled Release Society*, 109, 256-74.

YU, W., ZHAO, W., ZHU, C., ZHANG, X., YE, D., ZHANG, W., ZHOU, Y., JIANG, X. & ZHANG, Z. 2011. Sciatic nerve regeneration in rats by a promising electrospun collagen/poly( $\epsilon$ -caprolactone) nerve conduit with tailored degradation rate. *BMC neuroscience*, 12, 68-.

ZEUGOLIS, D. I., PAUL, G. R. & ATTENBURROW, G. 2009. Cross-linking of extruded collagen fibers--a biomimetic three-dimensional scaffold for tissue engineering applications. *Journal of biomedical materials research. Part A*, 89, 895-908.

ZHANG, J., FREDIN, N. J., JANZ, J. F., SUN, B. & LYNN, D. M. 2006. Structure/property relationships in erodible multilayered films: influence of polycation structure on erosion profiles and the release of anionic polyelectrolytes. *Langmuir : the ACS journal of surfaces and colloids*, 22, 239-45.



# 3 INTRODUCTION TO SKIN TISSUE ENGINEERING<sup>2</sup>

---

## 3.1 SYNOPSIS

Skin wounds are a major social and financial burden. However, current treatments are suboptimal. The gradual comprehension of the finely orchestrated nature of inter-cellular communication has stimulated scientists to investigate growth factor (GF) or stem cell (SC) incorporation into suitable scaffolds for local delivery into wound beds in an attempt to accelerate healing. This chapter provides a critical evaluation of the status quo of current research into GF and SC therapy and subsequent future prospects, including benefits and possible long-term dangers associated with their use. Additionally, the importance of a bottom-up approach in scaffold fabrication is highlighted to enable controlled factor incorporation as well as production of complex scaffold micro- and nanostructures resembling that of natural ECM.

---

<sup>2</sup> The following chapter has been adapted from Yildirimer et al. Trends Biotechnol. 2012;30(12):638-648.

### **3.2 INTRODUCTION – A MULTIMODAL COCKTAIL FOR SKIN REGENERATION**

Skin serves the onerous function of protecting our internal organs and tissues from external, potentially dangerous insults for a lifetime. Such temporal demands require not only impeccable integrity, but also mechanical strength and durability. Loss of large parts of this barrier, be it related to illness or injury, renders the individual susceptible to disability or death. The World Health Organisation (WHO) estimates that, annually, over 300 000 deaths are attributable to fire-related burn injuries with millions more suffering from the partly devastating physical and emotional consequences thereof. A further 6.5 million individuals suffer from chronic skin ulcers caused by prolonged pressure, venous stasis, or diabetes mellitus (Jones et al., 2002). The holistic goals of modern cutaneous wound care consist of rapid wound excision and closure with a functionally intact and aesthetically pleasing outcome. Currently available treatment options are lacking in establishing both functional and cosmetic satisfaction. Thus, combined with the burden of pain and the currently suboptimal therapy methods, the overall onus of cutaneous wounds appears vast. It seems of particular importance to dissociate oneself from the concept of aiming to replace lost skin tissue, and rather focus on promoting the regeneration of wounded tissues by stimulating the innate ability of the skin for self-renewal. Wound contracture and scarring, properties that can misleadingly be thought accountable for faster wound healing, should be avoided in terms of wound regeneration. The gradual understanding of the biological processes involved in wound healing has opened the gates for developing smart bio-constructs that actively promote tissue regeneration via appropriately engineered regeneration platforms, or scaffolds, as well as the incorporation of cell-signalling elements such as GFs and SCs. In this chapter, a review and critical appraisal of current research efforts concerned with dermal regeneration scaffolds incorporating bioactive elements to promote neovascularisation

and tissue regeneration is provided. The most recent advances in the field of nanoscaled tissue engineering will also be touched upon because cellular behaviour is significantly influenced by the surface nanotopography of scaffolds that promotes cellular adherence, differentiation, and proliferation, mimicking natural ECM (Egaña et al., 2009).

### 3.2.1 The Structure of Normal Skin

Skin is the outermost covering of human beings and the largest organ of the body, encompassing the entire body surface. It has a complex three-layered structure (Fig. 3.1) which, under physiological circumstances, is intrinsically self-renewable, so that a new layer of skin develops every 2-3 weeks while continuously shedding the older top layers.

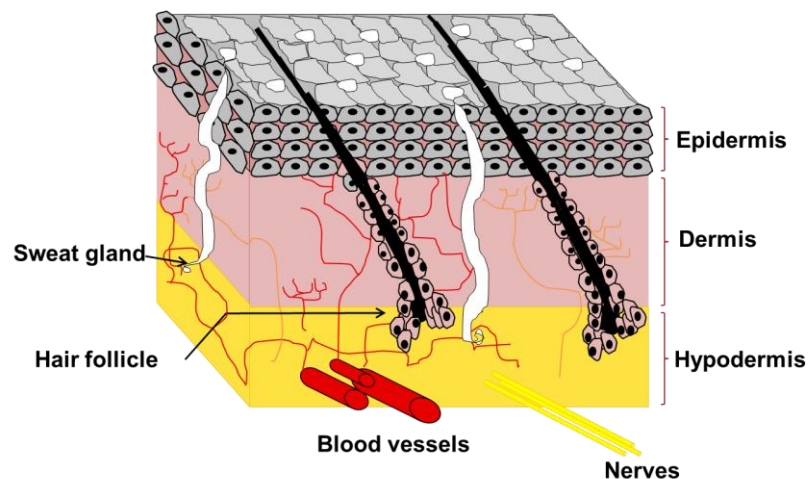


**Figure 3.1.** An illustration of human skin showing the three constituting layers and skin adnexae.

The three layers, from outermost to innermost are: (i) the epidermis which consists of multiple, ever renewing layers of keratinocytes; (ii) the dermis which is separated from the epidermis at the dermal-epidermal junction (basement membrane); and (iii) the hypodermis which is mainly made up of adipose tissue and collagen.

Skin appendages such as hair follicles, sebaceous glands and sweat glands are numerous intermingled along blood vessels, nerve endings, and pressure and touch

receptors. Regional variations exist regarding skin thickness, distribution of skin appendages, and melanocyte density. Skin mainly functions as a protecting interface, physically shielding internal organs and tissues from external insults. Once the external barrier is breached, innate surveillance mechanisms set off a cell-signalling cascade to limit pain, control infection, and accelerate wound healing naturally, ultimately creating a scar. However, extensive wounds such as those associated with full thickness burns rarely, if ever, heal spontaneously and thus require an external means of protection, be it temporary or permanent, to stimulate not only wound healing, but scarless self-regeneration. Current conventions hold that tissue-engineered skin constructs should resemble native skin both anatomically and functionally.

### **3.2.2 Normal Wound Healing**

Wounds are defined as breaks in the continuity of the structure of the skin, usually resulting from physical trauma and leading to either temporary or terminal loss of function. Healing is a complex dynamic process that results in the restoration of anatomic continuity and function (Fig. 3.2). It consists of 4 distinct but overlapping entities that depend on complex and finely orchestrated cell-signalling events. Firstly, haemostasis is triggered post-injury by platelets within the wound bed. These interact with the ECM to initiate the clotting cascade which results in a blood clot forming. This, in turn, provides a platform for cell migration. The second stage, inflammation, is triggered by PDGF and TGF- $\beta$  released by platelets. Neutrophils and monocytes are recruited to phagocytose foreign material and pathogens. Macrophages expressing CSF-1, TNF- $\beta$  and PDGF act as chemoattractants for fibroblasts. This leads on to the proliferative phase where PDGF, TGF- $\beta$  and ECM molecules induce fibroblast proliferation, new ECM deposition and integrin receptor expression to promote cell recognition and adherence.

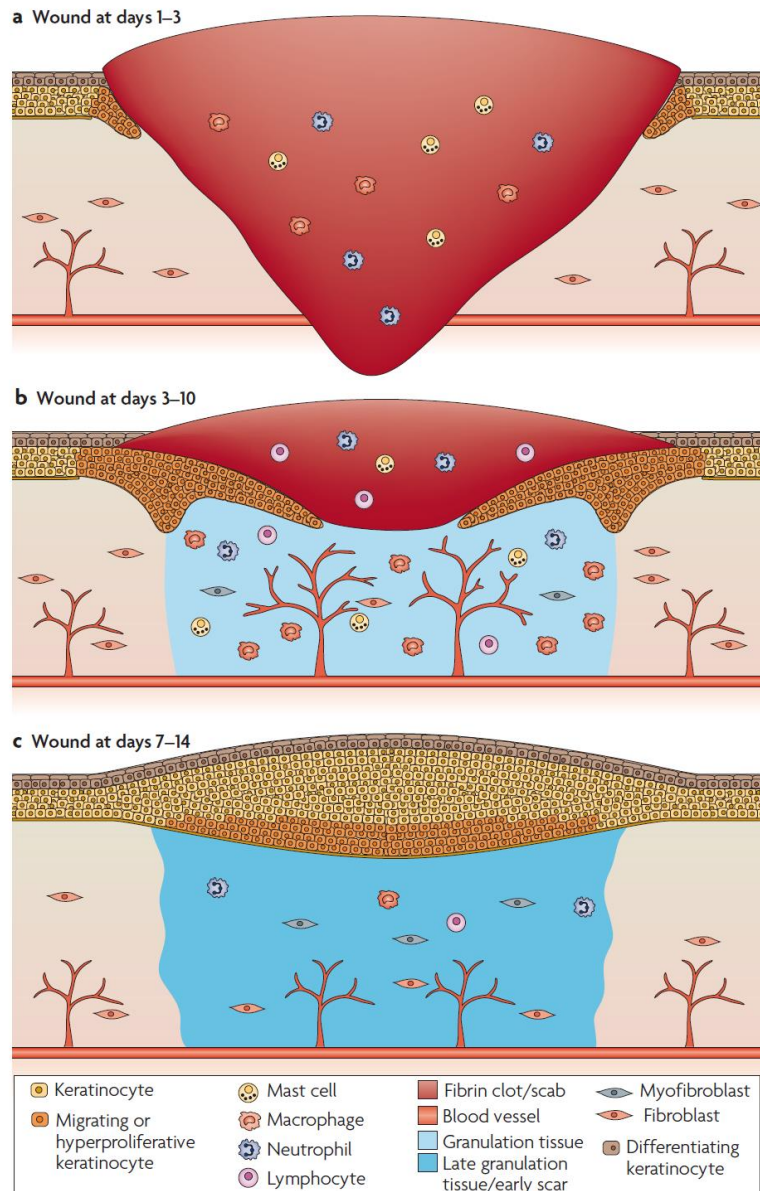


**Figure 3.2.** A schematic representation of the normal wound healing process incorporating various cell-signalling molecules (Schäfer and Werner, 2008).

The 4<sup>th</sup> remodelling stage involves the crosslinking of new collagen matrix. Fibroblast-derived enzymes including collagenases, plasminogen activators and gelatinases create pathways through tightly woven ECM for cellular movement. Over time, granulation tissue is replaced with an acellular, avascular scar.

### 3.2.3 Foetal Wound Healing

Foetal wound healing differs distinctly from adult healing, resulting in intrinsic and complete self-regeneration of a wound without scar formation. This is attributable to different healing mechanisms including a significantly reduced inflammatory response with fewer differentiated inflammatory cells in early gestational foetal wounds. Higher numbers of phagocytic cells and morphogenic factors result in collagen deposition akin to that of normal skin (i.e., large bundles of ECM in a normal reticular orientation as opposed to an adult-pattern abnormal deposition of parallel bundles of mainly collagen types I and III). Additionally, higher levels of hyaluronic acid (HA) and altered ratios of signalling molecules and genes are thought to play a vital role in scarless wound healing. However, scarless healing is only possible during the first two trimesters, attributable to a finely orchestrated interplay between several factors. During the third trimester, a transition occurs and the skin loses its ability to regenerate, resulting in the formation of fibrous scar tissues.

Previous assumptions that the sterile, GF-enriched intrauterine environment is the determining factor for scarless healing have been refuted by several seminal studies; a marsupial model for cutaneous healing demonstrated that the developing opossum retained its ability for scarless regeneration despite growing in a pouch devoid of amniotic fluid (Werner et al., 1994). Transplantation studies on sheep models have shown that wounded adult or late foetal skin transplanted onto early- gestation foetal lambs healed with scar formation (Staiano-Coico et al., 1993), whereas wounded early foetal human skin transplanted into nude mice regenerated with no scar formation (Peng et al., 2011). This demonstrates independence from environmental factors and an intrinsic ability for early- gestational foetal skin to regenerate without scar formation.



The complete elucidation of the intrinsic foetal wound healing mechanisms would allow for the meticulous re-establishment of signalling events within an ex-foetal environment, resulting in scarless dermal regeneration in adult wounds.

#### **3.2.4 Management of Thermal Wounds**

Thermal wounds have been divided into three zones of histopathological injury; (1) the zone of coagulation, or eschar, is the central area of a burn wound which undergoes complete and irreversible necrosis and denaturation of proteins. (2) The zone of stasis and oedema with partially denatured proteins and slow blood flow, and (3) the zone of hyperaemia which is characterised by gradually increasing blood flow.

In case of wound infection or poor perfusion, a seemingly superficial burn may in time develop into a more severe and deeper wound with necrotic areas extending into the zone of stasis. Current treatment standards of burn wounds comprise of (i) early and complete excision of eschar to prevent wound infection, (ii) in cases of full-thickness burns, wound coverage with an autologous split thickness skin graft harvested from intact areas of the patient's skin is used.

If larger parts of the total body surface area have been damaged, autologous skin grafts may still be taken and then meshed in order to enlarge the size of the graft. The disadvantages of such practices are morbidity, significant pain at the donor site, and the characteristic corrugated scar as the recipient site heals. In cases of total or near total full-thickness skin injuries, donor sites may be unavailable, necessitating the use of cadaveric skin to fulfil vital barrier functions. Cadaveric skin grafts are lyophilised, thus removing the cellular component to prevent graft immune rejection. They may either be obtained from non-profit skin banks or purchased as, for example, Karoskin. Such allografts represent temporary 'bridging' measures for immediate wound coverage in the acute

stages post-injury. Disadvantages of utilising human cadaveric skin are manifold and include donor organ shortage and limited skin bank availability, moral objections from the patient's or surgeon's perspective, and the potential risk of viral transmission from cadaveric tissues to the recipient. It is evident that there is an urgent need for fully synthetic, yet biocompatible and so-called 'smart' skin bio-constructs for the regeneration of scarfree skin.

### **3.3 CURRENT STATE OF TISSUE ENGINEERED SKIN SUBSTITUTES**

The pressing need for more suitable wound dressings has spurred on the search for alternative skin substitutes that actively promote wound regeneration. The era of dermal tissue engineering was heralded three decades ago with a bi-layered and biocompatible dermal scaffold based on a bovine collagen matrix, which successfully induced the synthesis of a neodermis (Burke et al., 1981). This novel bio-construct revolutionised current burns practice and even today, Integra® dermal regeneration scaffold is often used as the gold standard in severe full-thickness burns that are not amenable to autograft harvest, due to immediate availability, skin infiltration rates similar to that of skin allografts (85% versus 95%) and adequate cosmetic results (Jones et al., 2002).

Clinically available and novel skin substitutes can be broadly divided into epidermal, dermal, and dermo-epidermal (composite) tissue-engineered constructs (Shevchenko et al., 2010b). A multitude of choices and potential alternatives for tissue- engineering skin constructs exist and, in fact, numerous substitutes are being investigated for human usage; some of them already commercialised (Table 3.1).

The current lack of more sophisticated and superior skin alternatives requires a focus on regeneration rather than replacement. Current research is increasingly

integrating the concept of engineering dermal scaffolds that actively promote regeneration by incorporating SCs and external GFs to recreate a favourable cellular microenvironment. SCs have been central to the field of regenerative medicine for over three decades due to an ability to induce their differentiation into any cell type with subsequent cell-specific GF and cytokine release to enhance angiogenesis (Egaña et al., 2009). This approach is motivated by the understanding that numerous cell-cell and cell-ECM cues are required to achieve physiological functioning of the surrounding cells and tissues (Bianchi et al., 2007). Furthermore, naturally occurring ECM components, as well as physiological molecules involved in wound healing, have dimensions in the nanometre range (1-100 nm), thus suggesting a significant and exploitable potential for 'nano-engineered' particle delivery vehicles. For example, nanoparticles could be used to create advantageous surface nanostructures or nanotopography resembling natural structures, and further seeded with SCs or functionalised with GFs (Choi et al., 2008), cytokines, and peptides (Kim et al., 2009).

### **3.4 BIOENGINEERING 'SMART' SCAFFOLDS FOR SKIN REGENERATION: A BOTTOM-UP APPROACH**

The ultimate purpose of tissue-engineered skin grafts is to enable complete and natural, albeit accelerated, wound regeneration. A 3D supporting framework should serve as a template for tissue regeneration while simultaneously preventing wound bed contraction throughout the first stages of healing (Chevallay and Herbage, 2000). The framework, or scaffold, should further serve as a platform for cellular localisation, adhesion, and differentiation, as well as guide the development of new functional tissues (Kim and Mooney, 1998). A focus on the multitude of different scaffold materials and fabrication techniques is beyond the scope of this chapter but has been extensively

reviewed elsewhere (Edalat et al., 2012). Scaffold materials may be of natural, synthetic, or composite origin and engineered using a multitude of approaches including porogen leaching, electrospinning, molecular self-assembly, and phase separation. The mixing of materials of different classes to obtain composite scaffolds seems particularly promising because individual limitations of single material scaffolds (e.g. poor mechanical properties) are often overcome by the composite nature (Kannan et al., 2007a). The ideal skin regeneration scaffold should actively direct tissue formation and prevent scarring. Thus, much focus has been channelled into creating suitable biomimetic surface micro- and nanostructures that can act as delivery vehicles for SCs or GFs. The synergistic tissue regenerating effects of a smart scaffold cocktail comprising (i) favourable scaffold surface patterns, (ii) GFs, and (iii) SCs have the realistic potential of overcoming current barriers and enabling fast and complete skin regeneration.

During natural wound healing, dynamic and reciprocal interactions between components of the ECM and surrounding cell-signalling molecules are responsible for the expression of GFs and cytokines. These interactions elicit cellular responses that ultimately lead to new tissue formation. Overwhelming activation of the inflammatory system and prolific recruitment of contractile cells is thought to stem from prehistoric adaptations of human skin to close irregular and often contaminated wounds as rapidly as possible, to prevent microorganism invasion and potentially lethal infections (Sedaghati et al., 2014). Unfortunately, this response typically leads to scar formation, often resulting in disfigurement and functional disability. Nowadays, some wounds are closed aseptically using sutures that obviate the need for a vigorous contractile response, creating more time for complete tissue regeneration. Here, external modulation of cell-signalling events via a finely tuned delivery of GFs or SCs is thought to alter the wound

environment, enabling orderly regeneration. Modifying the micro- and nano-environment and surface architecture of the scaffold, termed nanotopography, actively influences cell migration, proliferation, and differentiation.

In the following sections, we focus on discussing incorporation of various GFs involved in wound healing into scaffolds and the possibilities of exploiting the latest SC technologies to accelerate skin regeneration. Potential advantages of cutting-edge nano-engineered scaffolds over macrosized skin substitutes as 3D stimulatory platforms for cellular growth and skin regeneration are highlighted. Overall, we support the argument that a bottom-up approach (i) enables tight control over important micro- and nanostructures within scaffold architecture; and (ii) facilitates incorporation of appropriate concentrations of bioactive factors as well as SCs.

### **3.5 GROWTH FACTOR FUNCTIONALIZED SKIN REGENERATION SCAFFOLDS**

#### **3.5.1 Epidermal Growth Factor (EGF)**

EGF is implicated in keratinocyte migration, fibroblast proliferation and differentiation, and granulation tissue formation. EGF significantly enhances wound healing (Alemdaroğlu et al., 2008) as well as the tensile strength of the resultant ECM (Throm et al., 2010). Prolonged exposure to EGF yielded a 200% increase in tensile strength when liposome-encapsulated EGF was delivered into murine dorsal cutaneous wounds (Brown et al., 1988). Similarly, EGF contained within a gelatine sheet applied to dorsa of hairless dogs accelerated wound closure and healing of superficial and partial-thickness wounds (Tanaka et al., 2005). Current challenges regarding the delivery of EGF at physiologically relevant concentrations and durations still prevail due to its rapid breakdown within the wound environment, encouraging research into effective immobilisation and delivery techniques. For example, biodegradable microspheres that

contain EGF provide sustained EGF delivery and hence more effective wound healing in a rabbit dorsal skin wound model (Ulubayram et al., 2001). Despite such encouraging results, supplemental EGF has a mitogenic effect upon cells and has been implicated in the spread of epithelial malignancies (Hardwicke et al., 2008). However, the beneficial effects of EGF in the wound healing process should not be denied, thus requiring further research.

### **3.5.2 Basic Fibroblast Growth Factor (bFGF)**

FGF comprises a large family of mitogens that are actively involved in the processes of wound healing, embryonic development, angiogenesis, and tumour progression (Thisse and Thisse, 2005, Dailey et al., 2005, Beenken and Mohammadi, 2009). Both acidic fibroblast growth factor (aFGF) and bFGF are found within the wound fluid at the earliest stages of healing (Nissen et al., 2003). aFGF, like bFGF, is a potent mitogen and chemo-attractant for vascular endothelial cells, dermal fibroblasts, and epidermal keratinocytes. In the initial phases of wound healing, bFGF participates by activating local macrophages and can still be identified within the healing tissue during the remodelling phase that occurs several weeks after injury (Kibe et al., 2000). bFGF accelerates neovascularisation as shown in a rabbit ear wound healing model, in which wounds supplemented with exogenous bFGF healed significantly faster compared to untreated controls (Komori et al., 2005). Radiation-induced cutaneous wounds created in miniature pig models treated with exogenous bFGF showed increased dermo-epidermal proliferation, new blood vessel formation, higher overall mechanical skin stability, and adnexae integrity (Kinoshita et al.). In 2001, genetically recombinant bFGF was approved for clinical use in Japan under the trade name Fiblast Spray (Kaken Pharmaceutical Co. Ltd., Tokyo, Japan). Clinical trials conducted on second-degree burn wounds in Japanese adults and children showed accelerated rates of wound healing and

superior mechanical properties of the resultant scars when topical bFGF was initiated relatively soon after creation of the burn injury (1-4 days, mean 2 days) (Akita et al., 2006, Akita et al., 2008). Despite such promising results, concerns over the carcinogenic potential of topical FGF application remain; bFGF has been identified as a major autocrine stimulant in melanoma and, in combination with UV light, is associated with tumour progression (Lázár-Molnár et al., 2000, Berking et al., 2001). Further research is needed to corroborate existing evidence of beneficial effects of bFGF on wound healing and refute any associations with the progression of skin cancers.

### **3.5.3 Keratinocyte Growth Factor (KGF)**

KGF is expressed within the dermis and hypodermis below the wound, whereas the KGF receptor is predominantly found on epithelial cells of the epidermis, suggesting a paracrine mediation of epithelial cell growth. Several animal and clinical studies have demonstrated the cytoprotective and epithelial regenerative properties of KGF (Wu et al., 2011, Yazbeck et al., 2011, Spielberger et al., 2004). Such favourable effects depend on several mechanisms including cell proliferation, migration, differentiation, survival, DNA repair, and detoxifying enzyme induction, which collectively act to strengthen the integrity of the epithelium (Finch and Rubin, 2004). During the initial 24 h of normal human wound healing, KGF expression is up-regulated 100-fold and remains elevated for several days (Marchese et al., 1995). This up-regulation in KGF is significantly dampened in genetically diabetic and glucocorticoid-treated mice (Brauchle et al., 1995, Werner et al., 1994). In a porcine partial-thickness wound model, topical application of recombinant KGF demonstrated an accelerated rate of re-epithelialisation compared to controls not receiving KGF (Staiano-Coico et al., 1993). In a murine full-thickness wound healing model, keratinocyte proliferation and angiogenesis were significantly retarded in KGF knockouts compared to wild-type mice (Peng et al., 2011). These results suggest a further

role of KGF in the control of wound bed angiogenesis. However, the use of KGF in epithelial cancer patients raises concerns regarding potential tumourigenicity of KGF because epithelial cells express KGF receptors. Several studies have identified a potential association between the overabundance of KGF and tumour growth progression (Chung et al., 1992). Further studies are warranted to examine the nature and extent of KGF involvement in tumour development.

#### **3.5.4 Vascular Endothelial Growth Factor (VEGF)**

The VEGF family encompasses VEGF-A, VEGF-B, VEGF- C, VEGF-D, and PlGF. During wound healing, VEGF-A is highly expressed by keratinocytes within the wound bed to promote new blood vessel formation essential for tissue regeneration (Drinkwater et al., 2002) and re-epithelialisation of wounds (Wise et al., 2012, Brem et al., 2009). VEGF is the major angiogenesis-promoting GF due to its combined ability to stimulate endothelial cell proliferation and migration (Ferrara and Henzel, 1989), basement membrane degradation (Unemori et al., 1992), tubular and luminal structure formation (Koolwijk et al., 1996), increased vascular permeability (Bates and Curry, 1996), and new vessel formation (Connolly et al., 1989). In a diabetic mouse model, mini-circle plasmid DNA encoding VEGF was successfully transfected into proliferating cells within wounded tissue, resulting in a high level of VEGF expression (Kwon et al., 2012). Wound healing rates were significantly accelerated in plasmid-exposed injuries compared to those exposed to empty vehicles. Similarly, vector-mediated VEGF transfer onto experimental murine burn wounds increased angiogenesis as well as epithelial proliferation and ECM maturation (Galeano et al., 2003). Despite extensive evidence for accelerated wound healing via increased blood vessel formation, the use of VEGF must be critically appraised within the context of potential negative effects; two relatively recent studies have reported associations between chronic burn injuries and the development of primary



cutaneous anaplastic large cell lymphoma (PCALCL) (Yeung et al., 2004, Morihara et al., 2007). According to these reports, the growth of PCALCL is fuelled by VEGF production and secretion by atypical large lymphocytes. Furthermore, skin biopsies from the erythematous region surrounding the PCALCL have revealed rich neovascularisation secondary to VEGF overexpression. Although the differing effects of VEGF on cutaneous wounds require a cautious approach, it seems of equal importance to investigate its beneficial effects further in order to avoid premature rejection of a potentially useful GF.

### **3.5.5 Insulin-Like Growth Factor (IGF)**

High levels of IGF-1 found within cutaneous wounds have been shown to accelerate epidermal wound healing and inhibit apoptosis pathways (Dasu et al., 2003, Spies et al., 2001), whereas reduced expression of IGF-1 is associated with retarded wound healing (Gartner et al., 1992). For example, IGF-1 receptor knockout mice (IGF-1r<sup>-/-</sup>) exhibited skin hypotrophy with fewer and smaller hair follicles (Liu et al., 1993). Wound healing by re-epithelialisation was accelerated by local overexpression of IGF-1, whereas no effects were observed on the underlying dermis (Semenova et al., 2008). *In vitro* studies, however, have found evidence for the stimulatory effects of IGF-1 on collagen and ECM production (Daian et al., 2003). Similarly, wound beds of IGF-1-depleted rats had significantly lower collagen content, as measured by the amount of hydroxyproline, a major component of collagen, compared to non-depleted animals, suggesting a reduced capacity for wound healing. Subsequent IGF-1 infusion returned concentrations to near-normal levels (Mueller et al., 1994). Such contrasting evidence for a role in ECM and collagen production is indicative of a dose-dependent activation of dermal fibroblasts by IGF-1. In a porcine diabetic full-thickness excisional wound model, transplantation of IGF-1-transfected keratinocytes increased local IGF-1 expression 900-fold, leading to significantly accelerated keratinocyte migration and wound closure (Hirsch et al., 2008).

Wound contracture, a possible confounder in the interpretation of wound closure rates, is not thought to have significantly influenced the wound healing process, because degrees of contractions were similar in transfected and control groups. Maintenance of appropriate IGF-1 concentrations within the wound bed is significantly important because overexpression has been linked to skin hyperplasia and tumour growth (DiGiovanni et al., 2000, Bol et al., 1997).

### **3.5.6 Platelet-Derived Growth Factor (PDGF)**

PDGF is involved throughout all stages of normal wound healing. PDGF is released by degranulating platelets and activated macrophages within the wound fluid. Later in the proliferative stage, PDGF is responsible for the differentiation of fibroblasts into their contractile phenotype, the myofibroblasts which through attachments of their filopodia to components of the ECM, drag or contract the tissues together (Clark, 1993). Several animal studies have demonstrated accelerated wound closure in normal and pathophysiological states when the wound bed was supplemented with exogenous PDGF (Uhl et al.). In a genetically diabetic mouse model (C57BL/Ks-J-db/db), large full-thickness skin wounds (1.5x1.5 cm<sup>2</sup>) created on the mid-back were exposed to recombinant human PDGF (Greenhalgh et al., 1990). At 21 days, more fibroblasts, enhanced capillary formation, and accelerated wound closure were observed in treated diabetic mice compared to littermates receiving empty vehicles. Furthermore, *in vivo* blockage of PDGF receptors with the PDGFR- $\beta$  inhibitor imatinib mesylate resulted in delayed wound healing, reduced wound closure, and abnormal microvascular morphology, normally observed in PDGFR- $\beta$  <sup>-/-</sup> mice, thus highlighting the pivotal role of PDGF in early wound healing (Rajkumar et al., 2006). However, similar results could not be obtained using the same animal model, same wound dimensions, but commercially available Regranex (Greenhalgh et al., 1990). In a recently published retrospective clinical study on the

healing efficiency of supplementary PDGF on diabetic heel ulcers larger than 4 cm (an independent predictor of limb loss), some beneficial effects were observed when the standard treatment regime (distal femoral bypass surgery, partial calcanectomy, intra-operative negative pressure wound treatment) was boosted with PDGF (Goudie et al., 2012) [68]. PDGF is thought to modulate beneficially the ulcer microenvironment, thereby accelerating wound healing and closure. However, the small cohort, lack of randomisation and blinding, as well as the absence of a control population minimise the significance of these results.

### **3.5.7 Transforming Growth Factor- $\beta$ (TGF- $\beta$ )**

TGF- $\beta$  exists in three isoforms - TGF- $\beta$ 1, TGF- $\beta$ 2, and TGF- $\beta$ 3 - which are all involved in the process of wound healing. After acute injuries, TGF- $\beta$ 1 is highly expressed by keratinocytes, platelets, monocytes, fibroblasts, and macrophages (Faler et al., 2006). TGF- $\beta$  acts in both autocrine and paracrine manners, inducing its own synthesis by target cells and activating nearby cells to synthesise and release other GFs involved in the healing process (Murphy et al., 2011). The autocrine action of TGF- $\beta$ 1 by fibroblasts sustains their activity beyond the initial inflammatory stimulus (Schmid et al., 1998) and is postulated to play a key role in myofibroblast differentiation (Tomasek et al., 2002). TGF- $\beta$ 2 expression is related to wound contracture and excessive collagen deposition, but has also been demonstrated to be a causative factor in scar formation (Shah et al., 1995). Early foetal skin is well known for its ability to regenerate wounds completely without the formation of scar tissue, which is thought to be largely associated with a significantly reduced expression of TGF- $\beta$ 1, coinciding with highly elevated levels of TGF- $\beta$ 3 (Lin et al., 1995). The exact underlying mechanism of action for scarless foetal wound regeneration has not been elucidated so far, leaving the respective roles of the TGF- $\beta$  isoforms to be fully uncovered.

The results obtained with the use of GFs to accelerate wound healing, while encouraging on both experimental and clinical levels, must be interpreted cautiously, because the same factors are often implicated in exuberant tissue and tumour growth. More basic and preclinical research is necessary to indicate when GF concentration moves from being beneficial to becoming potentially harmful. Such ambiguous circumstances demand careful evaluation for more than one reason.

First, it is of paramount importance that exposure to inappropriate amounts of GFs is prevented due to potentially carcinogenic tendencies *in vivo*, as previously mentioned. Any such long-term adverse effects must be excluded prior to commencing clinical trials. Only a few of the numerous GFs playing their part throughout the process of wound healing are approved by the Food and Drug Administration (FDA) and clinically available for the purpose of accelerating wound repair (e.g., Regranex, Kepivance). One may argue that worries about lasting adverse effects of GF use in the context of skin wound healing may be unfounded because their application is mostly local. Furthermore, GFs are rapidly degraded into natural metabolites by the wound fluid, thus eliminating any downstream effects. Such rapid elimination from the body is, however, avoidable via encapsulation techniques, enabling GFs to linger within the wound for longer prolonging their trophic effects.

Second, determining beneficial effects on wound healing is ongoing. Selective GF treatment leads to accelerated rates of healing both in experimental and preclinical trials. Potential reasons for failure might be inappropriate routes of GF delivery or overabundance of GFs that cancel out the anticipated beneficial effects on wound healing. This, again, demonstrates the critical need to investigate the optimal GF concentrations to stimulate appropriately skin regeneration while avoiding the risk of overstimulation

and tumour formation or receptor down-regulation. Below, a critical discussion on the benefits and disadvantages of SC usage for tissue engineering purposes is provided.

### **3.6 STEM CELL-SEEDED SKIN REGENERATION SCAFFOLDS**

Slow scaffold vascularisation is a critical limiting factor in skin wound regeneration due to inadequate supplies of nutrients and oxygen and a build-up of waste products within the tissues. SCs have the ability to self-renew and differentiate into lineage-specific progenies. Despite their ability to acquire any cell type of an organism, embryonic SC usage is retarded by ethical considerations. Adult SCs, on the other hand, have several advantages: (i) the ability to differentiate into several lineages within a tissue; (ii) the relative ease of access; and (iii) less stringent regulatory concerns and a higher degree of public acceptance compared to embryonic SC use. The beneficial effects of adult mesenchymal stem cells (MSCs) in wound bed neovascularisation and accelerated healing has been demonstrated in several preclinical models (Rustad et al., 2012, Wu et al., 2007). Yet, the mechanisms of action remain elusive; evidence for paracrine signalling subsists (Hocking and Gibran, 2010), although the role of MSC differentiation in wound healing is less clear, partially due to low engraftment efficiency of cells (Wagner et al., 2009). Thus, cell delivery vehicles have been applied to provide suitable cellular microenvironments and enhanced engraftment, survival and differentiation into appropriate mature cells (Rustad et al., 2012) (Fig. 3.3). Particular emphasis is placed on the integration of human adipose derived stem cells (hADSCs) into skin regeneration scaffolds due to their accessibility and facile *in vitro* expansibility. hADSCs are a source of MSCs that have shown a potential for therapeutic vascularisation due to the production of angiogenic GFs (Liu et al., 2011). This was demonstrated in an *in vivo* wound healing study using nude mice; two identical defects were created in the

dorsal skin of mice and exposed to either collagen gel preseeded with hADSCs or empty collagen vehicles (Kim et al., 2007). Angiogenic GF production was significantly enhanced in SC-seeded wounds compared to nonseeded wounds. Another study obtained similar results with ADSCs-impregnated microcarrier systems (Zhou et al., 2011). Despite substantial preclinical evidence for a beneficial role of SCs in the wound healing process, one should approach the clinical use of MSCs cautiously because evidence suggests a contributing role in cancer SC maintenance (Dazzi and Horwood, 2007). It remains to be seen how useful SC technology proves to be in clinical reality; the tendency to overplay the role of SCs for regenerative purposes, however, should not discourage scientists to evaluate further the substantial potential within the field of regenerative SC technology.

### **3.7 NANO-ENGINEERED SCAFFOLDS FOR A BOTTOM-UP APPROACH TO WOUND REGENERATION**

Regenerative medicine aims at recuperating lost tissues by guiding cell growth and restoring original tissue architecture. This requires the presence of a scaffold because isolated cells are unable to re-establish their native structures due to a lack in extracellular guidance. Figure 3.3 shows a schematic representation of the ideal skin regeneration scaffold.

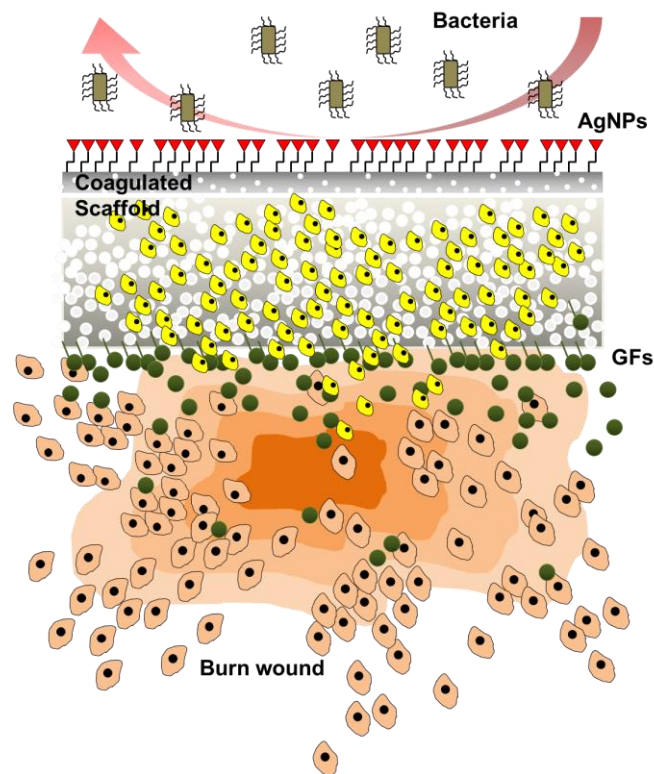


**Figure 3.3.** Schematic representation of the ideal scaffold to promote skin regeneration. Despite intense research efforts aiming at optimising available scaffolds, the proposed schematic has not been developed successfully yet. Abbreviations: AgNPs, silver nanoparticles; GFs, growth factors.

Although various scaffolds for skin regeneration are already on the market (Table 3.1), their clinical implementation remains riddled with flaws, ranging from poor take rates (Tremblay et al., 2005) and poor cosmesis to relatively high infection rates.

**Table 3.1.** Characteristics of the 'ideal' skin substitute.

	<i>Dermo-epidermal substitute (composite)</i>			<i>References</i>
	<b>Cadaveric skin (non-profit skin banks)</b>	<b>Karoskin® (*)</b>	<b>Apligraf® (*)</b>	
<b>Patient safety</b>	Potential for viral transmission Immune rejection	Potential for viral transmission Immune rejection	Potential for viral transmission	
<b>Scaffold degradability</b>	Rejection rather than degradation.	Rejection rather than degradation.	1-2 months	(Griffiths et al.)
<b>Duration of cover</b>	Temporary	Temporary	Temporary	

<b>Neo-dermis formation</b>	Dermis revascularizes and integrates into the wound bed. The epidermis is rejected 3-4 weeks post-transplantation.	Dermis revascularizes and integrates into the wound bed. The epidermis is rejected 3-4 weeks post-transplantation.	Delivers ECM components, cytokines and GF to the wound	(Ehrenreich and Ruszczak, 2006, Eaglstein and Falanga, 1998, Kim et al., 2006, Wood et al., 2006)
<b>Shelf life</b>	7-10 days if fresh. Unlimited if lyophilized.	Unlimited if lyophilized.	5-10 days	
<b>Cost (/cm<sup>2</sup>) (in 2007)</b>	donated	£0.60	£14.20	(Jones et al., 2002)
<b>Mechanical stability</b>	Lyophilization improves mechanical stability significantly.	Lyophilization improves mechanical stability significantly.	Requires delicate handling	
<b>Scaffold vascularisation (i.e. 'take')</b>	Cadaveric allografts 'take' initially, i.e. vascularization is observed however, subsequent graft rejection requires its eventual removal.	'Takes' initially, i.e. vascularization is observed however, subsequent graft rejection requires its eventual removal.	Take rates depend on the type of wound and are very variable ranging from 16%-41%	(Tremblay et al., 2005)
<b>N<sup>o</sup> of stages necessary for completion</b>	Multiple as cadaveric grafts require eventual replacement.	Multiple as cadaveric grafts require eventual replacement.	1-stage process but needs co-grafting with autologous epithelial cells in full-thickness burns.	

	<i>Dermal substitute</i>				<i>References</i>
	Alloderm® (*)	SureDerm® (*)	Integra® (*)	Dermagraft® (*)	
<b>Patient safety</b>	Potential for viral transmission	Potential for viral transmission	n/a	Potential for viral transmission	
<b>Scaffold degradability</b>	Incorporates into wound bed	Incorporates into wound bed	Half-live, T = 30 days	Degrades by hydrolysis	(Griffiths et al.)
<b>Duration of cover</b>	Permanent	Permanent	Semi-permanent	Temporary	
<b>Neo-dermis formation</b>	Repopulated by host cells, i.e. incorporates into host tissue.	Repopulated by host cells, i.e. incorporates into host tissue.	Neodermis formation complete in 15-20 days	Scaffolds degrade over 20-30 days. Fibroblasts simultaneously produce ECM components and GF	(Ehrenreich and Ruszczak, 2006, Eaglstein and Falanga, 1998, Kim et al., 2006, Wood et al., 2006)
<b>Shelf life</b>	2 years	Up to 2 years	2 years	Up to 6 months	
<b>Cost (/cm<sup>2</sup>) (in 2007)</b>	£5.90	n/f	£3.32	£7.14	(Jones et al., 2002)
<b>Mechanical stability</b>	Stable due to presence of basement membrane.	No adverse information regarding fragility and manual handling	Easy handling	Easy handling	
<b>Scaffold vascularisation (i.e. 'take')</b>	Uncertain rates of vascularization	No adverse information regarding	Takes relatively long time for	Take is facilitated by fibrovascular in growth and re-	(Tremblay et al., 2005)



		delayed or failed graft take.	vascularization (10-14 d).	epithelialization and wound closure by keratinocytes migration from wound edges.
<b>N° of stages necessary for completion</b>	1-stage process (using ultra-thin split-thickness graft)	2-stage process (using split-thickness graft)	2-stage process (using split-thickness graft)	2-stage process if used in burn injuries (using split-thickness graft)

	<i>Epidermal substitute</i>		<i>References</i>
	<b>MySkin™ (*)</b>	<b>CellSpray® (*)</b>	
<b>Patient safety</b>	Autologous keratinocytes are co-cultured with irradiated murine cells		n/a
<b>Scaffold degradability</b>	< 29 days		n/f (Griffiths et al.)
<b>Duration of cover</b>	Permanent	Permanent	
<b>Neo-dermis formation</b>	Only applicable in partial-thickness and graft donor side wounds, but not in full-thickness wounds	Only applicable in partial-thickness and graft donor side wounds, but not in full-thickness wounds	(Ehrenreich and Ruszczak, 2006, Eaglstein and Falanga, 1998, Kim et al., 2006, Wood et al., 2006)
<b>Shelf life</b>	3 days		n/f
<b>Cost (/cm<sup>2</sup>) (in 2007)</b>	n/f		n/f (Jones et al., 2002)
<b>Mechanical stability</b>	Easy handling and application due to a silicone support layer	Very fragile and difficult to handle	
<b>Scaffold vascularisation (i.e. 'take')</b>	Cannot be used for full-thickness wounds as dermal component missing.	Uncertain rate of take as it depends on cell-cell and cell-ECM adhesion rather than vascularization. Higher risk of bacterial contamination leading to graft loss.	(Tremblay et al., 2005)
<b>N° of stages necessary for completion</b>	Up to 12 individual applications	1-stage process	

Key: ECM, extra-cellular matrix; GF, growth factor; n/a, not applicable; n/f, not found; N°, number; (\*), commercialized product

Efforts at increasing their effectiveness include bioactivation, that is, expanding their role from being a simple structural framework to a delivery vehicle for GFs, cytokines, or genes (Yang et al., 2012, Barrientos et al.). In this way, tissue regeneration can be actively promoted rather than merely passively suggested. This should, however,

not discourage research into more suitable scaffold architectures, because accumulating evidence highlights the importance of biocompatible scaffold materials, appropriate pore sizes, and cell-growth-promoting surface topographies (Wong et al., 2011, Yildirimer et al., 2011). Although scientists agree on the importance of the extracellular microarchitecture for cell adherence and proliferation, studies have shown an abnormally elongated phenotype when cells were grown on microfibrillar materials. Cells cultured on nanofibrillar structures, however, demonstrated a phenotype resembling that of cells growing within natural environments. This may be explained by the close architectural approximation of nanofibrillar materials to natural ECM and collagen fibrils, which themselves exhibit nanometre dimensions. Thus, a natural cell environment can be feigned and cells guided along normal morphogenic lines. Additionally, natural ECM fibrils serve as storage vehicles for SCs and bioactive factors to regulate cell migration, proliferation, and differentiation. The bottom-up approach allows for tight control over scaffold micro- and nanoarchitecture, porosity, as well as the sequential incorporation of bioactive elements which, in turn, influence cellular interactions via the creation of a beneficial biomimetic micro- and nanoenvironment.

### **3.8 CONCLUSION AND FUTURE PERSPECTIVE**

The burden of cutaneous wounds is immense in both personal and financial terms. Clinically available and feasible treatment strategies are still lacking despite various skin substitutes being under thorough investigation. The emergence of nanotechnology combined with the latest SC technology and the ever-increasing appreciation of cell-signalling pathways in both adult and foetal wound healing models have opened up new avenues for precise biotechnological wound bed manipulations for accelerated healing.

Cutting-edge developments within the area of tissue-engineered scaffolds lead the way into a new era of organ consciousness with the ultimate goal of tissue regeneration rather than replacement.

Approved treatment strategies for skin wounds mostly aim to replace lost tissues rather than support intrinsic self-healing mechanisms. Technological advances now grant scientists the ability to manipulate precisely scaffold materials and engineering strategies within nanometre dimensions to create nanotopographies that mimic the natural ECM. The incorporation of SCs, GFs, and nanoparticles into scaffolds promotes the intricate interplay between naturally occurring cell-signalling factors to achieve full tissue regeneration. With such fast and current developments in nanotechnology and biomedical sciences, we are continuously improving skin regeneration and repair. The future trend of regenerative medicine in general, and tissue-engineering of skin in particular lies in: (i) the comprehension of intricate intercellular biochemical communications; (ii) the engineering of scaffold structures on a micro- and nanodimension; and (iii) the integration of GFs and SCs into such scaffolds to obtain a bioactive cocktail capable of active guidance in skin regeneration. Despite the presence of realistic benefits and dangers associated with GF or SC supplementation, ongoing research into their exploitation is fundamental if regenerative medicine is to have a future.

## References

- AKITA, S., AKINO, K., IMAIZUMI, T. & HIRANO, A. 2008. Basic fibroblast growth factor accelerates and improves second-degree burn wound healing. *Wound repair and regeneration : official publication of the Wound Healing Society [and] the European Tissue Repair Society*, 16, 635-41.
- AKITA, S., AKINO, K., IMAIZUMI, T., TANAKA, K., ANRAKU, K., YANO, H. & HIRANO, A. 2006. The quality of pediatric burn scars is improved by early administration of basic fibroblast growth factor. *Journal of burn care & research : official publication of the American Burn Association*, 27, 333-8.
- ALEMDAROĞLU, C., DEGİM, Z., CELEBI, N., SENGEZER, M., ALÖMEROĞLU, M. & NACAR, A. 2008. Investigation of epidermal growth factor containing liposome formulation effects on burn wound healing. *Journal of biomedical materials research. Part A*, 85, 271-83.
- BARRIENTOS, S., STOJADINOVIC, O., GOLINKO, M. S., BREM, H. & TOMIC-CANIC, M. Growth factors and cytokines in wound healing. *Wound repair and regeneration : official publication of the Wound Healing Society [and] the European Tissue Repair Society*, 16, 585-601.
- BATES, D. O. & CURRY, F. E. 1996. Vascular endothelial growth factor increases hydraulic conductivity of isolated perfused microvessels. *The American journal of physiology*, 271, H2520-8.
- BEENKEN, A. & MOHAMMADI, M. 2009. The FGF family: biology, pathophysiology and therapy. *Nature reviews. Drug discovery*, 8, 235-53.
- BERKING, C., TAKEMOTO, R., SATYAMOORTHY, K., ELENITSAS, R. & HERLYN, M. 2001. Basic fibroblast growth factor and ultraviolet B transform melanocytes in human skin. *The American journal of pathology*, 158, 943-53.
- BIANCHI, F., ROSI, M., VOZZI, G., EMANUELI, C., MADEDDU, P. & AHLUWALIA, A. 2007. Microfabrication of fractal polymeric structures for capillary morphogenesis: applications in therapeutic angiogenesis and in the engineering of vascularized tissue. *Journal of biomedical materials research. Part B, Applied biomaterials*, 81, 462-8.
- BOL, D. K., KIGUCHI, K., GIMENEZ-CONTI, I., RUPP, T. & DIGIOVANNI, J. 1997. Overexpression of insulin-like growth factor-1 induces hyperplasia, dermal abnormalities, and spontaneous tumor formation in transgenic mice. *Oncogene*, 14, 1725-34.
- BRAUCHLE, M., FÄSSLER, R. & WERNER, S. 1995. Suppression of keratinocyte growth factor expression by glucocorticoids in vitro and during wound healing. *The Journal of investigative dermatology*, 105, 579-84.
- BREM, H., KODRA, A., GOLINKO, M. S., ENTERO, H., STOJADINOVIC, O., WANG, V. M., SHEAHAN, C. M., WEINBERG, A. D., WOO, S. L. C., EHRLICH, H. P. & TOMIC-CANIC, M. 2009. Mechanism of sustained release of vascular endothelial growth factor in accelerating experimental diabetic healing. *The Journal of investigative dermatology*, 129, 2275-87.
- BROWN, G. L., CURTSINGER, L. J., WHITE, M., MITCHELL, R. O., PIETSCH, J., NORDQUIST, R., VON FRAUNHOFER, A. & SCHULTZ, G. S. 1988. Acceleration of tensile strength of incisions treated with EGF and TGF-beta. *Annals of surgery*, 208, 788-94.
- BURKE, J. F., YANNAS, I. V., QUINBY, W. C., BONDOC, C. C. & JUNG, W. K. 1981. Successful use of a physiologically acceptable artificial skin in the treatment of extensive burn injury. *Annals of surgery*, 194, 413-28.

- CHEVALLAY, B. & HERBAGE, D. 2000. Collagen-based biomaterials as 3D scaffold for cell cultures: applications for tissue engineering and gene therapy. *Medical & biological engineering & computing*, 38, 211-8.
- CHOI, J. S., LEONG, K. W. & YOO, H. S. 2008. In vivo wound healing of diabetic ulcers using electrospun nanofibers immobilized with human epidermal growth factor (EGF). *Biomaterials*, 29, 587-96.
- CHUNG, L. W., LI, W., GLEAVE, M. E., HSIEH, J. T., WU, H. C., SIKES, R. A., ZHAU, H. E., BANDYK, M. G., LOGOTHETIS, C. J. & RUBIN, J. S. 1992. Human prostate cancer model: roles of growth factors and extracellular matrices. *Journal of cellular biochemistry. Supplement*, 16H, 99-105.
- CLARK, R. A. 1993. Regulation of fibroplasia in cutaneous wound repair. *The American journal of the medical sciences*, 306, 42-8.
- CONNOLLY, D. T., HEUVELMAN, D. M., NELSON, R., OLANDER, J. V., EPPLEY, B. L., DELFINO, J. J., SIEGEL, N. R., LEIMGRUBER, R. M. & FEDER, J. 1989. Tumor vascular permeability factor stimulates endothelial cell growth and angiogenesis. *The Journal of clinical investigation*, 84, 1470-8.
- DAIAN, T., OHTSURU, A., ROGOUNOVITCH, T., ISHIHARA, H., HIRANO, A., AKIYAMA-UCHIDA, Y., SAENKO, V., FUJII, T. & YAMASHITA, S. 2003. Insulin-like growth factor-I enhances transforming growth factor-beta-induced extracellular matrix protein production through the P38/activating transcription factor-2 signaling pathway in keloid fibroblasts. *The Journal of investigative dermatology*, 120, 956-62.
- DAILEY, L., AMBROSETTI, D., MANSUKHANI, A. & BASILICO, C. 2005. Mechanisms underlying differential responses to FGF signaling. *Cytokine & growth factor reviews*, 16, 233-47.
- DASU, M. R. K., HERNDON, D. N., NESIC, O. & PEREZ-POLO, J. R. 2003. IGF-I gene transfer effects on inflammatory elements present after thermal trauma. *American journal of physiology. Regulatory, integrative and comparative physiology*, 285, R741-6.
- DAZZI, F. & HORWOOD, N. J. 2007. Potential of mesenchymal stem cell therapy. *Current opinion in oncology*, 19, 650-5.
- DIGIOVANNI, J., BOL, D. K., WILKER, E., BELTRÁN, L., CARBAJAL, S., MOATS, S., RAMIREZ, A., JORCANO, J. & KIGUCHI, K. 2000. Constitutive expression of insulin-like growth factor-1 in epidermal basal cells of transgenic mice leads to spontaneous tumor promotion. *Cancer research*, 60, 1561-70.
- DRINKWATER, S. L., SMITH, A., SAWYER, B. M. & BURNAND, K. G. 2002. Effect of venous ulcer exudates on angiogenesis in vitro. *The British journal of surgery*, 89, 709-13.
- EAGLSTEIN, W. H. & FALANGA, V. 1998. Tissue engineering for skin: an update. *Journal of the American Academy of Dermatology*, 39, 1007-10.
- EDALAT, F., SHEU, I., MANOUCHERI, S. & KHADEMHOSEINI, A. 2012. Material strategies for creating artificial cell-instructive niches. *Current opinion in biotechnology*.
- EGAÑA, J. T., FIERRO, F. A., KRÜGER, S., BORNHÄUSER, M., HUSS, R., LAVANDERO, S. & MACHENS, H.-G. 2009. Use of human mesenchymal cells to improve vascularization in a mouse model for scaffold-based dermal regeneration. *Tissue engineering. Part A*, 15, 1191-200.
- EHRENREICH, M. & RUSZCZAK, Z. 2006. Update on tissue-engineered biological dressings. *Tissue engineering*, 12, 2407-24.
- FALER, B. J., MACSATA, R. A., PLUMMER, D., MISHRA, L. & SIDAWY, A. N. 2006. Transforming growth factor-beta and wound healing. *Perspectives in vascular surgery and endovascular therapy*, 18, 55-62.

FERRARA, N. & HENZEL, W. J. 1989. Pituitary follicular cells secrete a novel heparin-binding growth factor specific for vascular endothelial cells. *Biochemical and biophysical research communications*, 161, 851-8.

FINCH, P. W. & RUBIN, J. S. 2004. Keratinocyte growth factor/fibroblast growth factor 7, a homeostatic factor with therapeutic potential for epithelial protection and repair. *Advances in cancer research*, 91, 69-136.

GALEANO, M., DEODATO, B., ALTAVILLA, D., SQUADRITO, G., SEMINARA, P., MARINI, H., STAGNO D'ALCONTRES, F., COLONNA, M., CALÒ, M., LO CASCIO, P., TORRE, V., GIACCA, M., VENUTI, F. S. & SQUADRITO, F. 2003. Effect of recombinant adeno-associated virus vector-mediated vascular endothelial growth factor gene transfer on wound healing after burn injury. *Critical care medicine*, 31, 1017-25.

GARTNER, M. H., BENSON, J. D. & CALDWELL, M. D. 1992. Insulin-like growth factors I and II expression in the healing wound. *The Journal of surgical research*, 52, 389-94.

GOUDIE, E. B., GENDICS, C. & LANTIS, J. C. 2012. Multimodal therapy as an algorithm to limb salvage in diabetic patients with large heel ulcers. *International wound journal*, 9, 132-8.

GREENHALGH, D. G., SPRUGEL, K. H., MURRAY, M. J. & ROSS, R. 1990. PDGF and FGF stimulate wound healing in the genetically diabetic mouse. *The American journal of pathology*, 136, 1235-46.

GRIFFITHS, M., OJEH, N., LIVINGSTONE, R., PRICE, R. & NAVSARIA, H. Survival of Apligraf in acute human wounds. *Tissue engineering*, 10, 1180-95.

HARDWICKE, J., SCHMALJOHANN, D., BOYCE, D. & THOMAS, D. 2008. Epidermal growth factor therapy and wound healing--past, present and future perspectives. *The surgeon : journal of the Royal Colleges of Surgeons of Edinburgh and Ireland*, 6, 172-7.

HIRSCH, T., SPIELMANN, M., VELANDER, P., ZUHAILI, B., BLEIZIFFER, O., FOSSUM, M., STEINSTRÄESSER, L., YAO, F. & ERIKSSON, E. 2008. Insulin-like growth factor-1 gene therapy and cell transplantation in diabetic wounds. *The journal of gene medicine*, 10, 1247-52.

HOCKING, A. M. & GIBRAN, N. S. 2010. Mesenchymal stem cells: paracrine signaling and differentiation during cutaneous wound repair. *Exp. Cell Res.*, 316, 2213-9.

JONES, I., CURRIE, L. & MARTIN, R. 2002. A guide to biological skin substitutes. *British journal of plastic surgery*, 55, 185-93.

KANNAN, R. Y., SALACINSKI, H. J., GHANAVI, J.-E., NARULA, A., ODLYHA, M., PEIROVI, H., BUTLER, P. E. & SEIFALIAN, A. M. 2007. Silsesquioxane nanocomposites as tissue implants. *Plastic and reconstructive surgery*, 119, 1653-62.

KIBE, Y., TAKENAKA, H. & KISHIMOTO, S. 2000. Spatial and temporal expression of basic fibroblast growth factor protein during wound healing of rat skin. *The British journal of dermatology*, 143, 720-7.

KIM, B. S. & MOONEY, D. J. 1998. Development of biocompatible synthetic extracellular matrices for tissue engineering. *Trends in biotechnology*, 16, 224-30.

KIM, K. L., HAN, D. K., PARK, K., SONG, S.-H., KIM, J. Y., KIM, J.-M., KI, H. Y., YIE, S. W., ROH, C.-R., JEON, E.-S., KIM, D.-K. & SUH, W. 2009. Enhanced dermal wound neovascularization by targeted delivery of endothelial progenitor cells using an RGD-g-PLLA scaffold. *Biomaterials*, 30, 3742-8.

KIM, P. J., DYBOWSKI, K. S. & STEINBERG, J. S. 2006. A closer look at bioengineered alternative tissues. *Podiatry Today*, 19, 38-55.

KIM, W. S., PARK, B. S., SUNG, J. H., YANG, J. M., PARK, S. B., KWAK, S. J. & PARK, J. S. 2007. Wound healing effect of adipose-derived stem cells: a critical role of secretory factors on human dermal fibroblasts. *Journal of dermatological science*, 48, 15-24.

- KINOSHITA, N., TSUDA, M., HAMUY, R., NAKASHIMA, M., NAKAMURA-KURASHIGE, T., MATSUU-MATSUYAMA, M., HIRANO, A. & AKITA, S. The usefulness of basic fibroblast growth factor for radiation-exposed tissue. *Wound repair and regeneration : official publication of the Wound Healing Society [and] the European Tissue Repair Society*, 20, 91-102.
- KOMORI, M., TOMIZAWA, Y., TAKADA, K. & OZAKI, M. 2005. A single local application of recombinant human basic fibroblast growth factor accelerates initial angiogenesis during wound healing in rabbit ear chamber. *Anesthesia and analgesia*, 100, 830-4, table of contents.
- KOOLWIJK, P., VAN ERCK, M. G., DE VREE, W. J., VERMEER, M. A., WEICH, H. A., HANEMAAIJER, R. & VAN HINSBERGH, V. W. 1996. Cooperative effect of TNF $\alpha$ , bFGF, and VEGF on the formation of tubular structures of human microvascular endothelial cells in a fibrin matrix. Role of urokinase activity. *The Journal of cell biology*, 132, 1177-88.
- KWON, M. J., AN, S., CHOI, S., NAM, K., JUNG, H. S., YOON, C. S., KO, J. H., JUN, H. J., KIM, T. K., JUNG, S. J., PARK, J. H., LEE, Y. & PARK, J.-S. 2012. Effective healing of diabetic skin wounds by using nonviral gene therapy based on minicircle vascular endothelial growth factor DNA and a cationic dendrimer. *The journal of gene medicine*, 14, 272-8.
- LÁZÁR-MOLNÁR, E., HEGYESI, H., TÓTH, S. & FALUS, A. 2000. Autocrine and paracrine regulation by cytokines and growth factors in melanoma. *Cytokine*, 12, 547-54.
- LIN, R. Y., SULLIVAN, K. M., ARGENTA, P. A., MEULI, M., LORENZ, H. P. & ADZICK, N. S. 1995. Exogenous transforming growth factor-beta amplifies its own expression and induces scar formation in a model of human fetal skin repair. *Annals of surgery*, 222, 146-54.
- LIU, J. P., BAKER, J., PERKINS, A. S., ROBERTSON, E. J. & EFSTRATIADIS, A. 1993. Mice carrying null mutations of the genes encoding insulin-like growth factor I (Igf-1) and type 1 IGF receptor (Igf1r). *Cell*, 75, 59-72.
- LIU, S., ZHANG, H., ZHANG, X., LU, W., HUANG, X., XIE, H., ZHOU, J., WANG, W., ZHANG, Y., LIU, Y., DENG, Z. & JIN, Y. 2011. Synergistic angiogenesis promoting effects of extracellular matrix scaffolds and adipose-derived stem cells during wound repair. *Tissue engineering. Part A*, 17, 725-39.
- MARCHESE, C., CHEDID, M., DIRSCH, O. R., CSAKY, K. G., SANTANELLI, F., LATINI, C., LAROCHELLE, W. J., TORRISI, M. R. & AARONSON, S. A. 1995. Modulation of keratinocyte growth factor and its receptor in reepithelializing human skin. *The Journal of experimental medicine*, 182, 1369-76.
- MORIHARA, K., TAKENAKA, H., MORIHARA, T. & KISHIMOTO, S. 2007. Primary cutaneous anaplastic large cell lymphoma associated with vascular endothelial growth factor arising from a burn scar. *Journal of the American Academy of Dermatology*, 57, S103-5.
- MUELLER, R. V., HUNT, T. K., TOKUNAGA, A. & SPENCER, E. M. 1994. The effect of insulinlike growth factor I on wound healing variables and macrophages in rats. *Archives of surgery (Chicago, Ill. : 1960)*, 129, 262-5.
- MURPHY, K. E., HALL, C. L., MCCUE, S. W. & SEAN MCELWAIN, D. L. 2011. A two-compartment mechanochemical model of the roles of transforming growth factor  $\beta$  and tissue tension in dermal wound healing. *Journal of theoretical biology*, 272, 145-59.
- NISSEN, N. N., GAMELLI, R. L., POLVERINI, P. J. & DIPIETRO, L. A. 2003. Differential angiogenic and proliferative activity of surgical and burn wound fluids. *The Journal of trauma*, 54, 1205-10; discussion 11.

PENG, C., HE, Q. & LUO, C. 2011. Lack of keratinocyte growth factor retards angiogenesis in cutaneous wounds. *The Journal of international medical research*, 39, 416-23.

RAJKUMAR, V. S., SHIWEN, X., BOSTROM, M., LEONI, P., MUDDLE, J., IVARSSON, M., GERDIN, B., DENTON, C. P., BOU-GHARIOS, G., BLACK, C. M. & ABRAHAM, D. J. 2006. Platelet-derived growth factor-beta receptor activation is essential for fibroblast and pericyte recruitment during cutaneous wound healing. *The American journal of pathology*, 169, 2254-65.

RUSTAD, K. C., WONG, V. W., SORKIN, M., GLOTZBACH, J. P., MAJOR, M. R., RAJADAS, J., LONGAKER, M. T. & GURTNER, G. C. 2012. Enhancement of mesenchymal stem cell angiogenic capacity and stemness by a biomimetic hydrogel scaffold. *Biomaterials*, 33, 80-90.

SCHÄFER, M. & WERNER, S. 2008. Cancer as an overhealing wound: an old hypothesis revisited. *Nature reviews. Molecular cell biology*, 9, 628-38.

SCHMID, P., ITIN, P., CHERRY, G., BI, C. & COX, D. A. 1998. Enhanced expression of transforming growth factor-beta type I and type II receptors in wound granulation tissue and hypertrophic scar. *The American journal of pathology*, 152, 485-93.

SEDAGHATI, T., JELL, G. & SEIFALIAN, A. 2014. Investigation of Schwann cell behaviour on RGD-functionalised bioabsorbable nanocomposite for peripheral nerve regeneration. *New biotechnology*.

SEMENOVA, E., KOEGEL, H., HASSE, S., KLATTE, J. E., SLONIMSKY, E., BILBAO, D., PAUS, R., WERNER, S. & ROSENTHAL, N. 2008. Overexpression of mIGF-1 in keratinocytes improves wound healing and accelerates hair follicle formation and cycling in mice. *The American journal of pathology*, 173, 1295-310.

SHAH, M., FOREMAN, D. M. & FERGUSON, M. W. 1995. Neutralisation of TGF-beta 1 and TGF-beta 2 or exogenous addition of TGF-beta 3 to cutaneous rat wounds reduces scarring. *Journal of cell science*, 108 ( Pt 3, 985-1002.

SHEVCHENKO, R. V., JAMES, S. L. & JAMES, S. E. 2010. A review of tissue-engineered skin bioconstructs available for skin reconstruction. *Journal of the Royal Society, Interface / the Royal Society*, 7, 229-58.

SPIELBERGER, R., STIFF, P., BENSINGER, W., GENTILE, T., WEISDORF, D., KEWALRAMANI, T., SHEA, T., YANOVICH, S., HANSEN, K., NOGA, S., MCCARTY, J., LEMAISTRE, C. F., SUNG, E. C., BLAZAR, B. R., ELHARDT, D., CHEN, M.-G. & EMMANOUILIDES, C. 2004. Palifermin for oral mucositis after intensive therapy for hematologic cancers. *The New England journal of medicine*, 351, 2590-8.

SPIES, M., NESIC, O., BARROW, R. E., PEREZ-POLO, J. R. & HERNDON, D. N. 2001. Liposomal IGF-1 gene transfer modulates pro- and anti-inflammatory cytokine mRNA expression in the burn wound. *Gene therapy*, 8, 1409-15.

STAIANO-COICO, L., KRUEGER, J. G., RUBIN, J. S., D'LIMI, S., VALLAT, V. P., VALENTINO, L., FAHEY, T., HAWES, A., KINGSTON, G. & MADDEN, M. R. 1993. Human keratinocyte growth factor effects in a porcine model of epidermal wound healing. *The Journal of experimental medicine*, 178, 865-78.

TANAKA, A., NAGATE, T. & MATSUDA, H. 2005. Acceleration of wound healing by gelatin film dressings with epidermal growth factor. *The Journal of veterinary medical science / the Japanese Society of Veterinary Science*, 67, 909-13.

THISSE, B. & THISSE, C. 2005. Functions and regulations of fibroblast growth factor signaling during embryonic development. *Developmental biology*, 287, 390-402.

THROM, A. M., LIU, W.-C., LOCK, C.-H. & BILLIAR, K. L. 2010. Development of a cell-derived matrix: effects of epidermal growth factor in chemically defined culture. *Journal of biomedical materials research. Part A*, 92, 533-41.



TOMASEK, J. J., GABBIANI, G., HINZ, B., CHAPONNIER, C. & BROWN, R. A. 2002. Myofibroblasts and mechano-regulation of connective tissue remodelling. *Nature reviews. Molecular cell biology*, 3, 349-63.

TREMBLAY, P.-L., HUDON, V., BERTHOD, F., GERMAIN, L. & AUGER, F. A. 2005. Inosculation of tissue-engineered capillaries with the host's vasculature in a reconstructed skin transplanted on mice. *American journal of transplantation : official journal of the American Society of Transplantation and the American Society of Transplant Surgeons*, 5, 1002-10.

UHL, E., RÖSKEN, F., SIRSIÖ, A. & MESSMER, K. Influence of platelet-derived growth factor on microcirculation during normal and impaired wound healing. *Wound repair and regeneration : official publication of the Wound Healing Society [and] the European Tissue Repair Society*, 11, 361-7.

ULUBAYRAM, K., NUR CAKAR, A., KORKUSUZ, P., ERTAN, C. & HASIRCI, N. 2001. EGF containing gelatin-based wound dressings. *Biomaterials*, 22, 1345-56.

UNEMORI, E. N., FERRARA, N., BAUER, E. A. & AMENTO, E. P. 1992. Vascular endothelial growth factor induces interstitial collagenase expression in human endothelial cells. *Journal of cellular physiology*, 153, 557-62.

WAGNER, J., KEAN, T., YOUNG, R., DENNIS, J. E. & CAPLAN, A. I. 2009. Optimizing mesenchymal stem cell-based therapeutics. *Current opinion in biotechnology*, 20, 531-6.

WERNER, S., BREEDEN, M., HÜBNER, G., GREENHALGH, D. G. & LONGAKER, M. T. 1994. Induction of keratinocyte growth factor expression is reduced and delayed during wound healing in the genetically diabetic mouse. *The Journal of investigative dermatology*, 103, 469-73.

WISE, L. M., INDER, M. K., REAL, N. C., STUART, G. S., FLEMING, S. B. & MERCER, A. A. 2012. The vascular endothelial growth factor (VEGF)-E encoded by orf virus regulates keratinocyte proliferation and migration and promotes epidermal regeneration. *Cellular microbiology*.

WONG, V. W., RUSTAD, K. C., GALVEZ, M. G., NEOFYTOU, E., NEOFYOTOU, E., GLOTZBACH, J. P., JANUSZYK, M., MAJOR, M. R., SORKIN, M., LONGAKER, M. T., RAJADAS, J. & GURTNER, G. C. 2011. Engineered pullulan-collagen composite dermal hydrogels improve early cutaneous wound healing. *Tissue engineering. Part A*, 17, 631-44.

WOOD, F. M., KOLYBABA, M. L. & ALLEN, P. 2006. The use of cultured epithelial autograft in the treatment of major burn injuries: a critical review of the literature. *Burns : journal of the International Society for Burn Injuries*, 32, 395-401.

WU, H., SUZUKI, T., CAREY, B., TRAPNELL, B. C. & MCCORMACK, F. X. 2011. Keratinocyte growth factor augments pulmonary innate immunity through epithelium-driven, GM-CSF-dependent paracrine activation of alveolar macrophages. *The Journal of biological chemistry*, 286, 14932-40.

WU, Y., CHEN, L., SCOTT, P. G. & TREDGET, E. E. 2007. Mesenchymal stem cells enhance wound healing through differentiation and angiogenesis. *Stem Cells*, 25, 2648-59.

YANG, Y., XIA, T., CHEN, F., WEI, W., LIU, C., HE, S. & LI, X. 2012. Electrospun fibers with plasmid bFGF polyplex loadings promote skin wound healing in diabetic rats. *Molecular pharmaceuticals*, 9, 48-58.

YAZBECK, R., HOWARTH, G. S., BORGES, L., GEIER, M. S., SMITH, C. L., DAVIDSON, G. P. & BUTLER, R. N. 2011. Non-invasive detection of a palifermin-mediated adaptive response following chemotherapy-induced damage to the distal small intestine of rats. *Cancer biology & therapy*, 12, 399-406.

YEUNG, C.-K., MA, S.-Y., CHAN, H. H.-L., TRENDELL-SMITH, N. J. & AU, W. Y. 2004. Primary CD30+ve cutaneous T-cell lymphoma associated with chronic burn injury in a

patient with longstanding psoriasis. *The American Journal of dermatopathology*, 26, 394-6.

YILDIRIMER, L., THANH, N. T. K., LOIZIDOU, M. & SEIFALIAN, A. M. 2011. Toxicology and clinical potential of nanoparticles. *Nano Today*, 6, 585-607.

ZHOU, Y., YAN, Z., ZHANG, H., LU, W., LIU, S., HUANG, X., LUO, H. & JIN, Y. 2011.

Expansion and delivery of adipose-derived mesenchymal stem cells on three microcarriers for soft tissue regeneration. *Tissue engineering. Part A*, 17, 2981-97.

# 4 SYNTHESIS AND CHARACTERIZATION OF BIODEGRADABLE POSS NANOCOMPOSITE POLY( $\epsilon$ -CAPROLACTONE UREA)URETHANE (POSS-PCLU)

---

## 4.1 SYNOPSIS

The field of tissue engineering and regenerative medicine aims to create biocompatible scaffolds capable of supporting cell attachment and proliferation whilst providing a 3D structural framework for the wound bed. Natural polymers such as collagen, whilst excellent in terms of cytocompatibility, are known to exhibit relatively weak mechanical properties and rapid degradation profiles. Synthetic polymers, on the other hand, provide excellent control over rates of degradation and display superior mechanical strength. It has been hypothesized that hard segment contents influence the degradability of PUs. Here, a novel biodegradable PU based on a poly( $\epsilon$ -caprolactone urea)urethane (PCLU) backbone integrated with polyhedral oligomeric silsesquioxane (POSS) nanoparticles was synthesized. Percentage variations of hard segment content resulted in 3 different formulations. The relationship between increasing hard segment content and material properties was systematically assessed.  $^1\text{H}$  nuclear magnetic resonance ( $^1\text{H}$  NMR) and attenuated total reflectance-Fourier transform infrared spectroscopy (ATR-FTIR) confirmed the molecular structure of POSS-PCLU. Increasing hard segment contents were reflected in increasing peaks at  $1551\text{ cm}^{-1}$  and  $1633\text{ cm}^{-1}$  which corresponded to the hard segment urethane and urea groups, respectively. Both differential scanning calorimetry (DSC) and X-ray crystallography (XRD) results demonstrated the mostly amorphous nature of POSS-PCLU which predictably was not

affected by the hard segment contents. Mechanical strength, however, increased with increasing hard segment without affecting the general viscoelasticity of the PU. Surface analysis with scanning electron (SEM) and atomic force microscopy (AFM) revealed a highly micro- and nano-structured topography which was mainly attributed to the inclusion of POSS nanoparticles. Despite less favourable cell interactions on POSS-PCLU scaffolds as opposed to PCLU scaffolds, POSS is believed to have significant anti-inflammatory properties important for *in vivo* applications.

## 4.2 INTRODUCTION

At all times, tangible materials have been the subject of profound curiosity for humankind. Pre-Socratic thinkers including Thales (ca. 624-546 BC), Anaximenes (died ca. 525 BC) and Heraclitus (ca. 535-475 BC) speculated about the fundamental elemental origins of the visible world and were amongst the first to contemplate water, air and fire, respectively, as the basic building blocks constituting every aspect of life and nature while Empedocles (ca. 495-435 BC) first highlighted the importance of interaction of the, now 4 elements, including earth. The particular importance of materials is further emphasized within the realms of archaeological classifications of ancient, pre-historic eras; the Stone Age, Bronze Age and Iron Age were each named after the prevailing hard material for the manufacture of basic implements and tools of each specific era (Rogers and Semaw, 2009). More recently, man-made entities including polymers have gained substantial scientific recognition, being one of the most versatile and heavily exploited materials in daily use. Whilst reinforcement of such materials at the microscale (microcomposites) has already been shown to improve mechanical properties, integrating the polymer with nano-dimensional particles (nanocomposites) is postulated to have characteristics unanticipated by conventional laws of physics due to the quantum confinement effect (Kannan et al., 2005b) which maintains that the band gap width, which determines the energy needed to promote an electron from the valence to the conduction band and thus is proportional to the potential energy which can be emitted on the electron's return to the valence band, is inversely proportional to the particle's size. This quantum phenomenon underlies the principle that when a certain size (usually  $< 10$  nm) is reached, energy levels exist not in continuous states but in discrete quanta, thus supporting the theorem of size-dependency. This concept of dimensional dependence further includes the physical arrangement of the material, i.e. its shape (Scholes and Rumbles, 2006).

In our laboratories, we have developed a novel biodegradable nanocomposite polymer based on a poly( $\epsilon$ -caprolactone urea)urethane (PCLU) backbone integrated with the silica nanoparticle polyhedral oligomeric silsesquioxane (POSS). POSS being the smallest of the silica nanoparticles with a mean diameter of 1.5 nm is believed to confer significant size-dependent advantages to any polymer system it may be introduced to. This has already been demonstrated with the non-biodegradable version of our nanocomposite polymer POSS-incorporated poly(carbonate urea)urethane (PCU) which has been transplanted into human patients during several compassionate cases in the forms of vascular bypass grafts, lacrimal drainage tubes and tracheal replacement scaffolds (Chaloupka et al., 2011, Jungebluth et al., 2011a). However, prior to being introduced to a clinical setting, biomaterials – particularly biodegradable ones – must undergo stringent quality control assessments ranging from surface property evaluations over determining their chemical composition to higher order structures such as glass transition temperatures, degree of crystallinity and mechanical properties. Following material characterization, *in vitro* and *in vivo* compatibility tests provide basic information regarding clinical suitability (Fig. 4.1).

In the following sections, the techniques used in this thesis to evaluate the novel polymer POSS-PCLU will be explained briefly following which the methods will be introduced. In subsequent chapters, recurring methods will be referred back to chapter 4 unless otherwise stated.

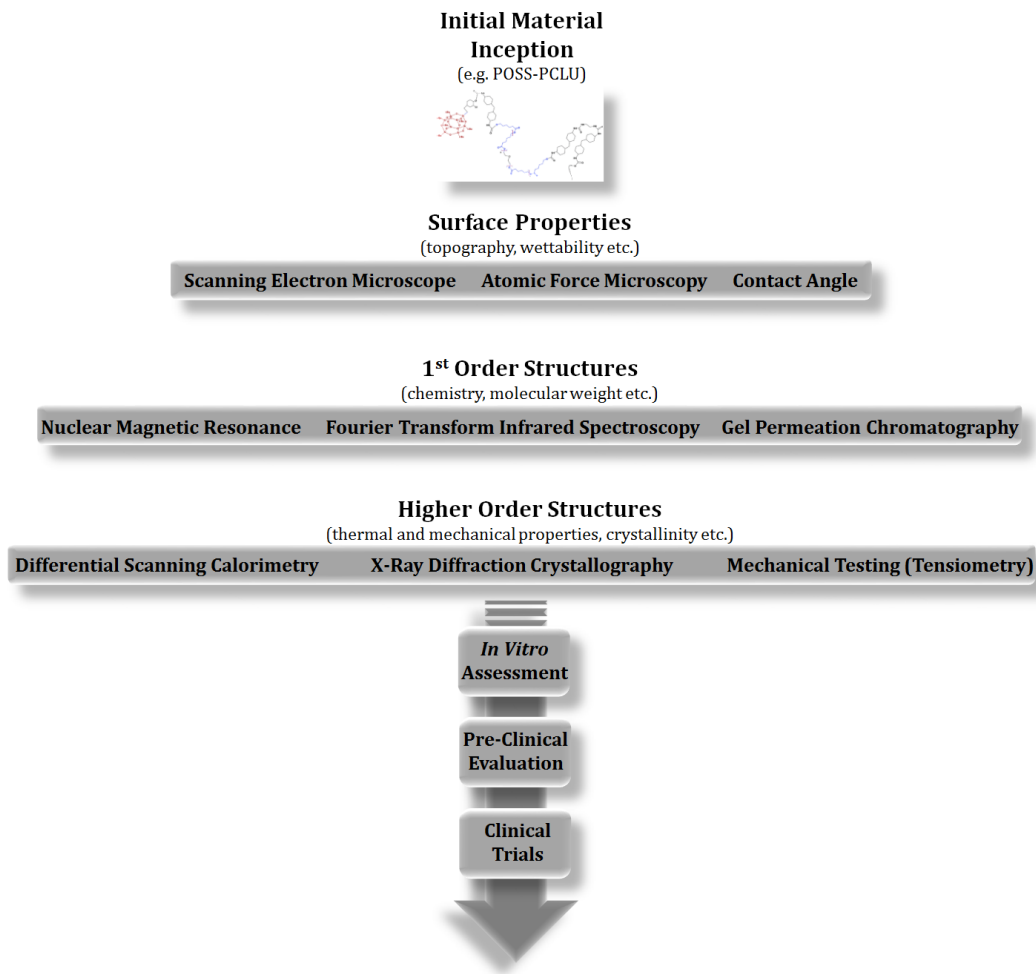


**Figure 4.1.** Diagrammatic illustration of the evaluation pathway for novel tissue engineering biomaterials.

*Scanning electron microscopy (SEM).* This type of microscope utilises a focused beam of electrons which scans the sample surface to produce highly magnified images of the sample. The obtained signals result from interactions of the electron beam with atoms at or near the sample surface. This enables mapping of the surface topography with resolutions as high as or even better than one nanometre. For non-conducting samples such as POSS-PCLU, an ultra-thin layer of gold is sputter-coated onto the mounted specimen as otherwise scanning faults, unsatisfactory signals and other artefacts may disrupt the image.

*Atomic force microscopy (AFM).* AFM has even better resolution than SEM in the order of fractions of a nanometre. This is particularly useful in assessing the degree of POSS-extrusion onto the polymers surface, e.g. following different types of sterilization treatments (chapter 5). Essentially, a cantilevered tip with a feedback mechanism is used to scan the sample surface. Being in extreme proximity to the sample surface results in interaction between the tip and the surface which in turn deflects the cantilever. The AFM measures this deflection and a 2-dimensional spatial map of the surface nanotopography is created.

*Contact angle measurement ( $\theta$ ).* The degree of biomaterial surface wettability is an important feature in the initial design and conception of a polymer system considering cell adhesion and proliferation are significantly influenced by it. Strongly hydrophobic ( $\geq 90^\circ$ ) surfaces result in strong protein adsorption onto such surfaces which leads to a loss in biological activity (de Mel et al., 2013, Tan et al., 2013, Tashnizi et al., 2013, Madani et al., 2013), associated inhibition of integrin binding (Shoae-Hassani et al., 2013a) and less cell-surface interaction. Several studies have demonstrated a contact angle between  $70^\circ$  and  $80^\circ$  to be optimal for fibroblast growth and proliferation (Shoae-Hassani et al., 2013b, Guasti et al., 2013).

*$^1H$  Nuclear Magnetic Resonance Spectroscopy ( $^1H$  NMR).* NMR is used to determine the molecular structure of organic compounds. Just as electrons have a  $+1/2$  and  $-1/2$  spin, certain atomic nuclei also have charged spins that create a magnetic field. Upon application of an external magnetic field, the nuclei orient themselves parallel ( $\alpha$ ) or antiparallel ( $\beta$ ) to the applied field. With the  $\alpha$ -spin having a lower energy state than the  $\beta$ -spin, the energy difference ( $\Delta E$ ) between those two spins depends on the applied magnetic field.



*Attenuated total reflectance-Fourier transform infrared spectroscopy (ATR-FTIR).*

FTIR spectra provide information about what molecules are present in the sample, whether or not two samples are the same and what concentrations of molecules are contained within the sample. The latter may be determined via the absorbance measured using FTIR. Using Beer's Law,

$$A = \epsilon lc$$

where A = absorbance,  $\epsilon$  = absorptivity, l = path length, and c = concentration, the height or area of a peak in the absorbance spectrum correlates to the concentrations and can thus be used to determine molecular concentrations. The use of ATR over transmission-IR spectroscopy alone is advantageous due to the limited path length into the sample required in ATR mode which avoids strong attenuation of the IR signal when travelling through a highly absorbing specimen.

*Gel permeation chromatography (GPC).* GPC is a molecular separation technique which uses columns packed with small, round and porous particles to separate molecules based on their size. The more association the molecule has with the stationary phase, the longer it takes to leave the column. Smaller molecules able to occupy most of the particles' pores are thus associated with them for longer whilst the largest molecules do not fit into any pores and thus elute first. Medium-sized molecules, on the other hand, fit into some pores but not all and thus occupy only some whilst a fraction of medium-weight molecules elute out. GPC is further used to determine molecular weight distributions of polymers. On a typical weight-distribution curve, the number average molecular weight ( $M_n$ ) marks the value at which there are equal numbers of higher and lower molecular weight molecules on each side. The importance of molecular weight values lies in the fact that they influence polymer properties including brittleness, toughness and elasticity.

*Differential scanning calorimetry (DSC).* DSC is used to detect changes in polymer phase transition temperatures including glass transition ( $T_g$ ) and melting temperature  $T_m$ . During polymer degradation, the detected  $T_g$  increases while  $T_m$  is lowered, providing an indication for the relative degree of degradation when comparing different polymers. Additionally, degradation of semicrystalline polymers such as POSS-PCLU results in phase separation of the amorphous and crystalline regions which, again, lead to changes in transition temperatures.

*X-ray diffraction crystallography (XRD).* XRD crystallography exploits the ability of crystalline substances to interact with X-rays resulting in a unique and reproducible diffraction pattern. It is a qualitative as well as quantitative method of identifying and characterising crystalline or semicrystalline polymers. It is a particularly useful tool for analysing degraded polymers as phase separation and crystallization induce changes in the XRD pattern.

*Tensiometry.* Assessment of mechanical properties remains a mainstay of polymer characterization. Evaluation of material toughness and elasticity being of particular importance for implantable devices such as tissue engineering scaffolds due to different properties being required for different applications.

## **4.3 MATERIALS AND METHODS**

### **4.3.1 Polymer Synthesis**

The polymer was prepared according to a previously published method (Kannan et al., 2006a). In brief, dry polycaprolactone diol ( $M_w$  2000) and *trans*-cyclohexanechloroydrinisobutyl-POSS were placed in a reaction flask equipped with a mechanical stirrer and nitrogen inlet. The mixture was heated to 135 °C to dissolve the

POSS nanocage and then cooled to 60 °C. To this, dicyclohexylmethane diisocyanate (Desmodur W, Bayer) was added and reacted under nitrogen at 70 °C for 90 minutes (min) to form a pre-polymer. Then, N,N-dimethylacetamide (DMAc) was added and the mixture cooled to 40 °C. A mixture of ethylenediamine and diethylamine in DMAc was added to allow chain extension of the pre-polymer. 1-Butanol in DMAc was added to the mixture to form an 18 % polyhedral oligomeric silsesquioxane-poly( $\epsilon$ -caprolactone urea)urethane (POSS-PCLU) solution. Polymers of three different percentage hard segments were synthesized by varying the amount of dicyclohexylmethane diisocyanate to obtain PUs of 24 %, 28 %, and 33 % hard segment. A control lacking POSS nanoparticles was synthesized to analyse the influence of silica nanoparticles on (i) *in vitro* cytocompatibility, (ii) *in vivo* biocompatibility, and (ii) any potential inhibitory effect of POSS nanoparticles on degradation. The polymer nomenclature was based on their main constituents and the weight percentage hard segment, as POSS-PCLU-24, POSS-PCLU-28, POSS-PCLU-33, and PCLU-24. All chemicals and reagents were purchased from Sigma Aldrich Ltd. (Gillingham, UK). Figures 4.2 and 4.3 schematically summarise the reaction steps and the composition is defined in Table 4.1.

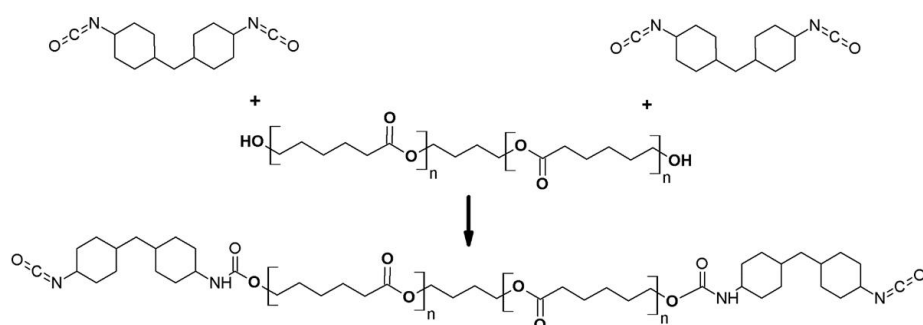


**Figure 4.2.** Synthesis of the aliphatic poly( $\epsilon$ -caprolactone urea)urethane prepolymer in a 2:1 ratio of 4,4'-methylenebis (cyclohexylisocyanate) to poly( $\epsilon$ -caprolactone)diol.

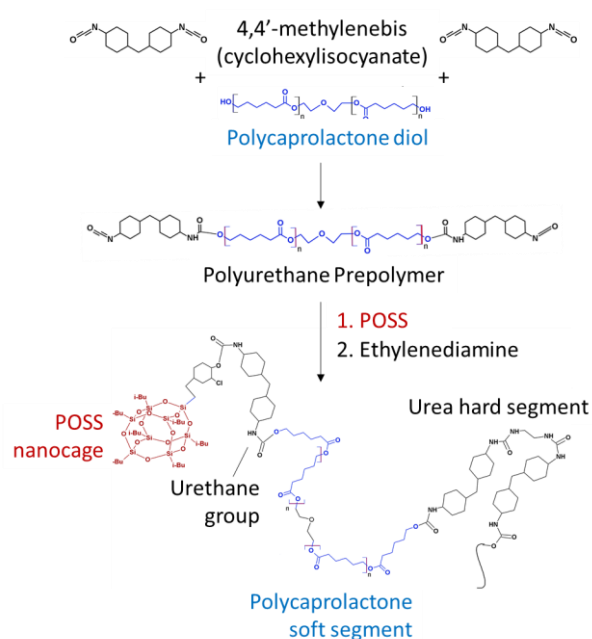


**Figure 4.3.** Chain extension reaction of the poly( $\epsilon$ -caprolactone urea)urethane prepolymer with ethylenediamine and integration of POSS nanoparticles as endcapped pendant chains. The final segmented PU consists of urea hard segments linked to PCL soft segment by urethane bonds.

**Table 4.1.** Composition of the 4 different PUs.

Material	POSS content (%)	Diisocyanate (%)	Polyol	Chain extender
PCLU-24	0	HMDI (24 %)	1-Butanol	Ethylenediamine/diethylamine
POSS-PCLU-24	2	HMDI (24 %)	1-Butanol	Ethylenediamine/diethylamine
POSS-PCLU-28	2	HMDI (28 %)	1-Butanol	Ethylenediamine/diethylamine
POSS-PCLU-33	2	HMDI (33 %)	1-Butanol	Ethylenediamine/diethylamine

Key: POSS, polyhedral oligomeric silsesquioxane; PCLU, poly( $\epsilon$ -caprolactone urea)urethane; HMDI, dicyclohexylmethane diisocyanate

#### 4.3.2 Scaffold Fabrication

Samples were fabricated by either casting or coagulation/phase inversion method to obtain non-porous films or porous sponges, respectively. Cast sheets were prepared by pouring diluted 15 wt. % POSS-PCLU polymer solution (~ 8 g) into a clean Petri dish ( $\approx$  10 cm) and allowing solvent evaporation overnight at constant temperature (65 °C).

Coagulated scaffolds were prepared by a sacrificial porogen leaching technique combined with a phase inversion coagulation method. The polymer solution was supplemented with 48 % (w/v) sodium bicarbonate ( $\text{NaHCO}_3$ ) particles (Brunner Mond, Cheshire, UK) and surfactant (Tween 20) to obtain a viscous slurry. This was poured over a surface modified stainless steel plate. Top surface modification was applied to avoid skin formation and increase percentage porosity. The polymer mixture was then extruded according to a protocol developed in-house. Overnight extrusion in sterile de-ionized water resulted in solvent exchange and  $\text{NaHCO}_3$  leaching and the fabrication of porous scaffolds. Washing over a period of 48 h using regular changes of sterile de-ionized water completely removed all remaining salt particles and DMAc, as confirmed by inductively coupled plasma optical emission spectrometry (Warwick Analytical Services, Coventry, UK).

#### **4.3.3 Scaffold Surface Modification**

Three distinct methods were evaluated to prevent an impermeable skin layer forming on the side facing the stainless steel plate. The aim was to obtain a uniformly porous and interconnected scaffold surface.

##### ***4.3.3.1 Different Porogen Sizes***

$\text{NaHCO}_3$  particles of two different diameters (65  $\mu\text{m}$  vs. 140  $\mu\text{m}$ ) were selected and scaffolds were fabricated as per section 4.3.2.

##### ***4.3.3.2 Pre-Modification of Stainless Steel Plates***

Stainless steel plates used for scaffold fabrication were pre-treated with a solution containing an excess of porogen particles. Evaporation of the liquid phase at 60 °C resulted in a rugged plate surface onto which the polymer mixture was poured.

#### 4.3.4 Scaffold Characterization

##### 4.3.4.1 Surface Structure Analysis

###### 4.3.4.1.1 Scanning Electron Microscopy

Microscopic scaffold features were evaluated using SEM digital photography at magnifications ranging from x 40 to x 1000. Cast or coagulated scaffolds were dried and post-fixed with 1% osmium tetroxide/1.5 % potassium ferricyanide for 1 h, unless otherwise stated. Scaffolds were then washed with de-ionised water and dehydrated using graded acetone series, unless otherwise stated. They were then mounted on aluminium stubs and sputter-coated with gold using an SC500 (EMScope) for electrical conductance. Photographs were taken using a Philips 501 scanning electron microscope. ImageJ (freeware) was used to analyse the specified parameters.

###### 4.3.4.1.2 Atomic Force Microscopy (AFM)

Surface nanotopographies of cast polymer samples were measured using a non-contact mode atomic force microscope (AFM, Bruker Dimensions 3100). Evaluation of the average surface roughness ( $R_a$ ), root mean square roughness ( $R_q$ ), and correlation length ( $\xi$ ) were carried out on a surface area of 20 x 20  $\mu\text{m}$  using Nanoscope Analysis software (Bruker Corporation, MA, USA). Commercially available AFM tips (radius of curvature 7 nm, PPP-NCH, Windsor Scientific) were used with intermediate contact mode.

###### 4.3.4.1.3 Hydrophobicity was assessed using Static Contact Angle Measurement ( $\theta$ )

Contact angle ( $\theta$ ) measurements were obtained using a goniometer (EasyDrop DSA20E, Kruss, Germany) equipped with a digital camera and image analysis software (DSA1 version 1.80, Kruss, Germany). De-ionized water (5  $\mu\text{L}$ ) was used as the wetting liquid which was deposited onto the samples using an automated syringe. Sessile drop method was used to analyse contact angles of the air-water-substrate interface of control

and sterilized cast samples which were measured three times in three samples of every group.

#### **4.3.4.2 First Order Structural Analysis**

##### 4.3.4.2.1 <sup>1</sup>H Nuclear Magnetic Resonance (NMR) Spectroscopy

The chemical structure and composition of all 4 PUs were determined by <sup>1</sup>H NMR spectroscopy using a Bruker AV 400 NMR spectrometer. The NMR spectrum was obtained at room temperature in deuterated dimethylformamide (DMF-*d*) (50 mg/mL) with tetramethylsilane (TMS) as an internal standard.

##### 4.3.4.2.2 Attenuated Total Reflectance (ATR) Fourier Transform Infrared (FTIR) Spectroscopy

Fourier Transform Infrared Spectra (FTIR) were obtained on a Jasco FT/IR 4200 Spectrometer equipped with a diamond attenuated total reflectance accessory (Diamond MIRacle ATR, Pike Technologies, US). A total number of 3 pieces per sterilization technique or control and 3 points on each scaffold were analysed. Spectra were produced from an average of 20 scans at 4 cm<sup>-1</sup> resolution over a range of 600 cm<sup>-1</sup> to 4000 cm<sup>-1</sup> wave numbers. A background scan was performed prior to each sample measurement.

##### 4.3.4.2.3 Gel Permeation Chromatography (GPC)

Average molecular weight of all 4 PUs was determined by gel permeation chromatography (GPC). The solvent phase was dimethylacetamide (DMAc) with 2 % LiBr serving as a stabiliser. The sample concentration was 2 mg/mL and the injection volume was 150 µL. The flow rate was set at 1 mL/min. The number and weight average molecular weights ( $M_n$  and  $M_w$ , respectively) were determined from the retention time using a calibration curve generated with polystyrene standards. The polydispersity index (PI) was obtained by  $M_w/M_n$ .

### 4.3.4.3 Higher Order Structural Analysis

#### 4.3.4.3.1 Differential Scanning Calorimetry (DSC)

A Q2000 DSC (TA instruments LLC) was used to study glass transition ( $T_g$ ), crystallization and melting behaviour of PUs. An indium standard ( $T_m = 156.6$  °C and  $\Delta H = 28.5$  J/g) was used to calibrate the instrument and ensure accuracy and reliability of the obtained data. Approximately 4-8 mg of polymer sample were loaded into aluminium Tzero pans and hermetically sealed. An empty aluminium pan, matched in weight to the sample pan, was used as a reference. Experiments were performed at heating rates of 10 °C/min from -80 °C to 200 °C for conventional DSC. Melting temperatures ( $T_m$ ) and heat of fusion ( $\Delta H$ ) were determined from DSC scans. Endothermic peak temperatures were taken as  $T_m$ , and percentage crystallinity was calculated using the following equation:

$$\% \text{ crystallinity} = \left( \frac{\Delta H_m}{\Delta H_{constant}} \right) \times 100\%$$

where  $\Delta H_m$  is the enthalpy of fusion of the sample and  $\Delta H_{constant}$  is the enthalpy of fusion of a 100 % crystalline PCL reference (136 J/g) (Crescenzi, V.; Manzini, G.; Calzolari, G.; Borri 1972; Heijkants et al. 2005).

#### 4.3.4.3.2 X-ray Diffraction (XRD) Crystallography

X-ray diffraction (XRD) data were recorded with a PW3830 (Philips, Netherlands) using a Cu K $\alpha$  X-ray source operated at 40 mA, 40 kV with an angular increment of 0.05°/s. Measurements were taken from 0 to 40° on the  $2\theta$  scale.

#### 4.3.4.3.3 Tensiometry

Tensile stress-strain properties were assessed according to British Standards (BS ISO 37:2005). Cast or coagulated POSS-PCLU samples were cut into dumbbell-shaped



pieces type 3 (shaft length 20 mm, width 4 mm, n=5) using a cutting press (Wallace Instruments, Surrey, UK). Thickness was measured using a digital electronic outside micrometer. Uniaxial tension was applied to either ends of the scaffolds until failure using an Instron-5565 tensile tester (Instron Ltd., Bucks, UK) equipped with a 500 N load, pneumatic grips with 1 kN capacity and at a rate of 100 mm/min. Bluehill software was used to analyse the scaffold's tensile strengths at room temperature. Stress (MPa) was calculated by dividing the force generated during stretching by the initial cross-sectional area. Strain was calculated as the ratio of the change in length in reference to the original sample length (%).

#### **4.3.5 Scaffold Cytocompatibility**

##### **4.3.5.1 Cell Culture**

Adult primary fibroblasts were isolated from human dermis (HDFa) and cultured in Dulbecco's Modified Eagle Medium (DMEM) supplemented with 1 mM L-glutamine, 10 % fetal bovine serum (FBS), 1 % penicillin/streptomycin and 1 % Fungizone (Invitrogen, Paisley, UK). HDFa were cultured to 80-90 % confluency, trypsinized and either re-plated or stored in 10 % DMSO/90 % FBS in liquid nitrogen until required.

A scratch test was conducted in order to qualitatively assess cellular proliferation. HDFa were seeded into 24-well plates in excess to obtain rapid confluency. The sterile sharp end of a plastic pipette tip was used to create a longitudinal scratch along the cell layer. Tips were changed each time a scratch was made to prevent cells from the previous well being laid down in the fresh scratch. At 0 hour (h), 24 h and 72 h, dead cells were stained with methylene blue and cell migration into the scratch path was observed using an inverted light microscope. Experiments were performed in triplicates.

The optimal cell seeding density was assessed over a period of 14 days. HDFa were seeded into 24-well plates at densities of  $2.5 \times 10^4$ ,  $3.75 \times 10^4$  and  $5 \times 10^4$  cells/cm<sup>2</sup>. Medium only wells served as controls. At 1, 3, 7 and 14 days, cell proliferative capacity was assessed using AlamarBlue® viability assay.

Next, viability and proliferation were assessed on cells cultured on cast PCLU films, cast POSS-PCLU films and coagulated POSS-PCLU scaffolds. HDFa cells were seeded onto DMEM pre-soaked POSS-PCLU scaffolds at a density of  $5 \times 10^4$  cells/150 µL/scaffold and incubated at 37 °C, 5 % CO<sub>2</sub> for 2 h. Then, 1 mL culture medium was added and cells were incubated for seven days. Previous tests determined 2 h sufficient for cell attachment (results not shown). A staggered seeding technique was utilized to ensure cell adhesion onto scaffolds rather than tissue culture plastic (TCP) (Noah et al., 2002). TCPs containing no scaffolds were seeded with an equal amount of cells (positive control) or medium only (negative control). Medium-soaked POSS-PCLU scaffolds not seeded with cells served as background noise which was subtracted from final results of cell-seeded scaffolds. Cells were incubated at 5 % CO<sub>2</sub> in air at 37 °C and culture medium was changed every 2-3 days for a total of 7 days.

In order to demonstrate the material's suitability as a tissue engineering platform, 3D porous scaffolds were seeded with HDFa at a density of  $5 \times 10^4$  cells/150 µL/scaffold and incubated at 37 °C, 5 % CO<sub>2</sub>.

On days 1, 3, and 7, cell morphology was visualised using the F-actin stain fluorescein isothiocyanate (FITC)-phalloidin and nuclei counterstained with Propidium Iodide (PI) (both Sigma-Aldrich, Dorset, UK). Cell viability and proliferative capacity were assessed using Live/Dead® stain and AlamarBlue® assay, respectively.

#### **4.3.5.2 Assessment of In Vitro Cytocompatibility and Cellular Proliferation using AlamarBlue® Cell Proliferation Assay**

Cell metabolism was assessed using AlamarBlue® assay (Invitrogen, Paisley, UK). HDFa were grown on cast or coagulated POSS-PCLU scaffolds and incubated for 1, 3 and 7 days. At each time point, media and non-adherent cells were removed with sterile phosphate buffered saline (PBS, 0.1 M, pH 7.4). AlamarBlue® solution in normal culture medium (ratio of 1:10) was added to each scaffold and incubated in 5 % CO<sub>2</sub> and 37 °C for 4 h. Fluorescent readings were recorded by Fluoroskan Ascent Fluorescence Microplate Reader (Thermo Scientific™, Hudson, US) with excitation at 530 nm and emission at 590 nm. Fluorescence readings for culture medium only were used for baseline corrections. Cell viability in terms of % of control cells grown on TCP is derived from the following equation (Mullick Chowdhury et al., 2013):

$$\% \text{ viability} = \frac{F_{test} - F_{blank}}{F_{control} - F_{blank}} \times 100$$

where  $F_{test}$  is the fluorescence of cells grown on test surfaces,  $F_{blank}$  is the fluorescence of medium only (no cells), and  $F_{control}$  is the fluorescence of cells grown on TCP.

#### **4.3.5.3 Live/Dead® Cell Survival Assay**

Cell viability on cast scaffolds was assessed at days 1, 3, and 7 using the Live/Dead® fluorescence assay (Invitrogen, Paisley, UK) according to the manufacturer's instructions and the number of attached live and uniformly green stained and non-viable/dead, pyknotic red cells was assessed immediately upon staining using an Eclipse C1 Plus Confocal microscope (Nikon, Surrey, UK) with a x 10 objective lens.

#### **4.3.5.4 Cytoskeletal Staining**

Cell attachment to cast scaffolds and their morphology were studied using FITC-labeled phalloidin according to the manufacturer's instructions. Cells grown on cast films

for 1, 3, and 7 days were fixed using 4% paraformaldehyde (PFA) in PBS, permeabilized with 0.1 % Triton-X 100 in PBS for 20 min and then blocked with 1 % bovine serum albumin (BSA) in PBS for 45 min. Cells were exposed to a 1:40 ratio FITC-phalloidin mixture in PBS supplemented with 0.1 % (w/v) BSA for 45 min for visualization of F-actin. Nuclei were counterstained using propidium iodide (PI) stain. Images were taken using an Eclipse C1 Plus Confocal microscope (Nikon, Surrey, UK) with a x 20 and x 40 objective lens.

#### **4.3.6 Statistical Analysis**

All data are presented as mean  $\pm$  standard deviation (SD). Experiments were repeated 6 times unless stated otherwise. Data comparisons were carried out by one-way ANOVA analysis of variance. Significant differences between experimental groups were determined using Bonferroni's test of multiple comparisons or Dunn's multiple comparison post-test in the case of surface roughness analysis. A *p*-value of  $< 0.05$  was considered statistically significant.

## **4.4 RESULTS AND DISCUSSION**

### **4.4.1 Synthesis and Molecular Characterization of POSS-PCLU Scaffolds**

The chemical structures of POSS-PCLU PUs were verified by  $^1\text{H}$  NMR and FTIR spectroscopy (Fig. 4.4 and 4.5). The chemical shift at 8.2 ppm was referred to the solvent peak of deuterated DMF. The signals at 4.1 ppm were attributed to the urethane linkage generated from the reaction between hydroxyl groups and isocyanate groups in HMDI ( $-\text{OH} + -\text{NCO} \rightarrow -\text{NHCOO}-$ ) (Li et al., 2012). The peaks at 3.9 ppm correspond to  $\text{CO-O-CH}_2$  in PCL diol (Nair and Ramesh, 2013), and the singlet at 3.64 ppm ( $\text{OCH}_2\text{CH}_2\text{O}$ ) is assigned to the diethyl ether bond linking the esters in PCL diol (Loh et al., 2008). The multiplet observed at 2.9 ppm ( $-\text{NH-CH}_2-$ ) relate to the secondary amines within the urea hard

segment (Sarkar et al., 2009). The multiplet at 1.6 ppm ( $\text{OCH}_2\text{CH}_2\text{CH}_2\text{CH}_2\text{CH}_2\text{CO}$ ) represents the PCL soft segment which corresponded to the hard segment content of the PUs. The integral value at 1.6 ppm of POSS-PCLU-24 with higher soft segment content was correspondingly higher compared to that of POSS-PCLU-33 (Fig. 4.4 inset box).

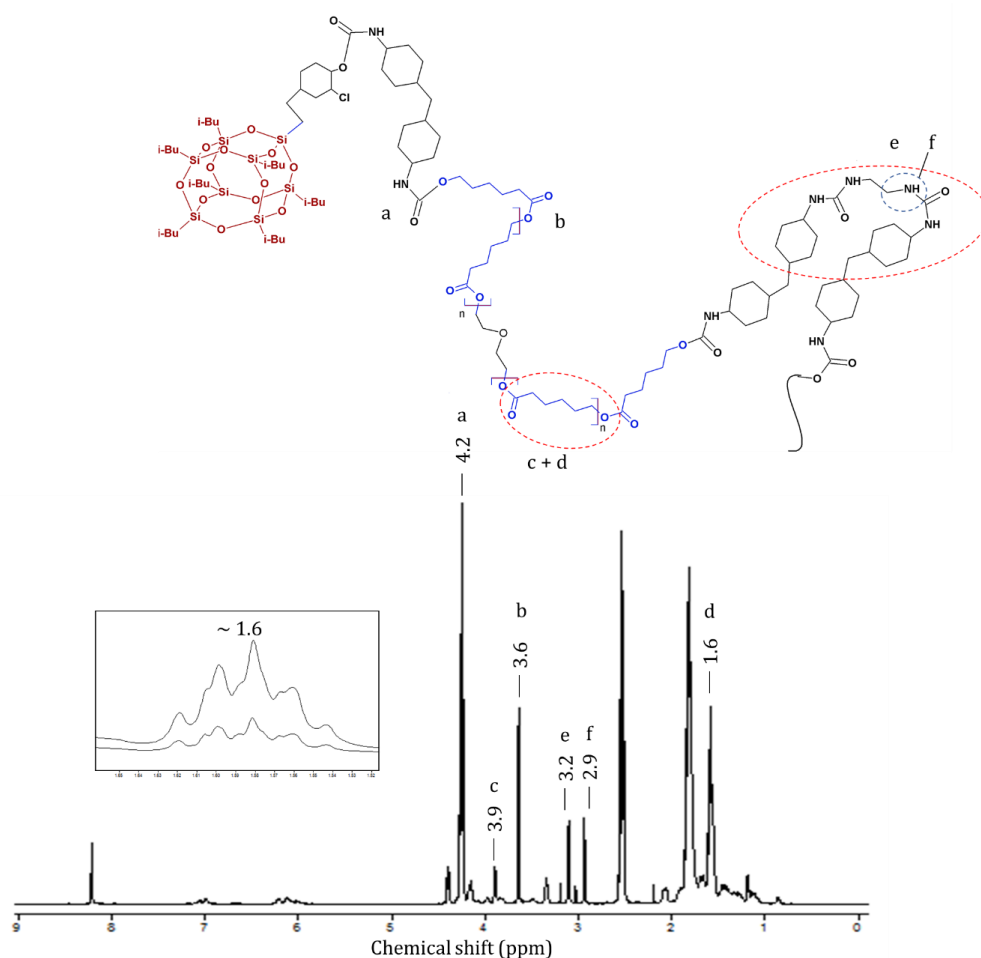


**Figure 4.4.**  $^1\text{H}$  nuclear magnetic resonance (NMR) spectrum of a representative POSS-PCLU PU. Inset is a magnification of the chemical shift at 1.6 ppm of POSS-PCLU-24 (top) and POSS-PCLU-33 (bottom).

Material surface chemistries of PCLU-24 and POSS-PCLU-24, POSS-PCLU-28 and POSS-PCLU-33 were analysed using attenuated total reflectance (ATR)-Fourier transform infrared (FTIR) spectroscopy and the spectra were overlaid for comparison (Fig. 4.5).

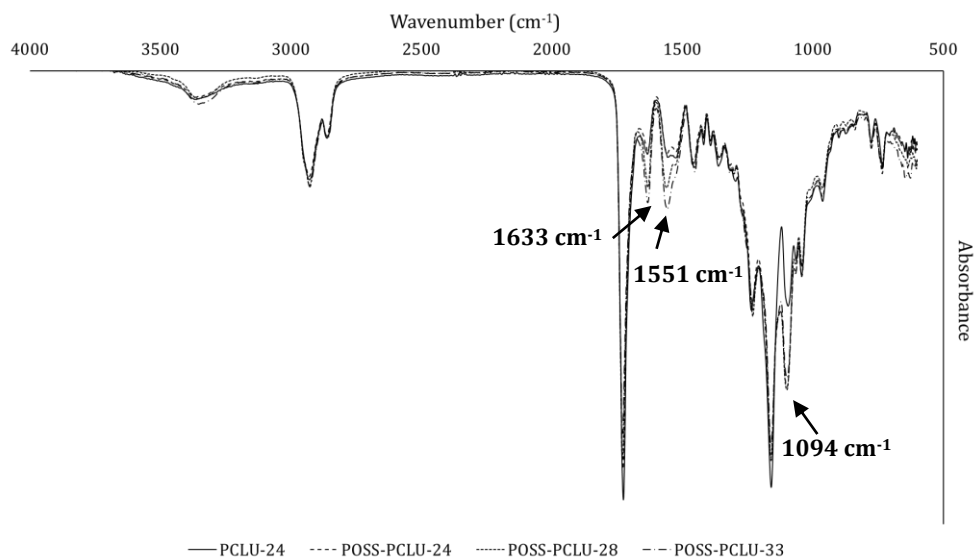


**Figure 4.5.** Overlaid attenuated total reflectance (ATR)-Fourier transform infrared (FTIR) spectrograph of cast PCLU-24, POSS-PCLU-24, POSS-PCLU-28 and POSS-PCLU-33 samples. Both urethane and urea groups at 1551  $\text{cm}^{-1}$  and 1633  $\text{cm}^{-1}$ , respectively, predictably increase with increasing hard segment content. The peak at 1094  $\text{cm}^{-1}$  represents the siloxane (Si-O-Si) bonds and is not present for PCLU-24 which lacks POSS nanoparticles.

All polymers exhibit common peaks at 2929  $\text{cm}^{-1}$  and 2861  $\text{cm}^{-1}$  which correspond to the alkyl groups of the hard segment, HDI. The peaks at 1726  $\text{cm}^{-1}$  and 1159  $\text{cm}^{-1}$  represent the carbonyl (C=O) region of non-hydrogen-bonded urethane and the ester (O-C-O) absorbance of the soft segment, respectively. The heights of the latter two peaks are negatively correlated with increasing hard segment content. In the case of the C=O bond of the non-hydrogen-bonded urethane bonds, the lower height with higher percentage hard segment is due to the fact that in high hard segment polymers, most urethane bonds are hydrogen-bonded, leaving a smaller fraction of urethane bonds non-bonded.

With increasing hard segment content, the spectral peaks corresponding to hydrogen-bonded urethane (1633  $\text{cm}^{-1}$ ) and urea (1551  $\text{cm}^{-1}$ ) bonds increase in height providing a qualitative measure of bond content. Both PCLU-24 and POSS-PCLU-24 containing the lowest amount of hard segment demonstrate relatively smaller peaks compared to the polymers of higher hard segment content. Similarly, polymers

containing POSS nanoparticles exhibit a high peak at around  $1094\text{ cm}^{-1}$  whilst PCLU-24 does not.

The molecular weight and distribution were analysed using GPC. Figure 4.6 illustrates a representative molecular weight distribution curve for the polymers.

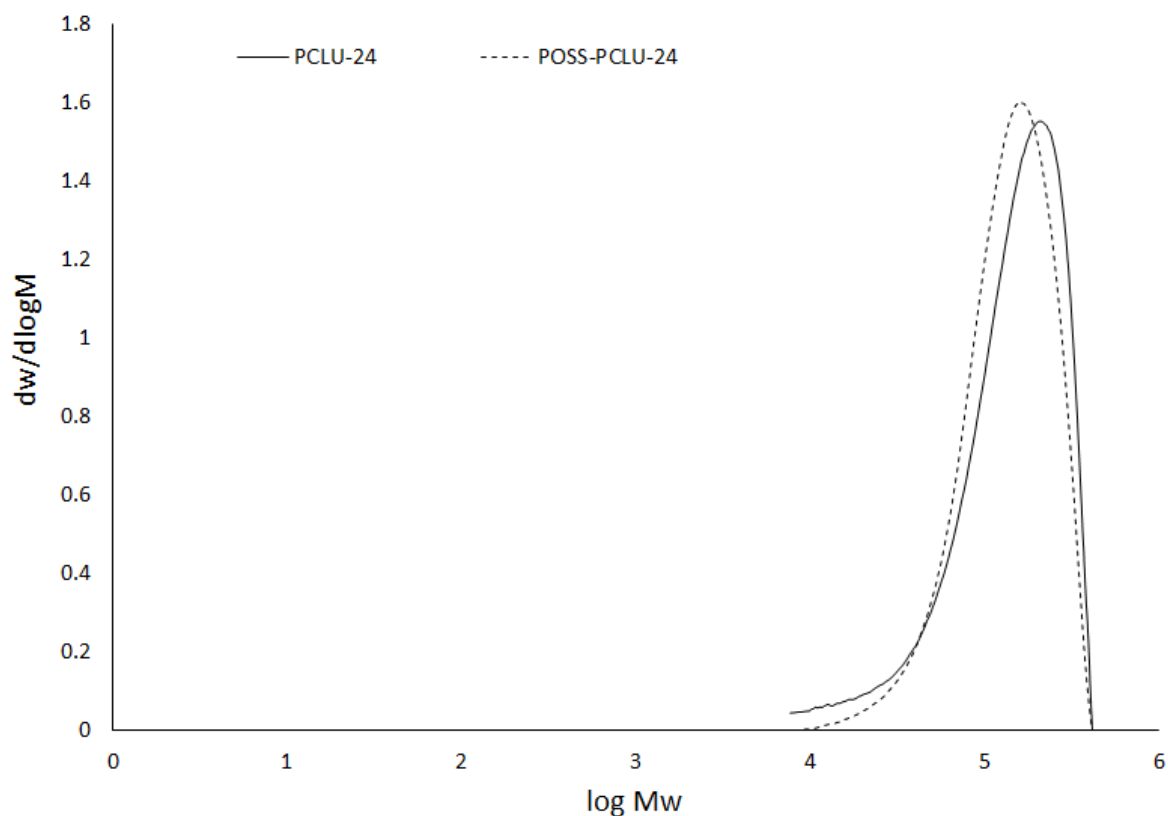


**Figure 4.6.** Representative molecular weight distribution curve of PCLU and POSS-PCLU polymer samples.

The symmetrical bell shape and narrow distribution demonstrate successful and complete polymerization. The molecular weights of the obtained PUs range from  $11.5 \times 10^4$  to  $11.9 \times 10^4$  g/mol with molecular weight distributions between 1.4 and 1.7. (Table 4.2).

**Table 4.2.** Composition, number average molecular weight ( $M_n$ ) and polydispersity indices (PDI) of PCLU and POSS-PCLU PUs.

Materials	$M_n$ ( $\times 10^4$ ) <sup>a</sup>	$M_w/M_n$ <sup>a</sup>
PCLU-24	11.5	1.7
POSS-PCLU-24	11.9	1.4
POSS-PCLU-28	-	-
POSS-PCLU-33	-	-

Key: POSS, polyhedral oligomeric silsesquioxane; PCLU, poly( $\epsilon$ -caprolactone urea)urethane

<sup>a</sup>  $M_n$  and  $M_w/M_n$  were determined by GPC. - = Values could not be obtained as samples did not dissolve in DMAc.

#### 4.4.2 Thermal Properties of POSS-PCLU Polyurethanes

The thermal properties of PCLU-24 and POSS-PCLU of varying hard segment content are summarised in Table 4.3.

**Table 4.3.** Thermal properties of POSS-PCLU PUs.

Material	$T_g$ ( $^{\circ}\text{C}$ ) <sup>a</sup>		$\chi$ (%) <sup>a</sup>
	Soft segment	Hard segment	
PCLU-24	- 54.8	51.1	-
POSS-PCLU-24	- 52.9	40.8	-
POSS-PCLU-28	- 55.4	52.6	-
POSS-PCLU-33	- 55.5	53.3	-

Key: POSS, polyhedral oligomeric silsesquioxane; PCLU, poly( $\epsilon$ -caprolactone urea)urethane

<sup>a</sup>  $T_g$  and  $\chi$  were determined by DSC

The DSC heating curves of the 4 different PUs all reveal a soft segment glass transition temperature ( $T_g$ ) between  $- 52.9$   $^{\circ}\text{C}$  to  $- 55.5$   $^{\circ}\text{C}$  and a hard segment  $T_g$  between  $+ 40.8$   $^{\circ}\text{C}$  and  $+ 53.3$   $^{\circ}\text{C}$  (Fig. 4.7).



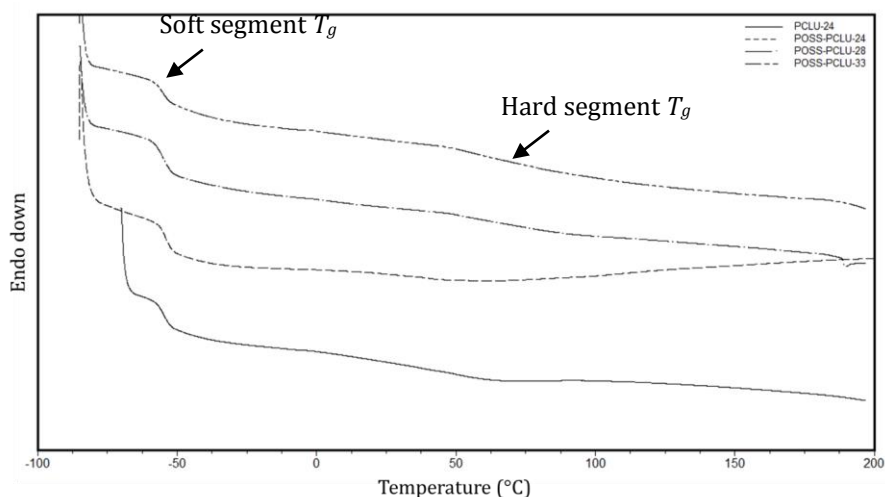


**Figure 4.7.** DSC heating curve of PCLU-24, POSS-PCLU-24, POSS-PCLU-28 and POSS-PCLU-33. Two distinct glass transitions,  $T_g$ s (soft segment) and  $T_g$ h (hard segment), can be seen.

In general, the soft segment  $T_g$  of both PCLU-24 and POSS-PCLU were independent of the hard segment content (24 %, 28 %, 33%) indicating limited hard segment mixing within the soft domain. The presence of  $T_g$  of both soft and hard segments alongside a lack of exothermic or endothermic peaks suggests a mostly amorphous polymer, hence no crystal formation was observed and percentage crystallinity was not calculated. This observation was supported by results obtained by XRD crystallography which is in accordance with previous reports (Bogdanov et al., 1999) (Fig. 4.8).

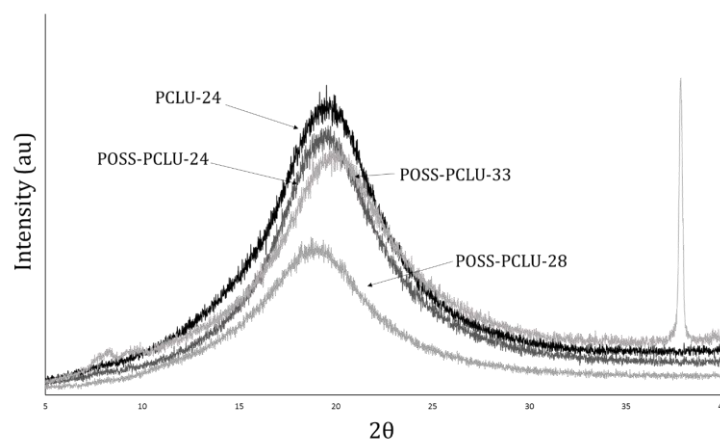


**Figure 4.8.** XRD pattern of non-degraded PU samples of varying hard segment contents.

#### 4.4.3 Microstructure and Surface Properties of POSS-PCLU Scaffolds

Scaffold micro- and nanotopographies were analysed using scanning electron microscopy (SEM), atomic force microscopy (AFM) and contact angle measurements. The SEM image of a salt-leached POSS-PCLU scaffold edge demonstrates a highly porous and interconnected microstructure with pore dimensions of approximately 140  $\mu\text{m}$  (Fig. 4.9 (A)).

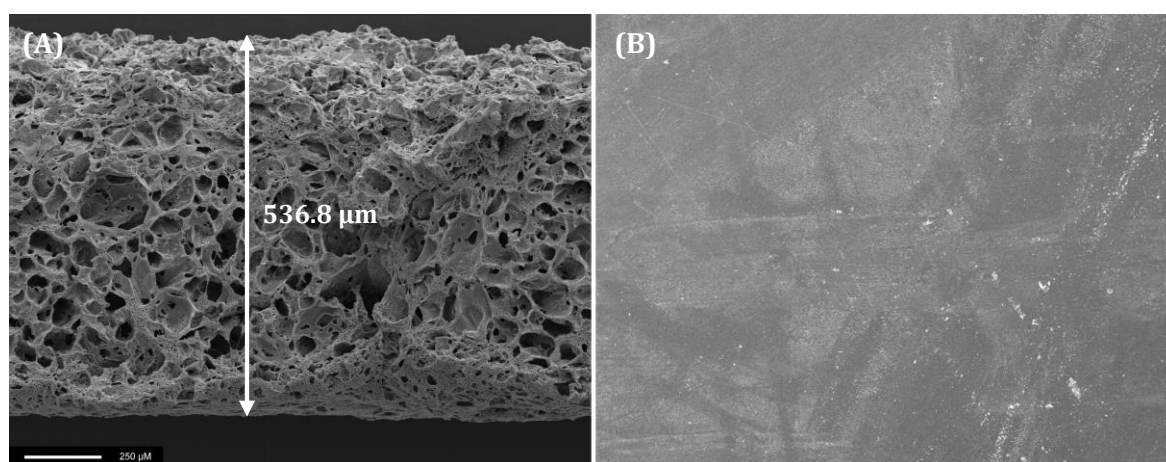


**Figure 4.9.** (A) Environmental scanning electron microscopy image of a salt-leached POSS-PCLU scaffold edge. Homogeneously distributed pores and high pore interconnectivity are important features for tissue engineering scaffolds to allow for diffusion of nutrients, waste and to promote the formation of a vascular network. (B) Top down view of a cast POSS-PCLU scaffold. Individual as well as small aggregates of POSS nanocages extrude onto the surface during solvent evaporation and can be seen as microscopic white dots. Magnification  $\times 80$  (A) and  $\times 100$  (B). Scales as shown.

Pores were found to be homogeneously distributed throughout the scaffold with slight variations in pore sizes likely due to a degree of porogen clumping during the fabrication process. Some significantly smaller pores are likely attributable to entrapped air bubbles which can serve as pore nucleation sites during polymer mixing (Chung et al., 2012). Non-porous cast POSS-PCLU scaffolds demonstrate a smooth surface with microscopic aggregates identified as white spots on the SEM image (Fig. 4.9 (B)). These micro-aggregates are hypothesized to represent individual or grouped POSS nanoparticles which are extruded onto the surface during solvent evaporation (Misra et

al., 2007, Fina et al., 2005). This theory is supported by the fact that PCLU-24 do not exhibit any white microaggregates.

Contact angle measurements of cast POSS-PCLU scaffolds reveal an inherent hydrophobic character with all POSS-containing PUs demonstrating a contact angle of  $> 90^\circ$  (Fig. 4.10).

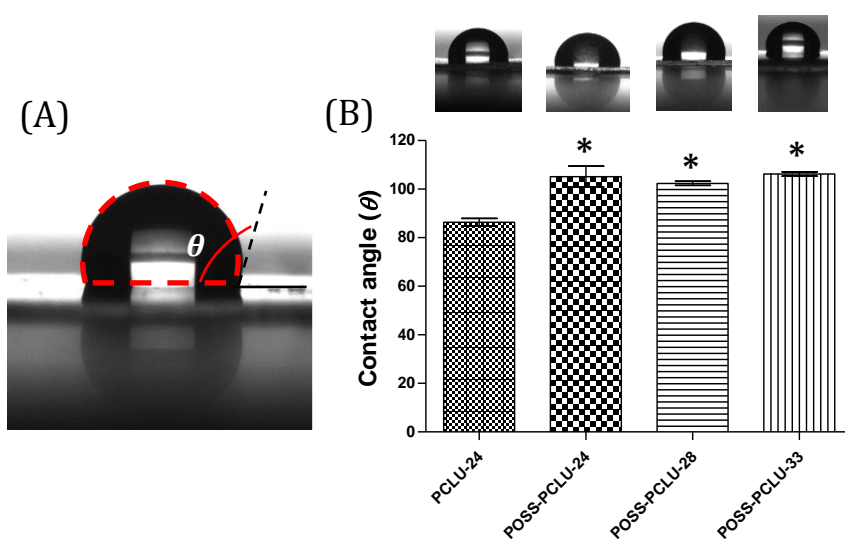


**Figure 4.10.** (A) Contact angle measurement of a cast POSS-PCLU disc demonstrates relative surface hydrophobicity ( $\theta > 90^\circ$ ). (B) Comparison of contact angle between cast discs of the 4 different polymer compositions. There is no statistically significant difference in  $\theta$  between polymers of different hard segments but a significantly reduced contact angle can be observed in PCLU-24 which lacks POSS nanoparticles. \* =  $p < 0.05$ . Values are given as mean  $\pm$  one SD.

No significant differences were found between polymers of different hard segment concentration ( $p > 0.05$ ) but lack of POSS nanoparticles resulted in a more hydrophilic nature with a contact angle of  $86.4^\circ$  as demonstrated by cast PCLU-24 discs. This is significantly more hydrophilic than any POSS-containing PU ( $p < 0.05$ ). Several previous study have demonstrated the change to a more hydrophobic character upon addition of POSS nanoparticles (Fina et al., 2005, Misra et al., 2007).

These results were further corroborated by surface roughness measurements using atomic force microscopy (AFM) (Fig. 4.11). The scaffold surface on a nano-level as well as the roughness profiles exhibited a random pattern of peak heights with relatively high mean surface roughness ( $R_a$ ) and root mean square roughness ( $R_q$ ) (54.1 nm and 89.1 nm, respectively) which corresponded to the contact angles of POSS-PCLU scaffolds. Such nanoscale roughness is hypothesized to stem from the extrusion of POSS-nanocages (average diameter including functional groups = 3.5 nm) onto the surface during the initial scaffold fabrication step.

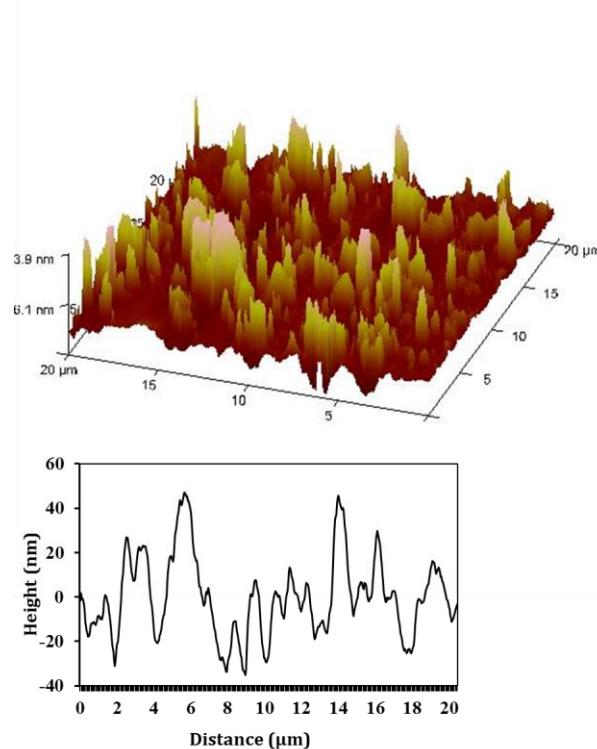


**Figure 4.11.** Atomic force microscopy (AFM) image illustrating a textured nanotopography of cast POSS-PCLU scaffolds. Multiple peaks provide points of attachment for cellular focal adhesion points.

#### 4.4.4 Mechanical Properties of POSS-PCLU Scaffolds

An overlay of the stress versus strain and Young's modulus versus strain curves of PCLU-24, POSS-PCLU-24, POSS-PCLU-28 and POSS-PCLU-33 are presented in Figure 4.12.

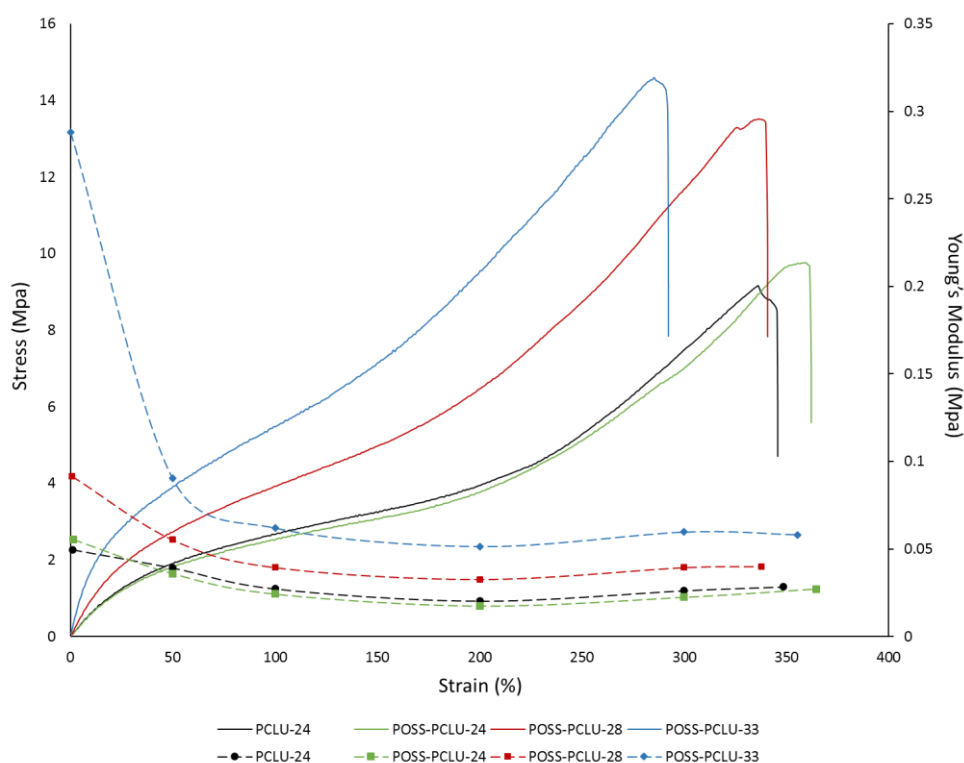


**Figure 4.12.** Overlaid stress versus strain and Young's modulus versus strain curves of PCLU and POSS-PCLU PUs at room temperature.

The characteristic values derived from these curves are summarised in Table 4.4.

**Table 4.4.** Mechanical properties of PCLU and POSS-PCLU PUs.

Material	Young's Modulus (MPa)	Strain at break (%)	Tensile strength (MPa)
PCLU-24	0.03	348.50	9.88
POSS-PCLU-24	0.03	364.48	10.24
POSS-PCLU-28	0.04	337.72	13.52
POSS-PCLU-33	0.06	355.45	20.66

Key: POSS, polyhedral oligomeric silsesquioxane; PCLU, poly( $\epsilon$ -caprolactone urea)urethane

In general, all samples displayed extension behaviour typical of semicrystalline polymers (Foks et al., 1991, Young and Lovell, 1991). At small strains, all PUs exhibited a steep linear slope culminating in a yield point for necking at around 20 % (2.5 MPa) after which further stretching results in irreversible plastic-like deformation. This was followed by a period of relatively linear elongation up to a strain of 150 % where an

upswing can be observed in all curves which is attributable to strain-induced crystallization of the soft segment portion. In general, a dependence of the permanent deformation stress and strain on the hard segment content can be observed which is in agreement with results obtained by other groups (Heijkants et al., 2005). With increasing hard segment content, the yield stress and ultimate tensile stress increase whilst the strain at break decreases. No significant differences in tensile strength could be observed between PUs with the same hard segment content but with (POSS-PCLU-24) or without (PCLU-24) POSS nanoparticle inclusion. This stands in contrast to previous findings (Gu et al., 2011) but is likely explained by the significantly smaller percentage of POSS included into our polymers (2 % versus 20 %). The values for Young's modulus, a measure for material stiffness, and yield stress are positively correlated with the hard segment content due to higher volume fractions and greater order in the hard segments (Lamba et al., 1998).

#### **4.4.5 *In Vitro* Cytocompatibility**

A light microscopy image of subconfluent HDFa cultured on TCP demonstrates the typical fibroblast morphology (Fig. 4.13). Elongated cell bodies give rise to two or more filamentous projections called filopodia which are slender cytoplasmic extensions anchoring the cells to the tissue culture plastic (or substrate) via focal adhesion points. They contain actin filaments cross-linked into actin-binding proteins which help in cellular locomotion (Mattila and Lappalainen, 2008, Hanein et al., 1997). Wound healing involves the stimulation of filopodia by environmental cues such as growth factors resulting in correct growth orientation (Bentley and Toroian-Raymond, 1986). The fibroblasts in demonstrate filopodial extension towards each other as well as towards the less confluent areas towards the bottom right of the image.

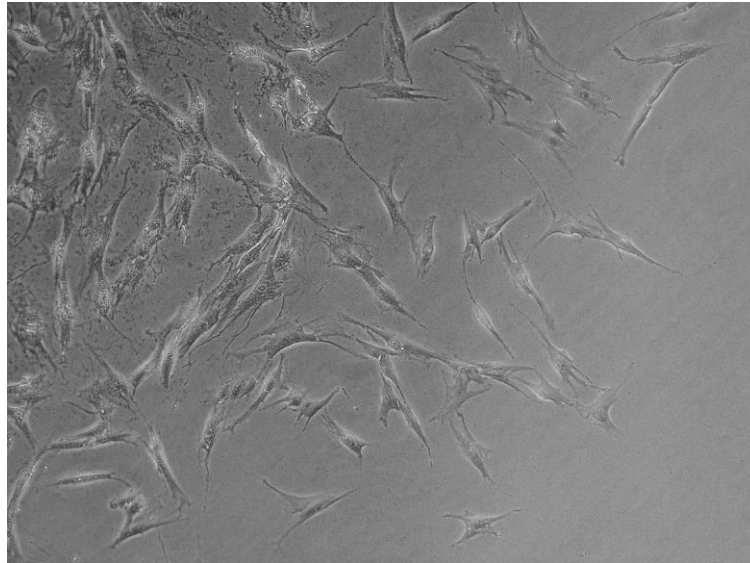


**Figure 4.13.** Light microscopy image of adult human dermal fibroblasts growing on tissue culture plastic. Magnification x 20.

In order to assess cell proliferative and migratory capacity more dynamically and over an extended period, a scratch test was conducted. A scratch assay is a widely used technique for investigating wound healing since manually created ‘wounds’ can be seen to close and ‘heal’ by cellular migration and proliferation of cells. At 0 h, a cell-free central scratch can be observed with live cells along the scratch margins (Fig. 4.14 (A)).



**Figure 4.14.** Scratch test qualitatively assessing cellular proliferation. Cells grown on tissue culture plastic, counterstained with Methylene Blue and imaged with light microscopy. Magnification x 4.

At 24 h, cells can be seen to migrate towards the centre of the gap (Fig. 4.14 (B)) and at 72 h, cells have migrated enough to fill the entire gap (Fig. 4.14 (C)). Trypan blue stains dead cells blue as the dye penetrates broken cell membranes but not intact ones.

In Figure 4.14 (C), very few cells are stained blue (arrow), indicating normal cell growth and migration.

Next, the optimal cell seeding density was assessed in 24-well plates over a period of 14 days. Usually, mammalian cells exhibit a characteristic semi-logarithmic growth pattern *in vitro* with an initial lag phase after seeding followed by an exponential growth phase (the log phase). Consumption of growth medium during the log phase and/or occupation of all available substrate results in the cells entering the stationary phase (the plateau phase) where proliferation stagnates or ceases. Ideally, cells should be subcultured prior to the plateau phase in order to prevent slowing of cell proliferation and changes in gene expression. We seeded HDFa in increasing concentrations ( $2.5 \times 10^4$ ,  $3.75 \times 10^4$  and  $5 \times 10^4$  cells/cm<sup>2</sup>) into the wells of a 24-well plate and cultured the cells over a period of 14 days. Normal medium containing no cells served as a control. Cell viability measurements taken at 1, 3, 7 and 14 days revealed a logarithmic increase in cell activity as expected (Fig. 4.15). Even at day 14, the plateau phase was not reached for any concentration, likely due to low starting densities. For subsequent cell studies, a seeding density of  $2.5 \times 10^4$  cells/cm<sup>2</sup> was chosen.

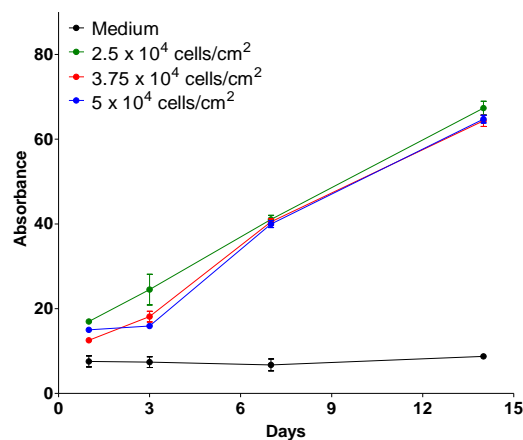


**Figure 4.15.** Evaluation of optimal cell seeding density on tissue culture plastic using three different cell seeding concentrations. Values are given as mean  $\pm$  one SD.



Basic cytocompatibility studies on both cast and coagulated POSS-PCLU scaffolds demonstrated good cell adherence and proliferation as well as healthy morphologies as expected. Staining with FITC-phalloidin revealed the cytoplasmic actin cytoskeleton responsible for maintaining cell shape and locomotion (Fig. 4.16 (A) and (B)). Depending on the surface topography, cell morphology, degree of spreading and alignment may vary. The relationship between surface micro- and nanotopography and cell shape will be discussed in more detail in chapter 5. Live/Dead® staining on HDFa cultured on cast POSS-PCLU films revealed mostly healthy living cells (Fig. 4.16 (C)) and very few dead cells (Fig. 4.16 (D)).

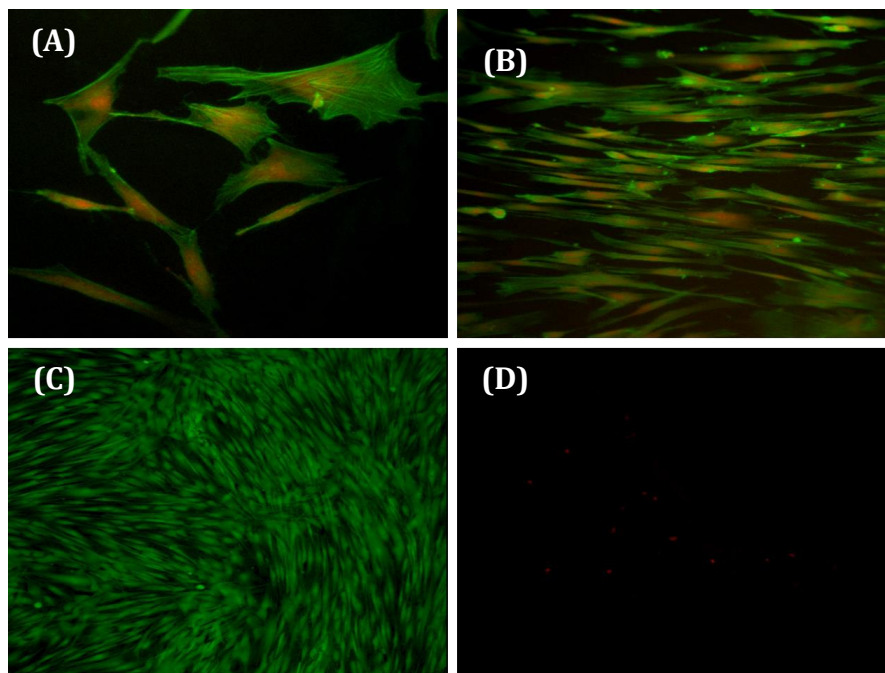


**Figure 4.16.** Top panel: Confocal laser scanning microscopy images of human dermal fibroblasts cultured on cast POSS-PCLU discs and stained for F-actin with fluorescein isothiocyanate (FITC)-labelled phalloidin. Nuclei are counterstained with propidium iodide. Bottom panel: Human dermal fibroblasts stained with (C) calcein AM (green) are live, whereas cells stained with (D) ethidium homodimer-1 (red) are dead.

In order to assess the material's suitability as a tissue regeneration scaffold, coagulated sponges were fabricated and seeded with HDFa (Fig. 4.17). Numerous cell nuclei can be seen to adhere to porous POSS-PCLU scaffolds.

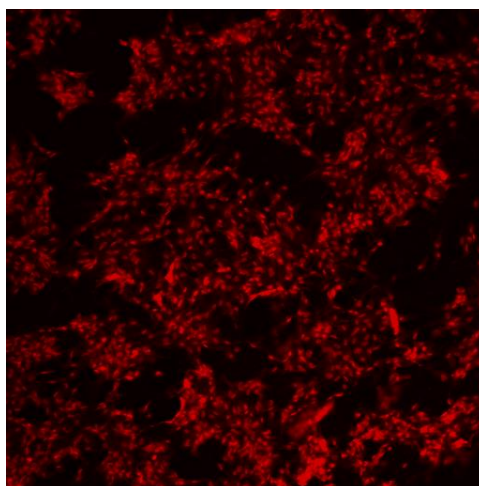


**Figure 4.17.** *Confocal laser scanning microscopy image of human dermal fibroblasts seeded onto porous POSS-PCL scaffolds after seven days of culture. Nuclei are counterstained with propidium iodide.*

Viability compared to cast POSS-PCLU appears to be slightly higher at days 1 and 3 (Fig. 4.18) which is likely due to the entrapment effect of cells within the porous scaffold structure. Viability was significantly higher on cast PCLU ( $p < 0.05$ ), possibly due to a more hydrophilic nature secondary to lacking POSS nanoparticles. Surface hydrophobicity is a known cell-repellent feature (Srinivasa Reddy et al., 2013), suggesting a removal of POSS nanoparticles from the PCLU system may benefit cell attachment and growth. From a more holistic point of view, however, POSS inclusion imparts tremendous benefits including superior mechanical characteristics, functionalisability and non-immunogenicity, rendering the overall nanocomposite polymer more versatile (Ahmed et al., 2011b, Bakhshi et al., 2011, de Mel et al., 2009, Ghanbari et al., 2011a, Ghanbari et al., 2011b, Ghanbari et al., 2010, Kannan et al., 2007b).

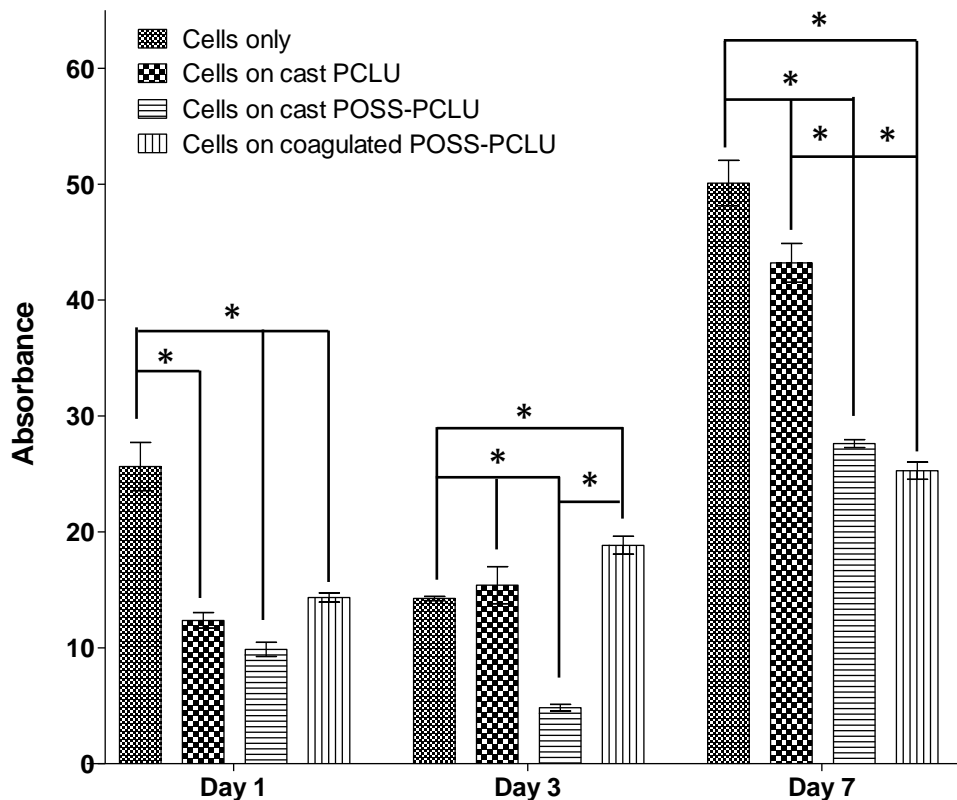


**Figure 4.18.** Cell cytocompatibility on tissue culture plastic (TCP), cast non-porous PCLU films, cast non-porous POSS-PCLU films and porous POSS-PCLU scaffolds over a period of 7 days as measured using AlamarBlue®. \* =  $p < 0.05$ . Values are given as mean  $\pm$  one SD.

## 4.5 CONCLUSION

Here, we have developed and characterized a novel biodegradable nanocomposite polymer system as a candidate material for tissue engineering purposes. Molecular characterization demonstrated POSS-PCLU polymers to be mostly amorphous as corroborated by  $T_g$  measurements. Mechanical analyses revealed a relationship between the hard segment content and tensile properties. No significant differences in tensile strength could be observed between PUs with the same hard segment content but with (POSS-PCLU-24) or without (PCLU-24) POSS nanoparticle inclusion. Surface analyses demonstrated microscopic POSS aggregates which are hypothesized to confer enhanced cytocompatibility and non-immunogenicity to the polymer system.

## References

- AHMED, M., GHANBARI, H., COUSINS, B. G., HAMILTON, G. & SEIFALIAN, A. M. 2011b. Small calibre polyhedral oligomeric silsesquioxane nanocomposite cardiovascular grafts: influence of porosity on the structure, haemocompatibility and mechanical properties. *Acta Biomater.*, 7, 3857-67
- BAKHSI, R., DARBYSHIRE, A., EVANS, J. E., YOU, Z., LU, J. & SEIFALIAN, A. M. 2011. Polymeric coating of surface modified nitinol stent with POSS-nanocomposite polymer. *Colloids Surf.B Biointerfaces.*, 86, 93-105.
- BENTLEY, D. & TOROIAN-RAYMOND, A. 1986. Disoriented pathfinding by pioneer neurone growth cones deprived of filopodia by cytochalasin treatment. *Nature*, 323, 712-5.
- BOGDANOV, B., TONCHEVA, V., SCHACHT, E. H., FINELLI, L., SARTI, B. & SCANDOLA, M. 1999. Physical properties of poly(ester-urethanes) prepared from different molar mass polycaprolactone-diols. *Polymer*, 40, 3171-82.
- CHALOUKKA, K., MOTWANI, M. & SEIFALIAN, A. M. 2011. Development of a new lacrimal drainage conduit using POSS nanocomposite. *Biotechnology and applied biochemistry*, 58, 363-70.
- CHUNG, E. J., SUGIMOTO, M., KOH, J. L. & AMEER, G. A. 2012. Low-pressure foaming: a novel method for the fabrication of porous scaffolds for tissue engineering. *Tissue Eng Part C Methods*, 18, 113-21.
- DE MEL, A., PUNSHON, G., RAMESH, B., SARKAR, S., DARBYSHIRE, A., HAMILTON, G. & SEIFALIAN, A. M. 2009. In situ endothelialization potential of a biofunctionalised nanocomposite biomaterial-based small diameter bypass graft. *Biomed.Mater Eng*, 19, 317-31.
- DE MEL, A., RAMESH, B., SCURR, D. J., ALEXANDER, M. R., BIRCHALL, M. & SEIFALIAN, A. M. 2013. Fumed Silica Nanoparticle Mediated Biomimicry for Optimal Cell-Material Interactions for Artificial Organ Development. *Macromolecular bioscience*.
- FINA, A., TABUANI, D., FRACHE, A. & CAMINO, G. 2005. Polypropylene-polyhedral oligomeric silsesquioxanes (POSS) nanocomposites. *Polymer*, 46, 7855-66.
- FOKS, J., JANIK, H. & POHL, M. 1991. Ruthenium tetroxide staining of semicrystalline polyester polyurethane films. *European Polymer Journal*, 27, 729-33.
- GHANBARI, H., COUSINS, B. G. & SEIFALIAN, A. M. 2011a. A nanocage for nanomedicine: polyhedral oligomeric silsesquioxane (POSS). *Macromolecular rapid communications*, 32, 1032-46.
- GHANBARI, H., DE, M. A. & SEIFALIAN, A. M. 2011b. Cardiovascular application of polyhedral oligomeric silsesquioxane nanomaterials: a glimpse into prospective horizons. *Int.J Nanomedicine*, 6, 775-86.
- GHANBARI, H., KIDANE, A. G., BURRIESCI, G., RAMESH, B., DARBYSHIRE, A. & SEIFALIAN, A. M. 2010. The anti-calcification potential of a silsesquioxane nanocomposite polymer under in vitro conditions: potential material for synthetic leaflet heart valve. *Acta Biomater.*, 6, 4249-60.
- GU, X., WU, J. & MATHER, P. T. 2011. Polyhedral oligomeric silsesquioxane (POSS) suppresses enzymatic degradation of PCL-based polyurethanes. *Biomacromolecules.*, 12, 3066-77.
- GUASTI, L., VAGASKA, B., BULSTRODE, N. W., SEIFALIAN, A. M. & FERRETTI, P. 2013. Chondrogenic differentiation of adipose tissue-derived stem cells within nanocaged POSS-PCU scaffolds: A new tool for nanomedicine. *Nanomedicine*.
- HANEIN, D., MATSUDAIRA, P. & DEROSIER, D. J. 1997. Evidence for a conformational change in actin induced by fimbrin (N375) binding. *J Cell Biol*, 139, 387-96.

HEIJKANTS, R. G. J. C., VAN CALCK, R. V., VAN TIENEN, T. G., DE GROOT, J. H., BUMA, P., PENNING, A. J., VETH, R. P. H. & SCHOUTEN, A. J. 2005. Uncatalyzed synthesis, thermal and mechanical properties of polyurethanes based on poly(epsilon-caprolactone) and 1,4-butane diisocyanate with uniform hard segment. *Biomaterials*, 26, 4219-28.

JUNGBLUTH, P., ALICI, E., BAIGUERA, S., LE, B. K., BLOMBERG, P., BOZOKY, B., CROWLEY, C., EINARSSON, O., GRINNEMO, K. H., GUDBJARTSSON, T., LE, G. S., HENRIKSSON, G., HERMANSON, O., JUTO, J. E., LEIDNER, B., LILJA, T., LISKA, J., LUEDDE, T., LUNDIN, V., MOLL, G., NILSSON, B., RODERBURG, C., STROMBLAD, S., SUTLU, T., TEIXEIRA, A. I., WATZ, E., SEIFALIAN, A. & MACCHIARINI, P. 2011a. Tracheobronchial transplantation with a stem-cell-seeded bioartificial nanocomposite: a proof-of-concept study. *Lancet*, 378, 1997-2004.

KANNAN, R. Y., SALACINSKI, H. J., BUTLER, P. E. & SEIFALIAN, A. M. 2005b. Polyhedral oligomeric silsesquioxane nanocomposites: the next generation material for biomedical applications. *Acc.Chem.Res.*, 38, 879-84.

KANNAN, R. Y., SALACINSKI, H. J., DE GROOT, J., CLATWORTHY, I., BOZEC, L., HORTON, M., BUTLER, P. E. & SEIFALIAN, A. M. 2006a. The antithrombogenic potential of a polyhedral oligomeric silsesquioxane (POSS) nanocomposite. *Biomacromolecules*, 7, 215-23.

KANNAN, R. Y., SALACINSKI, H. J., GHANAVI, J. E., NARULA, A., ODLYHA, M., PEIROVI, H., BUTLER, P. E. & SEIFALIAN, A. M. 2007b. Silsesquioxane nanocomposites as tissue implants. *Plast.Reconstr.Surg.*, 119, 1653-62.

LAMBA, N. M. K., VOODHOUSE, K. A. & COOPER, S. L. 1998. *Polyurethanes in Biomedical Applications*, Boca Raton, FL, CRC Press.

LI, Z., ZHANG, Z., LIU, K. L., NI, X. & LI, J. 2012. Biodegradable hyperbranched amphiphilic polyurethane multiblock copolymers consisting of poly(propylene glycol), poly(ethylene glycol), and polycaprolactone as in situ thermogels. *Biomacromolecules*, 13, 3977-89.

LOH, X. J., COLIN SNG, K. B. & LI, J. 2008. Synthesis and water-swelling of thermo-responsive poly(ester urethane)s containing poly(epsilon-caprolactone), poly(ethylene glycol) and poly(propylene glycol). *Biomaterials*, 29, 3185-94.

MADANI, S. Y., MANDEL, A. & SEIFALIAN, A. M. 2013. A concise review of carbon nanotube's toxicology. *Nano reviews*, 4.

MATTILA, P. K. & LAPPALAINEN, P. 2008. Filopodia: molecular architecture and cellular functions. *Nat Rev Mol Cell Biol*, 9, 446-54.

MISRA, R., FU, B. X. & MORGAN, S. E. 2007. Surface energetics, dispersion, and nanotribomechanical behavior of POSS/PP hybrid nanocomposites. *Journal of Polymer Science: Part B: Polymer Physics*, 45, 2441-55.

MULLICK CHOWDHURY, S., LALWANI, G., ZHANG, K., YANG, J. Y., NEVILLE, K. & SITHARAMAN, B. 2013. Cell specific cytotoxicity and uptake of graphene nanoribbons. *Biomaterials*, 34, 283-93.

NAIR, P. A. & RAMESH, P. 2013. Electrospun biodegradable calcium containing poly(ester-urethane)urea: synthesis, fabrication, in vitro degradation, and biocompatibility evaluation. *Journal of biomedical materials research. Part A*, 101, 1876-87.

NOAH, E. M., CHEN, J., JIAO, X., HESCHEL, I. & PALLUA, N. 2002. Impact of sterilization on the porous design and cell behavior in collagen sponges prepared for tissue engineering. *Biomaterials*, 23, 2855-61.

- ROGERS, M. J. & SEMAW, S. 2009. From Nothing to Something: The Appearance and Context of the Earliest Archaeological Record. *In*: M.CAMPS & P.CHAUHAN (eds.). New York: Springer.
- SARKAR, R., COMMENT, A., VASOS, P. R., JANNIN, S., GRUETTER, R., BODENHAUSEN, G., HALL, H., KIRIK, D. & DENISOV, V. P. 2009. Proton NMR of (15)N-choline metabolites enhanced by dynamic nuclear polarization. *J Am Chem Soc*, 131, 16014-5.
- SCHOLES, G. D. & RUMBLES, G. 2006. Excitons in nanoscale systems. *Nat.Mater.*, 5, 683-96.
- SHOAE-HASSANI, A., KEYHANVAR, P., SEIFALIAN, A. M., MORTAZAVI-TABATABAEI, S. A., GHADERI, N., ISSAZADEH, K., AMIRMOZAFARI, N. & VERDI, J. 2013a. lambda Phage Nanobioparticle Expressing Apoptin Efficiently Suppress Human Breast Carcinoma Tumor Growth In Vivo. *PLoS One*, 8, e79907.
- SHOAE-HASSANI, A., SHARIF, S., SEIFALIAN, A. M., MORTAZAVI-TABATABAEI, S. A., REZAI, S. & VERDI, J. 2013b. Endometrial stem cell differentiation into smooth muscle cell: a novel approach for bladder tissue engineering in women. *BJU Int*, 112, 854-63.
- SRINIVASA REDDY, C., REDDY VENUGOPAL, J., RAMAKRISHNA, S. & ZUSSMAN, E. 2013. Polycaprolactone/oligomer compound scaffolds for cardiac tissue engineering. *J Biomed Mater Res A*.
- TAN, A., GOH, D., FARHATNIA, Y., G, N., LIM, J., TEOH, S. H., RAJADAS, J., ALAVIJEH, M. S. & SEIFALIAN, A. M. 2013. An anti-CD34 antibody-functionalized clinical-grade POSS-PCU nanocomposite polymer for cardiovascular stent coating applications: a preliminary assessment of endothelial progenitor cell capture and hemocompatibility. *PLoS One*, 8, e77112.
- TASHNIZI, M. A., ALAMDARI, D. H., KHAYAMI, M. E., RAHIMI, H. R., MOEINIPOUR, A., AMOUZESHI, A. & SEIFALIAN, A. M. 2013. Treatment of non-healing sternum wound after open-heart surgery with allogenic platelet-rich plasma and fibrin glue-preliminary outcomes. *Indian J Plast Surg*, 46, 538-42.
- YOUNG, R. J. & LOVELL, P. A. 1991. *Introduction to Polymers*, Nelson Thornes.

# 5 AN OPTIMIZED STERILIZATION METHOD FOR BIODEGRADABLE POSS-PCLU

---

## 5.1 SYNOPSIS

The field of tissue engineering is rapidly evolving, generating numerous biodegradable materials suited as regeneration platforms. Material sterility is of fundamental importance for clinical translation, yet, few studies have systematically researched the effects of different sterilization methods on biodegradable material systems. Heat, chemical or radiation treatments can alter material topographies and surface chemistries, thereby inadvertently influencing cellular morphometry and function. Here, we exposed a novel bioabsorbable nanocomposite based on polyhedral oligomeric silsesquioxane-modified poly( $\epsilon$ -caprolactone urea)urethane (POSS-PCLU) to autoclave, microwave, antibiotics and 70 % ethanol sterilization and systematically correlated differences in material characteristics to the attachment, viability, proliferative capacity and shape of human dermal fibroblasts (HDFa). Nanotopographical profiling of autoclaved or microwaved surfaces revealed relatively deep nano-grooves, increasing total surface area, roughness and hydrophobicity which resulted in significantly fewer adherent cells. Antibiotics or 70 % ethanol-treated surfaces displayed shallower nano-grooves and a more hydrophilic character and significantly greater cellular adhesion ( $p < 0.05$ ). In fact, relative cell proliferation on ethanol-treated films surpassed that of cells grown on every other surface by a factor of 9 over 7 days. F-actin staining demonstrated spindle-like morphologies characteristic of HDFa when grown on ethanol-treated films as opposed to cells grown on other films which were significantly more spread out ( $p < 0.05$ ).

## 5.2 INTRODUCTION

The application of synthetic scaffolds for tissue engineering and regeneration is a rapidly expanding field with enormous clinical potential as demonstrated with the world's first synthetic trachea transplantation as well as in-human vascular bypass graft and lacrimal duct insertion using the non-biodegradable nanocomposite material POSS-PCU (Chaloupka et al., 2011, Jungebluth et al., 2011a). For a number of applications such as developmental and paediatric organ malformations, however, biodegradable scaffold systems are more favourable due to the potential of such scaffolds to 'grow' with the young patients. Additionally, biodegradable materials have demonstrated substantial clinical potential in tissue engineering of skin regeneration platforms where initial structural stability is essential to prevent wound bed contraction but subsequent gradual degradation necessary to free space for the ingrowing new skin (Mansilla et al., 2010, Kuppam et al., 2011). Polyhedral oligomeric silsesquioxane-modified poly(carbonate urea-urethane)caprolactone (POSS-PCLU) is a novel bioabsorbable nanocomposite material suited as a platform material for tissue regeneration applications (Ahmed et al., 2011b, Kannan et al., 2006c, J. Armstrong et al., 2004, Salacinski et al., 2005, Kannan et al., 2005b, Jungebluth et al., 2011b, de Mel et al., 2009). POSS-PCLU scaffolds can be fabricated in a number of ways including casting, coagulation using a salt leaching method, 3-D printing and electrospinning in order to suit individual applications. This versatility renders bioabsorbable POSS-PCLU a highly desirable platform material for tissue engineering of temporary implantable devices. However, a frequently underestimated, albeit highly relevant aspect in the development of implantable devices is the ability to ensure impeccable sterility. As micro-organismal contamination tends to falsify *in vitro* studies as well as elicit a potentially exuberant immune reaction towards such devices in the human, sterility remains a fundamental prerequisite for the transition



of tissue engineered scaffolds into the clinical arena. Sterilization is defined as the destruction of all forms of life by heat, chemical or radiation treatment (Ninemeier, 2003). Conventional laboratory-based sterilization techniques include high pressure steam sterilization (autoclaving) and exposure to microwaves. Whilst effectively removing surface-adherent bacteria, these methods often irreversibly damage hydrolytically unstable materials leading to material melting, collapse of internal porous architectures, unpredictable changes in mechanical and surface properties as well as altered rates of biodegradation. Chemical means of microbial removal such as exposure to 70 % ethanol or antibiotics, whilst strictly speaking not considered sterilising agents, have been routinely adopted as antimicrobial agents for laboratory cell studies (Shearer et al., 2006).

Besides the sterilizing effect, exposure to heat sources or potentially abrasive chemicals influences surface topographies (e.g. surface roughness) and can thereby significantly change cell-substrate interactions and cell function (Ma et al., 2007, Kikuchi and Okano, 2005, Flemming et al., 1999). Changes in cellular attachment, motility, proliferation and differentiation (Tonazzini et al., 2010) have been shown to be brought about by modulating material surface tension and chemical and mechanical properties (Rehfeldt et al., 2007). It is a recognized fact that 3D topographical features of polymers (Washburn et al., 2004), oxides (Winkelmann et al., 2003), carbon nanofibers (Price et al., 2004) and metals (Khang et al., 2008) are related to cyto- and biocompatibility of the respective materials. Surface topographies ranging within the nanometer scale are thought to facilitate cell-substrate interactions by mimicking the biological cues present on ECM components of natural tissues (Chen et al., 2013b, Loesberg et al., 2007, Pan et al., 2013, Miller et al., 2004). Since focal adhesion proteins located on the outer surface of

the cell membrane (e.g. integrins) have a diameter measuring ~10-15 nm, cell-substrate adhesion is enhanced by nanoscaled surface topographies (Hussain and Siedlecki, 2004).

The aim of this work was to systematically investigate (i) the effectiveness of 4 different, easily accessible sterilization methods for bioabsorbable POSS-PCLU material, and (ii) the influence of these sterilization methodologies on surface topography and chemistry as well as cell-substrate interactions.

## **5.3 MATERIALS AND METHODS**

### **5.3.1 Polymer Synthesis**

Please refer to section 4.3.1.

### **5.3.2 Manufacturing of Scaffolds**

Please refer to section 4.3.2.

### **5.3.3 Scaffold Sterilization Techniques**

#### ***5.3.3.1 Autoclave Sterilization***

Samples were exposed to saturated steam at 121°C for 15 min at pressures of 115 kPa (Classic Prestige Medical autoclave, Prestige Medical Limited, Blackburn, UK). Prior to use, samples were cooled to room temperature for 12-24 h.

#### ***5.3.3.2 Microwave Sterilization***

Samples were completely submerged in de-ionized water and placed into an unmodified domestic microwave and exposed to highest power radiation (750 Watt) for a total of 30 seconds (sec) (Cardoso 2007). Samples were allowed to cool down before use.

#### **5.3.3.3 Treatment with Antibiotic/Antimycotic solution**

Samples were placed in a 5 % (v/v) antibiotic antimycotic solution (10 000 U/mL penicillin G, 10 mg/mL streptomycin sulphate, and 25 mg/mL amphotericin B [Sigma-Aldrich, Dorset, UK]) in PBS for 24 h at 4 °C. Samples were washed 3 times with PBS under agitation before use.

#### **5.3.3.4 Treatment with 70 % Ethanol Solution**

Samples were ethanol-treated according to a method published by Kweon (Kweon et al., 2003). Samples were soaked in 2 changes of 70 % ethanol over 30 min under agitation, and subsequently washed in 4 changes of PBS solution over 2 h.

#### **5.3.3.5 Control Samples**

Non-sterilized samples served as a control for all tests.

### **5.3.4 Sterilization Efficiency**

Sterility testing was performed according to British Standards (ISO 11737-2:2009) on cast and coagulated samples immediately following sterilization. The samples were immersed in normal cell culture medium to cultivate micro-organisms and maintained at 37 °C for 7 days. Untreated scaffolds were used as the positive control and sterile medium alone served as the negative control. Samples were assessed daily for any turbidity which denotes infection and inefficient sterilization. All experiments were conducted in triplicates.

### **5.3.5 Scaffold Characterization**

#### **5.3.5.1 Scaffold Shrinkage**

Changes in scaffold diameter post-sterilization were used as an indicator for sterilization-induced scaffold degradation. Diameters were measured pre- and post-sterilization using a calliper.

### ***5.3.5.2 Scaffold Surface Micro- and Nanotopographical Assessment***

#### **5.3.5.2.1 Scanning Electron Microscopy**

Please refer to section 4.3.4.1.1.

#### **5.3.5.2.2 Atomic Force Microscopy**

Please refer to section 4.3.4.1.2.

### ***5.3.5.3 Surface Wettability Measurement using Contact Angle ( $\theta$ )***

Please refer to section 4.3.4.1.3.

#### **5.3.5.3.1 Attenuated Total Reflectance Fourier Transform Infrared (ATR/FTIR) Spectroscopy**

Please refer to section 4.3.4.2.2.

### ***5.3.5.4 Mechanical Properties of Scaffolds***

Please refer to section 4.3.4.3.3.

## **5.3.6 Cell Behaviour on Sterilized Surfaces**

Primary fibroblasts were isolated from human dermis (HDFa) and cultured in Dulbecco's Modified Eagle Medium (DMEM) supplemented with 1 mM L-glutamine, 10 % fetal bovine serum (FBS), 1 % penicillin/streptomycin and 1 % Fungizone (Invitrogen, Paisley, UK). HDFa were cultured to 80-90 % confluency, trypsinized and either re-plated or stored in 10 % DMSO/10 % FBS in liquid nitrogen until required.

To allow for isolated assessment of sterilization-induced variations in surface topography and the influence on cell adhesion and proliferation, HDFa cells were seeded onto DMEM pre-soaked and non-porous cast POSS-PCLU scaffolds at a density of  $5 \times 10^4$  cells/150  $\mu$ L/scaffold and incubated at 37 °C, 5 % CO<sub>2</sub> for 2 h. Then, 1 mL culture medium was added and cells were incubated until the pre-determined time points. Previous tests determined 2 h sufficient for cell attachment (results not shown). A staggered seeding

technique was utilized to ensure cell adhesion onto scaffolds rather than tissue culture plastic (TCP) (Noah et al., 2002). TCPs containing no scaffolds were seeded with an equal amount of cells (positive control) or medium only (negative control). Medium-soaked POSS-PCLU scaffolds not seeded with cells served as background noise which was subtracted from final results of cell-seeded scaffolds. Cells were incubated at 5 % CO<sub>2</sub> in air at 37 °C and culture medium was changed every 2-3 days for a total of 7 days.

In order to demonstrate the material's suitability as a tissue engineering platform, 3D porous scaffolds were seeded with HDFa at a density of 5 x 10<sup>4</sup> cells/150 µL/scaffold and incubated at 37 °C, 5 % CO<sub>2</sub> and cellular viability, proliferative capacity as well as migration into the scaffold's internal architecture were analysed.

On days 1, 3, and 7, cell morphology was visualised using the F-actin stain fluorescein isothiocyanate (FITC)-phalloidin and nuclei counterstained with Propidium Iodide (PI) (both Sigma-Aldrich, Dorset, UK). Cell viability and proliferative capacity were assessed using Live/Dead<sup>®</sup> stain and AlamarBlue<sup>®</sup> assay, respectively.

#### ***5.3.6.1 Assessment of Cell Viability using AlamarBlue<sup>®</sup> Cell Proliferation Assay***

Please refer to section 4.3.5.2.

#### ***5.3.6.2 Live/Dead<sup>®</sup> Cell Survival Assay***

Please refer to section 4.3.5.3.

#### ***5.3.6.3 Cytoskeletal Staining***

Please refer to section 4.3.5.4.

#### **5.3.7 Statistics**

Please refer to section 4.3.6.

## 5.4 RESULTS AND DISCUSSION

Tissue engineering of implantable biodegradable devices is increasingly advocated as an elegant solution to restore the diseased or imperfect human body to a pre-morbid state (Lavik and Langer, 2004, Vacanti and Langer, 1999, Langer and Vacanti, 1993). In particular, the paediatric population is thought to benefit from absorbable devices as is the field of skin reconstruction. Tissue engineered devices are often highly porous and therefore, by nature, display large surface areas with known incidences and histories for clinical infections (Kuijjer et al., 2007). Further, it has been shown that bacteria can remain dormant within the internal scaffold structure, only to manifest as pathogenic biofilms after implantation (Drenkard and Ausubel, 2002). Material sterility is of fundamental significance for all implantable biomedical devices and is a particularly important consideration for all bioabsorbable materials (Holy et al., 2001). Here, we introduced a novel biodegradable nanocomposite polymer based on a diisocyanate hard segment and a poly(urea urethane)caprolactone soft segment incorporating POSS nanoparticles for use as a tissue engineering scaffold. Major advantages of using a PCLU backbone as tissue engineering platforms include its inherent biocompatibility, non-immunogenicity and slow degradation into non-toxic metabolites. Unmodified POSS-PCLU, however, has a relatively hydrophobic nature which increases non-specific protein adsorption leading to poor cell attachment and proliferation (Cheng and Teoh, 2004). Several researchers investigated surface modification strategies including collagen and acrylic acid functionalisations in order to enhance cell adhesion and improve biocompatibility of PCL (Bae et al., 1999, Cheng and Teoh, 2004, Hutmacher, 2000). However, one fundamental aspect that most studies relating to biodegradable scaffolds fail to mention is the necessity for a terminal sterilization step. Depending on the sterilization method used, the biomaterial surface may undergo different degrees of modifications which may

influence cell-biomaterial interactions (Zhang et al., 1996, Baier et al., 1982). This may render any prior surface modifications obsolete resulting in unpredictable material properties. In this study, we present a one-step method to achieve both sterilization and enhance biocompatibility after the initial synthesis of the scaffold; a technique termed post-production processing.

#### 5.4.1 Effectiveness of Different Sterilization Techniques by Immersion in Culture Medium

Table 5.1 summarizes the results of the sterility tests. An incubation period of 7 days allowed sufficient time for any potential microbial migration.

**Table 5.1.** Sterility testing of cast and coagulated samples by immersion in culture medium for 7 days post-sterilization. Experiments were carried out in triplicates. Key: -ve control, medium only; +ve control, contaminated samples; x, no growth present; ✓, growth present.

		Number of Repeats		
Sterilization Technique		1	2	3
<b>Cast</b>	Autoclave	x	x	x
	Microwave	x	x	x
	Antibiotics	x	x	✓
	70 % Ethanol	x	x	x
	-ve control	x	x	x
	+ve control	✓	✓	✓
<b>Coagulated</b>	Autoclave	x	x	x
	Microwave	x	x	✓
	Antibiotics	x	x	✓
	70 % Ethanol	x	x	x
	-ve control	x	-	-
	+ve control	✓	-	-

After 7 days, all non-sterilized cast and coagulated control samples showed signs of infection and bacterial growth whereas medium-only controls did not exhibit turbidity, thus proving the feasibility of this testing technique. The results predictably showed

efficient microbial removal on non-porous, cast films using autoclave, microwave and 70 % ethanol sterilization; all of which have been proven effective in numerous studies (Holy et al., 2001, Machado et al., 2011, Athanasiou et al., 1996). However, extensive polymer deformation and shrinkage due to melting of the heat-sensitive POSS-PCLU were observed in the coagulated samples.

Exposure to microwaves for 30 sec sterilized cast samples. Porous scaffolds, however, were only inconsistently sterilized using microwave irradiation, retaining contaminants within some core structures that only surfaced days later to cause infection. Such delayed infection is indicative of incomplete microbial eradication due to microwave scattering along the rough polymer surface and wave reflection due to incomplete air elimination within the internal structures (Ulaby et al., 1978). The presence of such attenuating factors reducing microwave intensity has been confirmed in previous studies (Harvey, 1963, Skolnik, 1970). It has been suggested that the presence of water vapour favours microwave absorption, thereby attenuating its intensity. Conventionally, microwaves have been used in the disinfection of denture base resins (Machado et al., 2011) and the sterilization effect is thought to be due mainly to the heating effect. Studies investigating microwave sterilization of glass culture tubes demonstrated microbial growth when tube stoppers were purposefully opened to the ambient pressure, indicating a major role of pressurised steam in the killing of micro-organisms (Fitzpatrick et al., 1978).

Antibiotic treatment resulted in unreliable sterilization and clouding of the incubation medium for both cast and coagulated samples. To the best of our knowledge, antibiotic antimycotic solutions have only been used as sterilizing agents in a study by Shearer who recommended exposure over a period of 24 h (Shearer et al., 2006).



Contrary to Shearer's results, our investigation showed inefficient sterilization using antibiotic solutions.

Immersion of samples in two changes of 70 % ethanol over 30 min and subsequent washing with 4 changes of sterile PBS over 2 h resulted in effective removal of micro-organismal contaminants from both cast and coagulated samples. Exposure to 60-80 % ethanol is considered disinfectant rather than sterilizing due to its inability to destroy hydrophilic viruses or bacterial spores (Holy et al., 2001). However, ease of use and apparent effectiveness make ethanol a favourable tool for *in vitro* studies. Further, it has been demonstrated that ethanol treatment of a poly-L-lactide-co-glycolide polymer did not affect the molecular weight ( $M_w$ ) of the polymer (Holy et al., 2001).

#### **5.4.2 Sterilization Induced Microscopic Changes in Scaffold Architecture and Topography**

Surface micro- and nanotopographies of unsterilized and sterilized POSS-PCLU sheets were analysed using SEM (Fig. 5.1 and 5.2), FTIR spectroscopy (Fig. 5.3), goniometry (Fig. 5.4) and AFM (Fig. 5.5). Whilst all sterilization methods bar antibiotic solution had sterilizing effects, structural damage was evident in all cases. The SEM image of an unsterilized coagulated sample surface (Fig. 5.1 (E)) exhibits sub-micron scale tufts of polymer imprinted during the surface modification step of scaffold synthesis. Changes to this surface microtopography post-sterilization are suggestive of damage induced by these treatments. Surface tufts were lost after using autoclave, microwave and 70 % ethanol sterilisation with polymer melting and irregular re-formation into larger and flatter ridges (Fig. 5.1 (A), (B) and (D)).

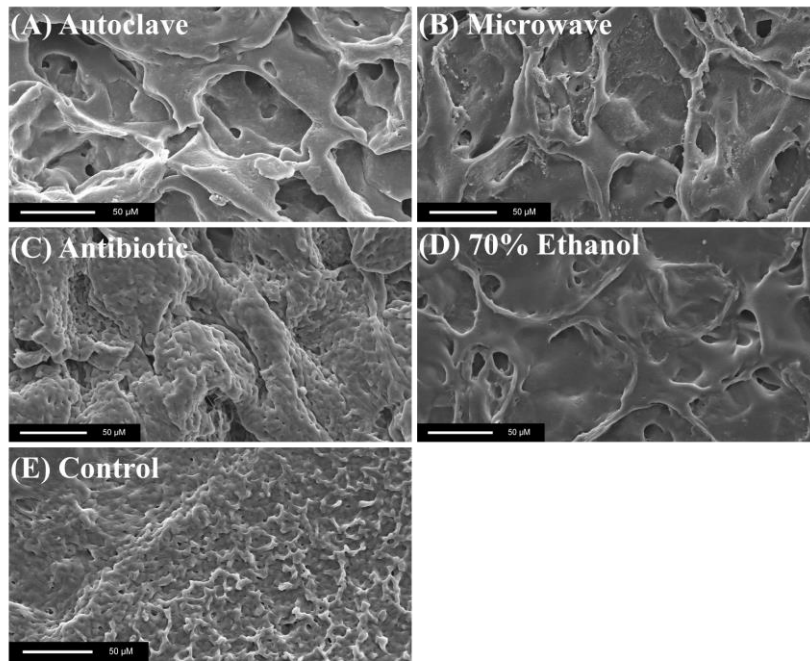
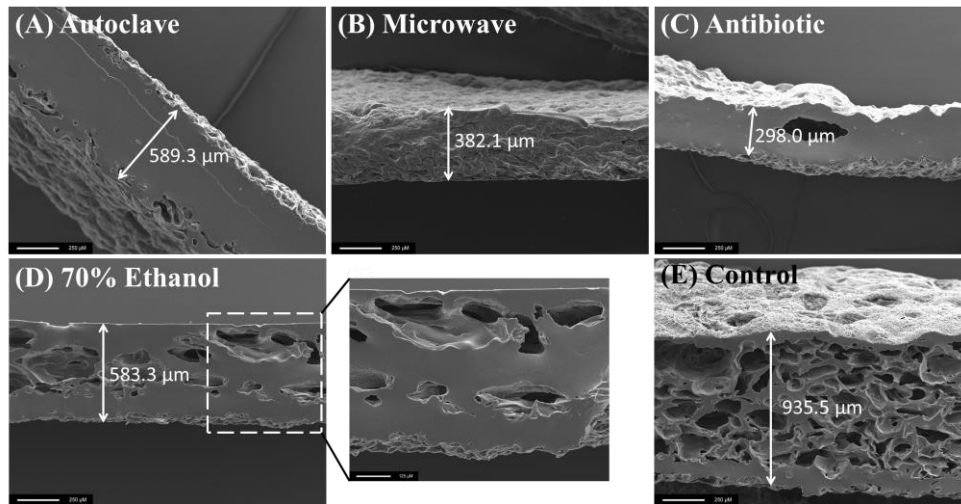


**Figure 5.1.** Representative SEM images of coagulated sterilized (A-D) and control (E) scaffold surfaces. Magnification x 320. Scale 50 μM.

Exposure to high pressure steam sterilization and microwaves expectedly resulted in extensive morphological damage of hydrolytically unstable POSS-PCLU (Rainer et al., 2010) indicative of partial dissolution of the polymer surface tufts due to hydrolysis. Subsequent fusion of polymer tufts into larger and flatter ridges is thought to be mainly driven by high polymer concentration at the polymer-moisture interface (Shearer et al., 2006). Antibiotic treatment seemed to have the least effect on surface melting (Fig. 5.1 (C)). However, the complete loss of internal porous structure observed on transverse cut SEM images was unexpected as antibiotic solution reportedly does not damage morphological or chemical characteristics of scaffolds (Richards et al., 1991). SEM images of vertically cut edges of an unsterilized coagulated scaffold revealed a spongy internal architecture characterized by numerous interconnected pores (Fig. 5.2 I (E)), whilst all sterilization methods resulted in a reduction (Fig. 5.2 I (D)) or complete loss of the porous internal architecture (Fig. 5.2 I (A), (B) and (C)).

(I)



(II)

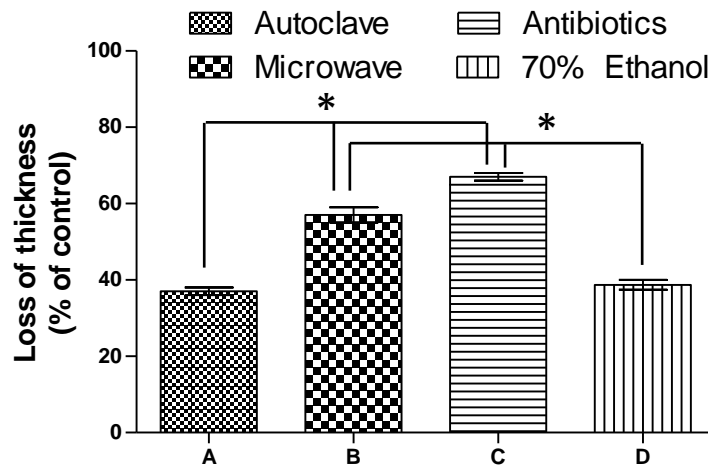


**Figure 5.2.** (I) Representative SEM images of cut scaffold edges. Magnification  $\times 80$ . Scale  $250 \mu\text{m}$ . Image analysis with ImageJ (freeware). (II) All sterilization methods significantly affected scaffold thickness ( $p < 0.001$ ) with a mean loss of 50.5 %. Most pronounced loss was observed in antibiotic treated scaffolds (C, mean loss of 68 %). Values are given as mean  $\pm$  one SD.

Scaffolds treated with 70 % ethanol were found to retain the porous internal architecture best compared to other sterilization methods (Fig. 5.2 I (E) and (F)) which is in accordance with the literature (Holy et al., 2001, Karp et al., 2003). Loss of scaffold thickness was statistically significant for all sterilization methods (Fig. 5.2 II,  $*p < 0.001$ , mean loss of thickness = 50.5 %) but was most pronounced in scaffolds treated with antibiotic solutions (Fig. 5.2 II (C)). Preserving internal porosity post-sterilization is of

fundamental importance for the in- and efflux of nutrients and waste products to and from the cells (Noah et al., 2002).

### 5.4.3 Chemical Bond Scission Demonstrated by ATR-FTIR

Material surface chemistry and sterilization induced changes were analysed using FTIR spectroscopy. Figure 5.3 shows an FTIR spectrum overlay of individual representative cast POSS-PCLU surfaces sterilized using each technique.

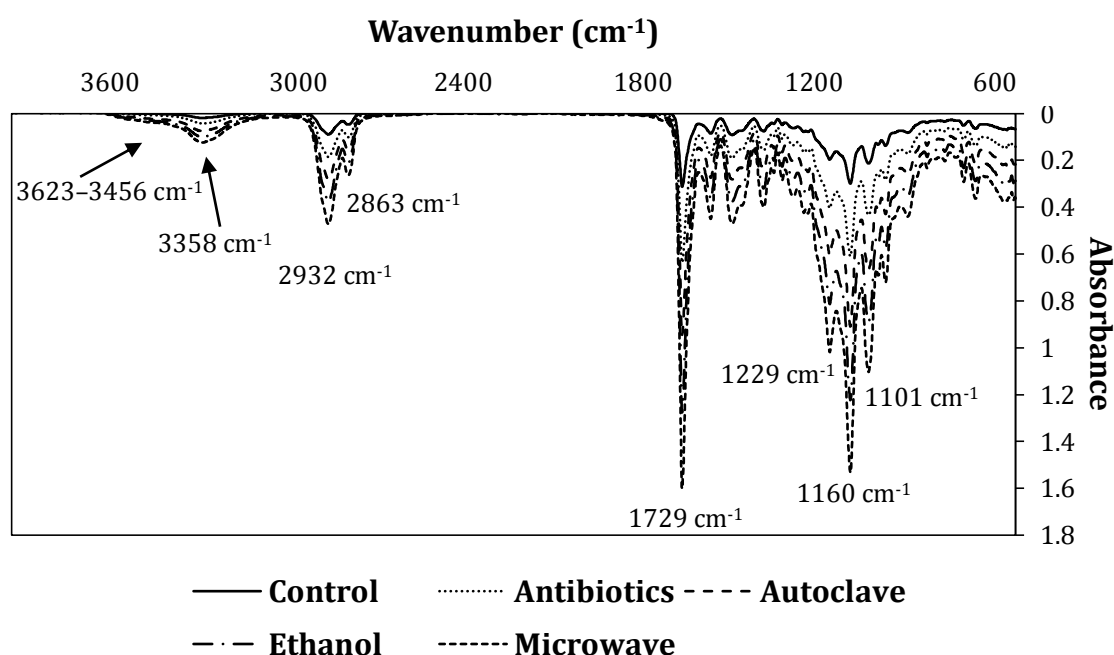


**Figure 5.3.** Overlaid attenuated total reflectance-Fourier transform infrared spectrum of cast sterilized and control samples. Particularly high temperature steam sterilization (autoclaving) induced a broadening of the OH peak at around 3550  $\text{cm}^{-1}$ . No reductions in peak intensity were observed at the methylene bridge at 2932  $\text{cm}^{-1}$  or the carbonyl region (1729  $\text{cm}^{-1}$ ) indicating the presence of both ester and urethane linkages and an intact hard segment.

All sterilization methods and in particular high temperature steam sterilization (autoclaving) induced an increase and broadening of the OH absorption peak at 3550  $\text{cm}^{-1}$  suggestive of an accumulation of carboxylic and hydroxyl groups secondary to the hydrolytic degradation of the soft segment of PCLU. Multiple cycles of high temperature steam sterilization confirmed a gradual increase in the OH band, indicative of successive

hydrolysis of the polymer (results not shown). No reductions in peak intensity were observed at the methylene bridge at  $2932\text{ cm}^{-1}$  or the carbonyl region at  $1729\text{ cm}^{-1}$  indicating the presence of both ester and urethane linkages and an intact hard segment. However, some evidence of hard segment exposure was evident with slight increases in peaks at  $1632$  (urethane carbonyl),  $1560$ - $1530$ ,  $1350$ ,  $1233$ ,  $992$  and  $793\text{ cm}^{-1}$ .

Soft segment breakdown is known to play a major role in chemical aging of thermoplastic PUs and negatively affects mechanical properties including tensile stress and maximal strain (Servay et al., 2000). Here, mechanical analysis post antibiotic treatment revealed significantly lower breaking strains of cast polymers, indicative of soft segment scission. TPUs are phase separated block copolymers and owe their elasticity to their biphasic morphology, i.e. a rigid and soft phase. While the soft segment provides the material with flexibility, the hard segment physically cross-links the phases to allow for elastic recovery (Servay et al., 2000). Thermal oxidation of the methylene bridge of the MDI and subsequent breakage of the material's hard segment has been observed at temperatures above  $150\text{ }^{\circ}\text{C}$  (Servay et al., 2000). However, in our studies, temperatures did not exceed  $121\text{ }^{\circ}\text{C}$  and thus no reductions in peak intensity were observed at the methylene bridge at  $2932\text{ cm}^{-1}$  or the carbonyl region ( $1729\text{ cm}^{-1}$ ) indicating the presence of both ester and urethane linkages. However, some evidence of hard segment exposure was evident with slight increases in peaks at  $1632$ ,  $1560$ - $1530$ ,  $1350$ ,  $1233$ ,  $992$  and  $793\text{ cm}^{-1}$  as similarly reported by Chan-Chan (Chan-Chan et al., 2010b).

#### **5.4.4 Surface Roughness Changed Significantly as Demonstrated with Contact Angle and AFM**

Sterilized and non-sterilized cast samples were also characterised in terms of wettability and nanotopograph. Contact angle measurements of non-sterilized control

samples demonstrated an inherent hydrophobic character of the POSS-PCLU polymer surface ( $\theta = 114^\circ$ , Fig. 5.4.).

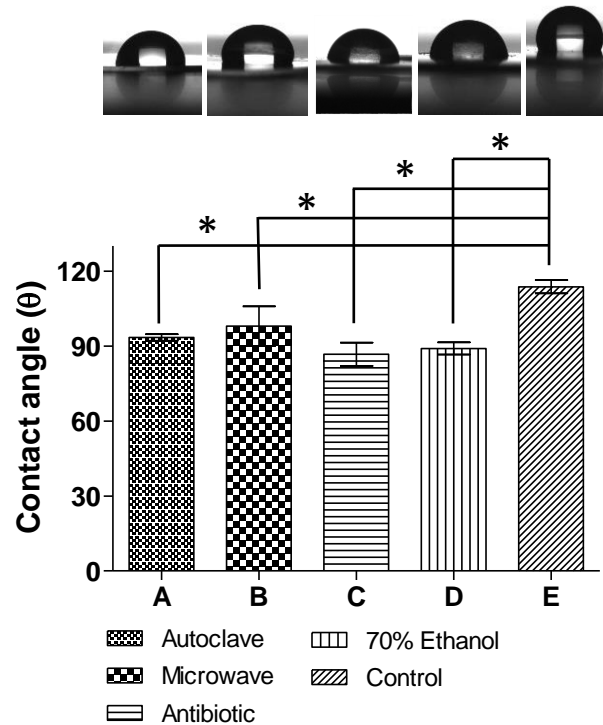


**Figure 5.4.** Contact angle ( $\theta$ ) measurements on cast sterilized (A-D) and control (E) POSS-PCL samples. Values are given as mean  $\pm$  one SD.

All sterilization methods induced a significant reduction in surface hydrophobicity which, according to the Wenzel phenomenon is due to a reduction in surface roughness which results in a smaller surface area and thus increases hydrophilicity (Wenzel, 1936) (Fig. 5.4,  $p < 0.05$ ). Polymers treated with antibiotics and 70 % ethanol exhibited the most extreme loss in  $\theta$  (mean loss of 23.7 % and 21.9 %, respectively) whilst exposure to microwaves had the least effect on contact angle (mean loss of 13.9 %). Treatment with antibiotics and 70 % ethanol resulted in the most hydrophilic surfaces with  $\theta$  of  $87^\circ$  and  $89^\circ$ , respectively.

The results obtained by goniometry were further corroborated by surface roughness measurements using AFM (Table 5.2 and Fig. 5.5 (II) + (III)).

**Table 5.2.** Surface topographical properties of cast sterilized POSS-PCL samples. Key: AFM, atomic force microscopy;  $\theta$ , contact angle; <sup>a</sup>, mean surface roughness (the arithmetic average of the absolute values of all points of the profile); <sup>b</sup>, root mean square roughness (RMS, the root mean square of the values of all points of the profile); <sup>c</sup>, correlation length ( $\xi$ , measure of how microscopic variables at different positions are correlated); \* =  $p < 0.05$ .

Sterilization Technique	$\theta$ (°)	AFM		
		$R_a$ (nm) <sup>a</sup>	$R_q$ (nm) <sup>b</sup>	$\xi$ (nm) <sup>c</sup>
Autoclave	93*	42.9	67.1	4.2*
Microwave	98*	44.0	89.0	45.8*
Antibiotics	87*	27.4*	74.7	31.8*
70 % Ethanol	89*	47.1	67.7	5.5*
Control	114	54.1	89.1	14.6

Figure 5.5 (I) shows the scaffold surfaces on a nano-level as well as the roughness profiles of sterilized and control surfaces. All surfaces exhibited a random pattern of peak heights with antibiotic or 70 % ethanol-treated surfaces demonstrating an overall shallower appearance of grooves compared to those of autoclaved or microwaved surfaces.  $R_a$  as well as  $R_q$  were highest in non-sterilized samples ( $R_a = 54.1$  nm and  $R_q = 89$  nm) whilst  $\xi$  of unmodified surfaces was in the mid-range ( $\xi = 14.6$  nm) (Table 5.2). Such nanoscale roughness is hypothesized to stem from the extrusion of POSS-nanocages (average diameter including functional groups = 1.5 nm) during the initial polymer synthesis step.

Based on the AFM data,  $R_a$  and  $R_q$  decreased in a parallel fashion to the reductions observed in contact angle measurements. Although one-way ANOVA did not yield a significant difference amongst most data sets of  $R_a$  and  $R_q$ , samples exposed to antibiotic solution experienced the most pronounced and statistically significant loss in  $R_a$  (50 % reduction compared to control,  $p < 0.05$ ).

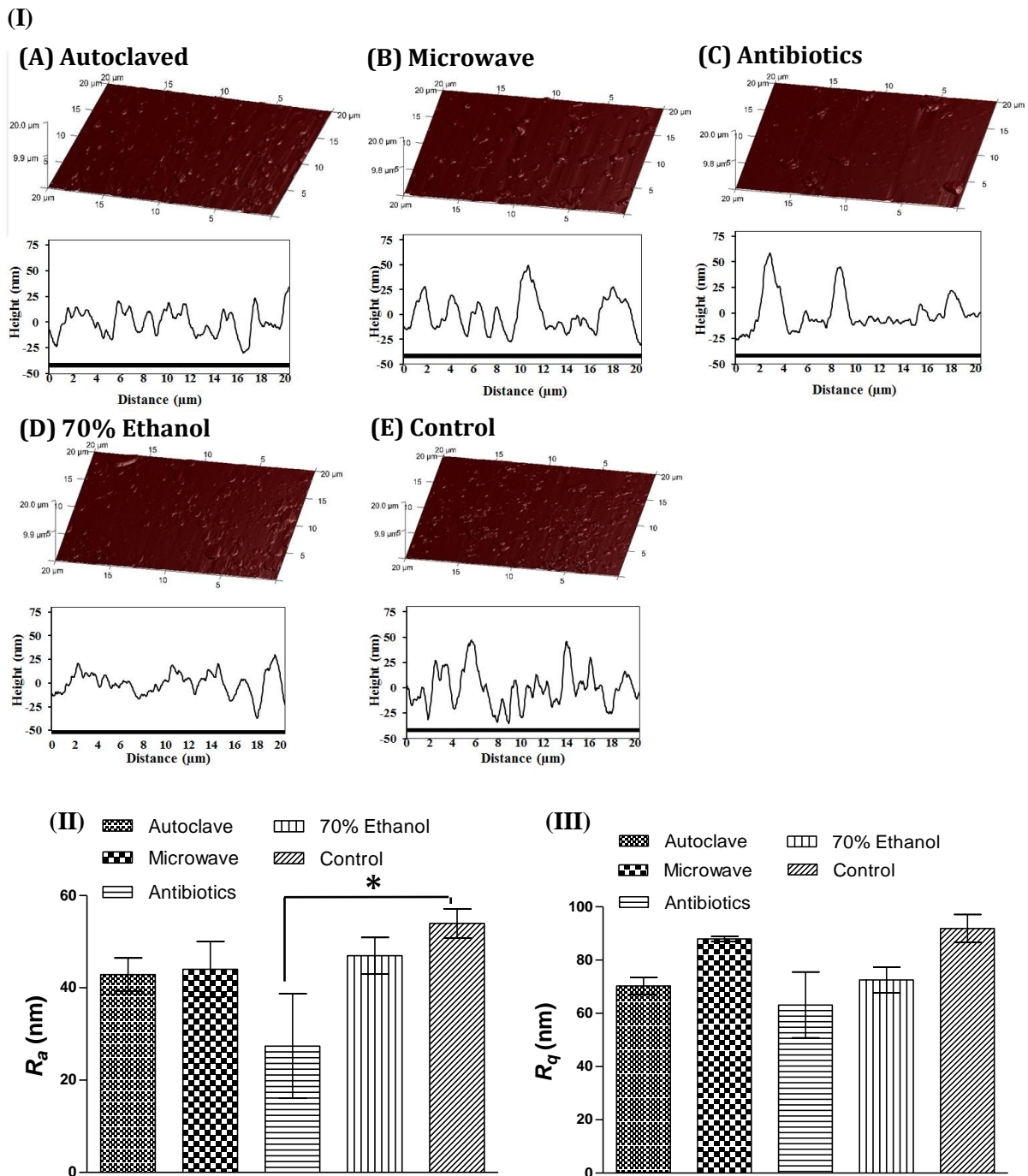


**Figure 5.5.** (I) Representative AFM images of cast sterilized (A-D) and non-sterilized control (E) POSS-PCL sheets. Dimensions 20x20 $\mu\text{m}$ . (II) Statistical analyses of mean surface roughnesses ( $R_a$ ). (III) Root mean square roughness ( $R_q$ ) analysis. All values are given as mean  $\pm$  one SD.

$R_q$ , whilst generally following a falling trend upon sterilization which indicates surface melting and irregular reformation on a nanoscale level as already demonstrated macroscopically using SEM (Fig. 5.1), did not exhibit statistically significant reductions in



values compared to control surfaces.  $\xi$  of sterilized surfaces differed significantly from control surfaces with microwave and antibiotic solution-exposed samples exhibiting a significantly increased  $\xi$  value (+68.1 % and +54.1 %, respectively) and autoclaved or 70 % ethanol-treated surfaces demonstrating a significant reduction in  $\xi$  (-71.2 % and -62.3 %, respectively). In summary, changes in contact angles corresponded to nanotopographical changes in roughness as demonstrated by AFM.

As depicted in Fig. 5.5, the roughness profiles of sterilized and control surfaces exhibit a random pattern of peak heights. Comparing the pattern of grooves along the length of the polymer surface, it is evident that antibiotic or 70 % ethanol treatment created an overall shallower appearance of grooves compared to those of autoclaved or microwaved surfaces. This is congruent with the lower contact angles of antibiotic or ethanol treated surfaces.

Consider the schematic in Fig. 5.6. A water droplet on a hydrophilic surface forms a low internal contact angle.

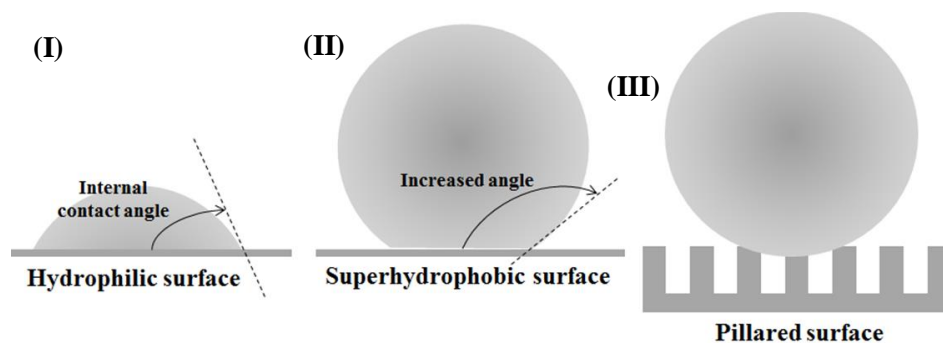


**Figure 5.6.** (I) Water drop on a hydrophilic surface forms a low internal contact angle. (II) Superhydrophobic non-wetting surfaces form a quasi-drop with a high internal contact angle. (III) A drop on a solid surface decorated with pillars with air filling the interpillar spaces. Yoshimitsu observed that the drop can sit on top of these pillars – the so-called ‘fakir regime’ – corresponding to an apparent contact angle larger than  $150^\circ$  (superhydrophobic behaviour) (Yoshimitsu et al., 2002). If the pillar height is shortened, the water contact angle decreases, because air is no longer trapped below the drop. Adapted from Quéré (Quéré, 2002).

A superhydrophobic surface, on the other hand, will form a quasi-drop with a high contact angle. A drop on a surface decorated with pillars long enough to trap air within the interpillar spaces (Cassie model) (Dettre and Johnson, 1963, Bico et al., 1999) will display an apparent contact angle of larger than  $150^\circ$ , as observed by Yoshimitsu (Yoshimitsu et al., 2002). The water drop consequently behaves as fakirs do on a bed of nails. Conversely, if the pillar height is shortened, as observed in our study with ethanol and antibiotic treatment of polymer surfaces, air can no longer be trapped in between the pillars and the water contact angle decreases, giving rise to a more hydrophilic surface (Quéré, 2002). Studies have shown that the topographical height threshold for fibroblast alignment lies at around 35 nm, below this value contact guidance no longer exists (Loesberg et al., 2007) giving rise to misaligned, broader cell morphologies.

Apart from pillar height, a further determining surface parameter is the correlation length ( $\xi$ ). In order to quantitatively describe spatial variations of surface parameters at ultrastructural levels,  $\xi$  analysis was carried out.  $\xi$ , a characteristic parameter of the covariance function was employed to estimate the fluctuations in surface roughness induced by different sterilization methods.  $\xi$  describes how microscopic variations in relative positions change the correlation patterns between such positions. E.g. if the distance between point A and point B is smaller than an arbitrary threshold  $\xi$ , then the interactions between A and B cause these points to be correlated. Peak-to-peak distance of surface micro- and nanostructures is known to influence cell-substrate behaviour, cell adhesion and proliferation. Studies analysing cellular responses to different surface structures demonstrated that smoother surfaces better supported cell attachment and subsequent proliferation compared to cells grown on nanorough surfaces (Chen et al.,

2012, Baharloo et al., 2005). This is in accordance with our cell proliferation and cell spreading results (see below). HDFa grown on surfaces treated with 70 % ethanol demonstrated highest proliferative capacity in accordance with surface topographical properties ( $\theta = 89^\circ$ ,  $R_a = 47$  nm,  $R_q = 68$  nm,  $\xi = 5.5$  nm). As can be seen in Fig. 5.9, cell morphology was influenced by surface topography. Surfaces with relatively higher  $\xi$  such as microwave or antibiotic treated surfaces ( $\xi = 46$  nm, and 32 nm, respectively) demonstrated more widely spread individual cells compared to the phenotypically more fibroblast-like spindle shaped cells seen on surfaces with lower  $\xi$  (70 % ethanol treated surfaces  $\xi = 5.5$  nm). Different surface topographies have previously been shown to markedly alter cell morphology of fibroblasts with smoother surfaces being more favourable for fibroblast proliferation (Chou et al., 1995, Könönen et al., 1992). Rough surfaces, on the other hand, were seen to provide multiple points of attachment (Wieland et al., 2002) which may influence the relatively broader spread of cells cultured on microwave or antibiotic treated surfaces.

$\xi$  of surfaces exposed to antibiotics or microwaves were found to be relatively higher compared to  $\xi$  of control surfaces (31.8 nm, 45.8 nm, and 14.6 nm, respectively).

A statistically significant reduction in surface roughness was observed in polymer sheets treated with antibiotic solution ( $p < 0.05$ ), but not for any other method of sterilization when compared to the unsterilized control sheet. Such findings diverge from earlier studies into effects of different polymer sterilization methods which found antibiotic treatment to significantly increase surface roughness of a poly(D,L-lactic-co-glycolic acid) flat sheet (Shearer et al., 2006). Such observations are suggestive of polymer-specific degradation modes towards the same treatment and thus display a non-

predictability in terms of which sterilization method is most effective while being least harmful.

#### 5.4.5 Mechanical Characteristics of Sterilized Scaffolds

Figure 5.7 (I) illustrates a representative stress-strain curve of a cast POSS-PCL sample. No differences in tensile strength were observed between differently sterilized scaffolds fabricated using the same technique (Fig. 5.7 (II) cast samples: top; coagulated samples: bottom), refuting earlier studies (Selim et al., 2011). Coagulated samples expectedly had significantly lower tensile properties compared to cast samples (Table 5.3;  $p < 0.05$ ). Maximal stress at break was found to be reduced in cast samples treated with all sterilization methods.

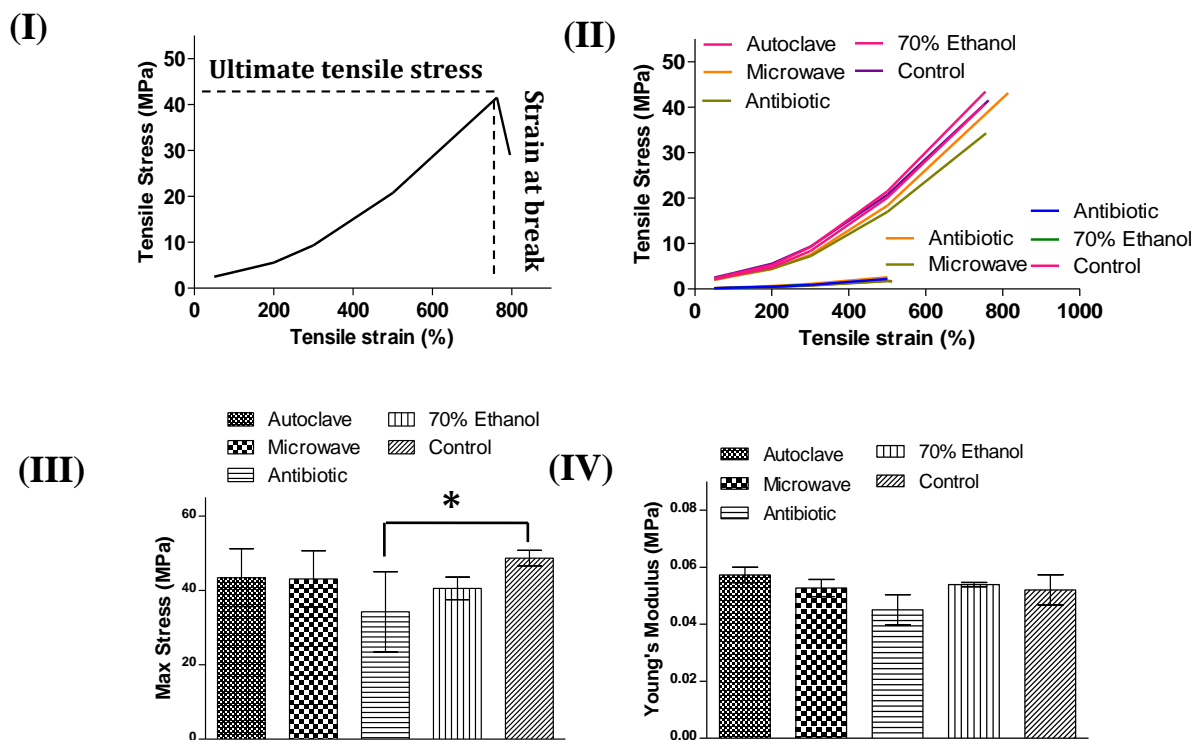


**Figure 5.7.** (I) A representative stress-strain curve of a cast POSS-PCLU sample. (II) A comparison of stress-strain curves of cast (top) and coagulated (bottom) scaffolds. Different fabrication techniques result in vastly different elastic moduli ( $E$ ). Mean elastic modulus ( $\bar{E}$ ) of cast scaffolds = 0.05 MPa vs  $\bar{E}$  of coagulated scaffolds = 0.003 MPa ( $p < 0.05$ ). (III) Treatment of cast samples using antibiotic solution reduced maximal stress values significantly compared to unsterilized controls

(C;  $p < 0.05$ ). (IV) Young's modulus was not significantly affected by any sterilization method (C). Values are given as mean  $\pm$  one SD.

Antibiotic treatment resulted in the most pronounced and statistically significant reduction in breaking stress (Fig. 5.7 (III),  $p < 0.05$ ), opposing a study conducted by Shearer who exposed coagulated and electrospun Poly(D,L Lactic-Co-Glycolic Acid) scaffolds to a 1 % (v/v) antibiotic antimycotic solution (Shearer et al., 2006). The observed differences may be due to dosage-dependent effects of antibiotics and/or differences in susceptibility of different polymers.

**Table 5.3.** Morphological and mechanical characteristics of differently sterilized POSS-PCLU scaffolds compared to human skin. Loss of scaffold diameter was assessed in porous samples. Mechanical properties of cast sheets were analysed to eliminate any potential variations induced by random pore distribution of the coagulated scaffolds, thus highlighting the mechanical properties of the pure polymer. Compared to human skin, coagulated scaffolds were significantly more elastic ( $E = 0.01$  vs  $E = 0.003$ , respectively;  $p < 0.05$ , paired  $t$ -test). Key: E. Young's modulus; d, diameter.

Sample	Sterilization Technique	Thickness (mm)	Loss in d (% of control)	Max. Tensile Strength (MPa)	Elongation at Break (%)	Young's Modulus (MPa)
Cast	Autoclave	0.28 $\pm$ 0.03	-	41.98 $\pm$ 9.90	919.80 $\pm$ 105.40	0.02
	Microwave	0.23 $\pm$ 0.02	-	47.61 $\pm$ 5.74	893.03 $\pm$ 34.19	0.02
	Antibiotics	0.27 $\pm$ 0.04	-	42.59 $\pm$ 4.08	890.68 $\pm$ 70.18	0.02
	70 % Ethanol	0.25 $\pm$ 0.012	-	54.31 $\pm$ 4.20	920.45 $\pm$ 68.81	0.02
	Control	0.26 $\pm$ 0.02	-	45.04 $\pm$ 8.40	898.54 $\pm$ 112.10	0.02
Coagulated	Autoclave	0.93 $\pm$ 0.04	22.0*	1.34 $\pm$ 0.12	568.07 $\pm$ 27.42	0.01
	Microwave	0.73 $\pm$ 0.03	10.0	1.63 $\pm$ 0.14	579.34 $\pm$ 16.59	0.01
	Antibiotics	0.98 $\pm$ 0.07	2.0	1.25 $\pm$ 0.11	496.48 $\pm$ 33.53	0.01
	70 % Ethanol	0.95 $\pm$ 0.05	7.5	1.14 $\pm$ 0.07	535.89 $\pm$ 29.69	0.01
	Control	0.83 $\pm$ 0.12	-	1.68 $\pm$ 0.55	512.34 $\pm$ 60.48	0.01
Human skin (Pailler-Mattei et al., 2008, Edwards and Marks, 1995)	n/a	1.00 – 3.00		21.50 $\pm$ 8.40	54.00 $\pm$ 17.00	0.01 – 0.02

#### 5.4.6 *In Vitro* Cell Viability and Proliferation

The percentage cell viability versus time and sterilization condition is represented as a bar chart in Figure 5.8. Viability of cells grown on normal TCP serves as the control total viability (i.e. 100 %). The general trend demonstrated increased cell adhesion and metabolic viability at each consecutive time point. However, AlamarBlue® metabolic assay demonstrated an initial lag in percentage viability of cells grown on 70 % ethanol treated films which is compensated for on day 7.

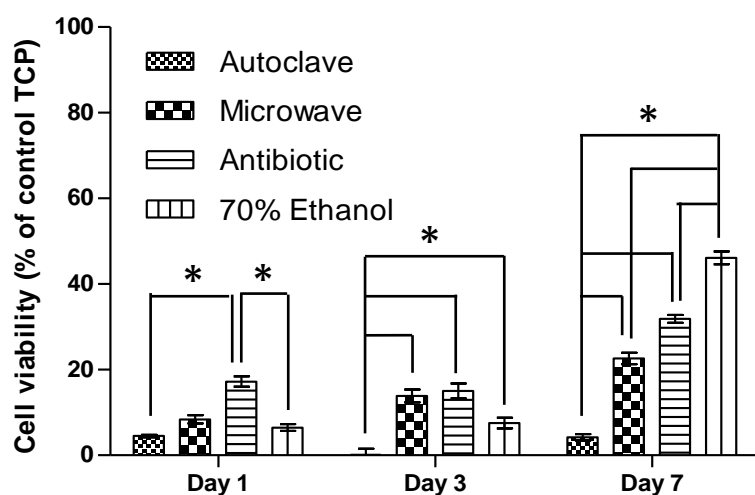


**Figure 5.8.** Percentage viability of HDFa grown on sterilized cast discs compared to cells grown on tissue culture plastic over a 7 day period assessed using AlamarBlue® cell viability assay. \* =  $p < 0.05$ . Values are given as mean  $\pm$  one SD.

In fact, relative cell proliferative capacity on ethanol treated films surpassed that of cells grown on every other surface (apart from TCP) by a factor of 9 over a period of seven days. Similarly, cell viability was found to be well supported by films treated with antibiotic solution. Autoclave treatment resulted in a cell-repellent surface with minimal to no cell adhesive capacity and significantly reduced cell viability. Exposure of films to microwaves supported cell proliferation but significantly less so compared to treatment with both antibiotic and 70 % ethanol solution ( $p < 0.05$ ). These results demonstrated

that optimal adhesion and alignment of HDFa onto differently sterilized POSS-PCLU polymer occurs with surfaces showing a combination of moderate wettability and relatively short peak-to-peak distance. It has previously been demonstrated that the cut-off contact angle for good cell attachment and spreading is  $\theta \leq 90^\circ$  (Förch et al., 2009). In terms of tissue engineering platforms, surface wettability of below  $90^\circ$  is regarded a highly important cue for the attachment of cells and the subsequent induction of tissue growth and regeneration (Olbrich et al., 2007, Yang et al., 2002). The enhanced adhesion of cells onto ethanol treated samples can be ascribed to the different surface chemistries, indicating a preference of cells for hydrophilic structures as ethanol treated films exhibited relatively more hydrophilic properties ( $\theta < 90^\circ$  in both cases). Surface wettabilities of under  $90^\circ$  are known to promote cell adhesion and proliferation by increasing surface free energy (Ishizaki et al., 2010, Zhao et al., 2010). Zhao previously demonstrated smaller water contact angles and higher values for surface free energy upon sterilization with ethanol compared to autoclaving (Zhao et al., 2010). These results are corroborated here. FTIR results demonstrated that hydrolysis of the soft segments converted the ester groups on the surface to hydrophilic hydroxyl and carboxyl groups which were favourable for cell attachment (Ng et al., 2001).

Live/Dead<sup>®</sup> images of cells cultured on sterilized cast films are shown in Figure 5.9. Films exposed to any of the sterilization methods demonstrated acceptable initial cell attachment (day one) but cell adhesion visibly declined on day 1 on autoclaved surfaces which was in accordance with AlamarBlue<sup>®</sup> studies (Fig. 5.8). All except autoclaved surfaces supported cell growth throughout the entire study period of 7 days. Autoclaved surfaces displayed an inherently cell-repellent character with minimal initial cell adhesion and no proliferation throughout the entire study period. In terms of cell

morphology, only cells grown on 70 % ethanol-treated films exhibited spindle-like morphologies typical for fibroblasts, similar to cells grown on control TCP.

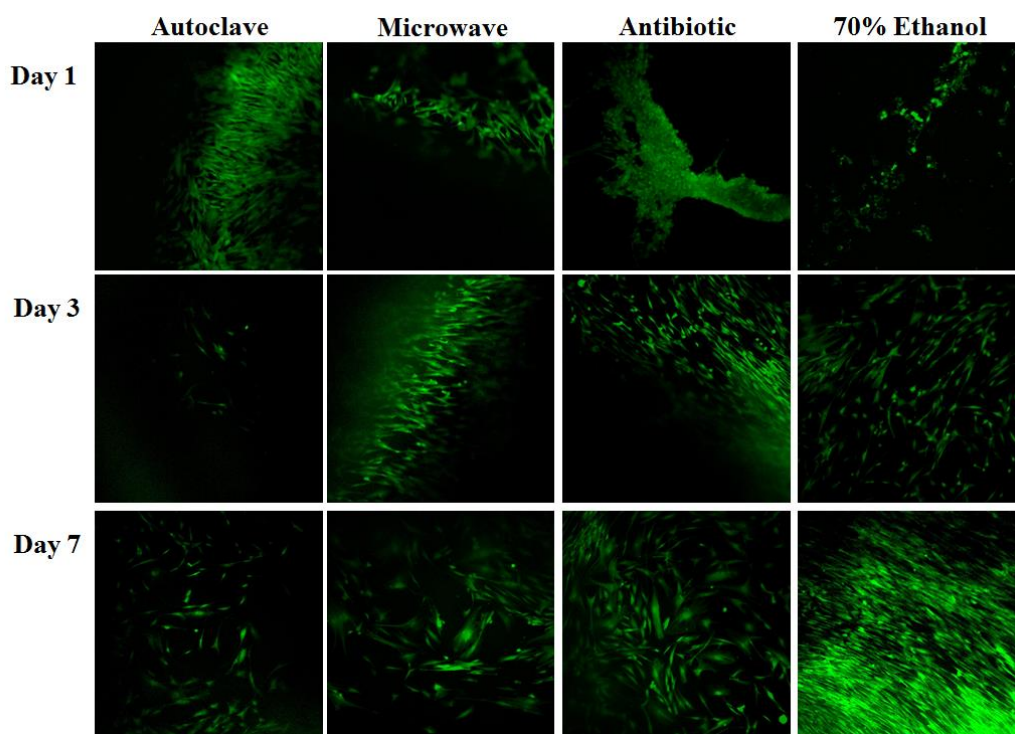


**Figure 5.9.** Representative laser scanning confocal microscopy images of HDFa cells grown on cast sterilized POSS-PCLU discs stained with Live/Dead® stain.

Generally, few or no dead cells (red) were visible on all sterilized or control surfaces. Films treated with 70 % ethanol supported cell adhesion and proliferation best.

#### 5.4.7 Cell Morphology and Attachment

Confocal laser scanning microscopy images indicated that fibroblasts developed different morphologies when grown on differently sterilized surfaces (Fig. 5.10 (I)). Cells grown on surfaces sterilised with microwaves or antibiotic solution exhibited a more spread out phenotype compared to cells grown on autoclaved surfaces or those exposed to 70 % ethanol which demonstrated an aligned and elongated spindle-like character. Due to a significantly higher  $\xi$  (peak to peak distance) of these surfaces, both microwaved



and antibiotic treated scaffolds provided more spread out points of attachment, thus anchoring the cells over a larger surface area (Fig. 5.10 (II),  $p < 0.05$ ).

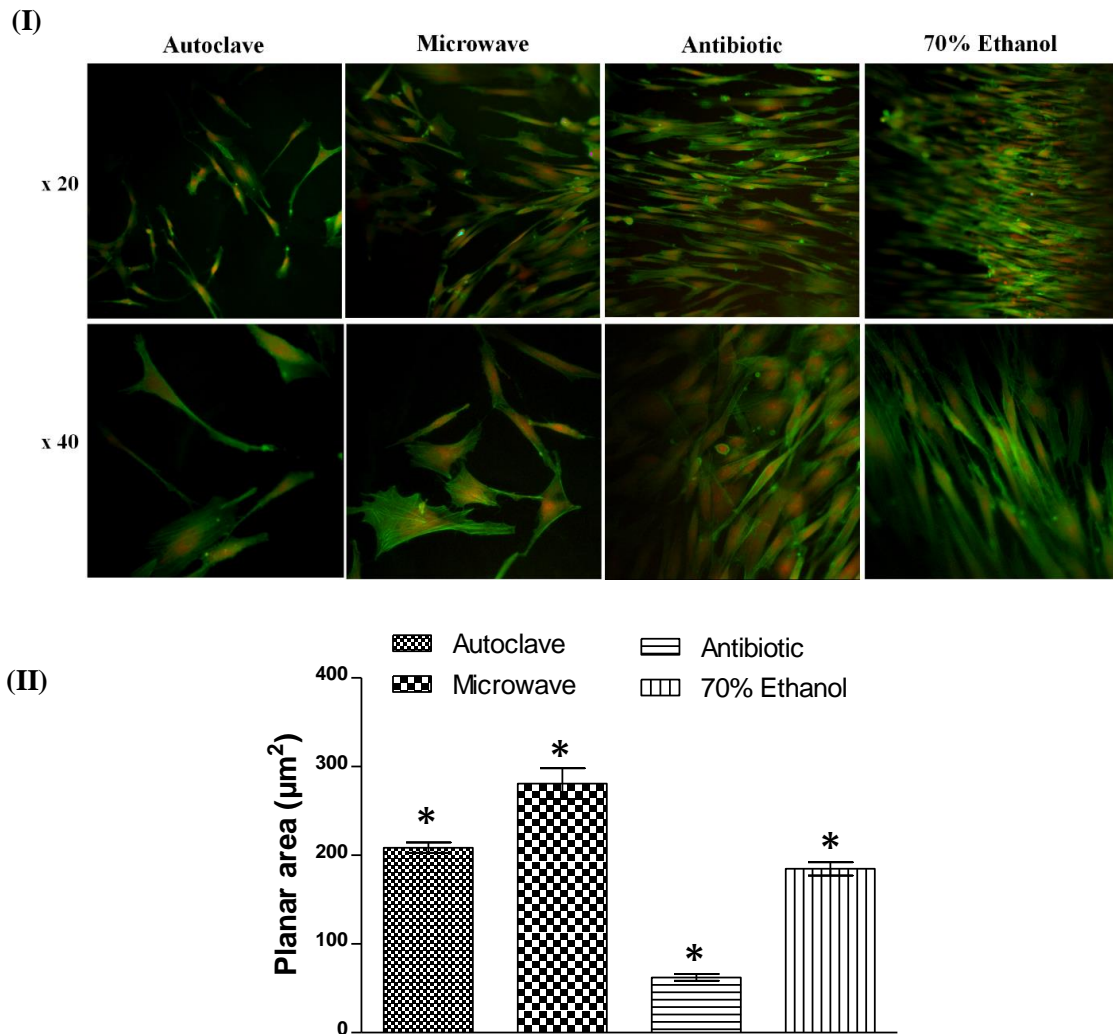


**Figure 5.10.** (I) Representative confocal images of HDFa cultured on sterilized cast POSS-PCLU films for 7 days. Filamentous actin (F-actin) was visualised with FITC-phalloidin and nuclei counterstained with propidium iodide. (II) Planar surface area calculations support the hypothesis that different sterilization methods induce changes in surface topographies which can influence cell spreading and alignment. \* indicates statistically significant differences ( $p < 0.05$ ). Values are given as mean  $\pm$  one SD.

#### 5.4.8 POSS-PCLU Scaffolds as Tissue Engineering Platforms

The ability of this novel polymer system to act as a tissue engineering scaffold was subsequently analysed on coagulated spongy POSS-PCLU scaffolds (Fig. 5.11). Scaffolds

were sterilized and subsequently seeded with HDFa at a density of  $5 \times 10^4$  cells/scaffold. % cell viability of control cells (grown on TCP) was derived from AlamarBlue® metabolic assay and found to steadily increase over a period of seven days (Fig. 5.11 (I)).

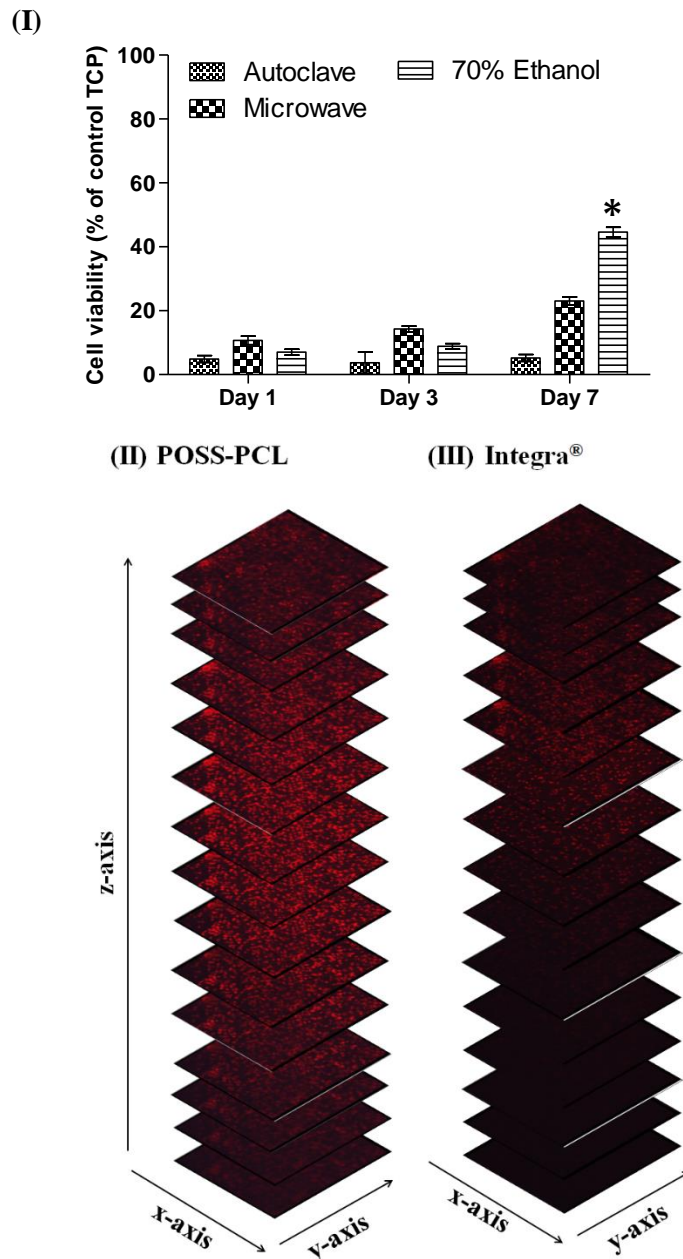


**Figure 5.11.** (I) Analysis of % cell viability on porous POSS-PCLU scaffolds compared to cells grown on tissue culture plastic. Antibiotic treated surfaces were excluded from statistical analysis due to recurrent contamination. \* =  $p < 0.05$ . Values are given as mean  $\pm$  one SD. (II) Z-stack of a porous POSS-PCLU scaffold and (III) Integra® dermal regeneration template seeded with HDFa and cultured for 7 days.

Autoclaved surfaces exhibited the least cytocompatible surface with % viabilities of less than 30 % at day seven. Similarly, surfaces exposed to microwaves had relatively stagnant cell growth and % viability also remained under 30 % of control. As expected, surfaces treated with 70 % ethanol had significantly higher cell proliferation ( $p < 0.05$ ). Surprisingly, however, there was significantly higher metabolic activity within antibiotic treated scaffolds. Subsequent immersion of aliquots of used culture medium into fresh sterile medium confirmed a suspected infection in the scaffolds treated with antibiotic solution. The results obtained with antibiotic treated scaffolds were therefore removed.

All other media remained clear of infection after 72 h. In order to visualise cellular penetration depth into the porous architecture of scaffolds, cells were cultured for seven days on 70 % ethanol sterilized sponges and nuclei were visualised with PI. Confocal imaging in conjunction with z-stacking demonstrated excellent cellular penetration into the internal architecture of the porous POSS-PCLU sponges (Fig. 5.11 (II)). A preliminary comparative study investigating the difference in cell adhesion and proliferation on POSS-PCLU scaffolds and Integra® dermal regeneration template (bovine collagen matrix, current clinical gold standard) demonstrated better adhesion and proliferative capacity as well as deeper migration of HDFa into POSS-PCLU scaffolds (Fig. 5.11 (II) versus (III)).

## 5.5 CONCLUSION

Cast and coagulated biodegradable POSS-PCLU scaffolds were exposed to 4 different sterilizing methods and their suitability as post-production processing tools to enhance biocompatibility were assessed. Autoclave and microwave treatments successfully sterilized cast POSS-PCLU films but significantly damaged the 3D porous structures of coagulated scaffolds. Additionally, autoclaved polymer surfaces displayed a hydrophobic, cell-repellent surface, overall making high pressure steam treatment an

unsuitable sterilization choice. Antibiotic antimycotic solution was ineffective in removing all micro-organisms and can therefore be excluded as a sterilizing agent. Exposure of both cast and coagulated scaffolds to 70 % ethanol resulted in the best overall sterilization efficiency combined with the least destructive effect on porosity and enhanced cytocompatibility. Ethanol treatment induced favourable surface topographical changes which positively influenced cell attachment, morphology, alignment as well as viability and proliferation. The present sterilization technique using 70 % ethanol can pave the way for future tissue engineering using bioabsorbable POSS-PCLU nanocomposite materials as regenerative platforms by addressing two current obstacles at once.

## References

- AHMED, M., GHANBARI, H., COUSINS, B. G., HAMILTON, G. & SEIFALIAN, A. M. 2011. Small calibre polyhedral oligomeric silsesquioxane nanocomposite cardiovascular grafts: influence of porosity on the structure, haemocompatibility and mechanical properties. *Acta Biomater.*, 7, 3857-67.
- ATHANASIOU, K. A., NIEDERAUER, G. G. & AGRAWAL, C. M. 1996. Sterilization, toxicity, biocompatibility and clinical applications of polylactic acid/polyglycolic acid copolymers. *Biomaterials*, 17, 93-102.
- BAE, J. S., SEO, E. J. & KANG, I. K. 1999. Synthesis and characterization of heparinized polyurethanes using plasma glow discharge. *Biomaterials*, 20, 529-37.
- BAHARLOO, B., TEXTOR, M. & BRUNETTE, D. M. 2005. Substratum roughness alters the growth, area, and focal adhesions of epithelial cells, and their proximity to titanium surfaces. *Journal of biomedical materials research. Part A*, 74, 12-22.
- BAIER, R. E., MEYER, A. E., AKERS, C. K., NATIELLA, J. R., MEENAGHAN, M. & CARTER, J. M. 1982. Degradative effects of conventional steam sterilization on biomaterial surfaces. *Biomaterials*, 3, 241-5.
- BICO, J., MARZOLIN, C. & QUÈRÈ, D. 1999. Perl drops. *Europhys. Lett.*, 47, 220-6.
- CHALOUPKA, K., MOTWANI, M. & SEIFALIAN, A. M. 2011. Development of a new lacrimal drainage conduit using POSS nanocomposite. *Biotechnology and applied biochemistry*, 58, 363-70.
- CHAN-CHAN, L. H., SOLIS-CORREA, R., VARGAS-CORONADO, R. F., CERVANTES-UC, J. M., CAUICH-RODRÍGUEZ, J. V., QUINTANA, P. & BARTOLO-PÉREZ, P. 2010. Degradation studies on segmented polyurethanes prepared with HMDI, PCL and different chain extenders. *Acta biomaterialia*, 6, 2035-44.
- CHEN, W., SUN, Y. & FU, J. 2013. Microfabricated nanotopological surfaces for study of adhesion-dependent cell mechanosensitivity. *Small (Weinheim an der Bergstrasse, Germany)*, 9, 81-9.
- CHEN, W., VILLA-DIAZ, L. G., SUN, Y., WENG, S., KIM, J. K., LAM, R. H. W., HAN, L., FAN, R., KREBSBACH, P. H. & FU, J. 2012. Nanotopography influences adhesion, spreading, and self-renewal of human embryonic stem cells. *ACS nano*, 6, 4094-103.
- CHENG, Z. & TEOH, S.-H. 2004. Surface modification of ultra thin poly (epsilon-caprolactone) films using acrylic acid and collagen. *Biomaterials*, 25, 1991-2001.
- CHOU, L., FIRTH, J. D., UITTO, V. J. & BRUNETTE, D. M. 1995. Substratum surface topography alters cell shape and regulates fibronectin mRNA level, mRNA stability, secretion and assembly in human fibroblasts. *Journal of cell science*, 108 (Pt 4), 1563-73.
- DE MEL, A., PUNSHON, G., RAMESH, B., SARKAR, S., DARBYSHIRE, A., HAMILTON, G. & SEIFALIAN, A. M. 2009. In situ endothelialization potential of a biofunctionalised nanocomposite biomaterial-based small diameter bypass graft. *Biomed.Mater Eng*, 19, 317-31.
- DETTRE, R. H. & JOHNSON, R. E. 1963. No Title. *Adv. Chem. Ser.*, 43, 136-44.
- DRENKARD, E. & AUSUBEL, F. M. 2002. Pseudomonas biofilm formation and antibiotic resistance are linked to phenotypic variation. *Nature*, 416, 740-3.
- EDWARDS, C. & MARKS, R. 1995. Evaluation of biomechanical properties of human skin. *Clinics in dermatology*, 13, 375-80.
- FITZPATRICK, J. A., KWAO-PAUL, J. & MASSEY, J. 1978. Sterilization of bacteria by means of microwave heating. *Journal of clinical engineering*, 3, 44-7.
- FLEMMING, R. G., MURPHY, C. J., ABRAMS, G. A., GOODMAN, S. L. & NEALEY, P. F. 1999. Effects of synthetic micro- and nano-structured surfaces on cell behavior. *Biomaterials*, 20, 573-88.

- FÖRCH, R., SCHÖNHERR, H. & JENKINS, A. T. A. 2009. *Surface design: applications in bioscience and nanotechnology*, Wiley-VCH.
- HARVEY, A. F. 1963. *Microwave Engineering*, New York, Academic Press.
- HOLY, C. E., CHENG, C., DAVIES, J. E. & SHOICHET, M. S. 2001. Optimizing the sterilization of PLGA scaffolds for use in tissue engineering. *Biomaterials*, 22, 25-31.
- HUSSAIN, M. A. & SIEDLECKI, C. A. 2004. The platelet integrin alpha(IIb) beta(3) imaged by atomic force microscopy on model surfaces. *Micron (Oxford, England : 1993)*, 35, 565-73.
- HUTMACHER, D. W. 2000. Scaffolds in tissue engineering bone and cartilage. *Biomaterials*, 21, 2529-43.
- ISHIZAKI, T., SAITO, N. & TAKAI, O. 2010. Correlation of cell adhesive behaviors on superhydrophobic, superhydrophilic, and micropatterned superhydrophobic/superhydrophilic surfaces to their surface chemistry. *Langmuir : the ACS journal of surfaces and colloids*, 26, 8147-54.
- J.ARMSTRONG, H.J.SALACINSKI, Q.MU, A.M.SEIFALIAN, L.PEEL, N.FREEMAN, C.M.HOLT & J.R.LU 2004. Interfacial adsorption of fibrinogen and its inhibition by RGD peptide: a combined physical study. *J Phys Condens Matter*, 16.
- JUNGEBLUTH, P., ALICI, E., BAIGUERA, S., LE, B. K., BLOMBERG, P., BOZOKY, B., CROWLEY, C., EINARSSON, O., GRINNEMO, K. H., GUDBJARTSSON, T., LE, G. S., HENRIKSSON, G., HERMANSON, O., JUTO, J. E., LEIDNER, B., LILJA, T., LISKA, J., LUEDDE, T., LUNDIN, V., MOLL, G., NILSSON, B., RODERBURG, C., STROMBLAD, S., SUTLU, T., TEIXEIRA, A. I., WATZ, E., SEIFALIAN, A. & MACCHIARINI, P. 2011a. Tracheobronchial transplantation with a stem-cell-seeded bioartificial nanocomposite: a proof-of-concept study. *Lancet*, 378, 1997-2004.
- KANNAN, R. Y., SALACINSKI, H. J., BUTLER, P. E. & SEIFALIAN, A. M. 2005. Polyhedral oligomeric silsesquioxane nanocomposites: the next generation material for biomedical applications. *Acc.Chem.Res.*, 38, 879-84.
- KANNAN, R. Y., SALACINSKI, H. J., ODLYHA, M., BUTLER, P. E. & SEIFALIAN, A. M. 2006. The degradative resistance of polyhedral oligomeric silsesquioxane nanocore integrated polyurethanes: an in vitro study. *Biomaterials*, 27, 1971-9.
- KARP, J. M., SHOICHET, M. S. & DAVIES, J. E. 2003. Bone formation on two-dimensional poly(DL-lactide-co-glycolide) (PLGA) films and three-dimensional PLGA tissue engineering scaffolds in vitro. *Journal of biomedical materials research. Part A*, 64, 388-96.
- KHANG, D., LU, J., YAO, C., HABERSTROH, K. M. & WEBSTER, T. J. 2008. The role of nanometer and sub-micron surface features on vascular and bone cell adhesion on titanium. *Biomaterials*, 29, 970-83.
- KIKUCHI, A. & OKANO, T. 2005. Nanostructured designs of biomedical materials: applications of cell sheet engineering to functional regenerative tissues and organs. *Journal of controlled release : official journal of the Controlled Release Society*, 101, 69-84.
- KÖNÖNEN, M., HORMIA, M., KIVILAHTI, J., HAUTANIEMI, J. & THESLEFF, I. 1992. Effect of surface processing on the attachment, orientation, and proliferation of human gingival fibroblasts on titanium. *Journal of biomedical materials research*, 26, 1325-41.
- KUIJER, R., JANSEN, E. J. P., EMANS, P. J., BULSTRA, S. K., RIESLE, J., PIEPER, J., GRAINGER, D. W. & BUSSCHER, H. J. 2007. Assessing infection risk in implanted tissue-engineered devices. *Biomaterials*, 28, 5148-54.
- KUPPAN, P., VASANTHAN, K. S., SUNDARAMURTHI, D., KRISHNAN, U. M. & SETHURAMAN, S. 2011. Development of poly(3-hydroxybutyrate-co-3-hydroxyvalerate)

fibers for skin tissue engineering: effects of topography, mechanical, and chemical stimuli. *Biomacromolecules*, 12, 3156-65.

LANGER, R. & VACANTI, J. P. 1993. Tissue engineering. *Science*, 260, 920-6.

LAVIK, E. & LANGER, R. 2004. Tissue engineering: current state and perspectives. *Applied microbiology and biotechnology*, 65, 1-8.

LOESBERG, W. A., TE RIET, J., VAN DELFT, F. C. M. J. M., SCHÖN, P., FIGDOR, C. G., SPELLER, S., VAN LOON, J. J. W. A., WALBOOMERS, X. F. & JANSEN, J. A. 2007. The threshold at which substrate nanogroove dimensions may influence fibroblast alignment and adhesion. *Biomaterials*, 28, 3944-51.

MA, L., ZHOU, J., GAO, C. & SHEN, J. 2007. Incorporation of basic fibroblast growth factor by a layer-by-layer assembly technique to produce bioactive substrates. *Journal of biomedical materials research. Part B, Applied biomaterials*, 83, 285-92.

MACHADO, A. L., GIAMPAOLO, E. T., VERGANI, C. E., SOUZA, J. F. D. & JORGE, J. H. 2011. Changes in roughness of denture base and reline materials by chemical disinfection or microwave irradiation: surface roughness of denture base and reline materials. *Journal of applied oral science : revista FOB*, 19, 521-8.

MANSILLA, E., SPRETZ, R., LARSEN, G., NUÑEZ, L., DRAGO, H., STURLA, F., MARIN, G. H., ROQUE, G., MARTIRE, K., DÍAZ AQUINO, V., BOSSI, S., GARDINER, C., LAMONEGA, R., LAUZADA, N., CORDONE, J., RAIMONDI, J. C., TAU, J. M., BIASI, N. R., MARINI, J. E., PATEL, A. N., ICHIM, T. E., RIORDAN, N. & MACEIRA, A. 2010. Outstanding survival and regeneration process by the use of intelligent acellular dermal matrices and mesenchymal stem cells in a burn pig model. *Transplantation proceedings*, 42, 4275-8.

MILLER, D. C., THAPA, A., HABERSTROH, K. M. & WEBSTER, T. J. 2004. Endothelial and vascular smooth muscle cell function on poly(lactic-co-glycolic acid) with nano-structured surface features. *Biomaterials*, 25, 53-61.

NG, K. W., HUTMACHER, D. W., SCHANTZ, J. T., NG, C. S., TOO, H. P., LIM, T. C., PHAN, T. T. & TEOH, S. H. 2001. Evaluation of ultra-thin poly(epsilon-caprolactone) films for tissue-engineered skin. *Tissue engineering*, 7, 441-55.

NINEMEIER, J. D. 2003. *Central Service Technical Manual*, International Association of Healthcare Central Service Material Management.

NOAH, E. M., CHEN, J., JIAO, X., HESCHEL, I. & PALLUA, N. 2002. Impact of sterilization on the porous design and cell behavior in collagen sponges prepared for tissue engineering. *Biomaterials*, 23, 2855-61.

OLBRICH, M., PUNSHON, G., FRISCHAUF, I., SALACINSKI, H. J., REBOLLAR, E., ROMANIN, C., SEIFALIAN, A. M. & HEITZ, J. 2007. UV surface modification of a new nanocomposite polymer to improve cytocompatibility. *J Biomater.Sci Polym Ed*, 18, 453-68.

PAILLER-MATTEI, C., BEC, S. & ZAHOUANI, H. 2008. In vivo measurements of the elastic mechanical properties of human skin by indentation tests. *Medical engineering & physics*, 30, 599-606.

PAN, H.-A., LIANG, J.-Y., HUNG, Y.-C., LEE, C.-H., CHIOU, J.-C. & HUANG, G. S. 2013. The spatial and temporal control of cell migration by nanoporous surfaces through the regulation of ERK and integrins in fibroblasts. *Biomaterials*, 34, 841-53.

PRICE, R. L., ELLISON, K., HABERSTROH, K. M. & WEBSTER, T. J. 2004. Nanometer surface roughness increases select osteoblast adhesion on carbon nanofiber compacts. *Journal of biomedical materials research. Part A*, 70, 129-38.

QUÉRÉ, D. 2002. Surface chemistry: Fakir droplets. *Nature materials*, 1, 14-5.

RAINER, A., CENTOLA, M., SPADACCIO, C., GHERARDI, G., GENOVESE, J. A., LICOCIA, S. & TROMBETTA, M. 2010. Comparative study of different techniques for the sterilization

of poly-L-lactide electrospun microfibers: effectiveness vs. material degradation. *The International journal of artificial organs*, 33, 76-85.

REHFELDT, F., ENGLER, A. J., ECKHARDT, A., AHMED, F. & DISCHER, D. E. 2007. Cell responses to the mechanochemical microenvironment--implications for regenerative medicine and drug delivery. *Advanced drug delivery reviews*, 59, 1329-39.

RICHARDS, M., DAHIYAT, B. I., ARM, D. M., BROWN, P. R. & LEONG, K. W. 1991. Evaluation of polyphosphates and polyphosphonates as degradable biomaterials. *Journal of biomedical materials research*, 25, 1151-67.

SALACINSKI, H. J., HANDCOCK, S. & SEIFALIAN, A. M. 2005. *Polymer for use in conduits and medical devices*.

SELIM, M., BULLOCK, A. J., BLACKWOOD, K. A., CHAPPLE, C. R. & MACNEIL, S. 2011. Developing biodegradable scaffolds for tissue engineering of the urethra. *BJU international*, 107, 296-302.

SERVAY, T., VOELKEL, R., SCHMIEDBERGER, H. & LEHMANN, S. 2000. Thermal oxidation of the methylene diphenylene unit in MDI-TPU. *Polymer*, 41, 5247-56.

SHEARER, H., ELLIS, M. J., PERERA, S. P. & CHAUDHURI, J. B. 2006. Effects of common sterilization methods on the structure and properties of poly(D,L lactic-co-glycolic acid) scaffolds. *Tissue engineering*, 12, 2717-27.

SKOLNIK, M. I. 1970. *Radar Handbook*, New York, McGraw Hill.

TONAZZINI, I., BYSTRENOVA, E., CHELLI, B., GRECO, P., STOLIAR, P., CALÒ, A., LAZAR, A., BORGATTI, F., D'ANGELO, P., MARTINI, C. & BISCARINI, F. 2010. Multiscale morphology of organic semiconductor thin films controls the adhesion and viability of human neural cells. *Biophysical journal*, 98, 2804-12.

ULABY, F. T., BATLIVALA, P. P. & DOBSON, M. C. 1978. Microwave Backscatter Dependence on Surface Roughness, Soil Moisture, and Soil Texture: Part I-Bare Soil. *Geoscience Electronics*, 16, 286-95.

VACANTI, J. P. & LANGER, R. 1999. Tissue engineering: the design and fabrication of living replacement devices for surgical reconstruction and transplantation. *Lancet*, 354 Suppl, S132-4.

WASHBURN, N. R., YAMADA, K. M., SIMON, C. G., KENNEDY, S. B. & AMIS, E. J. 2004. High-throughput investigation of osteoblast response to polymer crystallinity: influence of nanometer-scale roughness on proliferation. *Biomaterials*, 25, 1215-24.

WENZEL, R. N. 1936. No Title. *Ind. Eng. Chem*, 28, 988-94.

WIELAND, M., CHEHROUDI, B., TEXTOR, M. & BRUNETTE, D. M. 2002. Use of Ti-coated replicas to investigate the effects on fibroblast shape of surfaces with varying roughness and constant chemical composition. *Journal of biomedical materials research*, 60, 434-44.

WINKELMANN, M., GOLD, J., HAUERT, R., KASEMO, B., SPENCER, N. D., BRUNETTE, D. M. & TEXTOR, M. 2003. Chemically patterned, metal oxide based surfaces produced by photolithographic techniques for studying protein- and cell-surface interactions I: Microfabrication and surface characterization. *Biomaterials*, 24, 1133-45.

YANG, J., SHI, G., BEI, J., WANG, S., CAO, Y., SHANG, Q., YANG, G. & WANG, W. 2002. Fabrication and surface modification of macroporous poly(L-lactic acid) and poly(L-lactic-co-glycolic acid) (70/30) cell scaffolds for human skin fibroblast cell culture. *Journal of biomedical materials research*, 62, 438-46.

YOSHIMITSU, Z., NAKAJIMA, A., WATANABE, T. & HASHIMOTO, K. 2002. Effects of Surface Structure on the Hydrophobicity and Sliding Behavior of Water Droplets. *Langmuir*, 18, 5818-22.



- ZHANG, Y. Z., BJURSTEN, L. M., FREIJ-LARSSON, C., KOBER, M. & WESSLÉN, B. 1996. Tissue response to commercial silicone and polyurethane elastomers after different sterilization procedures. *Biomaterials*, 17, 2265-72.
- ZHAO, L., MEI, S., WANG, W., CHU, P. K., WU, Z. & ZHANG, Y. 2010. The role of sterilization in the cytocompatibility of titania nanotubes. *Biomaterials*, 31, 2055-63.



# 6 EFFECT OF HARD SEGMENT CHEMISTRY ON LONG-TERM *IN VITRO* OXIDATIVE AND HYDROLYTIC STABILITY OF POSS-PCLU SCAFFOLDS

---

## 6.1 SYNOPSIS

Biodegradable PU scaffolds are a popular choice for tissue engineering and regenerative applications, particularly in mechanically challenging settings (e.g. the skin). Previous investigations mainly focussed on the integration of more or less hydrolysable components to modulate degradation rates. In this chapter, however, the objective was to synthesize a family of novel biodegradable PUs with varying amounts of hard segments in order to investigate the influence of hard segment chemistry on the degradation rate and profile. Specifically, we synthesized a PU based on a poly( $\epsilon$ -caprolactone urea)urethane backbone integrating polyhedral oligomeric silsesquioxane (POSS-PCLU) nanoparticles using dry polycaprolactone diol as the soft segment and different concentrations (24 %, 28 % and 33 % (w/v)) of dicyclohexylmethane diisocyanate as the hard segment with ethylenediamine as a chain extender. PUs lacking POSS nanoparticles served to prove the important function of POSS in maintaining the viscoelasticity of the PUs before, during and after degradation. Polymer tensile strength and Young's moduli increase with increasing hard segment content whilst breaking strain was not significantly affected. Both *in vitro* and *in vivo* degradation studies revealed hard segment-dependent modulation of the materials' viscoelastic properties which was attributable to (i) degradation-induced changes in the PU crystallinities and (ii) the presence or absence of POSS. The data obtained in this study highlight the influence of

hard segment content and POSS nanoparticles on PU properties. This provide opportunities for a higher degree of control over degradation rates and mechanical properties which is important for scaffolds intended for tissue engineering and regenerative purposes.

## 6.2 INTRODUCTION

Segmented PUs are amongst the most favoured synthetic polymers used in the manufacture of biomedical devices due to their superior biomechanical properties and a unique combination of toughness, durability, flexibility and biocompatibility. Generally, PUs are synthesized by reacting soft segments of polyesters/polycarbonate with hard segment of diisocyanates. Since their discovery by Otto Bayer in 1937, the PU family has become the most versatile of any family of plastic materials gaining considerable popularity in the biomedical field as pacemaker leads, catheters, vascular grafts and prosthetic heart valves (Chawla et al. 1988; Izci et al. 2009; Rahmani et al. 2012; Desai et al. 2012). Whilst non-resorbable scaffolds are adequately suited for certain applications, their lack of degradation limits their use to the adult population and potentially necessitates revision surgeries to replace or remove such scaffolds. Bioresorbable scaffolds, on the other hand, must maintain temporary structural integrity within relatively harsh wound environments and degrade in a controllable fashion surrounded by enzymes and free radicals, pH as well as temperature fluctuations. Numerous investigations have studied the biodegradation behaviour of segmented PUs by integrating more or less hydrolysable components such as PEG, PLA, and PGA (G. Li et al. 2012; Rafiemanzelat et al. 2013; Z. Li et al. 2012). However, degradation-induced loss of mechanical properties and rapid acidification of the degradation media limit their clinical application. Additionally, commonly used biodegradable PUs are based on aromatic diisocyanates which break down into toxic by-products originating from the hard segments (Tang et al. 2003; Szycher, M.; Poirier, V.L.; Dempsey 1983b; Gogolewski 1988; Marchant, R.E.; Zhao, Q.; Anderson, J.M.; Hiltner 1987; Pinchuk 1994). Hard segments based on aliphatic 4,4'-methylenebis (cyclohexylisocyanate) (H<sub>12</sub>MDI), however, are

considered a safer alternative and we have thus developed a segmented nanocomposite PU based on degradable poly( $\epsilon$ -caprolactone)diol and H<sub>12</sub>MDI.

Biodegradation is influenced by both the chemical and physical properties of the PU; surface properties (e.g. surface area and wettability), first order structures (chemical structure, molecular weight and molecular weight distribution) as well as higher order structures (glass transition temperature, melting temperature, degree of crystallinity and elastic modulus) of polymers play fundamental roles in the biodegradation process (Tokiwa et al. 2009). It is well known that higher molecular weight PCL ( $M_n > 4000$ ) is more slowly degraded by *Rhizopus delemar* lipase than that with low  $M_n$  (Tokiwa, Y; Suzuki 1978). Similarly, polymer morphology, and by extension, their crystallinity affects degradation. Crystalline domains consist of tightly packed molecules which are more resistant than amorphous regions where hydrolytic or enzymatic attack mainly occurs. Within the amorphous region, molecules are loosely packed making them more susceptible to degradation. Thus, degradation rate is inversely proportional to the crystallinity of the polymer (Iwata and Doi, 1998). Here, we have synthesized POSS-PCLU polymers of incrementally increasing hard segment content to evaluate whether or not the diisocyanate content may be a suitable parameter in the fine-tuning of polymer degradation. Polymers lacking POSS nanoparticles were also synthesized in an effort to determine the influence of POSS inclusion on degradation as previous studies have attributed an increased resistance to degradative breakdown of PUs when supplemented with POSS (Gu et al., 2011). Degradation media spanning oxidative, hydrolytic and enzymatic conditions were selected in order to mimic as closely as possible the realistic environments encountered upon material implantation into the body. Under certain circumstances, *in vitro* degradation studies may even be considered superior to *in vivo*

implantation studies as each individual degradative condition and their effects exerted onto the polymer may be studied separately.

### **6.2.1 Oxidative degradation**

Implantable devices may encounter oxidative conditions as particularly leukocytes and macrophages involved in the early foreign body reaction are able to produce reactive oxygen species such as superoxides ( $O_2^-$ ), hydrogen peroxide ( $H_2O_2$ ), nitric oxide (NO) and hypochloric acid (HOCl) (Labow, Tang, et al. 2002; Williams, D. F.; Zhong 1994). Particularly, aliphatic polyesters as used in the present study have been found to be susceptible to degradation via the nucleophilic attack of  $O_2^-$  and subsequent cleavage of ester bonds (Lee & Chu 2000). This mechanism is believed to be a key component of the stress cracking phenomenon frequently observed in long-term implantable PU devices (Sutherland et al. 1993).

### **6.2.2 Hydrolytic degradation**

Water molecules can attack and break hydrolytically labile chemical bonds, breaking polymers into oligomers and finally monomers. Upon implantation, water can attack bonds located either on the surface or within the polymeric matrix via water uptake. Since hydrolysis can be catalysed by acids or enzymes (Williams, D. F.; Zhong 1994), implantation of polyesters such as PLA or PGA which have acidic degradation products, results in accelerated breakdown due to a process called autocatalysis. A further important factor influencing the mode and rate of degradation is the polymer's surface wettability with hydrophilic materials degrading more readily than hydrophobic ones. In terms of PUs, hard segment content as well as distribution within the amorphous region are postulated to significantly influence hydrolytic degradation as hydrolysable

bonds may be masked by compact hard segment micro-domains which can form by hydrogen bonding between individual hard segments.

### **6.2.3 Enzymatic degradation**

Enzymes are cell-derived proteins capable of accelerating hydrolytic degradation processes. Naturally occurring and principally important in the breakdown of substrates for facilitated nutrient uptake, enzymes have also been demonstrated to accelerate biomaterial degradation (Santerre et al. 1994). The content and distribution of hard segments within the polymeric surface was shown to influence the manner in which enzymes adsorb and express their activity on the material's surface so that increasing hard segment contents correlated with reduced degradation (Tang et al., 2001, Santerre and Labow, 1997).

## **6.3 MATERIALS AND METHODS**

### **6.3.1 Polymer Synthesis**

Please refer to section 4.3.1.1.

### **6.3.2 Scaffold Fabrication**

Please refer to section 4.3.1.2.

### **6.3.3 *In Vitro* Degradation**

Accelerated degradation experiments were carried out according to ISO 10993:12 specification under hydrolytic, enzymatic and oxidative conditions at 37 °C. Cast specimen of the different polymers were immersed in 5 mL of (i) sterile PBS, (ii) lipase (10 U/mL), (iii) collagenase (10 U/mL), (iv), cholesterol esterase (1 U/mL), or (v) 20 % H<sub>2</sub>O<sub>2</sub> in 0.1 M cobalt chloride (CoCl<sub>2</sub>). Degradation media were changed every week to replenish enzymatic/oxidative activities and supernatants containing the degradation products were collected for subsequent toxicological analysis. At selected time points,



specimen were washed thrice with sterile distilled water and the air-dried overnight before being subjected to analyses.

#### **6.3.4 Evaluation of *In Vitro* Degraded Films**

##### **6.3.4.1 <sup>1</sup>H Nuclear Magnetic Resonance (NMR) Spectroscopy**

Please refer to section 4.3.4.2.1.

##### **6.3.4.2 Gel Permeation Chromatography (GPC)**

Please refer to section 4.3.4.2.3.

##### **6.3.4.3 Differential Scanning Calorimetry (DSC)**

Please refer to section 4.3.4.3.1.

##### **6.3.4.4 X-Ray Diffraction (XRD) Crystallography**

Please refer to section 4.3.4.3.2.

##### **6.3.4.5 Attenuated Total Reflectance (ATR)-Fourier Transform Infrared (FTIR) Spectroscopy**

Please refer to section 4.3.4.2.2.

##### **6.3.4.6 Scanning Electron Microscopy (SEM) Evaluation of Surface Changes**

Differences in scaffold surface microscopic appearances were evaluated using SEM digital photography at magnifications of x 100, x 500 and x 1000. Degraded scaffolds were washed with PBS and air-dried for a minimum of 3 days. No dehydrating alcohol series was used for this purpose since exposure to ethanol significantly changes surface structures as demonstrated in chapter 5. Then, samples were mounted on aluminium stubs and sputter-coated with gold using an SC500 (EMScope) for electrical conductance. Photographs were taken using a Philips 501 scanning electron microscope.

##### **6.3.4.7 Static Contact Angle Measurement to Determine Surface Wettability**

Please refer to section 4.3.4.1.3.

##### **6.3.4.8 Tensiometry**

Please refer to section 4.3.4.3.3.

### **6.3.5 Cell Viability**

#### **6.3.5.1 Preparation of Medium Containing Degradation Products**

Throughout the polymer degradation study, the degradation medium was renewed once a week to replenish enzymatic or peroxide activity. The old medium was collected and stored in -80 °C until further use. Prior to starting extract cytotoxicity studies, the media containing polymer leachables were filter sterilized and mixed with fresh medium at a range of concentrations (0 – control, 10, 50, and 70 % v/v).

#### **6.3.5.2 In Vitro Cytocompatibility of Leachables**

The cytocompatibility of any products released by the degradation of POSS-PCLU with varying percentage hard segments and PCLU-24 was assessed according to ISO standard 10993-5 using HDFa. Cells were seeded onto tissue culture plastic of 24-well plates at low densities of  $2 \times 10^4$  cells/cm<sup>2</sup> in complete culture medium. After 24 h, cells were microscopically assessed and subconfluency was verified. Medium was removed and replaced with fresh medium containing PU leachables at different concentrations. 10 % dimethylsulfoxide (DMSO) served as the positive control (Bae et al. 2012; Hua, K.; Carlsson, D.O.; Alander, E.; Lindström, T.; Stromme, M.; Mihranyan, A.; Ferraz 2014) and cells grown in complete medium with no added leachables were the negative control. Cytotoxicity was defined as cell viability below 70 % of the negative control as defined by the ISO standard 10993-5.

At 6 h, 24 h, 72 h and 7 days, cell viability and proliferative capacity were assessed using AlamarBlue® cell proliferation assay.

### **6.3.6 Animals**

26 male healthy Sprague-Dawley rats weighing 270-300 g were acclimatized for 1 week prior to any experimental procedure. All animals were housed in special facilities

with controlled temperatures ( $24 \pm 1$  °C) and a 12 h light/dark cycle. Animals had liberal access to water and a standard rat diet.

#### **6.3.6.1 Scaffold Implantation into Animals**

Eight week old rats were anaesthetised with isoflurane and a dorsal midline incision was created. Two porous scaffolds were implanted subcutaneously on either side of the midline. Round scaffolds (1 mm thickness, 16 mm diameter) were obtained using a cutting press, sterilized in 70 % ethanol and then washed 3 times with sterile PBS before implantation. One central suture restricted disc migration and folding in on itself.

#### **6.3.6.2 In Vivo Blood Flow and Oxygenation of Scaffolds**

At 4, 8, and 12 weeks, animals were anaesthetized using isoflurane and scaffolds were exposed. Real-time blood flow and scaffold oxygenation were measured using MoorFLPI Laser Doppler imager (Moor Instruments, Devon, UK) and Visisens™ oxygen sensor (PreSens, Regensburg, Germany), respectively.

#### **6.3.6.3 Scaffolds and Organ Harvest and Preparation for Histology**

After assessment of scaffold blood flow and oxygenation, animals were sacrificed humanely and both scaffolds and end organs (liver, spleen, brain, lung, and kidney) were harvested and placed in 4 % paraformaldehyde. Fixed samples were processed conventionally to produce 4 mm thin paraffin sections and stained with haematoxylin and eosin (H&E) or MSB (Martius, Scarlet and Blue) stain. Sections were analysed by a consultant histopathologist blinded to the study objectives.

#### **6.3.6.4 Immunostaining of Explanted Scaffolds**

Vascular infiltration of scaffolds was determined using goat polyclonal anti-rat CD31 (Santa Cruz) which identifies endothelial cells. Formalin fixed samples were cut at 5mm, dewaxed, rehydrated and antigen retrieval performed for CD31 by microwaving in

500 mL Tris and EDTA for 3 min. Sections were then incubated in 5 % H<sub>2</sub>O<sub>2</sub> in methanol to block endogenous peroxidase and incubated with the primary antibodies with normal rabbit or horse serum for 1 h at room temperature at the following dilutions of 1:300. The sections were then washed in phosphate buffered saline and incubated with biotinylated secondary stage antibody (rabbit anti goat for CD31) for 30 min and the reaction product was visualised by DAB. Sections were counterstained using Harris haematoxylin.

### **6.3.7 Statistics**

Please refer to section 4.3.6.

## **6.4 RESULTS AND DISCUSSION**

### **6.4.1 Synthesis and Molecular Characterization of Degraded POSS-PCLU Films**

The PCLU or POSS-PCLU PUs were synthesized from polycaprolactone diol with different dicyclohexylmethane diisocyanate contents, i.e. 24 %, 28 % and 33 %, using an ethylenediamine chain extender. The synthesis pathway is described in Figures 4.2 and 4.3 and the composition is defined in Table 4.1. The chemical structures of POSS-PCLU PUs were verified by <sup>1</sup>H NMR spectroscopy (Fig. 4.4). The range of hard segment content was as stated since below 10 %, hard segments have been demonstrated to offer only insufficient crosslinking capacity resulting in poor mechanical performance (Li, F.K.; Zhang, X.; Hou, J.N.; Xu, M.; Lu, X.L.; Ma, D.Z.; Kim 1997). Too high a hard segment content, on the other hand significantly interferes with hydrolytic or oxidative degradation due to steric hindrance of chain scission sites by H-bonds. The synthesized PUs exhibited similar FTIR features but subtle NMR differences at 1.6 ppm. Such similarities are to be expected considering that PCLU is the major component. However, the small spectroscopic variations are congruent with the use of different concentrations of hard segment. Similarly, no significant differences were observed using DSC. Both soft and

hard segment Tg of all non-degraded polymers were in the range of -52.9 °C to -55.5 °C and +40.8 °C to +53.3 °C, respectively.

The number average molecular weight ( $M_n$ ) and molecular weight distributions (polydispersity index, PDI) of all polymers were analysed using GPC. Table 6.1 summarizes the number average molecular weights and PDI of all variations of the PU degraded in each buffer for the maximum period of 6 months.

**Table 6.1.** Composition, percentage crystallinity, number average molecular weight ( $M_n$ ) and polydispersity indices (PDI) of control non-degraded PU films and films degraded in various buffers for a period of 6 months.

Materials	Degradation buffer	$\chi$ (%) <sup>a</sup>	$M_n$ (x 10 <sup>4</sup> g/mol) <sup>b</sup>	$M_w/M_n$ <sup>b</sup>
PCLU-24	Control	-	11.5	1.7
	PBS	-	11.9	1.5
	Lipase	17.2	1.0	2.0
	Collagenase	0.4	10.4	1.7
	Cholesterol esterase	2.1	7.6	1.8
	Hydrogen peroxide + CoCl <sub>2</sub>	37.3	0.6	1.9
POSS-PCLU-24	Control	-	11.9	1.4
	PBS	-	10.4	1.5
	Lipase	19.4	1.0	1.9
	Collagenase	0.4	9.2	1.6
	Cholesterol esterase	1.3	7.6	1.7
	Hydrogen peroxide + CoCl <sub>2</sub>	35.8	0.5	1.8
POSS-PCLU-28	Control	-	-	-
	PBS	-	-	-
	Lipase	9.3	0.8	1.9
	Collagenase	9.0	13.4	2.1
	Cholesterol esterase	-	-	-
	Hydrogen peroxide + CoCl <sub>2</sub>	6.6	0.7	2.0
POSS-PCLU-33	Control	-	-	-
	PBS	-	-	-
	Lipase	3.4	-	-
	Collagenase	-	-	-
	Cholesterol esterase	-	-	-
	Hydrogen peroxide + CoCl <sub>2</sub>	11.8	0.7	1.9

Key: POSS, polyhedral oligomeric silsesquioxane; PCLU, poly( $\epsilon$ -caprolactone urea)urethane; <sup>a</sup> $\chi$  was determined by DSC. <sup>b</sup>  $M_n$  and  $M_w/M_n$  were determined by GPC. - = Values unavailable as samples did not dissolve in DMAc which suggests insignificant degrees of degradation.

The symmetrical bell shape and narrow distribution of the control non-degraded PUs demonstrate successful and complete polymerization. The molecular weights of these controls ranged from  $11.5 \times 10^4$  to  $11.9 \times 10^4$  g/mol with their corresponding molecular weight distributions between 1.4 and 1.7. (Table 5.1). The  $M_n$  was seen to decrease with increasing hard segment content due to a corresponding decrease in the proportion of PCL which is the highest  $M_n$  component in the PUs. In addition, POSS-containing PUs show a higher  $M_n$  than PCLU-24 without POSS nanoparticles due to the additional molecules (POSS  $M_w \sim 1$  kDa). Contrary to expectations, no significant trend could be observed between POSS inclusion and  $M_n$  post-degradation indicating too small a fraction of POSS inclusion (2 %).

Exposure to lipase and hydrogen peroxide buffers resulted in the most significant mass losses, highest PDI and relatively higher crystallinities, consistent with previous reports (Shoae-Hassani et al., 2013a, Shoae-Hassani et al., 2013b, Guasti et al., 2013). Increasing the hard segment content predictably resulted in better resistance to degradation as demonstrated by incrementally decreasing crystallinities coupled to higher molecular weights (Table 5.1). POSS nanoparticle addition, however, did not seem to induce any changes in degradation behaviour as postulated by Mather group (Gu et al., 2011). This discrepancy is likely due to the significantly smaller percentage fraction of POSS integrated into our polymeric systems (2 % versus 20 %). The normalized number average molecular weights ( $M_n$ ) for PCLU-24, POSS-PCLU-24, POSS-PCLU-28 and POSS-PCLU-33 exhibited a clear reduction during degradation (Fig. 6.1). At the final time point of this study (6 months in buffer solutions), PUs exposed to lipase and hydrogen peroxide buffer demonstrated the most significant reductions in  $M_n$  of > 90 %. This is consistent

with a combination of general bulk degradation coupled to some enzymatic surface erosion (Uhrich et al., 1999).

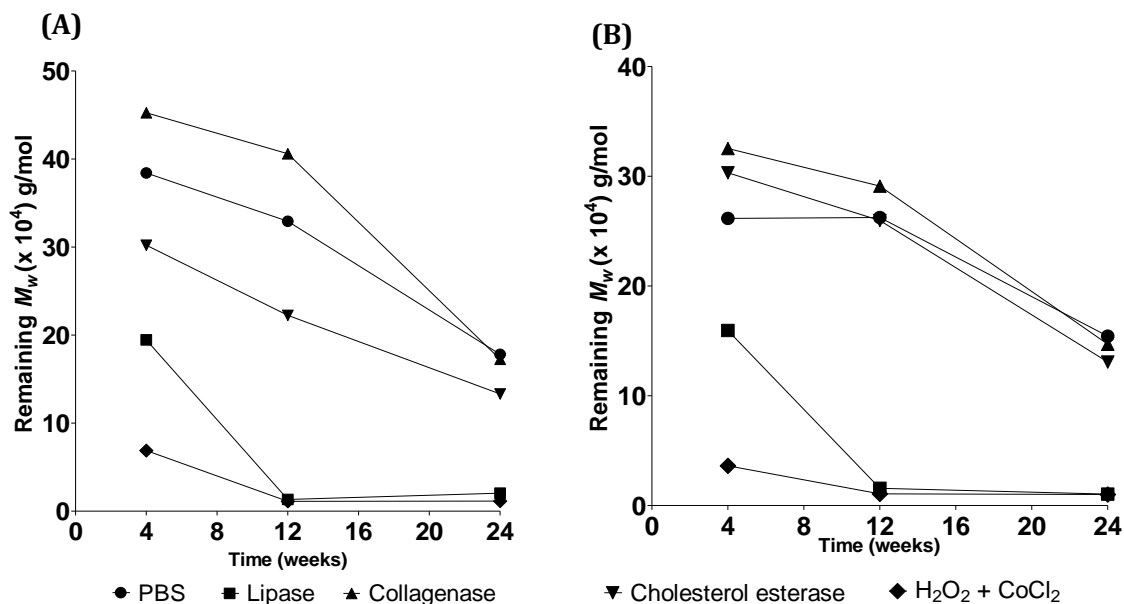


**Figure 6.1.** Mass loss over time after degradation in PBS, lipase, collagenase, cholesterol esterase and hydrogen peroxide buffers. (A) PCLU-24 and (B) POSS-PCLU-24. Degraded samples of POSS-PCLU-28 and POSS-PCLU-33 could not be sufficiently dissolved in solvent and data is therefore missing.

Exposure to PBS for 6 months resulted in only minor degradation (< 15 %) suggesting limited hydrolytic scission of water-labile ester linkages. Extensive hydrogen-bonding between hard segment micro-domains has previously been suggested to mask cleavage sites, thus retarding degradation (Santerre and Labow, 1997). Similarly, bathing in collagenase buffer for 6 months resulted in less severe degradation compared to exposure to lipase and hydrogen peroxide buffers. A maximum loss in  $M_n$  of < 25 % was evident for collagenase-degraded PUs. Again, correlations between hard segment content and mass loss were evident. This oft-suggested theory of hard segment content-dependent protective micro-domain formation is also reflected in our ATR-FTIR and DSC results (see below).

Material surface chemistries of non-degraded PCLU-24 and POSS-PCLU-24, POSS-PCLU-28 and POSS-PCLU-33 were analysed using attenuated total reflectance (ATR)-Fourier transform infrared (FTIR) spectroscopy and the spectra were overlaid for comparison (Fig. 6.2).

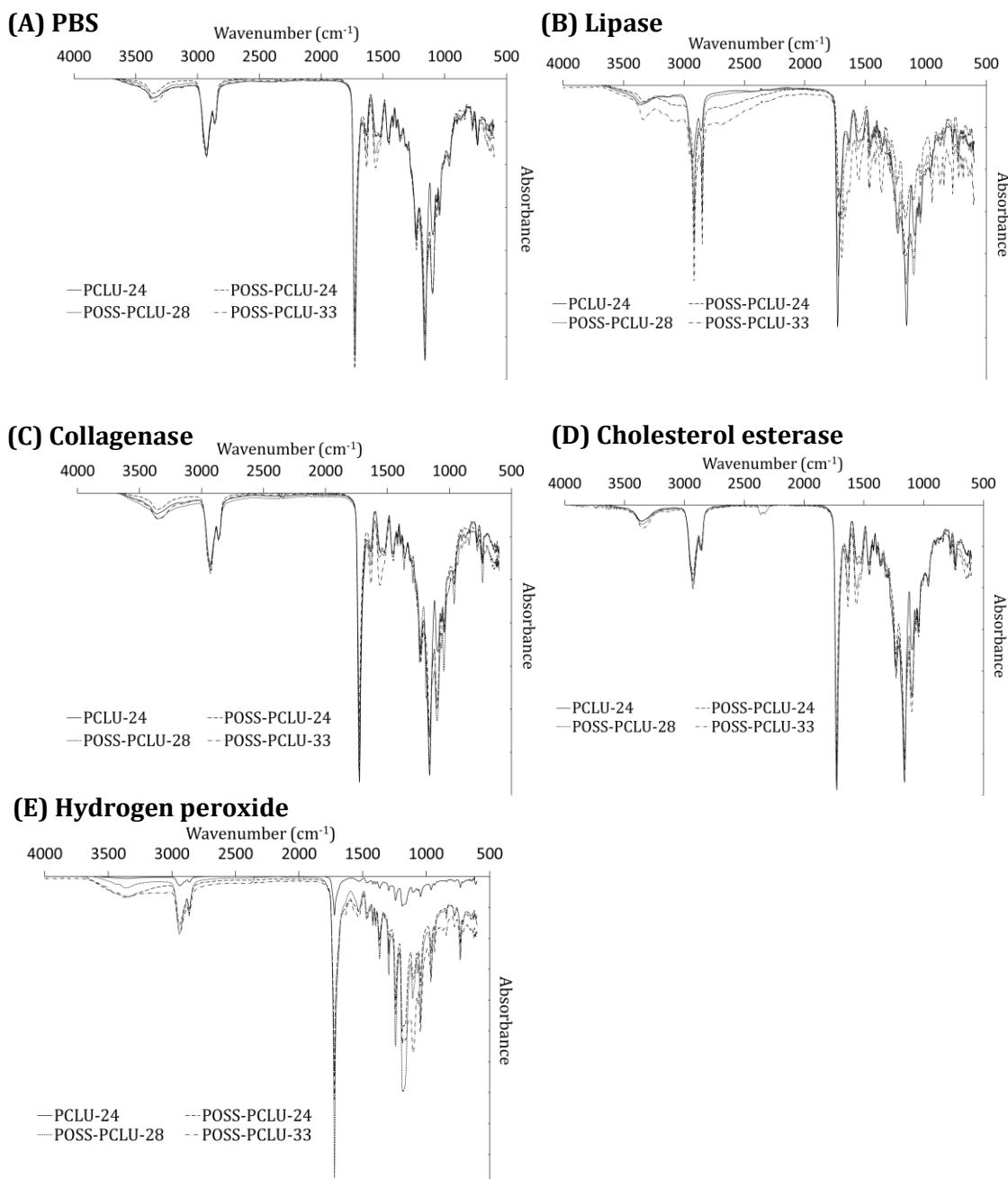


**Figure 6.2.** Overlaid attenuated total reflectance (ATR)-Fourier transform infrared (FTIR) spectra of films after 6 months in (A) PBS, (B) lipase buffer, (C) collagenase buffer, (D) cholesterol esterase buffer and (E) hydrogen peroxide +  $\text{CoCl}_2$  buffer.



All control polymers exhibit common peaks at 2929  $\text{cm}^{-1}$  and 2861  $\text{cm}^{-1}$  which correspond to the alkyl groups of the hard segment, H<sub>12</sub>MDI. The peaks at 1726  $\text{cm}^{-1}$  and 1159  $\text{cm}^{-1}$  represent the carbonyl (C=O) region of non-hydrogen-bonded urethane and the ester (O-C-O) absorbance of the soft segment, respectively. The heights of the latter two peaks are negatively correlated with increasing hard segment content. In the case of the C=O bond of the non-hydrogen-bonded urethane bonds, the lower height with higher percentage hard segment is due to the fact that in high hard segment polymers, most urethane bonds are hydrogen-bonded, leaving a smaller fraction of urethane bonds non-bonded.

With increasing hard segment content, the spectral peaks corresponding to hydrogen-bonded urethane (1633  $\text{cm}^{-1}$ ) and urea (1551  $\text{cm}^{-1}$ ) bonds increase in height providing a qualitative measure of bond content. Both PCLU-24 and POSS-PCLU-24 containing the lowest amount of hard segment demonstrate relatively smaller peaks compared to the polymers of higher hard segment content. Similarly, polymers containing POSS nanoparticles exhibit a high peak at around 1094  $\text{cm}^{-1}$  whilst PCLU-24 does not.

#### **6.4.2 Thermal Properties of Degraded POSS-PCLU**

Segmented PUs display several thermal transitions, corresponding to the microstructure of the soft and hard domains. The thermal properties of cast control and degraded POSS-PCLU films with different percentage hard segments are summarized in Table 6.2.

**Table 6.2.** Thermal properties of (A) PCLU-24, (B) POSS-PCLU-24, (C) POSS-PCLU-28 and (D) POSS-PCLU-33 PUs.

(A)

Materials	Degradation buffer	$T_g$ (°C) <sup>a</sup>		$T_m$ (°C) <sup>a</sup>	
		Soft segment	Hard segment		
PCLU-24	Control	-54.8	51.1	-	-
	PBS	-55.4	41.7	-	-
	Lipase	-50.4	14.8	38.8	47.7
	Collagenase	-55.1	-	43.7	-
	Cholesterol esterase	-55.9	0.0	41.4	-
	Hydrogen peroxide + CoCl <sub>2</sub>	-23.5	-	46.4	-

(B)

Materials	Degradation buffer	$T_g$ (°C) <sup>a</sup>		$T_m$ (°C) <sup>a</sup>	
		Soft segment	Hard segment		
POSS-PCLU-24	Control	-52.9	40.8	-	-
	PBS	-56.7	39.4	-	-
	Lipase	-49.4	14.4	39.5	51.8
	Collagenase	-54.9	-	41.8	-
	Cholesterol esterase	-56.8	-	41.4	-
	Hydrogen peroxide + CoCl <sub>2</sub>	-24.3	-	45.8	52.7

(C)

Materials	Degradation buffer	$T_g$ (°C) <sup>a</sup>		$T_m$ (°C) <sup>a</sup>	
		Soft segment	Hard segment		
POSS-PCLU-28	Control	-55.4	52.5	-	-
	PBS	-56.3	52.5	-	-
	Lipase	-51.7	12.8	37.8	48.7
	Collagenase	-52.6	-	39.4	50.2
	Cholesterol esterase	-56.5	53.8	-	-
	Hydrogen peroxide + CoCl <sub>2</sub>	-46.8	-	37.7	49.3

(D)

Materials	Degradation buffer	$T_g$ (°C) <sup>a</sup>		$T_m$ (°C) <sup>a</sup>	
		Soft segment	Hard segment		
POSS-PCLU-33	Control	-55.5	54.1	-	-
	PBS	-56.2	52.1	-	-

Lipase	-54.4	11.5	39.5	49.4
Collagenase	-56.3	-	-	-
Cholesterol esterase	-56.4	-	-	-
Hydrogen peroxide + CoCl <sub>2</sub>	-44.8	-	40.2	51.9

Key: POSS, polyhedral oligomeric silsesquioxane; PCLU, poly( $\epsilon$ -caprolactone urea)urethane

<sup>a</sup>  $T_g$ ,  $T_m$ ,  $\Delta H_m$  and  $\chi$  were determined by DSC

In general, soft segment glass transition temperatures,  $T_g$ , of POSS-PCLU and PCLU were independent of the hard segment content (ranging from 24 % - 33 %) indicating limited hard segment mixing within the soft domain. Similar results were found with PU systems based on poly(ethylene oxide), poly(tetramethylene oxide) and poly(propylene oxide) with comparable hard segment contents (Sung, C.S.P.; Hu, C.B.; Wu 1980; O'Sickey, M.J.; Lawrey, B.D.; Wilkes 2002; Korley et al. 2006).  $T_g$  of the PCLU soft segments ranged from approximately -60.0 °C for the control, non-degraded sample to -25 °C after oxidative degradation. The  $T_g$  shift to higher temperatures induced by the different degradation media indicates a degree of phase mixing between the soft and hard segment of the PU and crystallization of amorphous areas (Skarja & Woodhouse 1998). Oxidative conditions were seen to induce the most drastic increase in  $T_g$ , particularly in samples of relatively lower hard segment content, suggesting strong interactions between soft and hard segments secondary to degradation. Previous studies have confirmed the formation of hard segment micro-domain structures in segmented PUs which can protect or mask potential cleavage sites within their hard segments (i.e. urea and urethane bonds) via formation of an extensive network of hydrogen bonds (H-bonds) (Santerre & Labow 1997; Shibayama, M; Kawauchi, T.; Kotani, T.; Nomura, S.; Matsuda 1986). Thus, with increasing hard segment content, the extent of urethane H-bonding also increases, resulting in delayed degradation. This protective phenomenon was, indeed, present in the samples

with relatively higher hard segment content which resisted a significant increase in  $T_g$  post-degradation.

None of the control polymers exhibited hard segment crystallization and hard segment  $T_g$  ranging from approximately 40 °C to 55 °C which is just below that observed by Skarja *et al.* (Skarja & Woodhouse 1998). This means that the hard segments of all control polymers are amorphous at room or body temperature (Skarja & Woodhouse 1998) which may be due to a lack of efficient chain packing necessary for hard segment crystallization (Okkema & Cooper 1991) secondary to the mobile aliphatic diisocyanate (Szycher, M.; Poirier, V.L.; Dempsey 1983a) and the presence of bulky side-chains on the chain extender (ethylene diamine).

Endothermic melting peaks were observed in samples exposed to lipase, collagenase, cholesterol esterase and hydrogen peroxide between 35 °C and 50 °C which were attributed to the melting of the crystalline portions of the soft segment (Shibayama *et al.* 1991). Double endotherms could be observed in all films exposed to lipase and hydrogen peroxide (Fig. 6.3) whilst no endothermic peaks were seen in control and PBS exposed samples, indicative of a mostly amorphous starting polymer and negligible degradation in PBS-exposed samples. Collagenase exposure induced the formation of a double melting peak only in POSS-PCLU-28 after 6 months and a small single endothermic peak in POSS-PCLU-24 after the same exposure period. Cholesterol esterase exposure did not induce melting peaks in any of the samples except PCLU-24 where a single small endothermic valley can be observed after 6 months of exposure. Double endothermic peaks may indicate the presence of either two distinct types of crystals or the recrystallization of a metastable crystal into a more stable form with increasing temperatures within polymorphic structures.

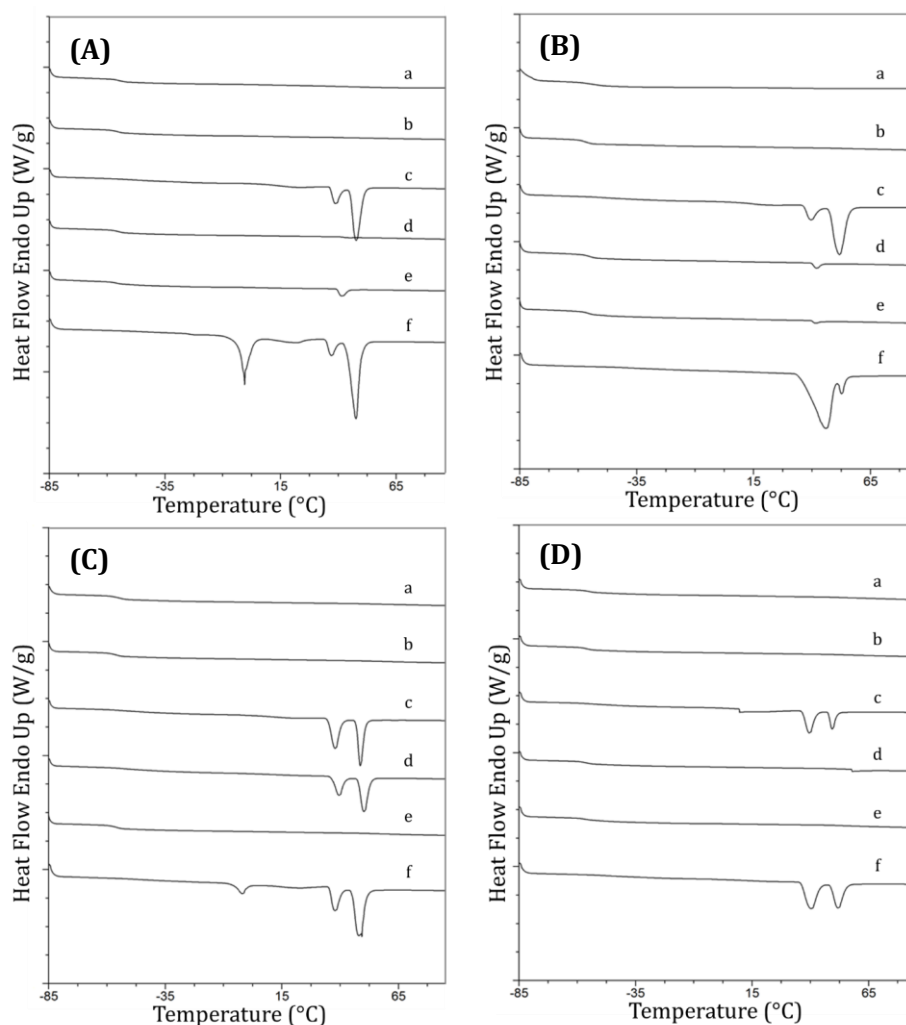


**Figure 6.3.** Differential scanning calorimetry graphs of (A) PCLU-24, (B) POSS-PCLU-24, (C) POSS-PCLU-28 and (D) POSS-PCLU-33 films; (a) non-degraded control film, (b) in PBS, (c) in lipase buffer, (d) in collagenase buffer, (e) in cholesterol esterase buffer and (f) in hydrogen peroxide +  $\text{CoCl}_2$  buffer. Incubation period for all was 6 months.

The latter underlies the principles of Ostwald's rule of stages which states that when a material crystallises, it will move to equilibrium from an initial high-energy state (e.g. glass) via a cascade of stages requiring minimal changes in free energy. This implies that the sample will crystallise in sequence beginning with the least stable polymorph and progressing through any further metastable polymorph to the stable crystalline form (Ostwald 1897).

The melting temperature and percentage crystallinity are affected by the soft segment content and its molecular weight (Tokiwa et al. 2009). After oxidative and enzymatic degradation with hydrogen peroxide and lipase, respectively, the degree of crystallinity was positively correlated with the relative amounts of soft segments in the study samples, such that percentage crystallinity followed: PCLU-24 > POSS-PCLU-24 > POSS-PCLU-28 > POSS-PCLU-33. The higher the hard segment content within the samples, the lower the relative soft, crystallizable portion which is reflected in the DSC thermograms. Additionally, increases in soft segment  $T_g$  were correlated with higher percentage crystallinity induced by degradation (Fig. 6.4) and increased crystallinity resulted in a reduction in  $T_g$  step height secondary to a reduction in the amorphous content (Fig. 6.5).

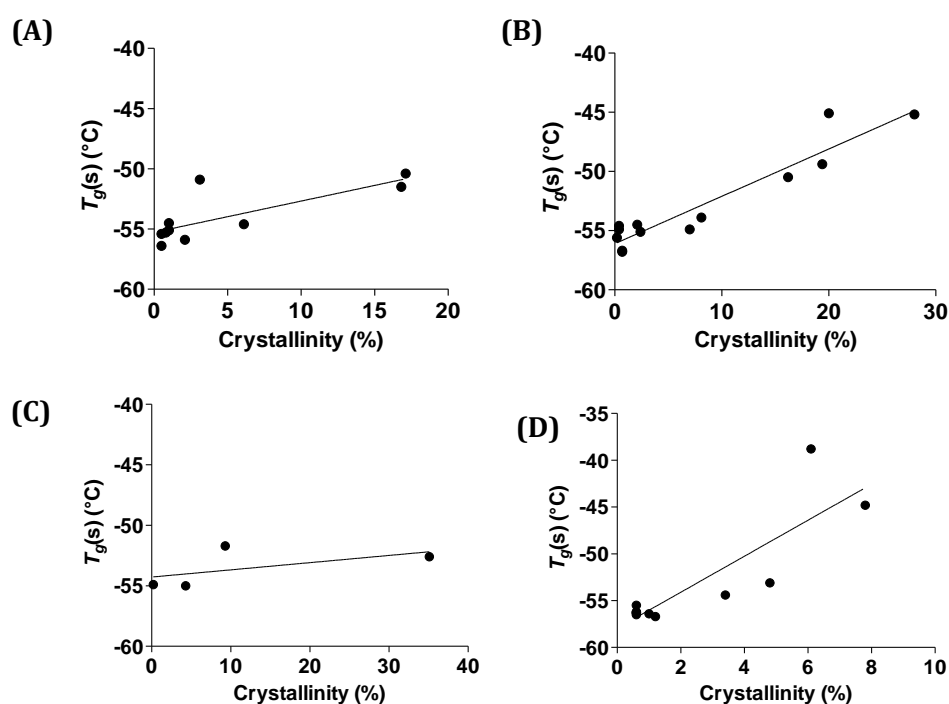


**Figure 6.4.** Soft segment glass transition temperatures ( $T_g(s)$ ) as a function of percentage crystallinity of control and degraded (A) PCLU-24, (B) POSS-PCLU-24, (C) POSS-PCLU-28 and (D) POSS-PCLU-33 polymers.

This is likely due to increased phase mixing secondary to shorter chain length and thus reduced molecular weight of the soft segment. For reference, the crystal melting temperature for pure PCL is 57 °C (Engelberg & Kohn 1991) which was higher than those observed in the degraded samples, suggestive of phase mixing.

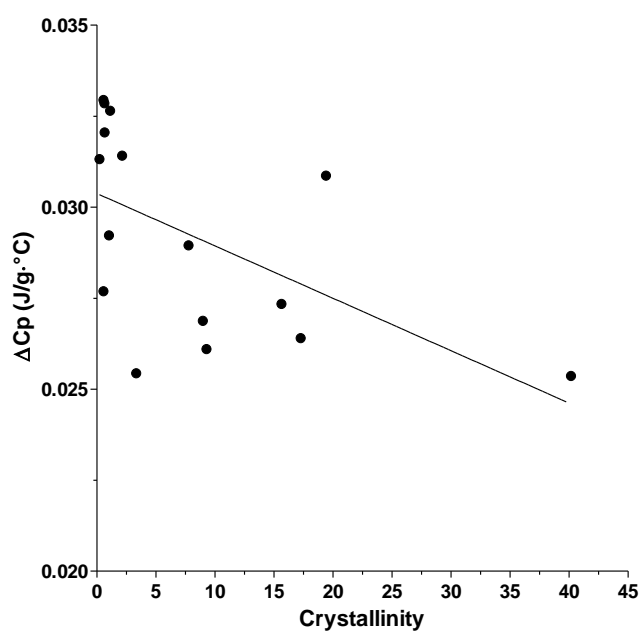


**Figure 6.5.** The normalized step height of the specific heat at  $T_g$  as a function of crystallinity.

A small exothermic transition was detected towards the lower temperature side of the main endothermic peaks in all those samples exhibiting melting peaks and was attributed to the crystallization transition ( $T_c$ ).

XRD studies on films exposed to oxidative medium for the total period of 6 months revealed PCL peaks at  $2\theta = 21.3^\circ$  and  $23.7^\circ$  for all PUs, in accordance with previous studies (Chan-Chan et al., 2010a). Similarly, exposure to lipase and collagenase buffers resulted in these PCL peaks, albeit at lower intensities (Fig. 6.6).

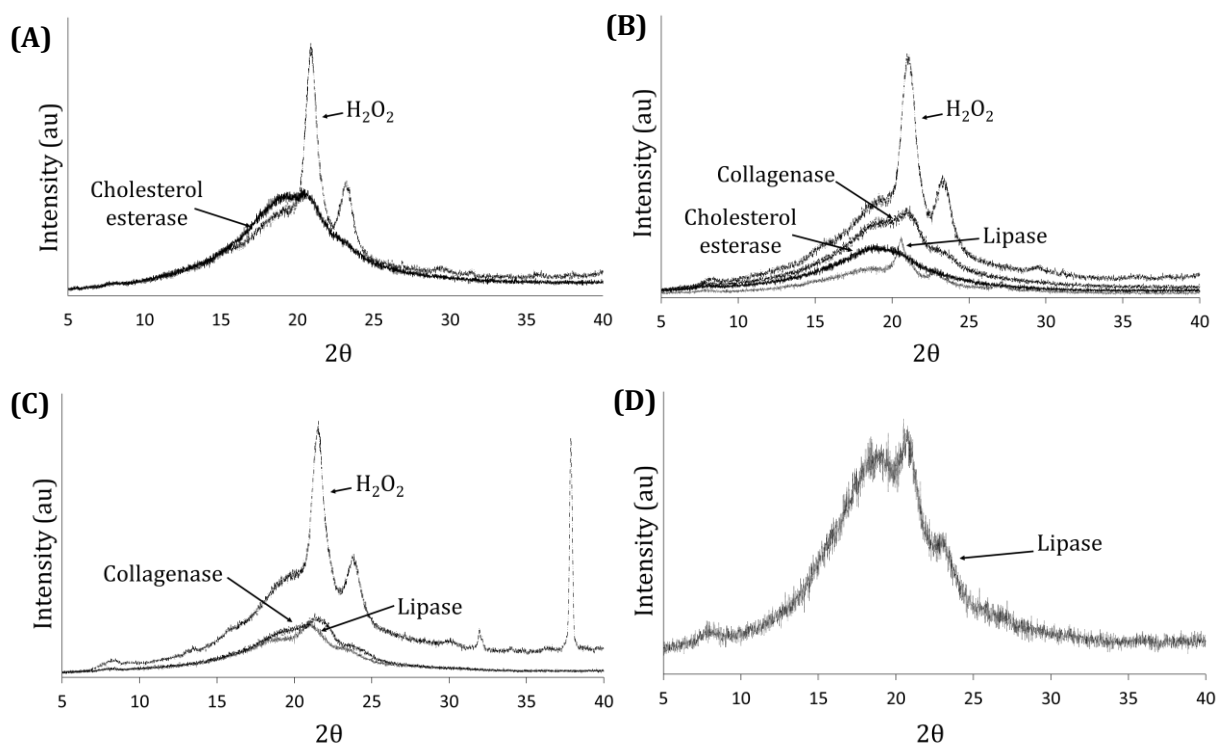


**Figure 6.6.** XRD patterns of degraded (A) PCLU-24, (B) POSS-PCLU-24, (C) POSS-PCLU-28 and (D) POSS-PCLU-33. Degradation time was 6 months.

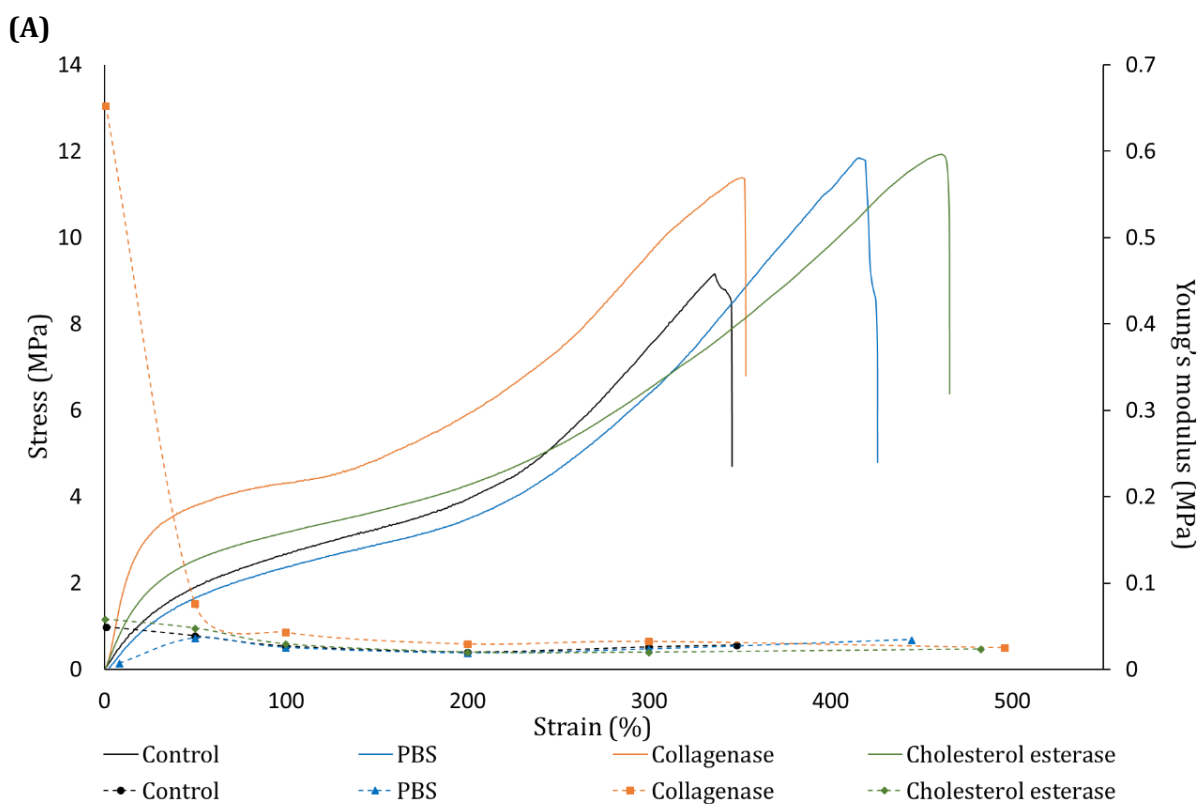
This so-called peak splitting is suggestive of the presence of different crystalline domains within some degraded films (Lee and Chu, 2008). This hypothesis is corroborated by the presence of double endothermic melting peaks on DSC traces of those samples which display peak splitting on XRD.

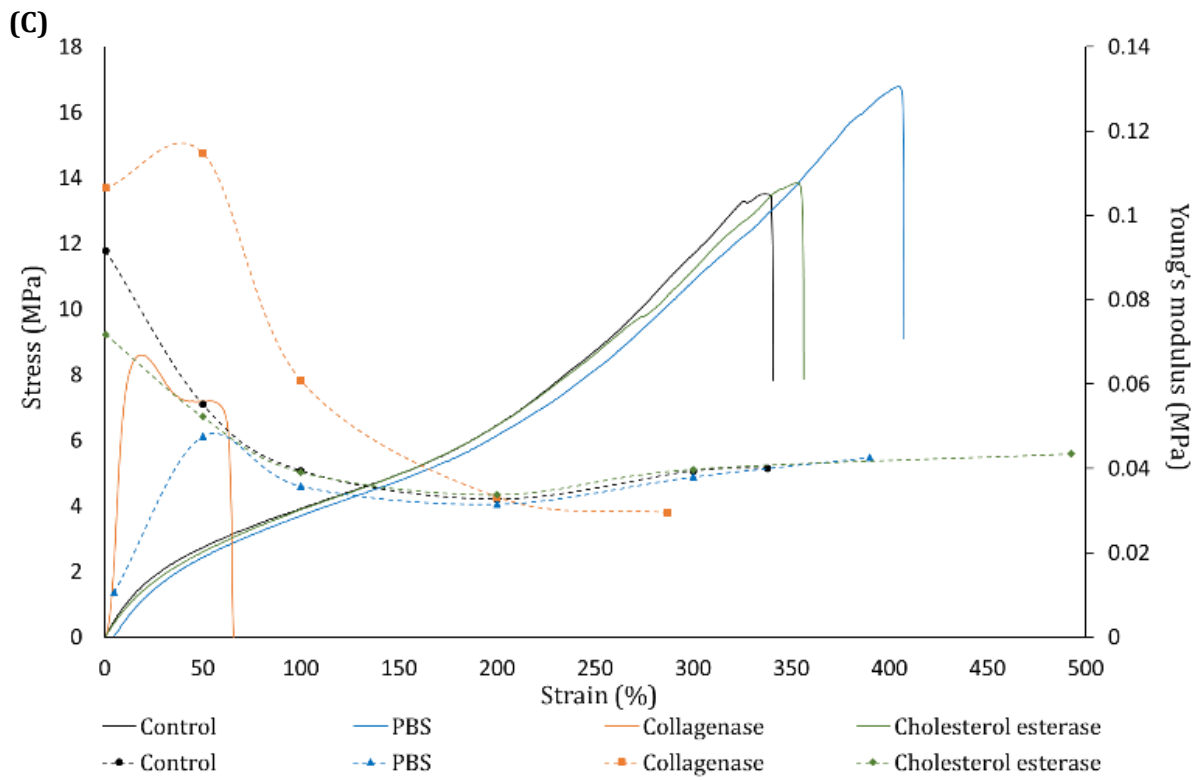
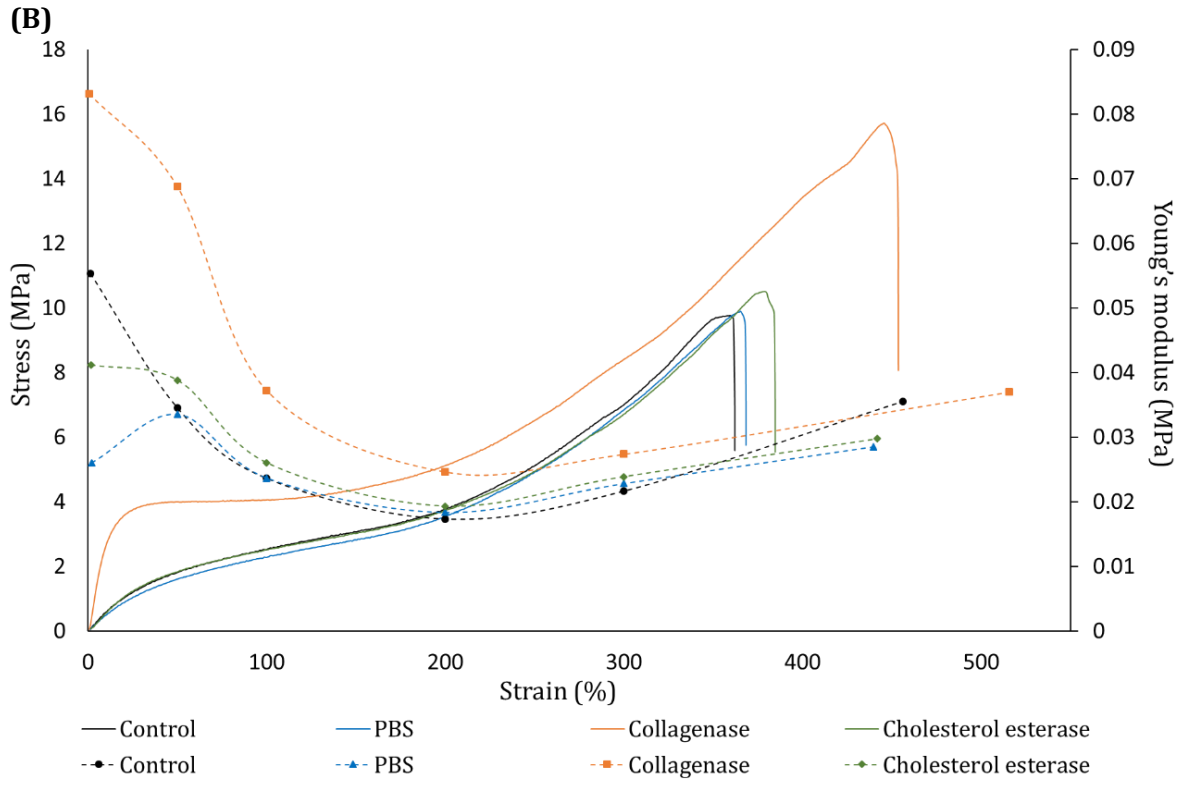
Diffraction patterns of films degraded in hydrogen peroxide revealed further peaks at  $2\theta = 8^\circ$  and  $29.6^\circ$  as well as broad shoulders at  $15.7^\circ$  and  $19.2^\circ$ . Neither cholesterol esterase buffer nor PBS incubation revealed peaks, suggestive of a lesser degree of degradation and relative conservation of the amorphous PU structure. Comparisons between different time points indicate a time-dependent formation of crystal structures which can also be observed in the DSC traces. These results suggest a condition- and time-dependent breakdown of the mostly amorphous PU into semicrystalline structures secondary to degradation-induced changes.



### 6.4.3 Degradation-Induced Changes in Mechanical Properties

Mechanical properties of all PUs were affected by incubation in all buffers. The representative stress-strain curves for all materials before and after incubation in normal saline, enzymatic or oxidative buffers are shown in Figure 6.7. Overlaid on those graphs are the Young's moduli, a measure for material stiffness. Specific degradation points (1, 4 and 6 months) were chosen for mechanical evaluation but even after 4 weeks, PCLU-24 incubated in lipase or hydrogen peroxide buffer disintegrated, making tensile testing impossible. In general, both tensile strength and Young's modulus increased with increasing hard segment content for control non-degraded films which is likely due to increased crystalline to amorphous content ratio within the PUs leading to better phase separation as well as urethane bond interactions (Tatai et al., 2007).





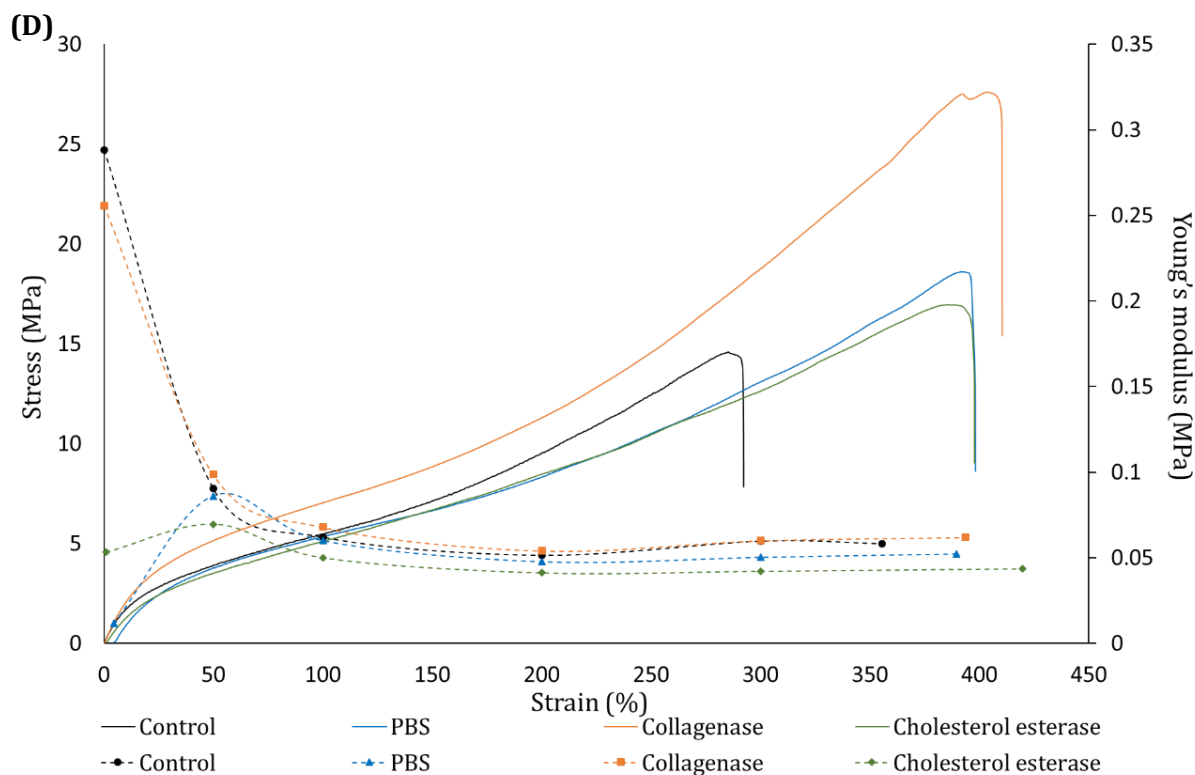


**Figure 6.7.** Stress-strain curves overlaid against Young's moduli for (A) PCLU-24, (B) POSS-PCLU-24, (C) POSS-PCLU-28 and (D) POSS-PCLU-33. Degradation time was 6 months.

Degradation of PU films resulted in significant changes in mechanical properties, contrary to previously published reports (Gu et al., 2011). Differences in outcomes may be attributable to major differences in incubation periods with short time spans (days rather than months) failing to induce changes and thus potentially misrepresenting long-term properties of investigated materials. In general, films incubated in any degradation buffer exhibited higher values for stress and strain at break, indicative of increased phase separation induced by degradation.

In the current study, films incubated in collagenase buffer for 6 months exhibited the largest increase in both Young's modulus and tensile strength whilst retaining dependence on the hard segment content as observed for non-degraded control films (films exposed to lipase buffer or hydrogen peroxide became too brittle to handle after 6

months and thus were not included for mechanical analysis). This suggests a degradation-induced influence on these mechanical parameters. However, films not containing any POSS nanoparticles (PCLU-24) demonstrated the highest increase in Young's modulus compared to their compositional equivalent containing POSS (POSS-PCLU-24). This suggests a major role for POSS in protecting PUs from degradation induced loss in material elasticity. We can hypothesize that POSS nanoparticles potentially act as cross-linking agents as suggested by Mather's group (Wu et al., 2009). Cholesterol esterase buffer did not significantly impact upon the Young's modulus after 6 months' of incubation, however, a negative trend in modulus after PBS exposure could be observed for all PU films. This is likely due to a lack in phase mixing which is usually expected during degradation. Thus, significant phase separation results in dispersion of the crystalline hard segment within the amorphous region of the PU as supported by the lack of crystallinity data obtained using DSC spectral results. Small Young's moduli are generally believed to suffer from high strain accumulation resulting in poor durability, thus compromising a material's *in vivo* stability (Bernacca et al., 2002).

#### **6.4.4 Contact Angle Measurements**

Polymer hydrophilicity is an important parameter in their hydrolytic degradation. Hydrolysis requires the reaction between water and labile ester bonds and the reaction velocity depends on the abundance of both water and ester bonds. Thus, hydrophilic polymers capable of attracting water molecules generally degrade more rapidly than hydrophobic polymers presuming the ester bond concentration remains relatively stable (Göpferich 1996). Control non-degraded POSS-PCLU polymers did not exhibit significant differences in contact angle with a mean hydrophobic  $\theta$  of 105°. PUs lacking POSS nanoparticles predictably were more hydrophilic as POSS is known to increase hydrophobicity when incorporated into polymeric systems (Schutzius et al., 2012).

Upon degradation, contact angles were shown to gradually decrease, in line with expectations (Fig. 6.8). As degradation progresses, the PCL component is preferentially broken down due to hydrolytically labile ester bonds. A reduced amorphous soft segment component thus favours relatively increased phase mixing which results in the polar hard segments aggregating at the material surface. This, in turn, reduces contact angle. It can further be observed that with higher starting hard segment content, degradation-induced increases in material hydrophilicity are more pronounced due to the relatively more polar segments within the degraded material.

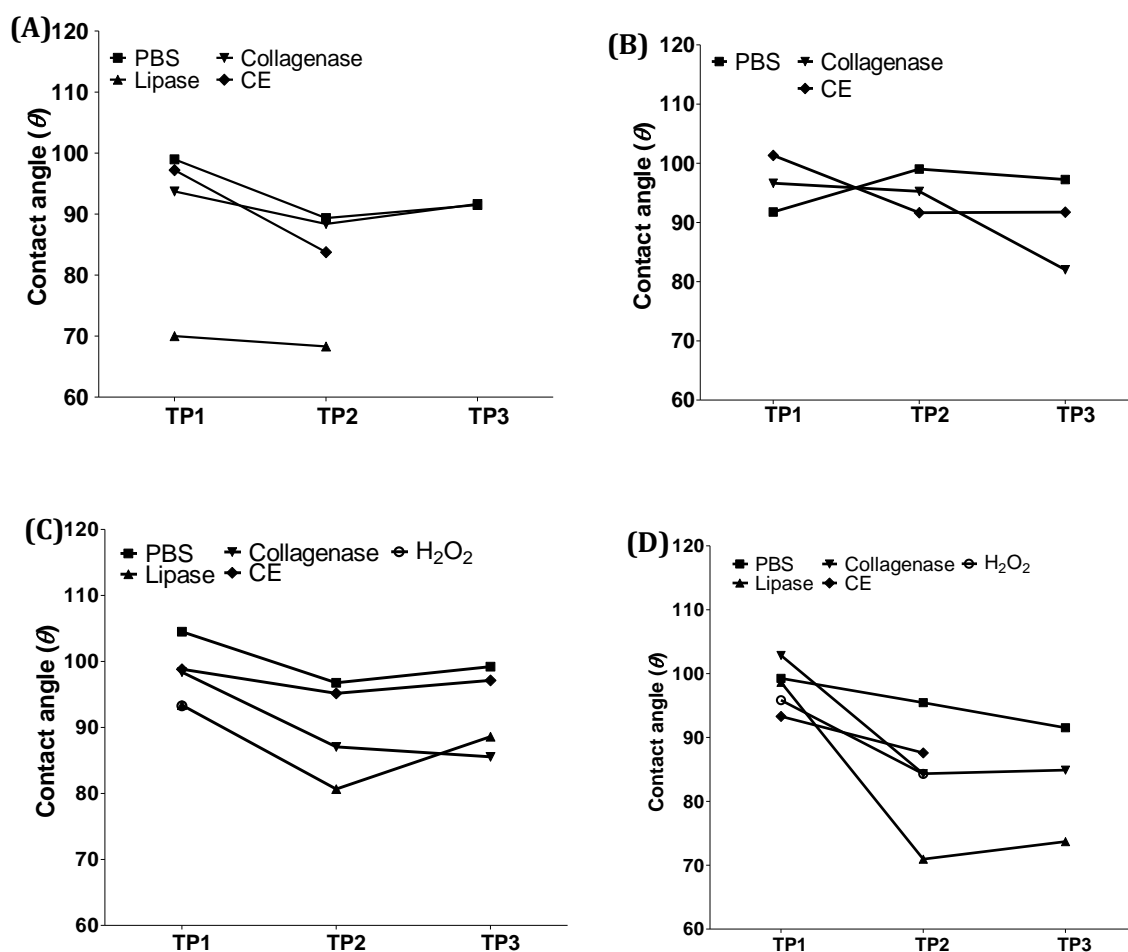
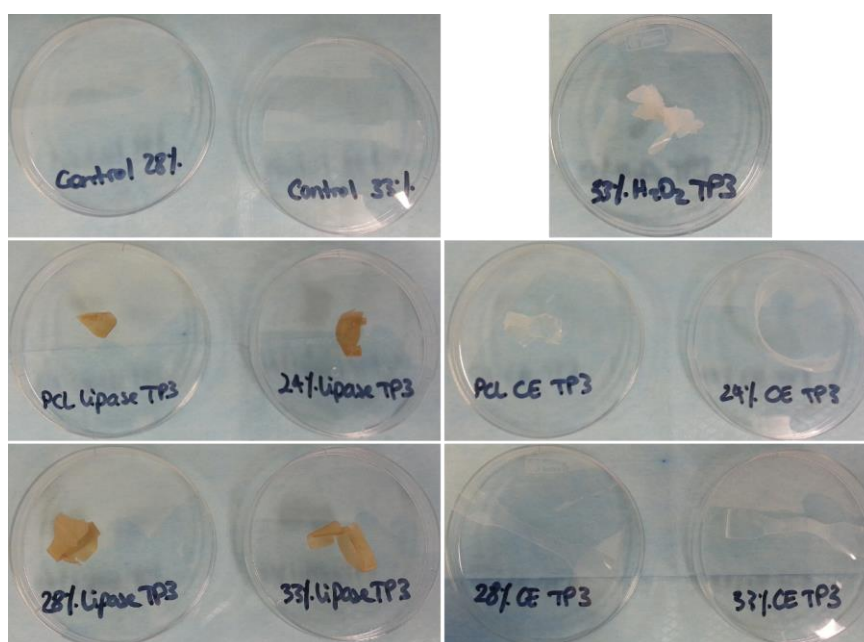


**Figure 6.8.** Water contact angles of (A) PCLU-24, (B) POSS-PCLU-24, (C) POSS-PCLU-28 and (D) POSS-PCLU-33 at 4 weeks (TP1), 12 weeks (TP2) and 24 weeks (TP3). No contact angles could be obtained for the following due to disintegration: PCLU-24 in lipase buffer TP3, PCLU-24 in hydrogen peroxide + CoCl<sub>2</sub> buffer TP1, TP2 and TP3, POSS-PCLU-24 in hydrogen peroxide + CoCl<sub>2</sub>

buffer TP1, TP2 and TP3, POSS-PCLU-28 in hydrogen peroxide + CoCl<sub>2</sub> buffer TP2 and TP3, POSS-PCLU-33 in hydrogen peroxide + CoCl<sub>2</sub> buffer TP3.

#### 6.4.5 Surface Changes Induced by Degradation

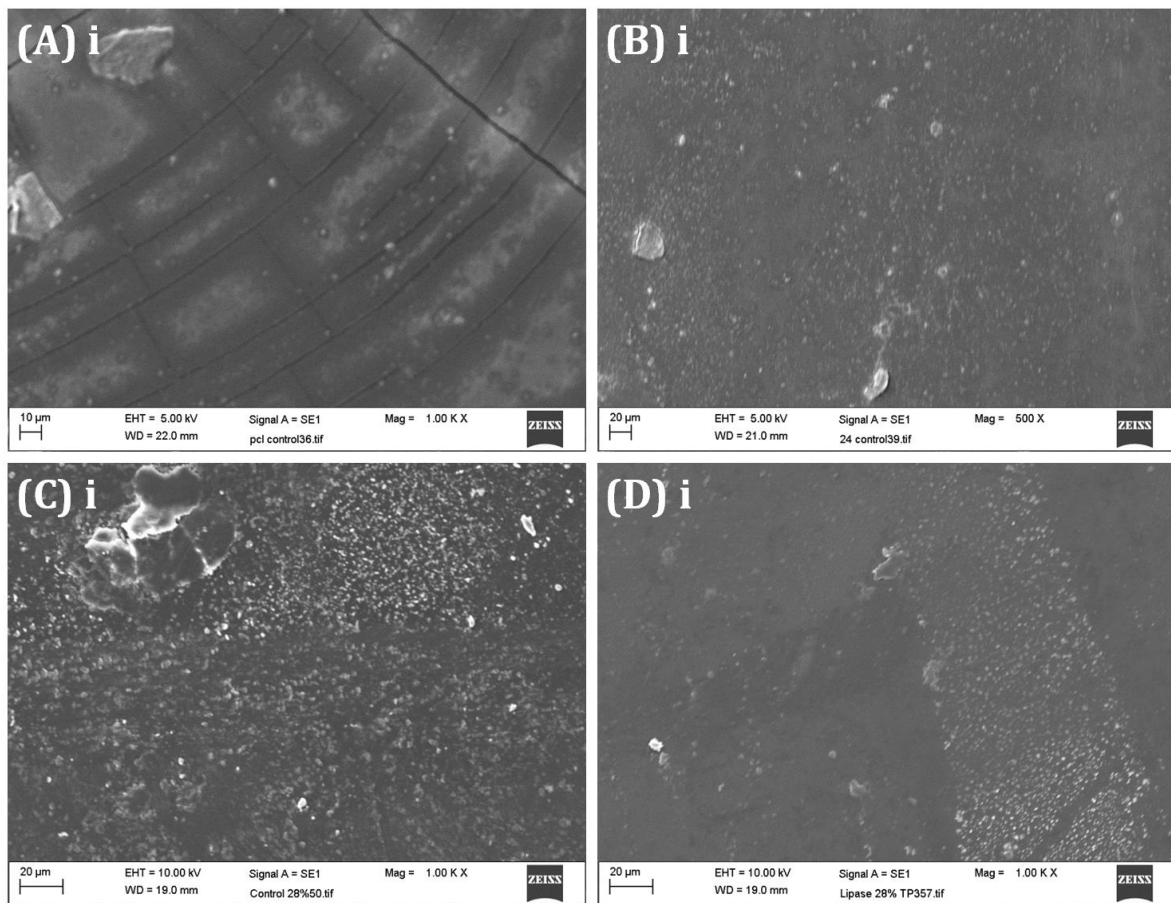
From a macroscopic point of view, degraded polymer films exhibited significant differences depending on the incubation buffer (Fig. 6.9).



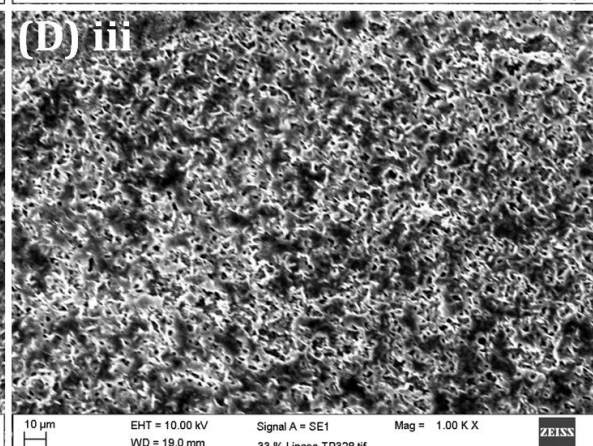
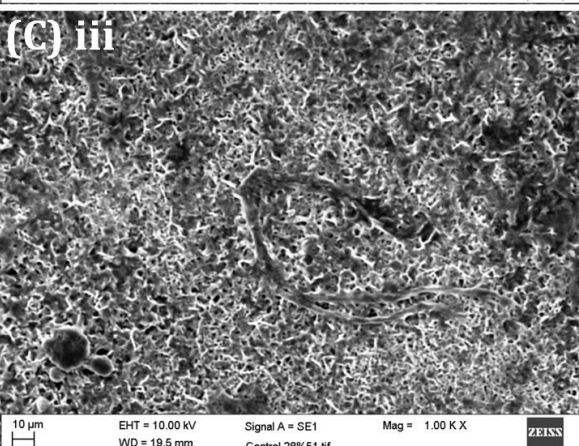
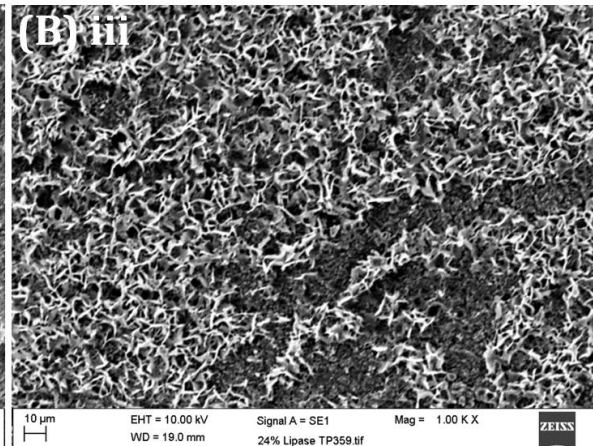
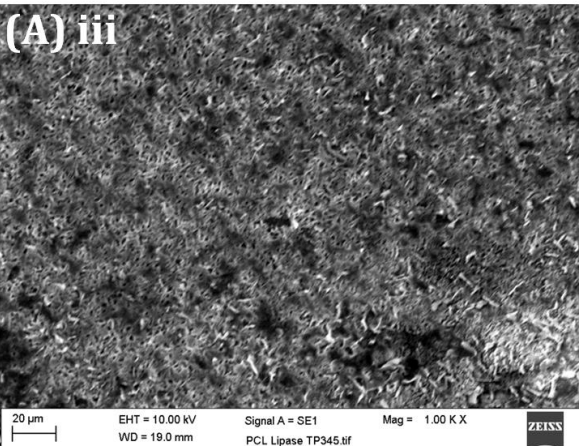
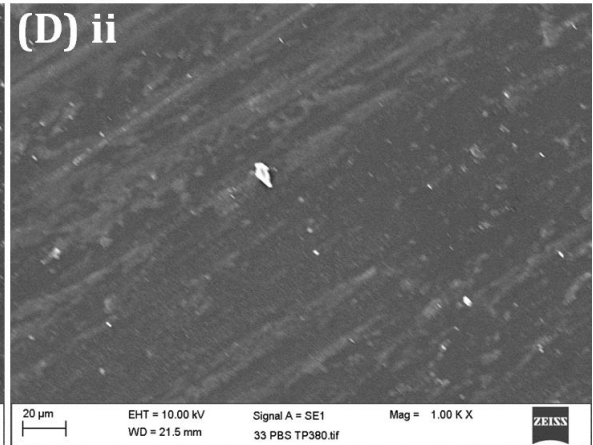
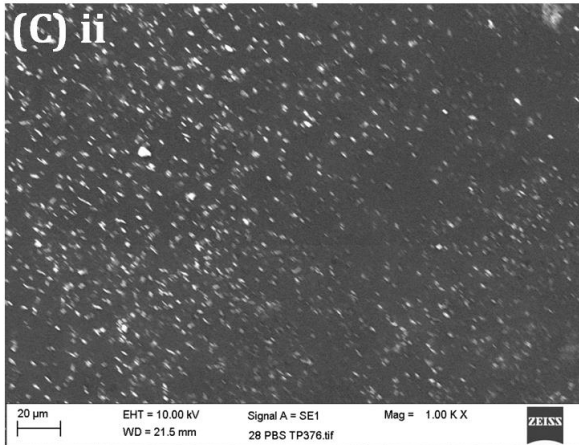
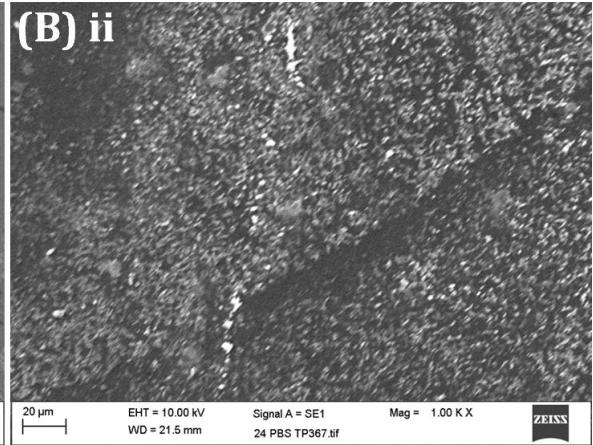
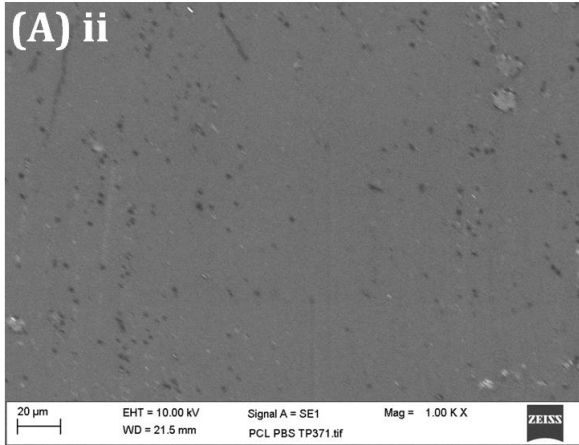
**Figure 6.9.** Macroscopic image of polymer films after 6 months in degradative media.

Similarly, the microscopic surface morphology of enzymatically degraded PUs demonstrated differences when investigated by SEM analysis and compared with non-degraded control PUs (Fig. 6.10). All films except PCLU-24 revealed spherical micro-particulates on their surfaces which we hypothesize can be assigned to micro-aggregates of POSS nanoparticles as they cannot be seen in films lacking POSS (Gao et al., 2004). Compared to control films, all degradation buffers induced surface changes in the tested PUs. All films incubated in lipase buffer displayed uniform roughened and porous surfaces, indicating a surface-erosion mechanisms which is typical of enzymatic attack

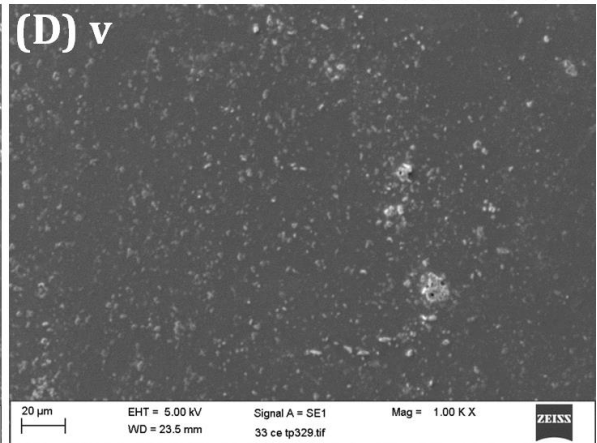
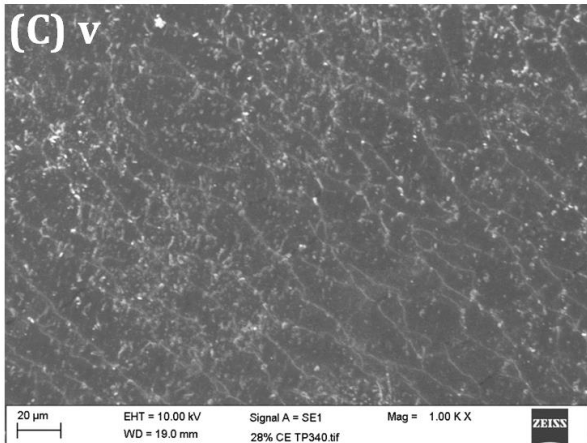
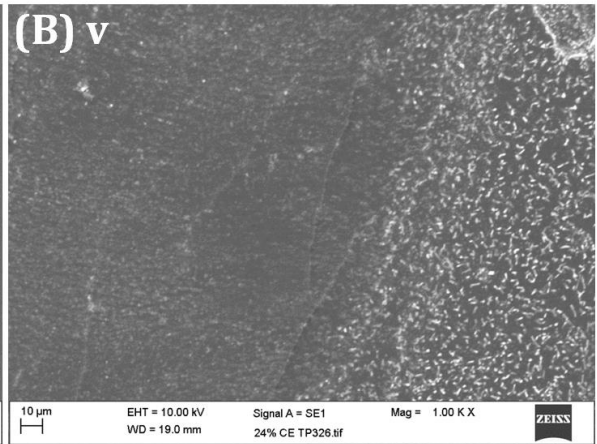
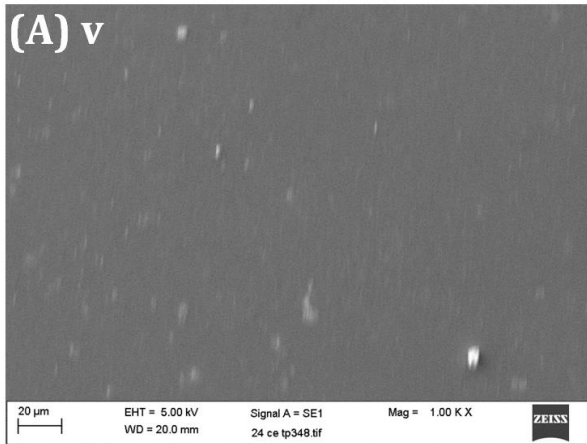
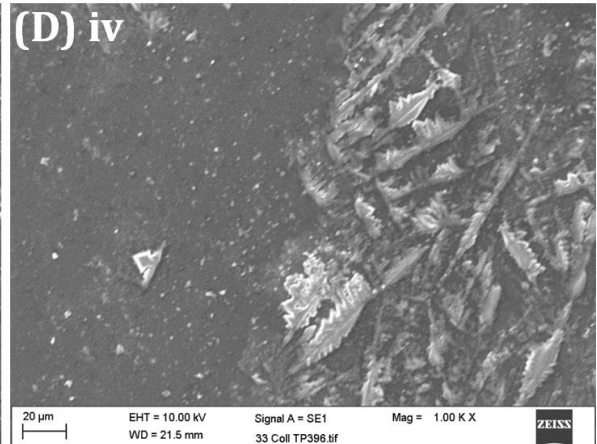
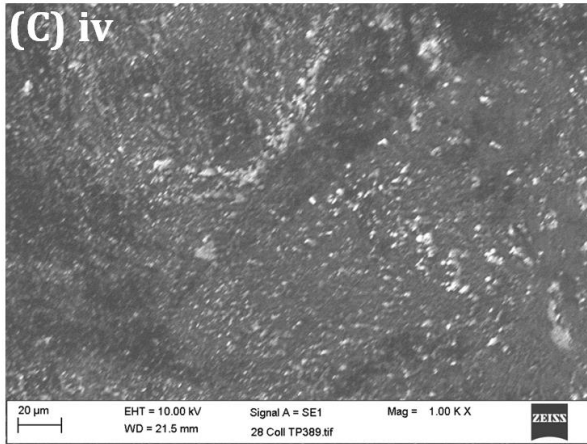
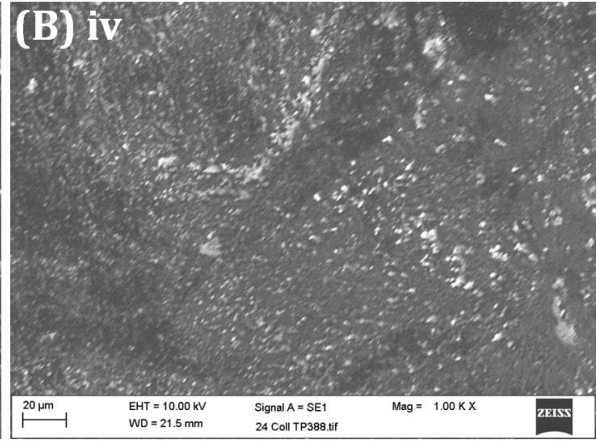
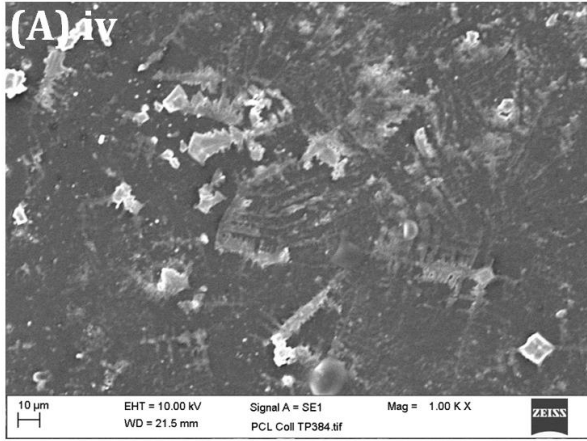
(Christenson et al., 2006). Gradual degradation from non-porous into porous films enables these PU scaffolds to be used as delivery vehicles for a multitude of molecules such as drugs or genes (Peng et al., 2013). Films exposed to cholesterol esterase and hydrogen peroxide buffer, on the other hand, revealed significant stress-cracking associated with degradation. This is of clinical significance as inflammatory cells including monocyte-macrophages release both cholesterol esterases and oxidants capable of degrading PUs (Tang et al., 2001, Li et al., 1997). Overall, most degradative changes could be observed in films exposed to lipase and hydrogen peroxide buffers which is in agreement with results obtained by GPC and mechanical characterization.











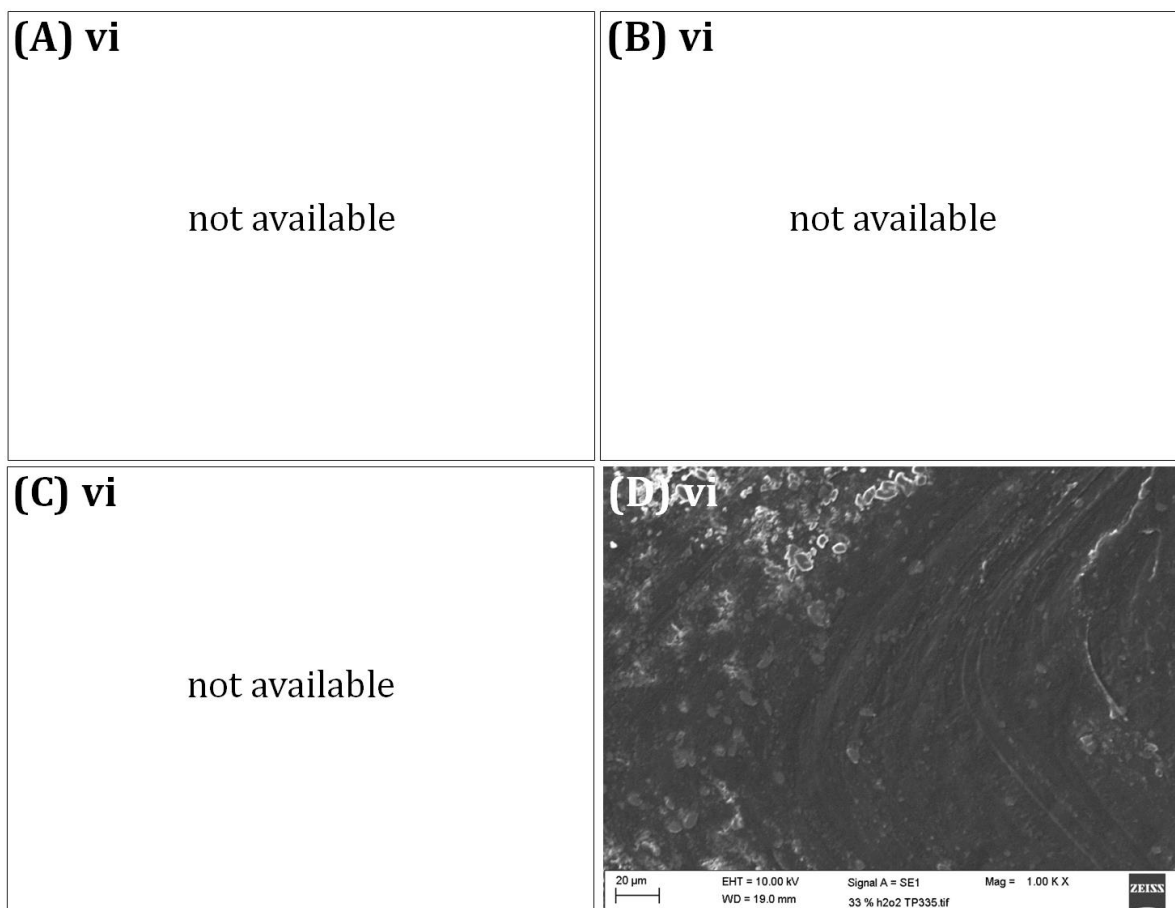


**Figure 6.10.** Scanning electron microscopy images of: (A) PCLU-24, (B) POSS-PCLU-24, (C) POSS-PCLU-28 and (D) POSS-PCLU-33: (i) control, (ii) in PBS for 6 months, (iii) in lipase buffer for 6 months, (iv) in collagenase buffer for 6 months, (v) in cholesterol esterase buffer for 6 months and (vi) in hydrogen peroxide +  $\text{CoCl}_2$  buffer for 6 months.

#### 6.4.6 Cytocompatibility of Degradation Products

Figure 6.11 shows the cell culture media supplemented with increasing concentrations of leachable solution.

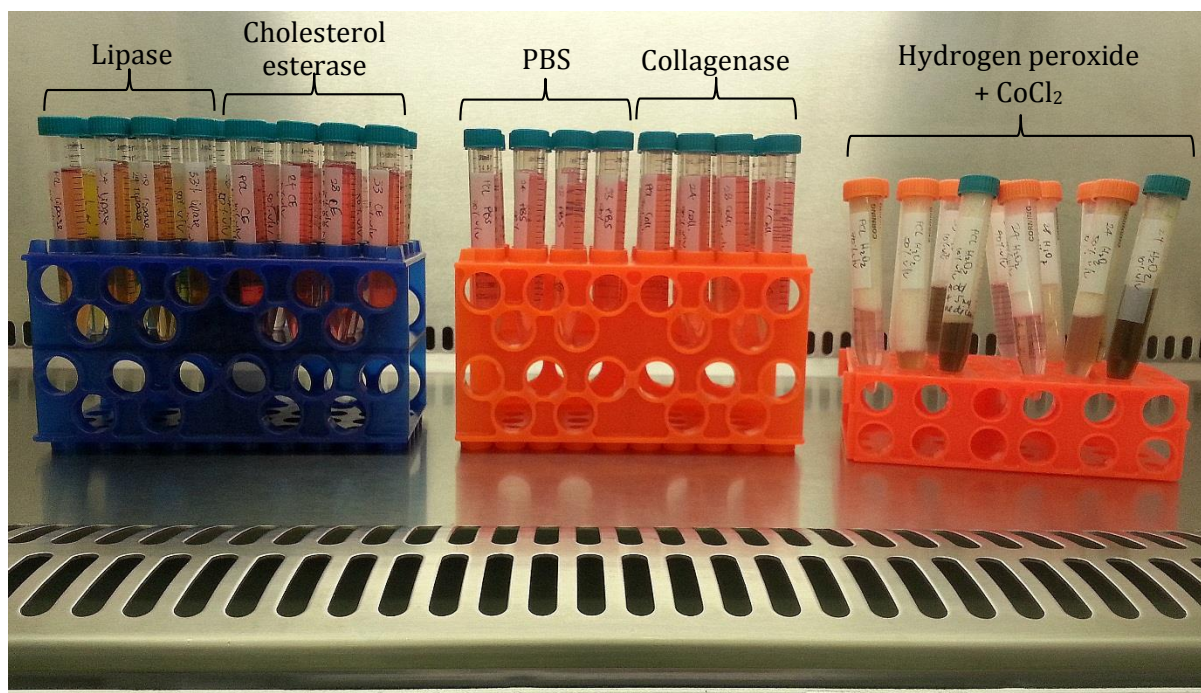


**Figure 6.11.** Media containing filter-sterilized leachables from degraded polymers at 10 % v/v, 50 % v/v and 70 % v/v.

In general, a time- and concentration-dependent decrease in cellular viability was observed when HDFa were incubated with degradation extracts of any PU (Fig. 6.12 to 6.16). In addition, toxicities seemed to be related to the hard segment content in the PUs. Higher hard segment PUs translated into lower cell viability. The results of this toxicity study were unexpected as theoretically, no component of the POSS-PCLU nanocomposite polymer is toxic individually (Rizvi et al., 2012). Similarly, H<sub>12</sub>MDI as opposed to MDI hard segment was utilized due to its superior biocompatibility (Hafeman et al., 2011). Most interestingly, previous studies using similar PU compositions to the one currently under investigation reported cytocompatibility and non-toxicity (Ahmed et al., 2013). Also, *in vivo* subcutaneous implantation studies of PCLU and POSS-PCLU variations revealed no significant inflammatory response (see below). We hypothesize that acidic degradation products were responsible for cell death rather than true cytotoxicity of the metabolites (Taylor et al., 1994). Taken together, these cytocompatibility results, whilst indicative of



potential toxicity, may not be extrapolated directly into an *in vivo* setting as the body's circulatory potential is expected to flush away materials which may cause harm at high concentrations. Here, we used volume percent concentrations of degradation extracts to simulate highest concentrations of leachables closest to the implanted PU scaffold with gradually decreasing concentrations further away. One limitation of this study appears to be the incrementally decreasing percentage of growth medium which may be an explanation as to the concentration-dependent decrease in cell viability. More realistic means of analysis, therefore, include *in vivo* exposure studies over a sufficient time period.

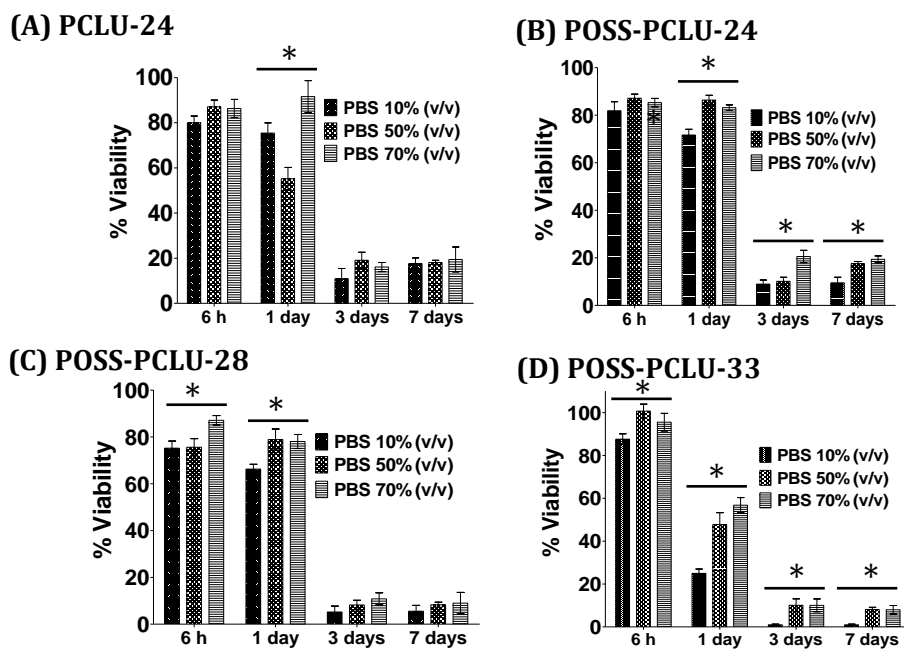


**Figure 6.12.** AlamarBlue® cell viability assay over a period of seven days. HDFa were cultured in media containing extracts of polymers degraded in phosphate buffered saline for 6 months. Increasing concentrations of extracts represent the *in vivo* scenario where highest extract concentrations can be found in close proximity to the polymer scaffold.

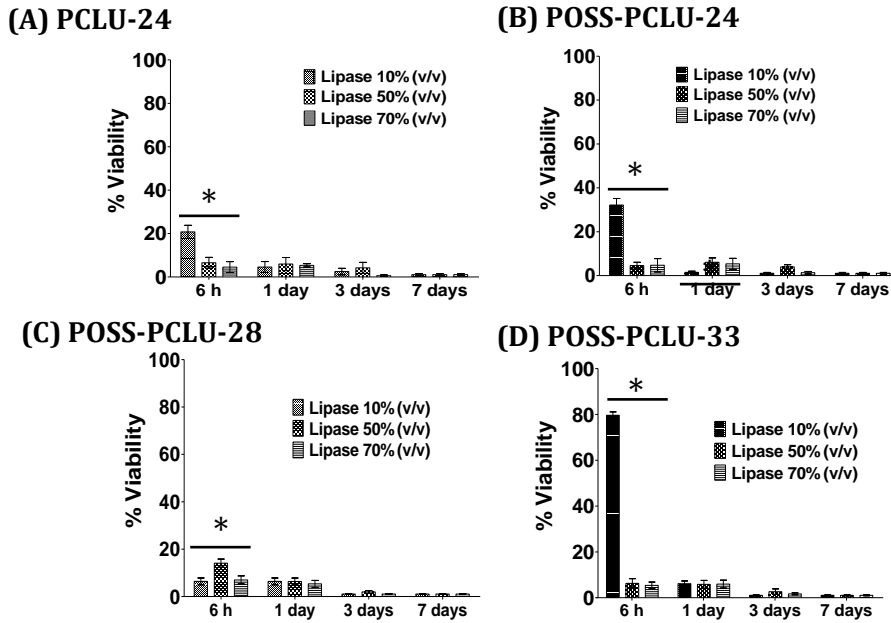


**Figure 6.13.** AlamarBlue® cell viability assay over a period of seven days. HDFa were cultured in media containing extracts of polymers degraded in lipase buffer for 6 months. Increasing concentrations of extracts represent the *in vivo* scenario where highest extract concentrations can be found in close proximity to the polymer scaffold.

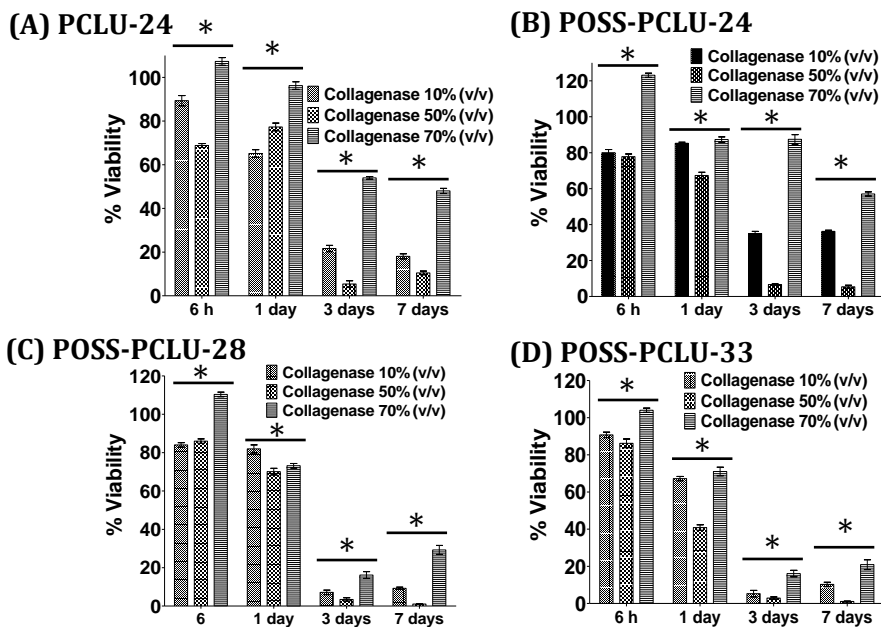


**Figure 6.14.** AlamarBlue® cell viability assay over a period of seven days. HDFa were cultured in media containing extracts of polymers degraded in collagenase buffer for 6 months. Increasing concentrations of extracts represent the *in vivo* scenario where highest extract concentrations can be found in close proximity to the polymer scaffold.

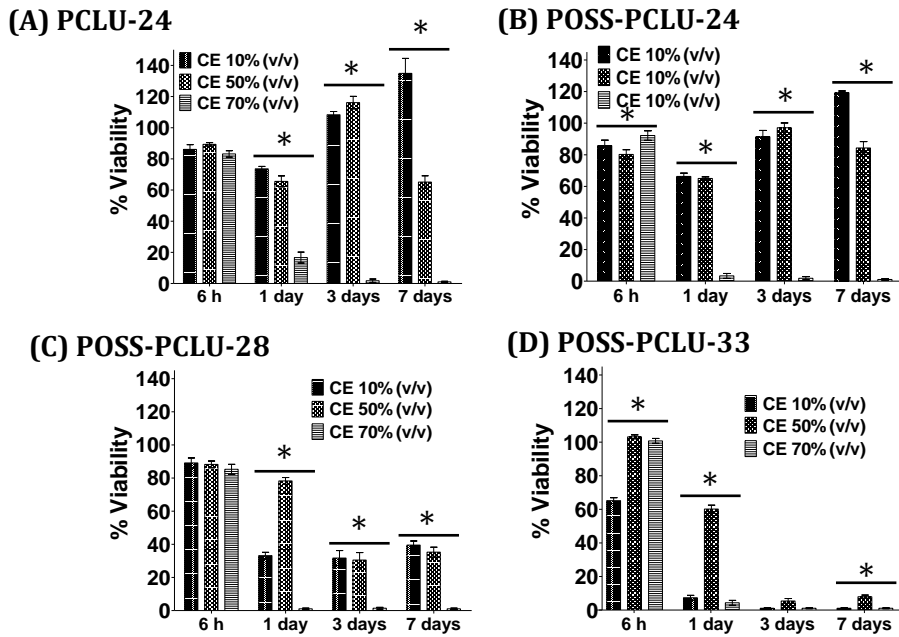


**Figure 6.15.** AlamarBlue® cell viability assay over a period of seven days. HDFA were cultured in media containing extracts of polymers degraded in cholesterol esterase buffer for 6 months. Increasing concentrations of extracts represent the *in vivo* scenario where highest extract concentrations can be found in close proximity to the polymer scaffold.

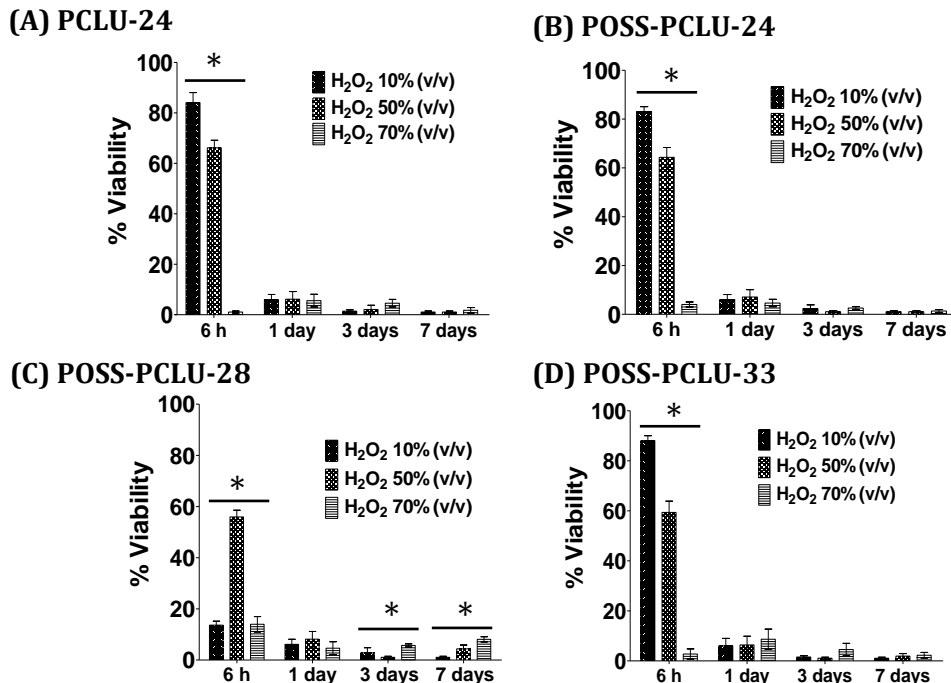


**Figure 6.16.** AlamarBlue® cell viability assay over a period of seven days. HDFA were cultured in media containing extracts of polymers degraded in hydrogen peroxide + CoCl<sub>2</sub> buffer for 6 months.

*Increasing concentrations of extracts represent the in vivo scenario where highest extract concentrations can be found in close proximity to the polymer scaffold.*

#### 6.4.7 *In Vivo* Blood Flow and Oxygenation

Subcutaneous integration and the extent of vascularization were assessed visually, using a laser Doppler imager and an oxygen sensor (Fig. 6.17). Animals were anaesthetized and scaffolds were exposed. Visual comparison between scaffolds of different hard segment and different lengths of implantation revealed obvious dimensional differences. POSS-PCLU-33 scaffolds implanted for the shortest period (4 weeks) appeared to retain most of their size compared to PCLU-24 scaffolds implanted for 12 weeks which were smallest.

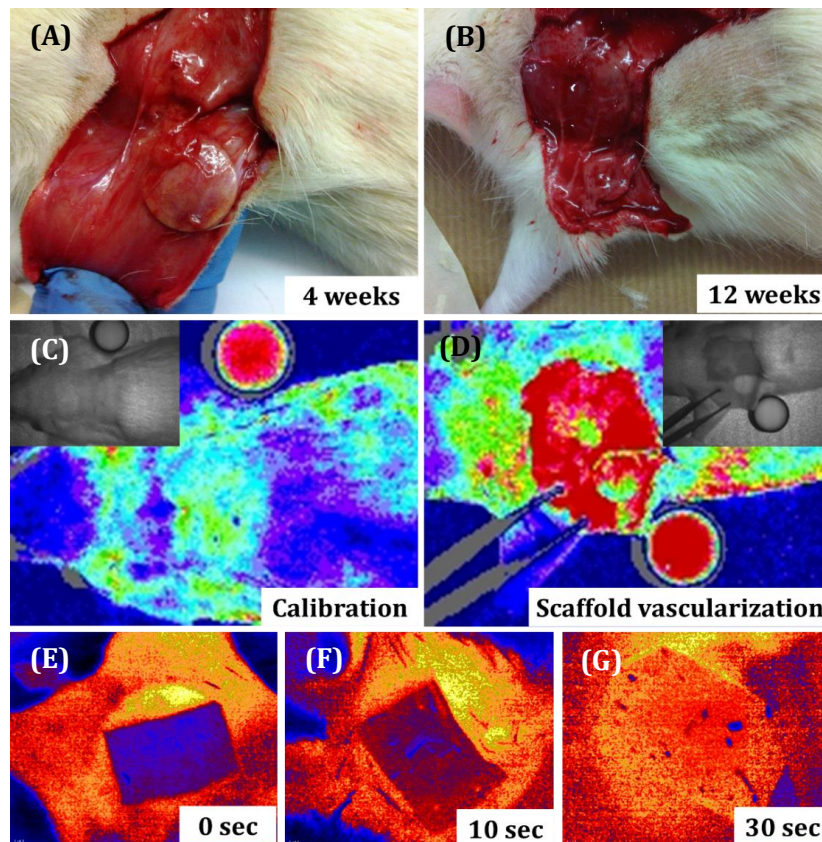


**Figure 6.17.** Macroscopic view of subcutaneously implanted scaffolds at (A) 4 weeks and (B) 12 weeks. (C) Laser Doppler calibration using full fat milk and (D) analysis of vascularized scaffolds

*prior to explantation. (E-G) Monitoring of oxygen transfer from scaffolds through an oxygen sensor film as a measure of scaffold vascularization.*

All scaffolds, however, appeared to be firmly integrated with the subcutaneous tissue and encapsulated in a highly vascularized fibrous sheath. Qualitative measurements of the extent of superficial scaffold vascularization were obtained using laser Doppler imaging and oxygen sensing, the premise being that vascularized scaffolds would be able to carry oxygen to the scaffold surface which could be detected by a sensor foil placed onto the scaffold. The intensity of the change in colour of the sensor foil determined the extent of vascularization. Whilst relatively non-specific as a stand-alone analytic tool, combined with histological and immunohistochemical analyses, the ability and extent of vascularization may be confidently determined.

#### **6.4.8 Histological and Immunohistochemical Analysis of Explanted Samples**

At 12 weeks post-implantation, gross evaluation of explanted scaffolds and surrounding tissues revealed no signs of infection (Fig. 6.18).

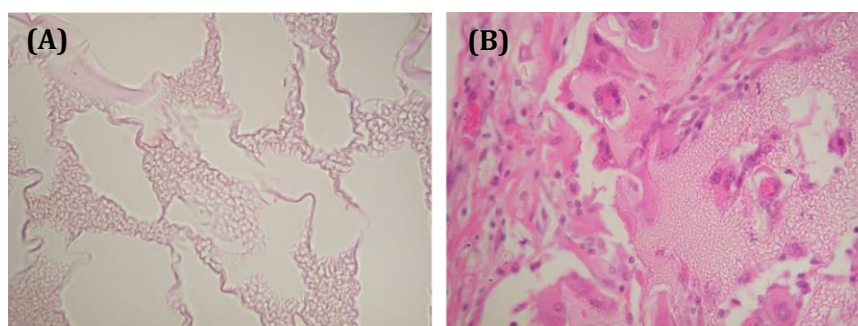


**Figure 6.18.** *Histological haematoxylin & eosin stain of (A) non-implanted control scaffold and (B) implanted scaffold. Magnification x 200.*

As expected, scaffold degradation visibly increased in the following order: POSS-PCLU-33, POSS-PCLU-28, POSS-PCLU-24 and PCLU-24 (Fig. 6.19). Arguably, PCLU-24 was



more degraded compared to its POSS-containing counterpart, supporting the hypothesis of POSS-induced slowing of degradation. Some polymers folded up on themselves despite the central suture. This, however, did not result in brittle fracture, underlining the elastic nature of these scaffolds.

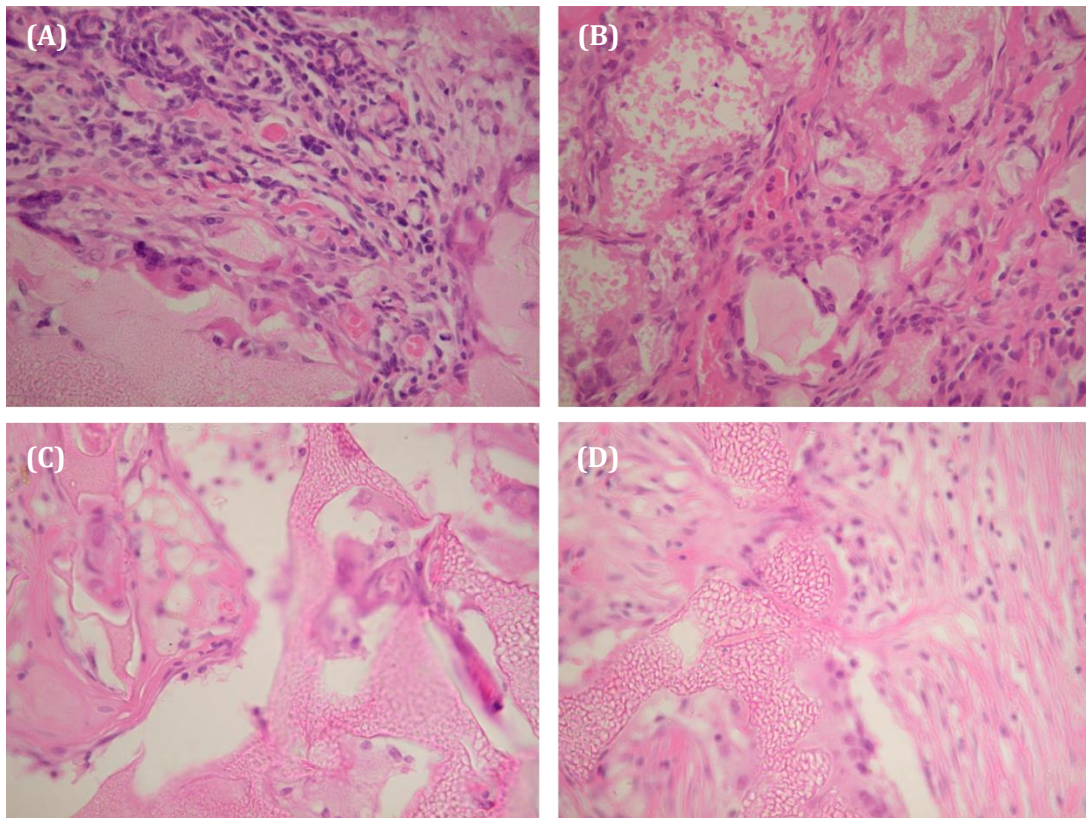


**Figure 6.19.** Histological comparison of the extent of connective tissue regeneration and *in vivo* degradation of scaffold groups. (A) PCLU-24, (B) POSS-PCLU-24, (C) POSS-PCLU-28 and (D) POSS-PCLU-33. Magnification x 200.

Histological examination of the polymer sections (H&E) demonstrated that each PU group supported cellular infiltration and connective tissue ingrowth which traversed from the periphery of the polymer scaffold through to the opposite side. Cells initially populated the pores of the scaffolds before breaking through the polymeric structures to infiltrate the scaffold proper. Matrix deposition was accompanied by blood vessel formation as can be seen in Figures 6.20 and 6.21 (arrows).

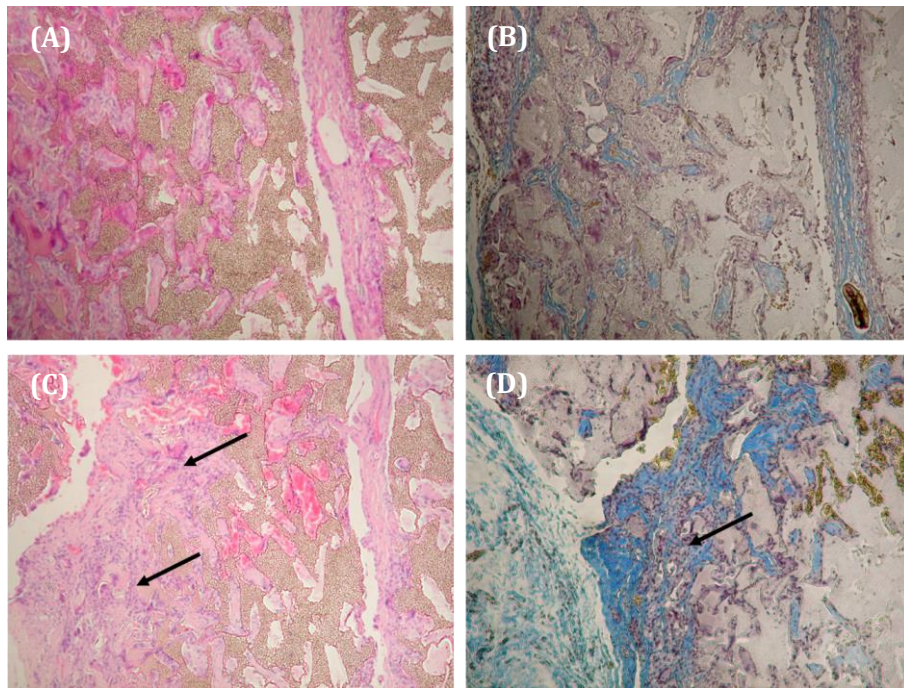


**Figure 6.20.** Haematoxylin & eosin stained images of PCLU-24 after 4 weeks (A) and 8 weeks (C) and corresponding MSB stained images (B and D). The arrows indicate noticeable integration of the tissue infiltrate with the scaffold (C) and marked collagen deposition (D). Magnification x 100.

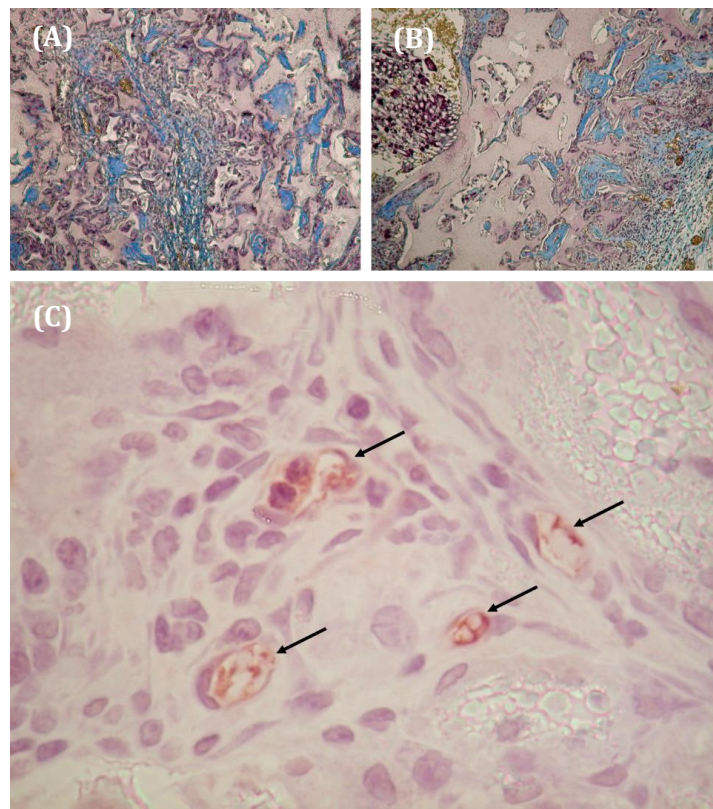


**Figure 6.21.** *MSB stained POSS-PCLU-24 (A) and POSS-PCLU-33 (B) at 4 weeks demonstrating increased degradation of scaffolds of lower hard segment. (C) Vascular infiltration visible at 4 weeks post-implantation. Magnification x 100 (A and B) and x 400 (C).*

At 4 weeks post-implantation, 50 % of the PCLU-24 graft was populated with cells and a moderate amount of vasculature and collagen formation. At 12 weeks post-implantation, collagen deposition was more abundant. Similar trends were observed for POSS-PCLU-24 scaffolds. However, more abundant collagen deposition and vascular infiltration was noticed at the 12 week time point. Scaffolds of higher hard segment content initially revealed significantly less cellular infiltration compared to softer scaffolds but demonstrated cellular proliferation rates similar to those observed in the softer scaffolds, indicating slower degradation of the PU scaffolds and thus slower tissue infiltration. After eight weeks, some degradation was noticeable in both PCLU-24 and POSS-PCLU-24 which presumably accelerated tissue infiltration.

Histological sections of end organs revealed no signs of inflammation when exposed to degradation products of any of the scaffolds (Fig. 6.22), suggesting excellent biocompatibility of both PCLU and POSS-PCLU scaffolds.



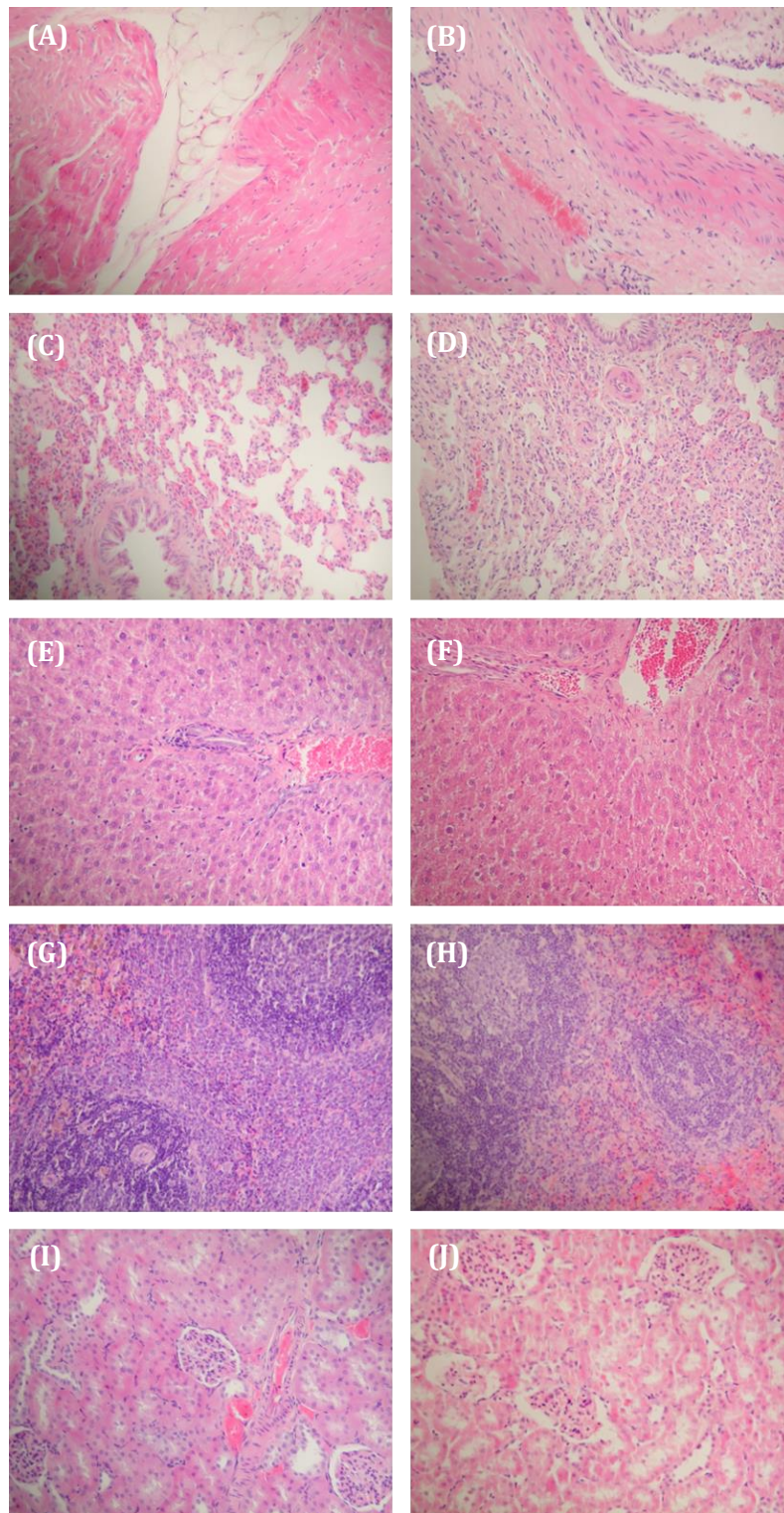


**Figure 6.22.** Representative haematoxylin & eosin stains of in vivo response to PCLU and POSS-PCLU scaffolds. (A) Heart, (C) lung, (E) liver, (G) spleen and (I) kidney tissues with the corresponding sham-treated tissues (B, D, F, H and J). Magnification x 100.

## 6.5 CONCLUSION

We synthesized a novel nanocomposite PU based on a poly( $\epsilon$ -caprolactone urea)urethane backbone integrating POSS nanoparticles. Differences in hard segment content and presence or absence of POSS particles were analysed with respect to their influence on *in vitro* and *in vivo* degradative behaviour. Degradation was strongly dependent upon hard segment micro-domain formation with PUs containing the highest number of hydrolytically labile urea and urethane bonds exhibiting the least degradation. Additionally, the mode of degradation was strongly influenced by POSS nanoparticle inclusion due to its ability to influence degradation.

Rather than degrading into a stiff and brittle film which may compromise functionality of the implanted device, POSS nanoparticles were able to tailor material degradation whilst retaining vital elasticity. This is of great importance for tissue engineering applications involving tissues such as the skin or vasculatures.

## References

- AHMED, M., PUNSHON, G., DARBYSHIRE, A. & SEIFALIAN, A. M. 2013. Effects of sterilization treatments on bulk and surface properties of nanocomposite biomaterials. *J Biomed Mater Res B Appl Biomater*, 101, 1182-90.
- BAE, S. H., CHE, J.-H., SEO, J.-M., JEONG, J., KIM, E. T., LEE, S. W., KOO, K.-I., SUANING, G. J., LOVELL, N. H., CHO, D.-I. D., KIM, S. J. & CHUNG, H. 2012. In vitro biocompatibility of various polymer-based microelectrode arrays for retinal prosthesis. *Investigative ophthalmology & visual science*, 53, 2653-7.
- BERNACCA, G. M., O'CONNOR, B., WILLIAMS, D. F. & WHEATLEY, D. J. 2002. Hydrodynamic function of polyurethane prosthetic heart valves: influences of Young's modulus and leaflet thickness. *Biomaterials*, 23, 45-50.
- CHALOUPKA, K., MOTWANI, M. & SEIFALIAN, A. M. 2011. Development of a new lacrimal drainage conduit using POSS nanocomposite. *Biotechnol Appl Biochem*, 58, 363-70.
- CHAN-CHAN, L. H., SOLIS-CORREA, R., VARGAS-CORONADO, R. F., CERVANTES-UC, J. M., CAUICH-RODRIGUEZ, J. V., QUINTANA, P. & BARTOLO-PEREZ, P. 2010. Degradation studies on segmented polyurethanes prepared with HMDI, PCL and different chain extenders. *Acta Biomater*, 6, 2035-44.
- CHAWLA, A. S., BLAIS, P., HINBERG, I. & JOHNSON, D. 1988. Degradation of explanted polyurethane cardiac pacing leads and of polyurethane. *Biomaterials, artificial cells, and artificial organs*, 16, 785-800.
- CHRISTENSON, E. M., PATEL, S., ANDERSON, J. M. & HILTNER, A. 2006. Enzymatic degradation of poly(ether urethane) and poly(carbonate urethane) by cholesterol esterase. *Biomaterials*, 27, 3920-6.
- CRESCENZI, V., MANZINI, G., CALZOLARI, G. & BORRI, C. 1972. Thermodynamics of fusion of poly- $\beta$ -propiolactone and poly- $\epsilon$ -caprolactone. Comparative analysis of the melting of aliphatic polylactone and polyester chains. *Eur Polym*, 449-63.
- DESAI, M., BAKHSHI, R., ZHOU, X., ODLYHA, M., YOU, Z., SEIFALIAN, A. M. & HAMILTON, G. 2012. A sutureless aortic stent-graft based on a nitinol scaffold bonded to a compliant nanocomposite polymer is durable for 10 years in a simulated in vitro model. *J Endovasc Ther*, 19, 415-27.
- ENGELBERG, I. & KOHN, J. 1991. Physico-mechanical properties of degradable polymers used in medical applications: a comparative study. *Biomaterials*, 12, 292-304.
- GAO, Y., EGUCHI, A., KAKEHI, K. & LEE, Y. C. 2004. Efficient preparation of glycoclusters from silsesquioxanes. *Org Lett*, 6, 3457-60.
- GÖPFERICH, A. 1996. Mechanisms of polymer degradation and erosion. *Biomaterials*, 17, 103-14.
- GU, X., WU, J. & MATHER, P. T. 2011. Polyhedral oligomeric silsesquioxane (POSS) suppresses enzymatic degradation of PCL-based polyurethanes. *Biomacromolecules*, 12, 3066-3077.
- GUASTI, L., VAGASKA, B., BULSTRODE, N. W., SEIFALIAN, A. M. & FERRETTI, P. 2013. Chondrogenic differentiation of adipose tissue-derived stem cells within nanocaged POSS-PCU scaffolds: A new tool for nanomedicine. *Nanomedicine*.
- GUELCHER, S. A. 2008. Biodegradable polyurethanes: synthesis and applications in regenerative medicine. *Tissue Eng Part B Rev*, 14, 3-17.
- GUELCHER, S. A., GALLAGHER, K. M., DIDIER, J. E., KLINEDINST, D. B., DOCTOR, J. S., GOLDSTEIN, A. S., WILKES, G. L., BECKMAN, E. J. & HOLLINGER, J. O. 2005. Synthesis of biocompatible segmented polyurethanes from aliphatic diisocyanates and diurea diol chain extenders. *Acta Biomater*, 1, 471-84.
- HAFEMAN, A. E., ZIENKIEWICZ, K. J., ZACHMAN, A. L., SUNG, H.-J., NANNEY, L. B., DAVIDSON, J. M. & GUELCHER, S. A. 2011. Characterization of the degradation mechanisms of lysine-derived aliphatic poly(ester urethane) scaffolds. *Biomaterials*, 32, 419-29.
- HEIJKANTS, R. G. J. C., VAN CALCK, R. V., VAN TIENEN, T. G., DE GROOT, J. H., BUMA, P., PENNING, A. J., VETH, R. P. H. & SCHOUTEN, A. J. 2005. Uncatalyzed synthesis, thermal and mechanical properties of polyurethanes based on poly( $\epsilon$ -caprolactone) and 1,4-butane diisocyanate with uniform hard segment. *Biomaterials*, 26, 4219-28.

HUA, K., CARLSSON, D. O., ALANDER, E., LINDSTRÖM, T., STROMME, M., MIHRANYAN, A. & FERRAZ, N. 2014. Translational study between structure and biological response of nanocellulose from wood and green algae. *RSC Advances*, 2892-2903.

IWATA, T. & DOI, Y. 1998. Morphology and enzymatic degradation of poly(L-lactic acid) single crystals. *Macromolecules*, 31, 2461-2467.

IZCI, Y., SECER, H., AKAY, C. & GONUL, E. 2009. Initial experience with silver-impregnated polyurethane ventricular catheter for shunting of cerebrospinal fluid in patients with infected hydrocephalus. *Neurological research*, 31, 234-7.

JUNGEBLUTH, P., ALICI, E., BAIGUERA, S., LE BLANC, K., BLOMBERG, P., BOZOKY, B., CROWLEY, C., EINARSSON, O., GRINNEMO, K. H., GUDBJARTSSON, T., LE GUYADER, S., HENRIKSSON, G., HERMANSON, O., JUTO, J. E., LEIDNER, B., LILJA, T., LISKA, J., LUEDDE, T., LUNDIN, V., MOLL, G., NILSSON, B., RODERBURG, C., STROMBLAD, S., SUTLU, T., TEIXEIRA, A. I., WATZ, E., SEIFALIAN, A. & MACCHIARINI, P. 2011. Tracheobronchial transplantation with a stem-cell-seeded bioartificial nanocomposite: a proof-of-concept study. *Lancet*, 378, 1997-2004.

KANNAN, R. Y., SALACINSKI, H. J., DE GROOT, J., CLATWORTHY, I., BOZEC, L., HORTON, M., BUTLER, P. E. & SEIFALIAN, A. M. 2006. The antithrombogenic potential of a polyhedral oligomeric silsesquioxane (POSS) nanocomposite. *Biomacromolecules*, 7, 215-23.

KORLEY, L. T. J., PATE, B. D., THOMAS, E. L. & HAMMOND, P. T. 2006. Effect of the degree of soft and hard segment ordering on the morphology and mechanical behavior of semicrystalline segmented polyurethanes. *Polymer*, 47, 3073-3082.

LABOW, R. S., TANG, Y., MCCLOSKEY, C. B. & SANTERRE, J. P. 2002. The effect of oxidation on the enzyme-catalyzed hydrolytic biodegradation of poly(urethane)s. *Journal of biomaterials science. Polymer edition*, 13, 651-65.

LEE, K. H. & CHU, C. C. 2000. The role of superoxide ions in the degradation of synthetic absorbable sutures. *Journal of biomedical materials research*, 49, 25-35.

LEE, W. C. & CHU, I. M. 2008. Preparation and degradation behavior of polyanhydrides nanoparticles. *J Biomed Mater Res B Appl Biomater*, 84, 138-46.

LI, F. K., ZHANG, X., HOU, J. N., XU, M., LU, X. L., MA, D. Z. & KIM, B. K. 1997. Studies on Thermally Stimulated Shape-Memory Effect of Segmented Polyurethanes. *Journal of Applied Polymer Science*, 64, 1511-1516.

LI, G., LIU, Y., LI, D., ZHANG, L. & XU, K. 2012a. A comparative study on structure-property elucidation of P3/4HB and PEG-based block polyurethanes. *Journal of biomedical materials research. Part A*, 100, 2319-29.

LI, Z., ZHANG, Z., LIU, K. L., NI, X. & LI, J. 2012b. Biodegradable hyperbranched amphiphilic polyurethane multiblock copolymers consisting of poly(propylene glycol), poly(ethylene glycol), and polycaprolactone as in situ thermogels. *Biomacromolecules*, 13, 3977-89.

MARCOS-FERNÁNDEZ, A., ABRAHAM, G. A. & VALENTÍN, J. L., ROMÁN, J.S. 2006. Synthesis and characterization of biodegradable non-toxic poly(ester-urethane-urea)s based on poly( $\epsilon$ -caprolactone) and amino acid derivatives. *Polymer*, 47, 785-798.

O'SICKEY, M. J., LAWREY, B. D. & WILKES, G. L. 2002. Structure-Property Relationships of Poly(urethane urea)s with Ultra-low Monol Content Poly(propylene glycol) Soft Segments. 1. Influence of Soft Segment Molecular Weight and Hard Segment Content. *Journal of Applied Polymer Science*, 84, 229-229.

OKKEMA, A. Z. & COOPER, S. L. 1991. Effect of carboxylate and/or sulphonate ion incorporation on the physical and blood-contacting properties of a polyetherurethane. *Biomaterials*, 12, 668-76.

OSTWALD, W. Z. 1897. Studien über die Bildung und Umwandlung fester Körper. *Zeitschrift Für Physikalische Chemie*, 22, 289-330.

PENG, L. H., MAO, Z. Y., QI, X. T., CHEN, X., LI, N., TABATA, Y. & GAO, J. Q. 2013. Transplantation of bone-marrow-derived mesenchymal and epidermal stem cells contribute to wound healing with different regenerative features. *Cell and tissue research*, 352, 573-83.

RAFIEMANZELAT, F., FATHOLLAHI ZONOUI, A. & EMTIAZI, G. 2013. Synthesis of new poly(ether-urethane-urea)s based on amino acid cyclopeptide and PEG: study of their environmental degradation. *Amino acids*, 44, 449-59.

RAHMANI, B., TZAMTZIS, S., GHANBARI, H., BURRIESCI, G. & SEIFALIAN, A. M. 2012. Manufacturing and hydrodynamic assessment of a novel aortic valve made of a new nanocomposite polymer. *J Biomech*, 45, 1205-11.

RIZVI, S. B., YILDIRIMER, L., GHADERI, S., RAMESH, B., SEIFALIAN, A. M. & KESHTGAR, M. 2012. A novel POSS-coated quantum dot for biological application. *Int J Nanomedicine*, 7, 3915-27.

SANTERRE, J. P. & LABOW, R. S. 1997. The effect of hard segment size on the hydrolytic stability of polyether-urea-urethanes when exposed to cholesterol esterase. *Journal of biomedical materials research*, 36, 223-32.

SANTERRE, J. P., LABOW, R. S., DUGUAY, D. G., ERFLE, D. & ADAMS, G. A. 1994. Biodegradation evaluation of polyether and polyester-urethanes with oxidative and hydrolytic enzymes. *Journal of biomedical materials research*, 28, 1187-99.

SCHUTZIUS, T. M., BAYER, I. S., JURSIK, G. M., DAS, A. & MEGARIDIS, C. M. 2012. Superhydrophobic-superhydrophilic binary micropatterns by localized thermal treatment of polyhedral oligomeric silsesquioxane (POSS)-silica films. *Nanoscale*, 4, 5378-85.

SHIBAYAMA, M., KAWAUCHI, T., KOTANI, T., NOMURA, S. & MATSUDA, T. 1986. Structure and properties of fatigued segmented poly(urethaneurea)s I. Segment orientation mechanism due to fatigue. *Polym. J.*, 18, 719-733.

SHIBAYAMA, M., SUETSUGU, M., SAKURAI, S., YAMAMOTO, T. & NOMURA, S. 1991. Structure characterization of polyurethanes containing poly(dimethylsiloxane). *Macromolecules*, 24, 6254-6262.

SHOAE-HASSANI, A., KEYHANVAR, P., SEIFALIAN, A. M., MORTAZAVI-TABATABAEI, S. A., GHADERI, N., ISSAZADEH, K., AMIRMOZAFARI, N. & VERDI, J. 2013a. lambda Phage Nanobioparticle Expressing Apoptin Efficiently Suppress Human Breast Carcinoma Tumor Growth In Vivo. *PLoS One*, 8, e79907.

SHOAE-HASSANI, A., SHARIF, S., SEIFALIAN, A. M., MORTAZAVI-TABATABAEI, S. A., REZAIIE, S. & VERDI, J. 2013b. Endometrial stem cell differentiation into smooth muscle cell: a novel approach for bladder tissue engineering in women. *BJU Int*, 112, 854-63.

SKARJA, G. A. & WOODHOUSE, K. A. 1998. Synthesis and characterization of degradable polyurethane elastomers containing an amino acid-based chain extender. *Journal of Biomaterials Science, Polymer Edition*, 9, 271-295.

SUNG, C. S. P., HU, C. B. & WU, C. S. 1980. Properties of Segmented Poly(urethaneureas) Based on 2,4-Toluene Diisocyanate. 1. Thermal Transitions, X-ray Studies, and Comparison with Segmented Poly(urethanes). *Macromolecules*, 13, 111-111.

SUTHERLAND, K., MAHONEY, J. R., COURRY, A. J. & EATON, J. W. 1993. Degradation of biomaterials by phagocyte-derived oxidants. *The Journal of clinical investigation*, 92, 2360-7.

SZYCHER, M., POIRIER, V. L. & DEMPSEY, D. J. 1983. Development of an aliphatic biomedical-grade polyurethane elastomer. *J Elastom Plast*, 81.95-81.95.

TANG, Y. W., LABOW, R. S. & SANTERRE, J. P. 2001. Enzyme-induced biodegradation of polycarbonate polyurethanes: dependence on hard-segment concentration. *Journal of biomedical materials research*, 56, 516-28.

TATAI, L., MOORE, T. G., ADHIKARI, R., MALHERBE, F., JAYASEKARA, R., GRIFFITHS, I. & GUNATILLAKE, P. A. 2007. Thermoplastic biodegradable polyurethanes: the effect of chain extender structure on properties and in-vitro degradation. *Biomaterials*, 28, 5407-17.

TAYLOR, M. S., DANIELS, A. U., ANDRIANO, K. P. & HELLER, J. 1994. Six bioabsorbable polymers: in vitro acute toxicity of accumulated degradation products. *J Appl Biomater*, 5, 151-7.

TOKIWA, Y., CALABIA, B. P., UGWU, C. U. & AIBA, S. 2009. Biodegradability of plastics. *International journal of molecular sciences*, 10, 3722-42.

TOKIWA, Y. & SUZUKI, T. 1978. Hydrolysis of polyesters by *Rhizopus delemar* lipase. *Agric. Biol. Chem.*, 42, 1071-1072.

UHRICH, K. E., CANNIZZARO, S. M., LANGER, R. S. & SHAKESHEFF, K. M. 1999. Polymeric systems for controlled drug release. *Chem Rev*, 99, 3181-98.

WANG, G. B., LABOW, R. S. & SANTERRE, J. P. 1997. Biodegradation of a poly(ester)urea-urethane by cholesterol esterase: isolation and identification of principal biodegradation products. *Journal of biomedical materials research*, 36, 407-17.



- WILLIAMS, D. F. & ZHONG, S. P. 1994. Biodeterioration/biodegradation of polymeric medical devices in situ. *International Biodeterioration & Biodegradation*, 34, 95-130.
- WU, J. & MATHER, P.T. 2009. POSS Polymers: Physical Properties and Biomaterials Applications. *Journal of Macromolecular Science, Part C: Polymer Reviews*, 49, 25-63.



# 7 PHOTO-POLYMERIZABLE GELATIN AS SKIN TISSUE ENGINEERING SCAFFOLDS: MECHANICAL, DEGRADATION AND BIOLOGICAL CONSIDERATIONS <sup>3</sup>

---

## 7.1 SYNOPSIS

Biomimetic composite hydrogels based on natural polymers have generated significant interest in the field of tissue engineering and regenerative medicine. Gelatin which is the hydrolysed derivative of collagen retains the bio-functionality of its parent polymer and is biodegradable under physiological conditions. Additionally, collagen is the most abundant protein in extracellular matrix (ECM) of most tissues. Whilst gelatin hydrogels have been investigated for various tissue engineering applications, their suitability as a skin regeneration scaffold has not been researched so far. In this chapter, hydrogels based on methacrylated gelatin (GelMA) were generated. Their physical and biological properties were tunable by using different concentrations of gelatin with or without the addition of polyethylene glycol-diacrylate (PEG-DA) which has previously been shown to enhance mechanical properties. Physical properties including swelling ratio, degradation and mechanical properties were investigated. Moreover, *in vitro* cellular responses of an immortalized human keratinocyte cell line (HaCaT) and their potential for creating an epidermal layer were investigated. It was found that higher concentrations of GelMA and PEG-DA correlated with increased compressive moduli and decreased swelling as well as degradation rates. HaCaT culture at the air-liquid interface

---

<sup>3</sup> In collaboration with the Khademhosseini laboratories at Harvard-MIT, Boston, USA.

resulted in the reconstruction of a stratified epidermis resembling that of normal human skin.

## 7.2 INTRODUCTION

Skin is the largest organ of the human body and is composed of three layers including epidermis, dermis and hypodermis (Metcalf and Ferguson, 2007). These three layers play an important role in protecting the body from any mechanical damage and against pathogens and microorganisms (Groeber et al., 2011). Loss of integrity of large portions of skin due to injury or illness may result in significant disability or even death. Healing of cutaneous wounds involves the regeneration of surface epidermis and repair of connective tissues by events that are largely independent of one another. If the wound is a shallow one, epidermal regeneration precedes repair in the dermis, but if the injury extends to the full thickness of the skin, epidermal regeneration and growth of granulation tissue takes place concurrently. In the past 30 years, great efforts have therefore been made to create substitutes that mimic human skin. Ideally, tissue-engineered skin needs to (i) provide a barrier layer of renewable keratinocytes which (ii) provides an elastic structural support for skin and (iii) is securely attached to the underlying dermis (MacNeil, 2007). Currently, however, no commercially available tissue-engineered skin replacement material possesses all of the above-mentioned properties (Shevchenko et al., 2010a).

Current strategies to develop an ideal keratinocytes layer involves the use of suitable biocompatible and biodegradable scaffolds, such as collagen, hyaluronic acid and other biopolymers capable of supporting keratinocyte growth (Liu et al., 2010). Amongst these, collagen is one of the most popular materials for production of tissue engineered human skin equivalents (e.g. Integra® dermal regeneration template, Apligraf®) as it is the major component of skin and constitutes the major part of the ECM (Harley and Yannas, 2007). Advantages of collagen are, however, offset by possible toxicities caused

by residual catalysts, initiators and unreacted or partially reacted chemical cross-linking agents that are generally employed to improve stability and mechanical properties (Yeh et al., 2011). One collagen derivative, namely gelatin (hydrolysed collagen), has a relatively lower antigenicity compared to collagen whilst maintaining the properties of biocompatibility and biodegradability and has thus become a popular alternative. In addition, gelatin is significantly less expensive than collagen (Yeh et al., 2011). Methacrylated gelatin (GelMA) maintains its unique properties, but additionally allows the material to be solidified from liquid to solid permanently upon light exposure whereas solidified gelatin may return to liquid state upon warming, limiting their usefulness in the body to temporary structures. We hypothesized that as a light polymerizable hydrogel based on collagen motifs, GelMA could successfully be micropatterned into a variety of shapes and configurations for tissue engineering and microfluidic applications, while retaining its high encapsulated cell viability and cell-responsive elements (i.e. binding and degradation). In this chapter, gelatin methacrylate was used as scaffold material to achieve an ideal keratinocyte layer for further development of a multi-layered epidermis.

Previously, it was reported that keratinocytes increased adhesion density on stiffer hydrogel surfaces (Xu et al., 2012). Additionally, it was found that keratinocyte spreading and differentiation was associated with stiffness of polyacrylamide (PAAm) hydrogel (Trappmann et al., 2012). Currently, there are few studies researching the effects of stiffness on keratinocyte culture to produce a viable epidermis comprised of a stratified layer of keratinocytes. The aim of the present study is to understand the effect of material properties (i.e., stiffness, degradation and biological properties) on the reconstruction of an artificial epidermis to control proliferation, differentiation and stratification of human

keratinocytes. Firstly, hydrogels consisting of GelMA of incrementally increasing stiffness were fabricated. Then, HaCaT cells were seeded onto these hydrogels to develop a confluent cell monolayer which was then lifted to the air-liquid interface (ALI) to reconstruct a multilayer of keratinocytes (stratified epidermis). The effect of hydrogel properties on cell morphology, attachment, proliferation and stratification was quantified and eventually the optimum formulation was selected for the development of an artificial epidermis (Fig. 7.1).

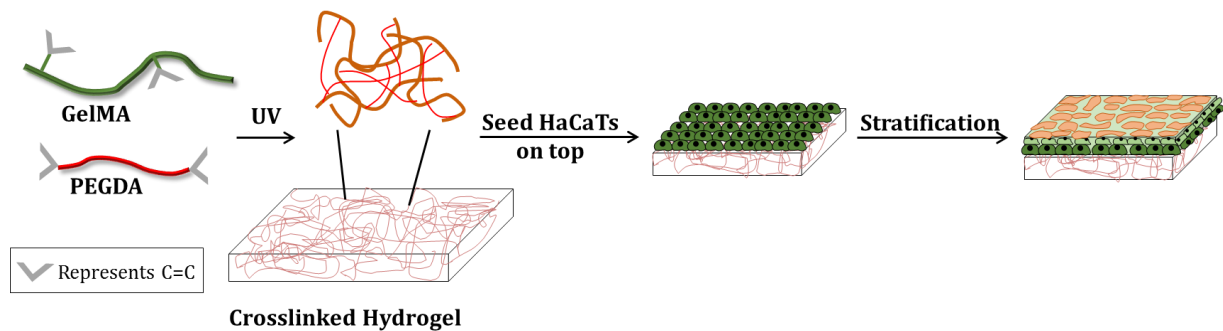


**Figure 7.1.** Schematic illustration of the synthesis steps involved in creating an artificial epidermis on gelatin methacrylate (GelMA) hydrogels.

## 7.3 MATERIALS AND METHODS

### 7.3.1 Materials

Porcine skin gelatin, methacrylic anhydride were purchased from Sigma-aldrich, St. Louis, MO; Dulbecco's phosphate buffered saline (DPBS), fetal bovine serum (FBS), live/dead<sup>®</sup> assay, rhodamine-phalloidin, 4',6-diamidino-2-phenylindole (DAPI), Quanti-iT<sup>™</sup> PicoGreen<sup>®</sup> dsDNA reagent kits were from Invitrogen, San Diego, CA; proteinase k were from HyClone, Logan, UT; 2-hydroxy-1-(4-(hydroxyethoxy)phenyl)-2-methyl-1-propanone (Irgacure 2959) from CIBA Chemicals, Basel, Switzerland; polyethylene glycol-diacrylate (PEG-DA;  $M_w$  4000) was purchased from Sigma-Aldrich Chemical Co. (St. Louis, MO, US).

### **7.3.2 Synthesis of Gelatin Methacrylate (GelMA)**

GelMA was synthesized as described previously (Van Den Bulcke et al., 2000). Briefly, 10 g of type A porcine skin gelatin was mixed at 10 % (w/v) into DPBS at 60 °C and stirred until fully dissolved. 8 mL of methacrylic anhydride was added until the target volume was reached at a rate of 0.5 mL/min to the gelatin solution under stirred conditions at 50 °C and allowed to react for 3 h. Following a 5 x dilution with additional warm (40 °C) DPBS to stop the reaction, the mixture was dialyzed against distilled water using 12–14 kDa cut-off dialysis tubing for 1 week at 40 °C to remove salts and unreacted methacrylic anhydride. The solution was lyophilized for 1 week to generate white porous foam and stored at –80 °C until further use. The degree of methacrylation was quantified using <sup>1</sup>H NMR spectroscopy. The spectra were collected at room temperature in deuterium oxide at a frequency of 600 MHz using a Varian INOVA NMR spectrometer with a single axis gradient inverse probe.

### **7.3.3 Preparation of GelMA Hydrogels with Varying Degrees of Methacrylation**

Incrementally increased amounts of freeze-dried GelMA macromer was mixed into DPBS containing 0.5 % (w/v) 2-hydroxy-1-(4-(hydroxyethoxy)phenyl)-2-methyl-1-propanone (used as photo-initiator) at 80 °C to make final concentration of GelMA at 5, 7.5, 10, 12.5, 15, 17.5 and 20 % (w/v). The prepolymer solution was then pipetted into a polydimethylsiloxane (PDMS) mold, covered with 3 - (Trimethoxysilyl) propyl methacrylate (TMSPMA) treated glass slide and exposed to 6.9 mW/cm<sup>2</sup> UV light (360 - 480 nm). For mechanical, swelling ratio and degradation study, samples of 6 mm diameter and 3 mm thickness were fabricated upon 180 s UV exposures whereas for biological studies, samples of 8 mm diameter and 200 μm thickness were produced upon 30 s UV exposure. For all test, 4 replicates were used unless otherwise stated.



### **7.3.3.1 Introduction of PEG+**

To a subset of GelMA prepolymer solutions of 5, 10, 15 and 20 % (w/v), PEG-DA ( $M_w$  4000) at concentrations of 1 % (v/v) of the initial GelMA concentrations (i.e. 0.5, 1, 1.5 and 2 % (v/v)) was added and processed into hydrogels as described in section 7.3.3.

## **7.3.4 Characterization of GelMA Hydrogels**

### **7.3.4.1 Mechanical Testing**

Cross-linked samples were detached from the glass slide and incubated in DPBS at 37 °C for 24 h. The samples were blotted dry and compressed at a rate of 1 mm/min using an Instron 5542 mechanical tester. The compressive modulus was determined as the slope of the linear region of stress-strain curve corresponding with 0–10 % strain.

### **7.3.4.2 Water Content Analysis**

Detached samples were incubated in DPBS at room temperature for 24 h, removed from DPBS, lightly blotted dry and weighted ( $W_s$ ). Samples were then lyophilized and weighed to determine the dry weight ( $W_D$ ). The water content of the swollen gel (SR) was calculated according to the following equation:

$$SR = \frac{W_s - W_D}{W_s} - 100 \%$$

### **7.3.4.3 Determination of diffusibility of hydrogel formulations**

All diffusibility studies were performed at 37 °C. Samples of 5 % (v/v) or 20 % (v/v) were placed in 1.5 mL Eppendorf tubes with 500  $\mu$ L of FITC-labelled BSA in DPBS. At 0, 1, 2, 4, 6, 8 and 24 h, samples were collected and fluorescence was visualised under a fluorescent microscope at x 4 magnification.

#### **7.3.4.4 Degradation Study**

Samples were placed in 1.5 mL Eppendorf tubes with 500  $\mu$ L of DPBS with 2 U/mL of collagenase type II at 37 °C. At time points 0, 2, 10, 24, 48, 72 and 96 h, the collagenase solution was removed and the samples were washed twice with sterile deionized water, freeze-dried and weighed. The percentage degradation ( $D_P$ ) of the gels was determined using the following equation:

$$D_P = \frac{W_0 - W_t}{W_0} \times 100 \%$$

where  $W_0$  is the initial sample dry weight and  $W_t$  is the dry weight after time  $t$ .

#### **7.3.5 Culture of Human Keratinocytes (HaCaT)**

HaCaTs were incubated at 37 °C in DMEM supplemented with 10 % FBS and 1 % penicillin/streptomycin. The cells were maintained in tissue culture polystyrene (TCP) and passaged 1:6 when the cells reached 70 % confluence.

##### **7.3.5.1 Culture of HaCaT Monolayer**

###### **7.3.5.1.1 Cell Adhesion**

HaCaT cell suspension was seeded on surfaces of samples of different GelMA concentration at a seeding density of  $2 \times 10^6$  cells/cm<sup>2</sup>. Rhodamine-labelled phalloidin/DAPI for F-actin/cell nuclei staining was used according to the manufacturer's instructions to examine cell adhesion on samples following 1, 4, 24 h, 4, and 7 days of culture in medium. Briefly, following 3 washing steps with PBS, samples were fixed in 4 % paraformaldehyde (PFA) for 30 min, permeabilized using 0.1 % Triton X-100 for 20 min, then blocked in 1 % BSA for 45 min. Rhodamine-labelled phalloidin solution (dilution 1:40) was then added and incubated with the cells at 37 °C for 45 min. The samples (at 7 days) were doubly stained with E-Cadherin antibodies (a cell adhesion molecule and epithelial cell marker) diluted 1:200 in PBS containing 1 % BSA for 45 min at room

temperature. Samples were subsequently incubated with FITC-labelled goat-anti-mouse secondary antibody (dilution 1:800) for 45 min in dark conditions. Last, DAPI solution (dilution 1:1000) was added to the cells and incubated at 37 °C for 5 min. The cells were then imaged and the cell number and cell area were measured using NIH ImageJ software.

#### 7.3.5.1.2 Cell Proliferation

Cell proliferation was evaluated using PicoGreen® DNA quantification assay. At each time point (0, 1, 4 and 7 days), the samples were lysed for 2 h with 500 µL of 50 µg/mL proteinase K at 37 °C, and pelleted by centrifugation at 18000 x g at 4 °C for 10 min. Samples were then incubated with PicoGreen® working solution, dilution 1:200, for 5 min at room temperature, protected from light. Fluorescence of the whole sample mixture was measured in 96-well plates (Thermo Fisher Scientific, Waltham, MA), at excitation and emission wavelengths of 485 and 520 nm, respectively, using a microplate reader (Fluostar, Ortenberg, Germany).

#### 7.3.5.1.3 Epidermal Differentiation of HaCaT Monolayers

Differentiation of HaCaT monolayers was monitored using Involucrin, a differentiation marker of HaCaT. After cells were cultured in submerged conditions for 1, 4 and 7 days, the samples were fixed in -20 °C methanol for 10 min, permeabilized in 0.5 % Triton for 5 min, then blocked twice using a mixture of 5 % BSA and 10 % goat serum for 30 min each. Cells were subsequently incubated with the primary antibodies to Involucrin at 1:1000 for 45 min at room temperature and then with Alexa Fluor 488-conjugated secondary antibody (goat-anti-mouse antibody, dilution 1:800) for 45 min in dark conditions at room temperature. Cell nuclei were then counter-stained with DAPI for 5 min. All samples were imaged immediately without mounting.

### **7.3.5.2 Reconstruction of Human Epidermis**

After one week of culture under submerged condition, cells were conditioned in serum-free medium for 2 h before being lifted to the ALI. Cells remained at the ALI for 2 weeks with regular changes of differentiation medium (3:1 DMEM:F12, 1 % Pen/Strep, 5 % FBS). In order to view the stratified multilayer of the resultant epidermis, samples were fixed in 4 % PFA, embedded in paraffin and cut at 5  $\mu$ m using a Reichert-Jung 2035 microtome. Sections were picked up on 2 % 3-aminopropyltriethoxysilane (APES) in acetone coated slides and stained with hematoxylin and eosin (H&E). After deparaffinization and rehydration, the sections were boiled in 10 mM citrate buffer. Endogenous peroxidase activity was quenched with 3 % hydrogen peroxide in methanol. The sections were then incubated following the protocol described by the manufacturer. Slides were incubated with blocking buffer followed by the application of the primary antibody Ki-67 at 1:100 and Involucrin at 1: 100 overnight at 37 °C. Sections were then labelled with secondary antibodies (Alexa Fluor 488-conjugated secondary antibody (goat-anti-mouse antibody, dilution 1:500) and Alexa Fluor 594-conjugated secondary antibody (goat-anti-rabbit antibody, dilution 1:800), respectively). Visualization of samples was performed using a Nikon Eclipse Ti-S fluorescence microscope.

### **7.3.6 Statistics**

Please refer to section 4.3.6.

## **7.4 RESULTS AND DISCUSSION**

### **7.4.1 Effects of Methacrylation Degree, PEG and Surface Modifications on GelMA Hydrogel Properties**

#### **7.4.1.1 Tunable Compressive Moduli and Degradation Rates**

Mechanical properties of hydrogels are well documented to influence cellular behaviour, function and differentiation (Engler et al., 2006, Engler et al., 2007). To

compare mechanical properties of photocrosslinked hydrogels of different GelMA concentrations, constant strain-rate compression tests were performed over time on samples incubated in DPBS. In general, statistical analysis illustrated a significant effect of increasing GelMA concentrations on the compressive modulus of hydrogels indicating a tunability of their compressive moduli ( $p < 0.05$ ; Fig. 7.2). Addition of PEG-DA, however, did not significantly increase the compressive modulus compared to corresponding control formulations without PEG-DA, contradicting previous reports (Hutson et al., 2011), except for hydrogels of 20 % (w/v) GelMA where addition of PEG-DA resulted in a synergistic effect on the compressive modulus, enhancing the modulus more than an increase in GelMA concentration alone. We hypothesize that at 20 % GelMA concentration, covalent crosslinking reduced gelatin dissolution enough allowing for increased gelatin resident time within the matrix, thus increasing the duration of its biofunctionality. Increasing the GelMA concentration from 5 % to 20 % increased the compressive modulus by > 50-fold whilst increasing the equivalent hydrogel to 20 % + PEG-DA increased compressive moduli by > 80-fold. These data reveal a tunable increase in the compressive modulus of composite hydrogels.

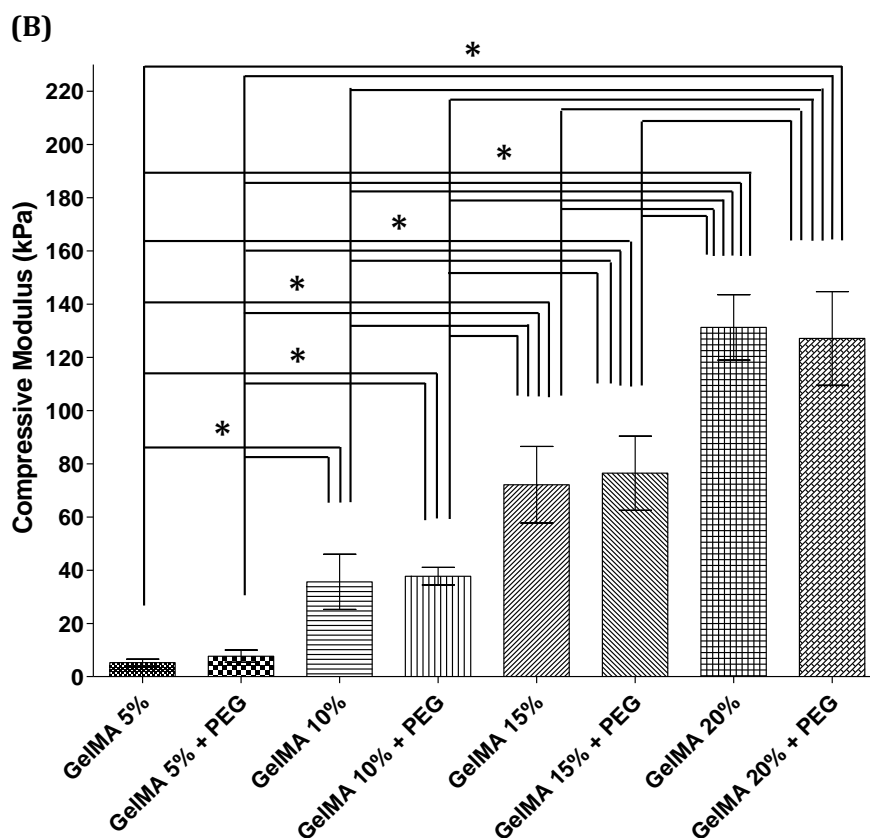
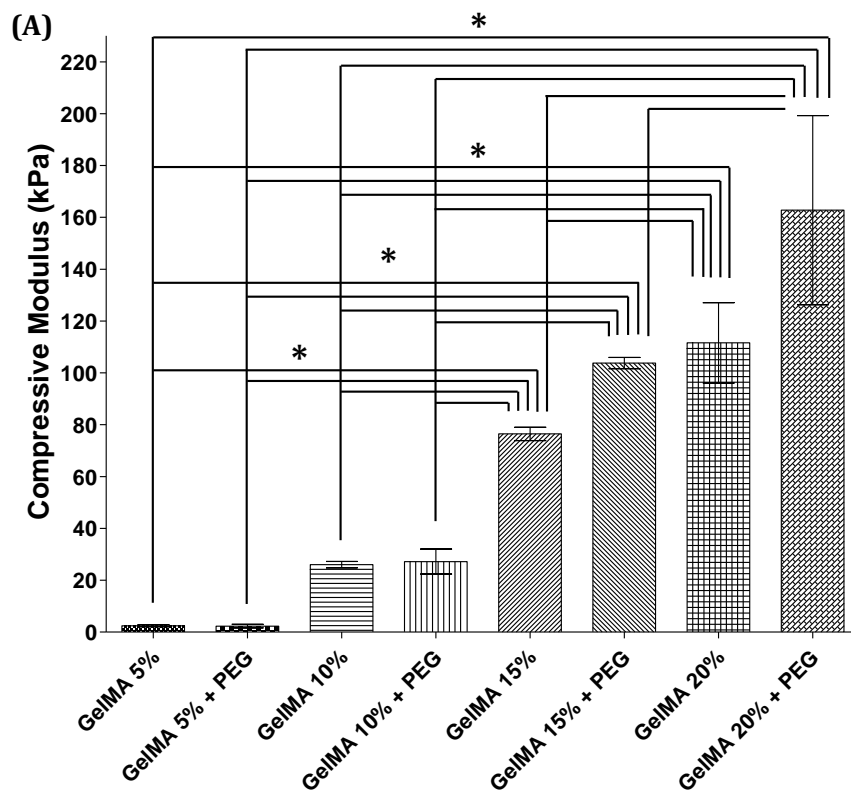


**Figure 7.2.** Compressive moduli of hydrogels of different GelMA concentrations with or without PEG-DA supplementation. (A) Results for hydrogels after synthesis and (B) after dehydration and subsequent rehydration. Results are given as mean  $\pm$  one SD. \* =  $p < 0.05$ .

Table 7.1 summarizes the different GelMA formulations with and without the addition of PEG-DA and the resultant mechanical properties and degradation behaviours.

**Table 7.1.** Differences in mechanical properties, water content and degradation rate with incrementally increasing GelMA content.

Formulations	Compressive Modulus (kPa)	Water Content (%)	Degradation after 96 h (%)
GelMA 5 %	2.5 ± 0.4	94.2 ± 0.8	100 ± 0.0
GelMA 7.5 %	14.1 ± 3.1	92.9 ± 1.4	100 ± 0.0
GelMA 10 %	26.0 ± 1.2	87.8 ± 0.4	39.5 ± 3.2
GelMA 12.5 %	43.2 ± 4.1	86.3 ± 0.2	30.0 ± 3.5
GelMA 15 %	88.8 ± 21.6	85.0 ± 0.4	21.2 ± 4.3
GelMA 17.5 %	97 ± 24.5	84.1 ± 0.4	17.5 ± 3.1
GelMA 20 %	107.6 ± 18.0*	82.5 ± 0.3	13.5 ± 3.9
GelMA 5 % + 0.5 % PEG	2.3 ± 0.7	93.7 ± 0.1	58 ± 5.6*
GelMA 10 % + 1 % PEG	27.2 ± 4.8	88.0 ± 0.5	32.1 ± 3.1
GelMA 15 % + 1.5 % PEG	103.8 ± 2.2	84.6 ± 0.4	10.8 ± 2.1*
GelMA 20 % + 2 % PEG	162.8 ± 36.5*	82.0 ± 0.7	4.5 ± 1.1*

\*statistically significant difference compared with control formulations without PEG.

From a macroscopic perspective, varying degrees of methacrylation do not result in obvious differences in GelMA hydrogel appearance (Fig. 7.3).

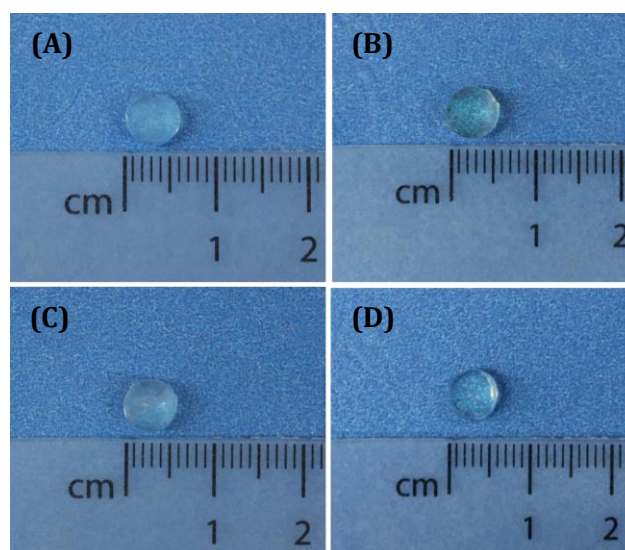


**Figure 7.3.** Macroscopic view of GelMA hydrogels of increasing methacrylation degree. (A) 5 % GelMA, (B) 10 % GelMA, (C) 15 % GelMA and (D) 20 % GelMA.

However, upon handling the hydrogels, those of lowest GelMA percentage (5 % (w/v)) unsurprisingly appeared more watery due to a lesser degree of cross-linking and subsequent inability to store water.

The water content and swelling characteristics of hydrogels are critical in tissue engineering applications, as they can greatly affect the pore size, mechanical properties and diffusivity of oxygen, drugs, nutrients and other water-soluble metabolites (Bayramoglu et al., 2014, Peppas et al., 2006). This was of particular importance considering subsequent elevation of GelMA hydrogels to the air-liquid interface (ALI) for keratinocyte stratification and epidermal reconstitution. As such, the effects of incrementally increasing GelMA concentrations as well as PEG-DA on the swelling profiles of composite hydrogels was evaluated. Figure 7.4 (II) and (III) show the water content and degree of swelling as a function of GelMA concentration. Statistical analysis revealed a significant effect of GelMA concentrations in driving the swelling properties of the hydrogels ( $p < 0.05$ ). The general trend for the tested formulations is a decreased water content and swelling degree with increasing GelMA concentrations as a higher GelMA concentration resulted in a higher amount of cross-links which altered the bulk properties of the resulting hydrogels by increasing the cross-linking density. This, in turn, reduced the space between gel networks and resulted in a decreased swelling ratio secondary to the development of higher elastic constraints when the gels were swelled in water. For the hydrogels containing the smallest GelMA concentration, the swelling percentage is about 170 % at swelling equilibrium. For the gels containing the highest amount of GelMA, the swelling percentage is about 15 % at equilibrium. Water content for all GelMA formulations was > 80 % supporting results obtained by swelling tests.



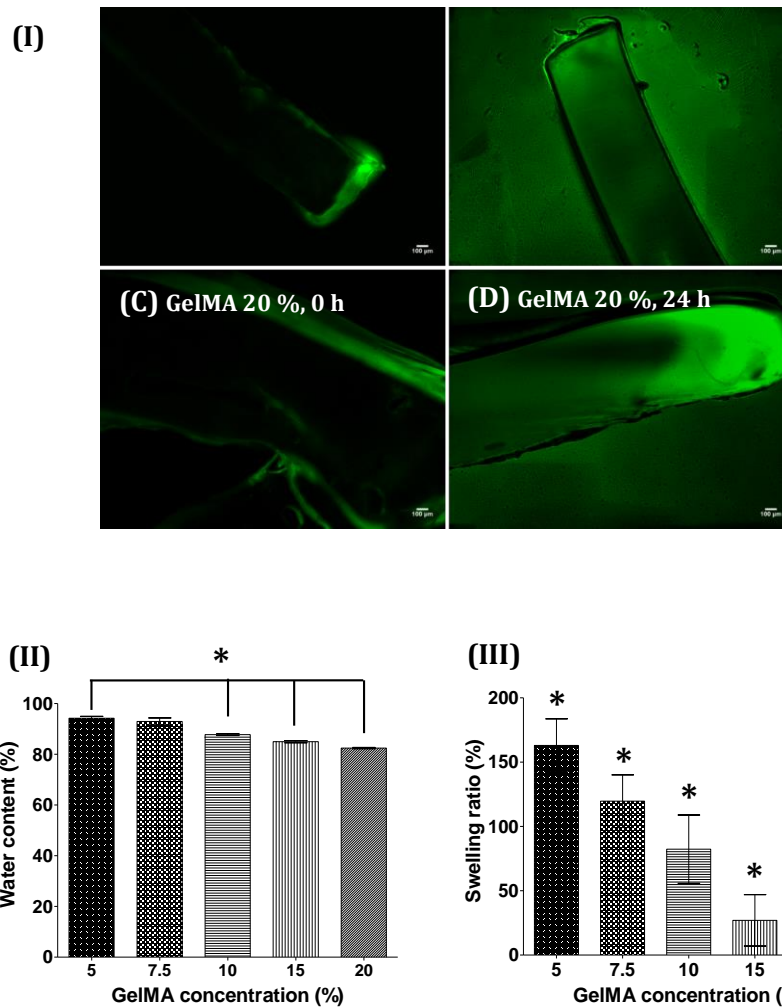


**Figure 7.4.** (I) Diffusion study on 5 % and 20 % GelMA using Fluorescein isothiocyanate (FITC)-labelled bovine serum albumin (BSA). (A) GelMA 5 % at 0 h, (B) GelMA 5 % at 24 h, (C) GelMA 20 % at 0 h and (D) GelMA 20 % at 24 h. Magnification  $\times 4$ . Scale 100  $\mu\text{M}$ . (II) Water content analysis as a function of GelMA concentration. (III) Hydrogel swelling capacity as a function of GelMA concentration. Results are given as mean  $\pm$  one SD. \* =  $p < 0.05$ .

However, PEG-DA supplementation did not result in statistically significant differences in swelling ratio or water content. Due to collagen being a hydrophilic structure, large intake of water by the cross-linked gel network was observed.

Similar to native gelatin, GelMA maintains its susceptibility to enzymatic degradation. PEG hydrogels, on the other hand, cannot be degraded enzymatically (Benton et al., 2009). Previous studies investigating the degradation profiles of GelMA with or without PEG-DA used 2.5 U/mL of type II collagenase (Benton et al., 2009, Hutson

et al., 2011). Here, we implemented a similar method to analyse degradation patterns of composite hydrogels. The remaining mass of photocrosslinked hydrogels over time was determined as a measure of degradation. Statistical analysis of the obtained results revealed a significant effect of incrementally increasing GelMA concentrations on the rate of degradation ( $p < 0.05$ ).

Similarly, a significant effect of PEG-DA concentration on degradation rates was observed with PEG-DA synergistically acting with GelMA to reduce degradation rates. Over a period of 96 h, hydrogels with the lowest GelMA concentration (5 % (w/v)) completely degraded while incrementally increased methacrylation degrees corresponded to slower degradation rates (Fig. 7.5 (A)).

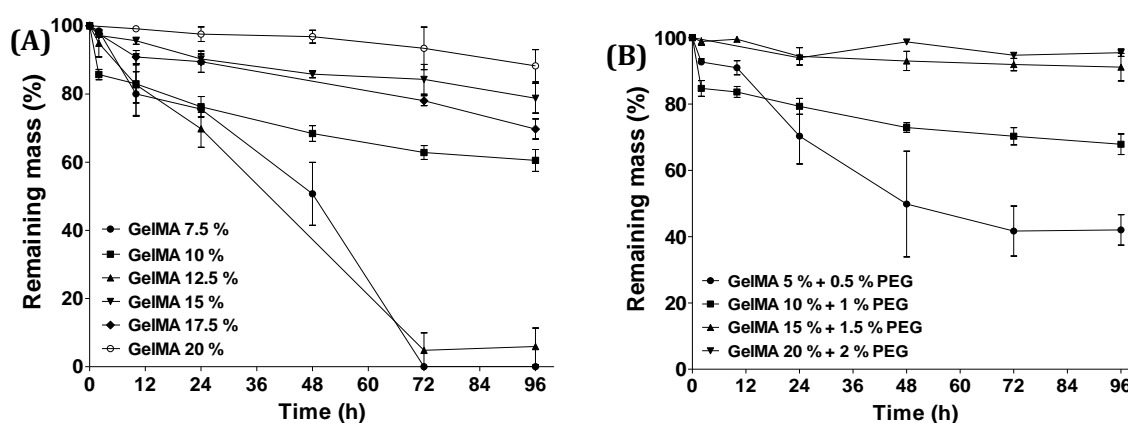


**Figure 7.5.** Remaining mass as a function of time for (A) GelMA hydrogels of different methacrylation degrees and (B) GelMA PEG-DA composite hydrogels. Results are given as mean  $\pm$  one SD.

GelMA hydrogels containing PEG-DA demonstrated even higher resistance to degradation compared to the same percentage GelMA without PEG-DA, indicating a bimodal tunability of degradation rates. After 96 h of degradation, hydrogels of 10 % GelMA concentration retained 60.5 % of their mass whilst hydrogels of 10 % GelMA +

PEG-DA retained 67.9 % of their mass which is a 7.4 % increased mass compared to GelMA alone. The difference in mass between 15 % GelMA and 15 % GelMA + PEG-DA after 96 h of degradation was even higher at 12.3 %. These data illustrate that PEG-GelMA composite hydrogels display tunable degradation rates which can be altered by changing the concentrations of either GelMA, PEG-DA or both.

#### **7.4.1.2 Cellular Response to Surface Mechanical Properties**

The ECM provides mechanical, biochemical and biophysical cues able to influence surrounding cellular behaviour. These are largely due to the ECM composition (i.e. glycoproteins, matrix proteins, proteoglycans and glycosaminoglycans (Badylak, 2005)) which provides a 3D micro-environment for cell growth (Cukierman et al., 2001). In addition to such molecular signals, certain anchorage-dependent cells further sense and can respond to changes in a biomaterial's modulus of elasticity, or stiffness (Discher et al., 2005) by altering cellular behaviours including cell proliferation, locomotion, adhesion, spreading, morphology, striation and differentiation in the case of stem cells (Discher et al., 2009, Engler et al., 2004, Flanagan et al., 2002, Khatiwala et al., 2006, Pelham and Wang, 1997, Reinhart-King et al., 2005, Wang et al., 2000). For example, NIH 3T3 murine fibroblasts have been demonstrated to undergo more apoptosis and reduced proliferation on relatively soft as opposed to stiff substrates (Wang et al., 2000). On the other hand, when grown on stiff polyacrylamide (PAA) hydrogels, NIH 3T3 cellular spreading was seen to increase. Similarly, keratinocytes cultured on gelatin hydrogels of different gelatin concentrations reinforced with different concentrations of PEG-DA demonstrated increased adhesion density and more intercellular connections on stiffer hydrogel surfaces (Xu et al., 2012). Higher gelatin concentrations which corresponded to increased stiffness provided more cell-binding motifs such as Arg-Gly-Asp (RGD) for cell adhesion. PEG, on the other hand, lacks these cell binding sequences but allows for the

fine-tuning of the hydrogel's mechanical and degradation properties. First, in order to investigate the effects of different GelMA concentrations on cellular adhesion and proliferation, HaCaT cells were seeded onto GelMA hydrogels, cultured for 7 days and stained with FITC-labelled phalloidin and DAPI to visualise F-actin fibres and the cell nucleus, respectively (Fig. 7.6).

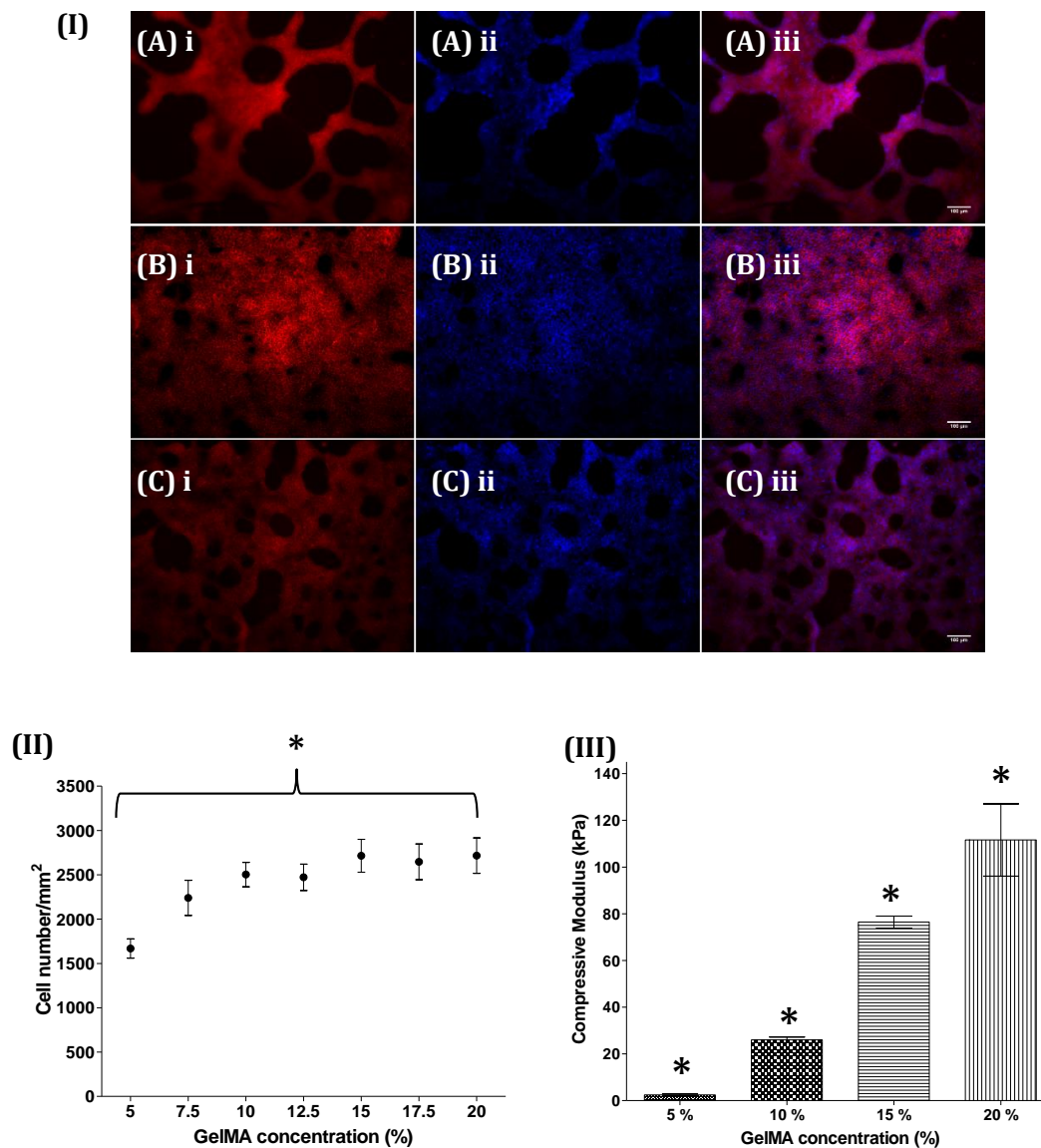
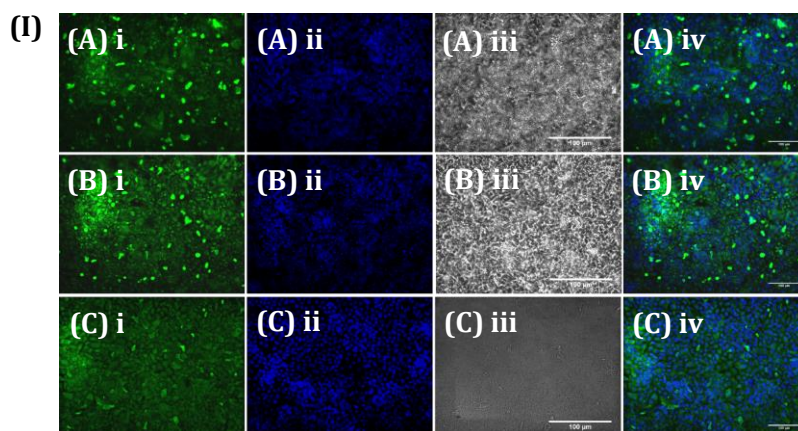


**Figure 7.6.** (I) Cell proliferation on GelMA hydrogels of (A) 5 %, (B) 10 % and (C) 20 % GelMA concentration. Cells were stained for FITC-labelled Phalloidin (i) and nuclei were counterstained with DAPI (ii). Images were merged in (iii). (II) Cell counts per mm<sup>2</sup> as a function of GelMA concentration. (III) Influence of GelMA concentration and resultant compressive moduli on cell proliferation over a period of 7 days. Results are given as mean  $\pm$  one SD. \* =  $p < 0.05$ .

Statistical analysis revealed a significant effect of GelMA concentration on cell proliferation ( $p < 0.05$ ). The data demonstrated that an increased concentration in GelMA increased cellular attachment, suggesting that stiffer hydrogels supported more attachment.

Significantly more cells attached and subsequently proliferated on hydrogels of at least 7.5 % GelMA percentage as opposed to 5 % GelMA hydrogels ( $p < 0.05$ ). In addition, there was no statistically significant increase in cell numbers on hydrogels of > 10 % GelMA concentration, suggesting that hydrogels containing 10 % GelMA are the most suitable formulation for cell adhesion and proliferation.

Therefore, for subsequent cell studies, 10 % (w/v) GelMA hydrogels were used. In order to investigate the effects of PEG-DA on cellular adherence and proliferation on the GelMA hydrogel, composite GelMA-PEG gels were synthesized and HaCaT's cultured for a period of 7 days. Cells were stained for cytokeratin and E-Cadherin. No differences in either proliferation or extent of differentiation were observed between cells grown on 10 % GelMA, 10 % GelMA + 1 % PEG or tissue culture plastic (Fig. 7.7), the latter being surface-modified for ideal cell attachment and growth.



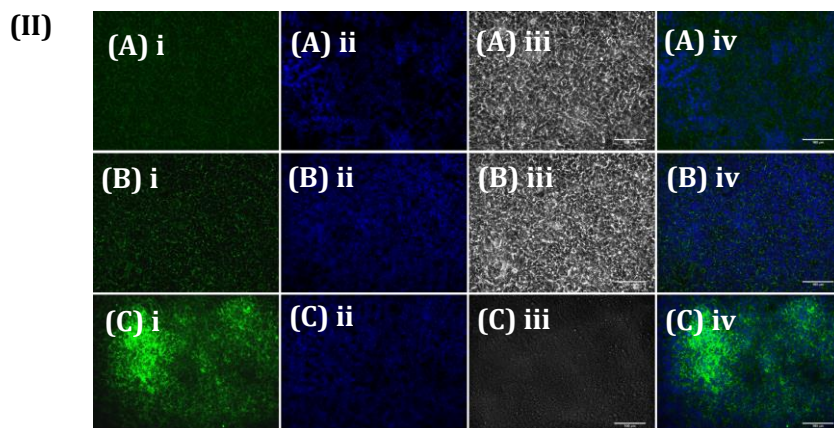


**Figure 7.7.** Fluorescent images of HaCaTs grown on GelMA hydrogels of different compositions or surface coatings. (A) 10 % GelMA, (B) 10 % GelMA + PEG and (C) tissue culture plastic. Cells were stained for (I) cytokeratin (i) or (II) E-Cadherin (i) and nuclei were counterstained with DAPI (ii). Stained images were overlaid with differential interference contrast (DIC) images (iii) to give merged images (iv). Magnification x 20. Scale 100  $\mu$ M.

These data indicate optimal cytocompatibility of GelMA hydrogels. However, whilst GelMA displays many desirable attributes as a hydrogel for tissue engineering, supplementation with PEG-DA has been demonstrated to enable tuning of swelling as well as degradation rates without compromising cytocompatibility.

#### 7.4.2 Reconstructed Human Epidermis

Previously, studies about the development of artificial epidermis relied on the observations that keratinocytes can be grown *in vitro* to produce thin epithelial sheet graft (Rheinwald and Green, 1975). However, the need for a fibroblast feeder layer as well as low plating efficiency shifted efforts into developing alternative culture techniques involving the use of biocompatible and biodegradable scaffolds such as collagen or hyaluronic acid which are capable of favouring keratinocyte growth (Liu et al., 2010, Machens et al., 2000). Such composite dermal-epidermal skin substitutes, however, may only survive provided the epidermal layer is firmly attached to the dermal substrate (Cooper et al., 1990). We thus sought to use a hydrogel which favoured skin cell adhesion and proliferation, facilitated ECM deposition and were biocompatible. Our results



demonstrated the 10 % (w/v) GelMA hydrogel fulfilled all those three requirements. H&E stained images demonstrated the development of a multi-layered and stratified epidermis after 4 weeks of culture at the air-liquid interface (ALI) not dissimilar to human skin (Fig. 7.8 (A) and (C)). Next, epidermal layers grown on GelMA hydrogels and human skin were stained for Ki67, a proliferation marker which is usually confined to the proliferative compartment of the basal keratinocyte layer (McCormick et al., 1993) and Involucrin, an early marker of terminal differentiation normally detected in the upper stratum corneum and stratum granulosum.

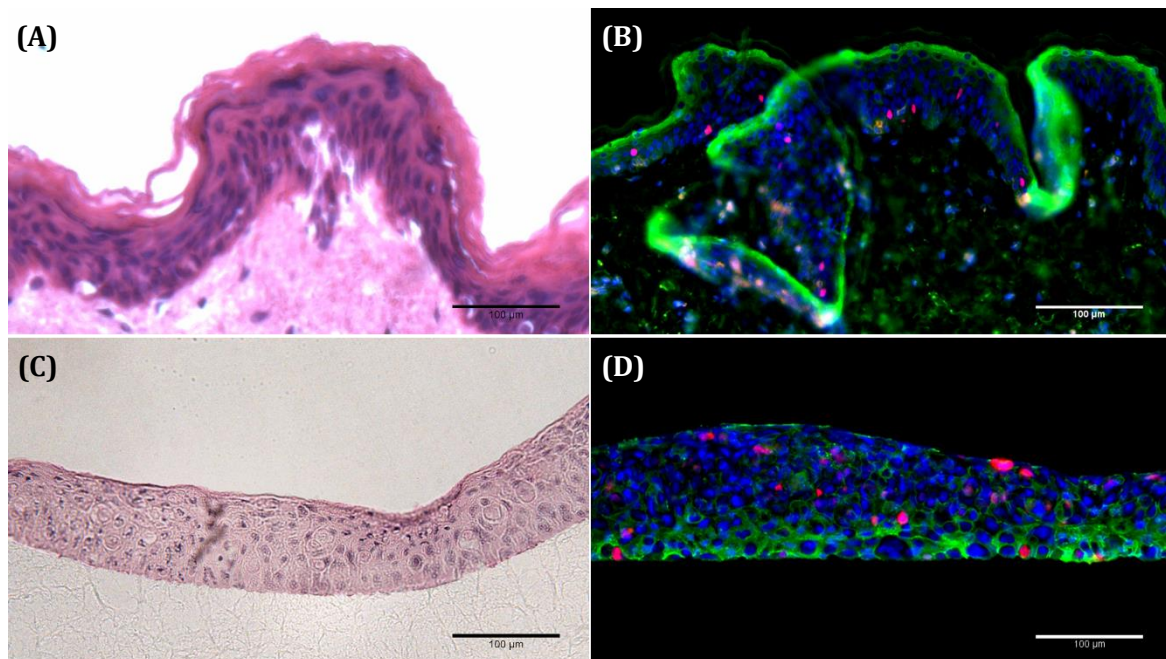


**Figure 7.8.** (A) Haematoxylin and eosin (H&E) histological section of human skin and (B) fluorescent image human skin stained for Ki61 and involucrin. (C and D) Corresponding images of HaCaTs cultured on GelMA hydrogels at the air-liquid interface for 4 weeks. Magnification x 4. Scale 100 µM.

Immunohistochemical examination revealed Involucrin positive cells in the entire stratum granulosum of human skin but only few within the reconstructed epidermis after 4 weeks of ALI. Ki67 positive cells were seen to be confined within the basal layer in

human skin but scattered throughout all epidermal layers when cultured on GelMA (Fig. 7.8 (B) and (C)). These results indicate that whilst the constructed composite skin substitute can form a multi-layered epidermis with histological similarities to that of normal skin, the organisation of the distinct layers found within healthy skin was somewhat distorted. It is possible that both the use of the immortalized HaCaT cell line as well as a lack of a dermis proper resulted in a lack of vital paracrine signalling factors for structural organization of the epidermis. It has previously been demonstrated that HaCaT cells grown on collagen gels containing human dermal fibroblasts produced a well-structured and differentiated squamous epithelium with a nearly complete basement membrane after 3 weeks of organotypic co-culture (Schoop et al., 1999).

## **7.5 CONCLUSION**

This chapter highlights the ability to influence mechanical, degradation and cell behaviour on GelMA hydrogels by tuning the concentrations of GelMA, PEG-DA or both. We created an artificial skin comprising of a stratified layer of keratinocytes and a dermal matrix consisting of GelMA hydrogel. The obtained data suggest that GelMA-PEG-DA composite hydrogels may be customised to meet necessary requirements for skin tissue engineering.



## References

- BADYLAK, S. F. 2005. Regenerative medicine and developmental biology: the role of the extracellular matrix. *Anatomical record. Part B, New anatomist*, 287, 36-41.
- BAYRAMOGLU, G., GOZEN, D., ERSOY, G., OZALP, V. C., AKCALI, K. C. & ARICA, M. Y. 2014. Examination of fabrication conditions of acrylate-based hydrogel formulations for doxorubicin release and efficacy test for hepatocellular carcinoma cell. *J Biomater Sci Polym Ed*.
- BENTON, J. A., FAIRBANKS, B. D. & ANSETH, K. S. 2009. Characterization of valvular interstitial cell function in three dimensional matrix metalloproteinase degradable PEG hydrogels. *Biomaterials*, 30, 6593-603.
- COOPER, M. L., HANSBROUGH, J. F. & FOREMAN, T. J. 1990. In vitro effects of matrix peptides on a cultured dermal-epidermal skin substitute. *The Journal of surgical research*, 48, 528-33.
- CUKIERMAN, E., PANKOV, R., STEVENS, D. R. & YAMADA, K. M. 2001. Taking cell-matrix adhesions to the third dimension. *Science (New York, N.Y.)*, 294, 1708-12.
- DISCHER, D. E., JANMEY, P. & WANG, Y.-L. 2005. Tissue cells feel and respond to the stiffness of their substrate. *Science (New York, N.Y.)*, 310, 1139-43.
- DISCHER, D. E., MOONEY, D. J. & ZANDSTRA, P. W. 2009. Growth factors, matrices, and forces combine and control stem cells. *Science (New York, N.Y.)*, 324, 1673-7.
- ENGLER, A. J., GRIFFIN, M. A., SEN, S., BÖNNEMANN, C. G., SWEENEY, H. L. & DISCHER, D. E. 2004. Myotubes differentiate optimally on substrates with tissue-like stiffness: pathological implications for soft or stiff microenvironments. *The Journal of cell biology*, 166, 877-87.
- ENGLER, A. J., REHFELDT, F., SEN, S. & DISCHER, D. E. 2007. Microtissue elasticity: measurements by atomic force microscopy and its influence on cell differentiation. *Methods in cell biology*, 83, 521-45.
- ENGLER, A. J., SEN, S., SWEENEY, H. L. & DISCHER, D. E. 2006. Matrix elasticity directs stem cell lineage specification. *Cell*, 126, 677-89.
- FLANAGAN, L. A., JU, Y.-E., MARG, B., OSTERFIELD, M. & JANMEY, P. A. 2002. Neurite branching on deformable substrates. *Neuroreport*, 13, 2411-5.
- GROEBER, F., HOLEITER, M., HAMPEL, M., HINDERER, S. & SCHENKE-LAYLAND, K. 2011. Skin tissue engineering - In vivo and in vitro applications. *Advanced Drug Delivery Reviews*, 63, 352-66.
- HARLEY, B. A. & YANNAS, I. V. 2007. *In Vivo Synthesis of Tissues and Organs*.
- HUTSON, C. B., NICHOL, J. W., AUBIN, H., BAE, H., YAMANLAR, S., AL-HAQUE, S., KOSHY, S. T. & KHADEMOSSEINI, A. 2011. Synthesis and characterization of tunable poly(ethylene glycol): gelatin methacrylate composite hydrogels. *Tissue Eng Part A*, 17, 1713-23.
- KHATIWALA, C. B., PEYTON, S. R. & PUTNAM, A. J. 2006. Intrinsic mechanical properties of the extracellular matrix affect the behavior of pre-osteoblastic MC3T3-E1 cells. *American journal of physiology. Cell physiology*, 290, C1640-50.
- LIU, J., BIAN, Z., KUIJPERS-JAGTMAN, A. M. & VON DEN HOFF, J. W. 2010. Skin and oral mucosa equivalents: construction and performance. *Orthodontics & craniofacial research*, 13, 11-20.
- MACHENS, H. G., BERGER, A. C. & MAILAENDER, P. 2000. Bioartificial skin. *Cells Tissues Organs*, 167.
- MACNEIL, S. 2007. Progress and opportunities for tissue-engineered skin. *Nature*, 445, 874-80.

- MCCORMICK, D., CHONG, H., HOBBS, C., DATTA, C. & HALL, P. A. 1993. Detection of the Ki-67 antigen in fixed and wax-embedded sections with the monoclonal antibody MIB1. *Histopathology*, 22, 355-60.
- METCALFE, A. D. & FERGUSON, M. W. J. 2007. Bioengineering skin using mechanisms of regeneration and repair. *Biomaterials*, 28, 5100-13.
- PELHAM, R. J. & WANG, Y. L. 1997. Cell locomotion and focal adhesions are regulated by substrate flexibility. *Proceedings of the National Academy of Sciences of the United States of America*, 94, 13661-5.
- PEPPAS, N. A., HILT, J. Z., KHADEMHOSEINI, A. & LANGER, R. 2006. Hydrogels in Biology and Medicine: From Molecular Principles to Bionanotechnology. *Advanced materials*, 18, 1345-60.
- REINHART-KING, C. A., DEMBO, M. & HAMMER, D. A. 2005. The dynamics and mechanics of endothelial cell spreading. *Biophysical journal*, 89, 676-89.
- RHEINWALD, J. G. & GREEN, H. 1975. Serial cultivation of strains of human epidermal keratinocytes: the formation of keratinizing colonies from single cells. *Cell*, 6, 331-43.
- SCHOOP, V. M., MIRANCEA, N. & FUSENIG, N. E. 1999. Epidermal organization and differentiation of HaCaT keratinocytes in organotypic coculture with human dermal fibroblasts. *J Invest Dermatol*, 112, 343-53.
- SHEVCHENKO, R. V., JAMES, S. L. & JAMES, S. E. 2010a. A review of tissue-engineered skin bioconstructs available for skin reconstruction. *Journal of the Royal Society Interface*, 7, 229-58.
- TRAPPMANN, B., GAUTROT, J. E., CONNELLY, J. T., STRANGE, D. G. T., LI, Y., OYEN, M. L., STUART, M. A. C., BOEHM, H., LI, B. J., VOGEL, V., SPATZ, J. P., WATT, F. M. & HUCK, W. T. S. 2012. Extracellular-matrix tethering regulates stem-cell fate (vol 11, pg 642, 2012). *Nature Materials*, 11, 742-.
- VAN DEN BULCKE, A. I., BOGDANOV, B., DE ROOZE, N., SCHACHT, E. H., CORNELISSEN, M. & BERGHMANS, H. 2000. Structural and rheological properties of methacrylamide modified gelatin hydrogels. *Biomacromolecules*, 1, 31-8.
- WANG, H. B., DEMBO, M. & WANG, Y. L. 2000. Substrate flexibility regulates growth and apoptosis of normal but not transformed cells. *American journal of physiology. Cell physiology*, 279, C1345-50.
- XU, K., FU, Y., CHUNG, W., ZHENG, X., CUI, Y., HSU, I. C. & KAO, W. J. 2012. Thiol-ene-based biological/synthetic hybrid biomatrix for 3-D living cell culture. *Acta biomaterialia*, 8, 2504-16.
- YEH, M.-K., LIANG, Y.-M., CHENG, K.-M., DAI, N.-T., LIU, C.-C. & YOUNG, J.-J. 2011. A novel cell support membrane for skin tissue engineering: Gelatin film cross-linked with 2-chloro-1-methylpyridinium iodide. *Polymer*, 52, 996-1003.

# 8 OVERALL CONCLUSIONS AND FUTURE OUTLOOK

---

## 8.1 LIMITATIONS OF SYNTHETIC POLYURETHANES AND COLLAGEN-BASED HYDROGELS AND A PROPOSAL FOR A FUTURE BIO-SYNTHETIC COMPOSITE MATERIAL

### 8.1.1 Advantages and Disadvantages of Polyurethanes as Tissue Engineering Platforms

The majority of PUs used in the manufacture of degradable tissue engineering platforms belongs to the polyester family. Scaffolds based on biodegradable PGA, PLA, their copolymers and PCL have been extensively researched for their use as tissue regeneration platforms, not only due to their degradability, but primarily due to their controllable manufacture and facile modifiability which enables exact tailoring of the polymeric structure to suit individual applications (Shirakata et al., 2014, Jiang et al., 2014, Tsao et al., 2014). The major clinical uses for such degradable systems include resorbable sutures, drug delivery systems and orthopaedic fixation devices (Behravesh et al., 1999, Middleton and Tipton, 2000). More recently, the field of tissue engineering and regenerative medicine has increased their focus on biodegradable scaffolds to regenerate not only tissues but whole organs using synthetic polyester urethanes due to the ability to fabricate these materials into various shapes with desired surface and pore morphologies conducive to tissue in-growth and vascularization. Additionally, synthetic polymers can be specifically designed to display chemical functional groups to further induce tissue regeneration. The ability to modulate mechanical parameters of synthetic polyester-based PU scaffolds is a further advantage which should not be underestimated since the viscoelastic character as well as the material stiffness have far-reaching implications with respect to cellular behaviour as demonstrated in chapter 7. Lastly, synthetic PUs are cost-effective compared to biological polymers as the starting materials

are cheap and material synthesis usually produces a high yield with reproducible structures.

A material intended for the purpose of implantation not only has to be versatile to suit numerous applications but must also satisfy biocompatibility requirements; it must degrade into non-toxic metabolites whilst supporting appropriate cell growth and proliferation. Many synthetic polyester PUs, however, demonstrate room for improvement since frequently, their degradation products acidify the surrounding tissues resulting in cell damage or death. Further, their inherently hydrophobic character is unfavourable to cell attachment. Thus it appears that many of the currently available degradable synthetic PU polymers do not fulfil all of the requirements and significant chemical changes to their structure may be required if they are to be formulated for tissue regenerative applications.

### **8.1.2 Advantages and Disadvantages of Collagen/Gelatin Hydrogels as Tissue Engineering Platforms**

Collagen, being the most abundant protein in the human body and the main structural protein in connective tissues, appears to be the evident first choice for tissue engineering applications, in particular for skin regenerative purposes. Collagen is inherently biocompatible as it naturally displays cell-binding motifs and has a hydrophilic cell-attracting nature. Gelatin, being the hydrolysed derivative of collagen, retains its biological properties and hydrogels made from gelatin, in particular, demonstrate beneficial properties as (i) hydrogels are mostly comprised of water and thus display excellent transport properties allowing for facile diffusion of nutrients and waste products, and (ii) gelatin has been found to improve wound healing as indicated by significantly earlier re-epithelialization and dermal maturation of the defective area (Huang et al., 2009).

Such benefits, however, are offset to a degree by their generally poor mechanical properties and premature degradation rates which, whilst tunable to a degree, display finite levels of control, unlike synthetic polymers. Further disadvantages of naturally-derived polymers include their potential immunogenicity and ability to transmit pathogens when originating from animal sources, the batch variability and poor processability and the relatively low cost-efficiency. Poor mechanical strength may ultimately lead to difficulty handling such hydrogels which poses problems during surgical implantation of such scaffolds. The ability to tune both mechanical and degradation profiles by varying the cross-linking density, whilst initially appearing to solve the mechanical issues, almost proves to be a curse in disguise as incomplete cross-linking and subsequent cross-linker toxicities are known to have detrimental effects on cells.

Scaffolds made from synthetic and natural polymers, i.e. composite scaffolds, have therefore emerged as the proclaimed answer to the individual components' drawbacks. The aim to exploit the undisputed benefits of both synthetic and natural polymers whilst addressing their respective disadvantages has concerned scientists for decades. Thus for future studies, a combinatorial approach to obtain a synergistically acting 'super-platform' is suggested for functional tissue regeneration.

## **8.2 CONCLUSIONS**

The investigations carried out in this thesis resulted in several major conclusions.

- 1) Loss of skin tissue remains a major problem with infection-related morbidity and mortality being a leading cause of death. Additionally, the frequently suboptimal cosmetic outcomes for most skin-loss victims should not be underestimated as it may

have a considerable psychosocial impact upon the affected individuals. Currently available treatment strategies are lacking both in availability (i.e. limited numbers of organ donors) and total safety – the latter pertaining to skin substitutes derived from both cadaveric human donors as well as dermal substitutes derived from animal origins (e.g. Integra® dermal regeneration template) which bear the risks of pathogen transmission. Thus, an alternative treatment strategy needs to be sought and the emergence of tissue engineering is believed to have the potential to achieve just that. Conceptually, tissue engineering aims to create a biocompatible platform able to provide a 3D scaffolding for the wound bed which cells can recognise and integrate into in order to regenerate lost tissues. Ideally, the scaffold should be resorbable in time to create space for the newly developing structures whilst providing an optimum level of mechanical support for the surrounding tissues and cells. However, the ideal biomaterial has yet to be developed.

- 2) As such, in this thesis, a suitable scaffolding material was sought. The ideal tissue engineering scaffold should possess the following characteristics; (i) biocompatibility, (ii) biodegradability into non-toxic metabolites, (iii) non-immunogenicity and (iv) suitability in terms of cell attachment and proliferation. Here, we developed a novel biodegradable nanocomposite PU based on a poly( $\epsilon$ -caprolactone urea)urethane backbone integrated with POSS nanoparticles (POSS-PCLU). The non-degradable family member POSS-PCU (a poly(carbonate urea)urethane) has already demonstrated clinical feasibility with several first-in-man compassionate cases. PUs are desirable candidate materials for tissue engineering scaffolds due to their tunable mechanical properties and degradation profiles as well as their straight-forward synthesis. Advantages of incorporating POSS nanoparticles include its non-immunogenicity and an increase in surface nano-

structuring which is hypothesized to enhance cell recognition and subsequent adherence.

- 3) The main focus of this thesis was to characterize this novel nanocomposite polymer and attempt to demonstrate tunable degradation rates in addition to *in vitro* cytocompatibility. With this in mind, PUs of varying hard segment content were developed and characterised. <sup>1</sup>H NMR and ATR-FTIR spectral analysis confirmed the formation of PUs with varying hard segment contents. Molecular weight analysis revealed no significant differences in  $M_n$  between the formulations. DSC and XRD studies confirmed the mostly amorphous nature of PCLU and POSS-PCLU. Compared to bulk properties, surface analyses of PCLU differed significantly from POSS-PCLU, most notably with the appearance of microscopic surface particulates which are hypothesized to be POSS aggregates which extrude out onto the polymer surface upon scaffold fabrication. Differences between PCLU and POSS-PCLU surfaces were further confirmed by contact angle measurements which demonstrated that addition of POSS leads to an increased angle.
- 4) Prior to commencing *in vitro* cytocompatibility studies, however, the degradable polymer scaffolds needed to be sterilized. Conventional steam sterilization (autoclaving) or any other means of sterilization applying either heat or water molecules are suboptimal due to their potential to degrade the samples leading to changes in mechanical and degradation properties. Alternative methods such as exposure to ethylene oxide gas was also considered unsafe due to the presence of residual toxic fumes within the scaffolds. Several different sterilization as well as disinfectant methods were trialled. However, it appeared that microbial eradication using laboratory-available techniques inevitably resulted in changes to the surface structures as seen on SEM and AFM images. Interestingly, scaffolds treated with a 70 %

ethanol solution appeared to not only clean the scaffolds sufficiently but also enhanced cell adherence and proliferation. Upon further investigation of the literature, ethanol treatment had been suggested to be used as a post-production processing tool in order to enhance cytocompatibility.

- 5) Despite reasonable cytocompatibility, POSS-PCLU scaffolds remain suboptimal due to their inherent hydrophobicity. In an attempt to develop a scaffold with favourable cytocompatibility whilst retaining the viscoelastic properties of POSS-PCLU, a composite scaffold based on synthetic POSS-PCLU and a naturally-derived polymer was conceptualized. In collaboration with the Khademhosseini laboratories at Harvard-MIT, a biological hydrogel consisting of methacrylated gelatin (GelMA) was synthesized and its *in vitro* compatibility with an immortalized human keratinocyte cell line (HaCaT) was assessed. As expected, hydrophilic GelMA hydrogels were superior in terms of cytocompatibility compared to POSS-PCLU scaffolds. The results demonstrated that GelMA hydrogels were tunable, to a degree, with respect to their mechanical properties and degradation profiles – both factors are important for keratinocyte growth. HaCaTs cultured on GelMA hydrogels of different methacrylation degrees revealed better spreading on stiffer gels. Eventually, an *in vitro* reconstructed stratified epidermal layer was created on GelMA hydrogels which demonstrated similarities to natural human skin. Regrettably, however, it was not possible to combine GelMA with POSS-PCLU due to issues surrounding intellectual property rights.
- 6) Subsequently, focus was placed back onto the evaluation of POSS-PCLU. *In vitro* degradation studies involved the exposure of the different PU formulations to hydrolytic, oxidative and enzymatic conditions to simulate the *in vivo* scenario. Hard segment content was demonstrated to influence degradation significantly, thus



confirming our hypothesis of rate tunability. Furthermore, the integration of POSS nanoparticles was shown to affect the mode of degradation, allowing for a bulk loss whilst retaining its viscoelasticity as opposed to developing a brittle nature as was seen with the same PU lacking POSS. This was thought to be due to the protective function exerted by POSS nanoparticles on the soft segments of the PU which are responsible for the material's elasticity.

- 7) Subcutaneous implantation studies demonstrated that POSS nanoparticle incorporation into the scaffold conferred a degree of immune tolerance to the composite system. Additionally, POSS-PCLU demonstrated the ability to become fully integrated into the host system as shown by extensive vascularization and connective tissue deposition into the scaffold. Simultaneous scaffold degradation could be observed, suggesting that POSS-PCLU may fulfil the important criterium of timely degradation.

### **8.3 CLOSING REMARKS AND FUTURE OUTLOOK**

Despite inexhaustible efforts having contributed significantly to the status quo of the field of tissue engineering and regenerative medicine, the ultimate panacea in terms of biomaterial scaffold is yet to be developed. Obstacles including the incomplete elucidation of the extensive biomolecular cascades leading to complete tissue regeneration and the current inability to fully mimic human disease or injury states *in vitro* or *in vivo* remain to be overcome. Little by little, each tiny piece of new information will contribute to the colossal puzzle that is nature.

## References

- BEHRAVESH, E., YASKO, A. W., ENGEL, P. S. & MIKOS, A. G. 1999. Synthetic biodegradable polymers for orthopaedic applications. *Clin Orthop Relat Res*, S118-29.
- HUANG, S., ZHANG, Y., TANG, L., DENG, Z., LU, W., FENG, F., XU, X. & JIN, Y. 2009. Functional bilayered skin substitute constructed by tissue-engineered extracellular matrix and microsphere-incorporated gelatin hydrogel for wound repair. *Tissue engineering. Part A*, 15, 2617-24.
- JIANG, J., XIE, J., MA, B., BARTLETT, D. E., XU, A. & WANG, C. H. 2014. Mussel-inspired protein-mediated surface functionalization of electrospun nanofibers for pH-responsive drug delivery. *Acta Biomater*, 10, 1324-32.
- MIDDLETON, J. C. & TIPTON, A. J. 2000. Synthetic biodegradable polymers as orthopedic devices. *Biomaterials*, 21, 2335-46.
- SHIRAKATA, Y., NAKAMURA, T., SHINOHARA, Y., TANIYAMA, K., SAKODA, K., YOSHIMOTO, T. & NOGUCHI, K. 2014. An exploratory study on the efficacy of rat dedifferentiated fat cells (rDFATs) with a poly lactic-co-glycolic acid/hydroxylapatite (PLGA/HA) composite for bone formation in a rat calvarial defect model. *J Mater Sci Mater Med*, 25, 899-908.
- TSAO, C. K., KO, C. Y., YANG, S. R., YANG, C. Y., BREY, E. M., HUANG, S., CHU, I. M. & CHENG, M. H. 2014. An ectopic approach for engineering a vascularized tracheal substitute. *Biomaterials*, 35, 1163-75.

## Appendix

# 9 SURFACE AND MECHANICAL ANALYSIS OF EXPLANTED POLY IMPLANT PROSTHÈSE SILICONE BREAST IMPLANTS <sup>4</sup>

---

## 9.1 SYNOPSIS

The recent events surrounding Poly Implant Prosthèse (PIP) breast implants have renewed the debate about the safety profile of silicone implants. The intentional use of industrial-grade instead of certified medical-grade silicone is thought to be responsible for reportedly higher frequencies of implant rupture *in vivo*. The differences in mechanical and viscoelastic properties between PIP and medical-grade silicone implant shells were investigated. Surface characterization of shells and gels was carried out to determine structural changes occurring after implantation. Breast implants were obtained from women at the Royal Free Hospital (London, UK). PIP implants were compared with medical-grade control silicone implants. Tensile strength, tear resistance and elongation at break were assessed using a tensile tester. Surfaces were analysed using attenuated total reflectance–Fourier transform infrared (ATR-FTIR) spectroscopy. Spearman correlation analyses and Kruskal–Wallis one-way statistical tests were performed for mechanical data. There were 18 PIP and 4 medical-grade silicone implants. PIP silicone shells had significantly weaker mechanical strength than control shells ( $p < 0.009$ ). There were negative correlations between mechanical properties of PIP shells and implantation times, indicative of deterioration of PIP shells over time *in vivo* ( $r^2 = -0.75$ ;  $p = 0.009$  for tensile strength;  $r^2 = -0.76$ ;  $p = 0.001$  for maximal strain). Comparison

---

<sup>4</sup> The following chapter has been adapted from Yildirimer et al. Br J Surg 2013;100(6):761-767.

of ATR-FTIR spectra of PIP and control silicones demonstrated changes in material characteristics during the period of implantation suggestive of time-dependent bond breakage and degradation of the material. This study demonstrated an increased weakness of PIP shells with time and therefore supports the argument for prophylactic removal of PIP breast implants.

## 9.2 INTRODUCTION

Breast augmentation using implantable silicone devices remains among the most commonly performed procedures in aesthetic and reconstructive surgery, with more than 8000 patients undergoing breast enhancement annually in the UK alone (choices, 2012). Despite the routine use of silicone breast implants, complications such as capsular contraction and implant rupture are common, necessitating the removal and replacement of such devices after several years. According to a recent report issued by the US Food and Drug Administration, the reoperation rate after receiving breast implants for cosmetic augmentation was between 20-40 %, whereas the rate for patients having reconstruction was as high as 70 %, at 8–10 years after implantation (FDA, 2011). The recent Poly Implant Prosthèse (PIP; La Seynesur-Mer, France) breast implant scandal has revived realistic worries about the mechanical stability of implanted silicones. PIP breast implants, manufactured by the eponymous French company, were distributed globally beginning in 2001 until their recent ban in 2010. The intentional use of breast fillers manufactured with industrial silicone intended for use as mattress fillers, rather than acceptable medical-grade materials, has led to the withdrawal of PIP implants for breast augmentation. This decision was enforced by the Medicines and Healthcare products Regulatory Agency on 31 March 2010. Other European countries swiftly followed suit. Over 300 000 PIP breast implants have been distributed worldwide, with approximately 47 000 women affected in the UK alone (NHS, 2012). With reportedly higher and more variable rupture and leakage rates compared with approved medical-grade silicone implants (AFSSAPS, 2011), PIP breast fillers have instilled significant concern in both patients and surgeons. This study was designed to compare the mechanical properties of medical-grade silicone shells used to manufacture standard breast implants and shells of PIP silicone implants, and to evaluate the impact of the local environment after

implantation on the mechanical, morphological and chemical properties of PIP silicone shells and gels.

### **9.3 MATERIALS AND METHODS**

PIP silicone gel-filled breast implants were obtained from the Department of Plastic and Reconstructive Surgery, Royal Free Hampstead NHS Trust Hospital (London, UK) throughout January to March 2012. These prostheses had been implanted in women between February 2001 and May 2011. Retrieved implants were disinfected manually using alcohol wipes, labelled and stored until further analysis. Explanted prostheses was assessed by visual inspection and implants were subsequently separated into two groups (intact or ruptured) depending on shell integrity. In preparation for testing, the gel was removed from the shell, and the shell was once again disinfected as described above. Medical-grade silicone implants (Natrella™, Allergan, Marlow, UK; Mentor MemoryGel®, Johnson & Johnson Medical Limited, Wokingham, UK; Impleo, Nagor, Glasgow, UK) explanted from other women were used as controls.

#### **9.3.1 Mechanical and Viscoelastic Properties of Implanted Silicone Shells**

Please refer to section 4.3.4.3.3.

#### **9.3.2 Surface Characterization of Silicone Shells and Gels**

Please refer to section 4.3.4.2.2.

#### **9.3.3 Statistical Analysis**

Two-tailed Spearman rank correlation analyses were performed for tensile strength, strain at break and tear resistance. Kruskal-Wallis test was used for group comparison, followed by Mann-Whitney *U* test if significant.  $p < 0.050$  was considered statistically significant. Graph-Pad Prism® version 5 (GraphPad, La Jolla, California, USA) was used for statistical analysis.

## 9.4 RESULTS AND DISCUSSION

The recent PIP scandal has led to renewed debates about the safety of implantable silicone devices for the augmentation of breast tissues. In February 2012, the Scientific Committee on Emerging and Newly Identified Health Risks (SCENIHR) published a report focusing on the physical, chemical and toxicological profiles of both the filler and shell of PIP implants (SCENIHR, 2012). The intentional use of lower quality industrial-grade silicone underlies the demonstrable mechanical fragility of the PIP shells and accelerated biodegradability of gels. This has been confirmed by the final report of the expert group commissioned by the medical director of the National Health Service in the UK (Keogh, 2012). A study conducted by the Australian Government Therapeutic Goods Administration, analysing low molecular weight (LMW) impurities of PIP and medical-grade silicone gels, found higher levels of LMW cyclic silicones (octamethylcyclotetrasiloxane, decamethylcyclopentasiloxane and dodecamethylmethylcyclohexasiloxane) in PIP implants (2012). Although these impurities have not been associated with health risks, they are thought to accelerate outer shell weakening, allowing silicone to leach across the shell into the surrounding tissues (SCENIHR, 2012). Despite negative *in vitro* genotoxicity results (AFSSAPS, 2011), *in vivo* irritancy tests provided evidence for local development of sores, lymphadenopathy and breast pain, which were deemed to be related to the amount of extruded silicone gel and the duration of exposure.

In the present study, 18 PIP breast implants were explanted from ten women, following implantation for a median of 126 (range 46-150) months. 4 control medical-grade silicone implants were explanted during the same time interval (Table 9.1).

**Table 9.1. Patient age, duration of implantation and reasons for removal of implants.**

Patient age (years)	Period of implantation	Duration of implantation (months)	Reason for explantation
Intact PIP shell			
40	05/2008 – 03/2012	46	Prophylactic removal following breast discomfort
40	05/2008 – 03/2012	46	Prophylactic removal following breast discomfort
66	04/2005 – 03/2012	83	
55	06/2004 – 02/2012	102	Left implant ruptured (not obtained)
42	02/2003 – 03/2012	109	
71	05/2003 – 03/2012	118	Capsular contracture
71	05/2003 – 03/2012	118	Capsular contracture
50	06/2001 – 02/2012	126	
50	06/2001 – 02/2012	126	Sharp pain around implant
35	08/2001 – 03/2012	128	Contralateral implant rupture
44	02/2001 – 02/2012	132	Prophylactic removal following nipple discharge
47	02/2001 – 02/2012	132	Prophylactic implant removal
47	02/2001 – 02/2012	132	
35	06/1999 – 02/2012	150	Bilateral tenderness around implants
35	06/1999 – 02/2012	150	Bilateral tenderness around implants
Ruptured PIP shell			
42	02/2003 – 03/2012	109	
35	08/2001 – 03/2012	128	Implant rupture + white exudates
44	02/2001 – 02/2012	132	Prophylactic implant removal following nipple discharge
Medical-grade silicon (control) shell			
67	11/2005 – 12/2012	85	Capsular contracture & displacement
47	12/2011 – 12/2012	12	Implant exchange post-reconstruction
43	04/2009 – 12/2012	32	Implant exchange for cosmetic reasons
43	04/2009 – 12/2012	32	Implant exchange for cosmetic reasons

Reasons for breast augmentation in the study population included primary reconstruction after mastectomy, cosmetic enhancement, and implant revision or exchange procedures. Reasons for implant removal ranged from prophylactic explantation, discomfort or tenderness around implants and nipple discharge to clinically determined implant rupture. Visual inspection of the implanted silicone shells and comparison of gels from ruptured versus intact implants demonstrated significant yellowing of exposed gels (Fig. 9.1).



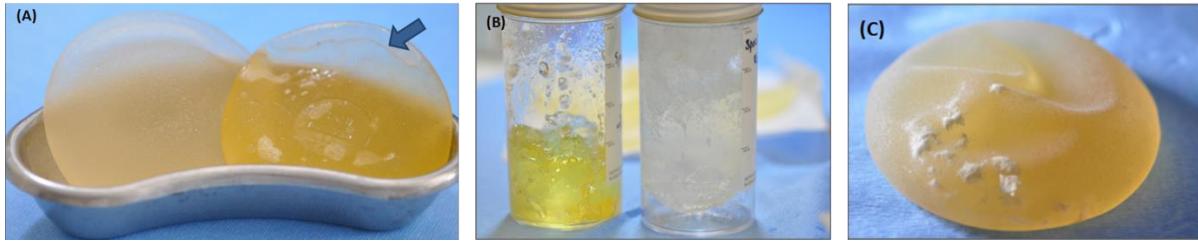
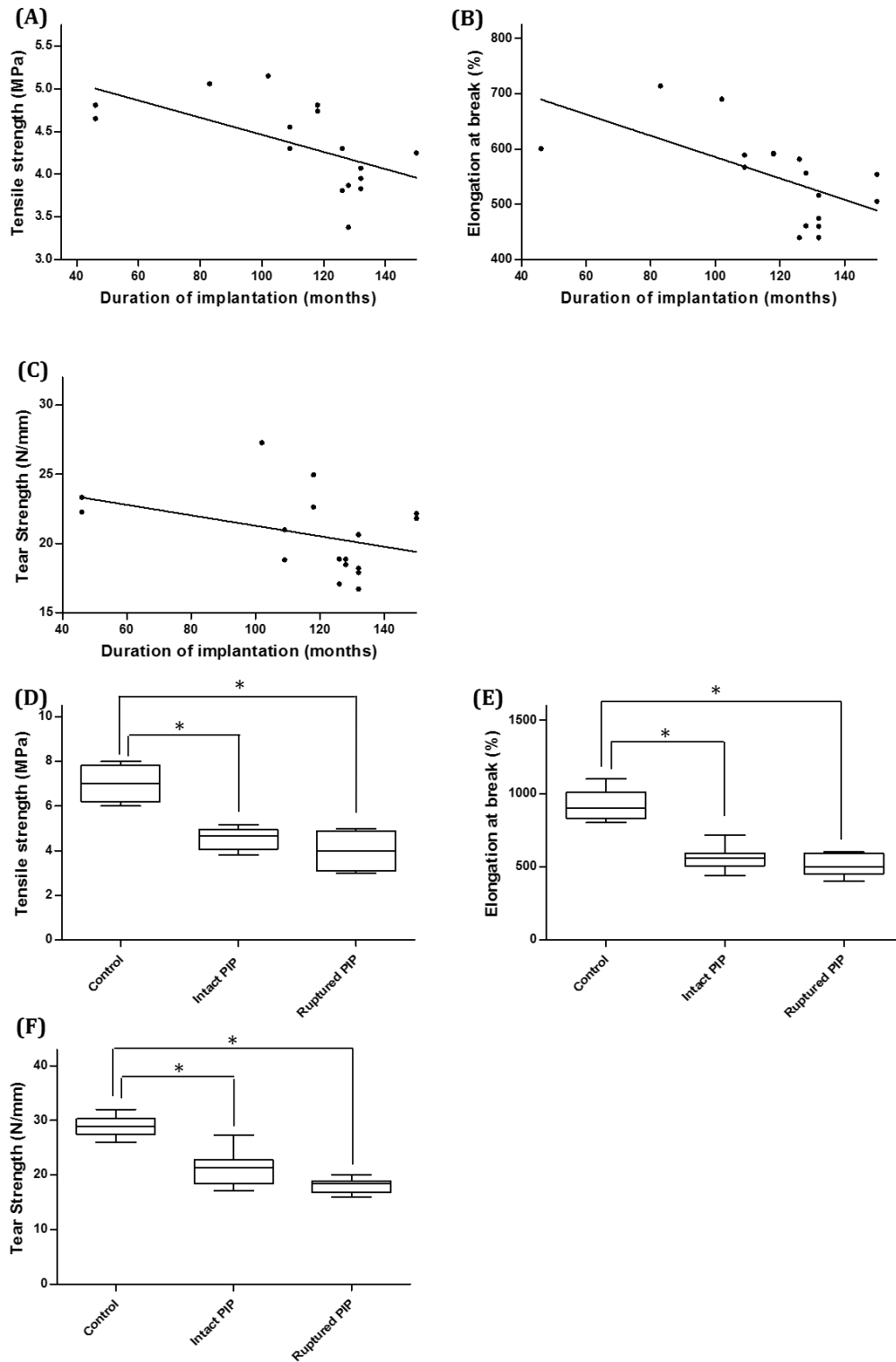


**Figure 9.1.** (A) Ruptured Poly Implant Prosthèse (PIP) breast implant (arrow) revealing yellow discoloration of the industrial-grade silicone gel within. (B) Direct comparison between silicone gels removed from ruptured (yellow) and intact (white) implants. (C) Yellowing and calcifications can be seen on the surface of an explanted, non-ruptured PIP implants.

Further, gels revealed variable consistency, ranging from highly cohesive to soft, non-adhesive and brittle. Gel cohesiveness increases as the number of cross-links increases, resulting in implants with superior shape retention. Gels removed from ruptured PIP implants were more likely to be non-adhesive and prone to breakdown on manual handling compared with gels taken from intact PIP and control implants. The probable reason for this is that *in vivo* exposure of the silicone gel leads to degradation and cross-link scission.

#### 9.4.1 Mechanical Testing of Silicone Shells

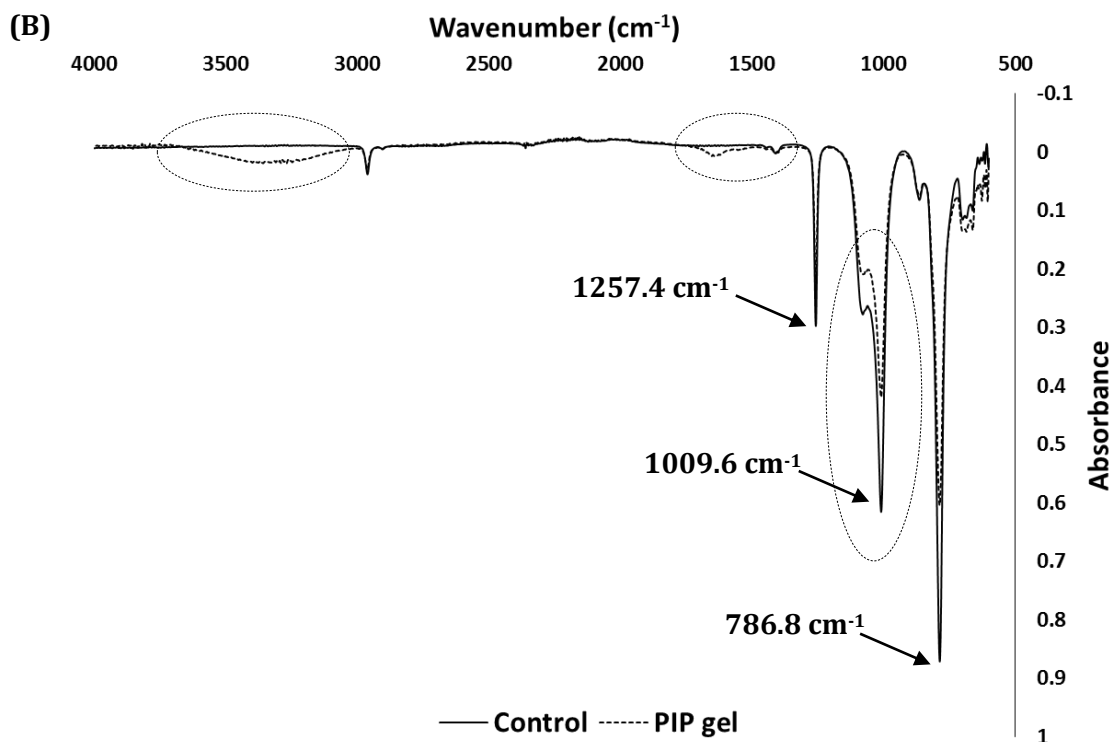
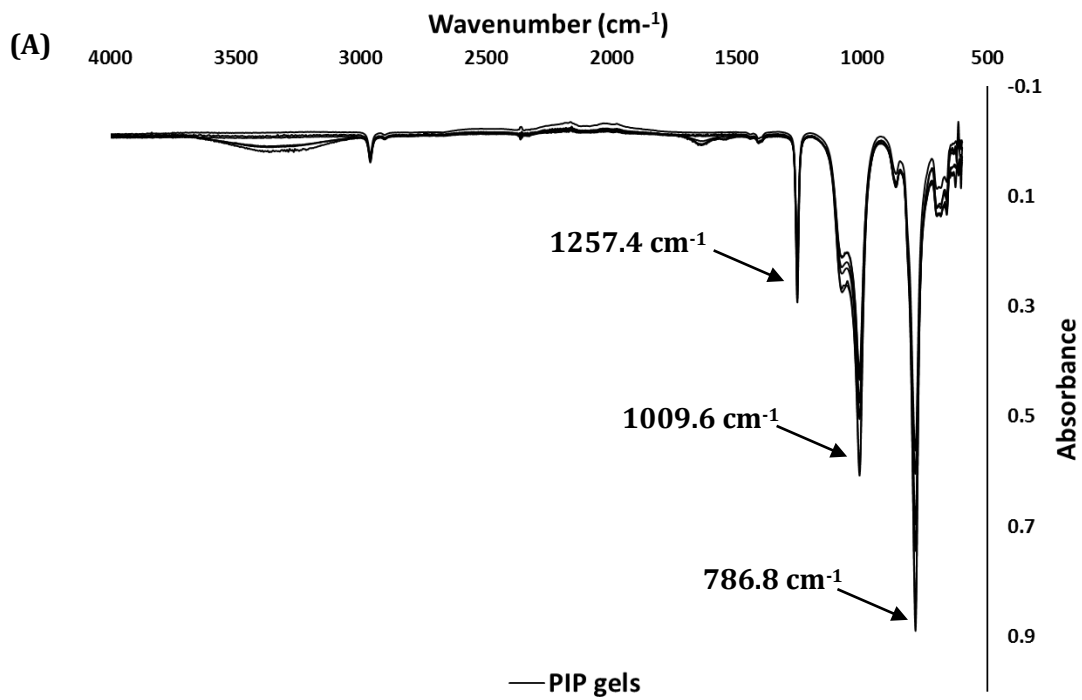
Correlation analyses demonstrated that tensile strength, maximal strain at rupture and tear strength were negatively correlated with shell implantation times (Fig. 9.2 (A-C)). There were statistically significant differences in tensile strength, maximal strain (elongation at break) and tear strength between intact and ruptured PIP compared with control shells ( $p = 0.009$  and  $p < 0.001$ , respectively) (Fig. 9.2 (D-F)).



**Figure 9.2.** (A-C) Spearman rank correlation between duration of implantation and mechanical parameters of Poly Implant Prosthèse (PIP) silicone shells: (A) tensile strength ( $r^2 = -0.75$ ;  $p = 0.009$ ), (B) elongation at break ( $r^2 = -0.76$ ;  $p = 0.01$ ), and (C) tear strength ( $r^2 = -0.49$ ;  $p = 0.047$ ). (D-F) Box plots comparing tensile strength (D), elongation at break (E), and tear strength (F) between medical-grade silicone control implants and intact and ruptured PIP shells. 6 pieces per implant shell were analysed. Values are presented as median (horizontal line within box), 5-95<sup>th</sup> percentile (box) and range (error bars). \*  $p < 0.05$  (Mann-Whitney U test).

#### 9.4.2 Surface Characterization of Silicone Shells and Gels

ATR-FTIR spectroscopy was performed on silicone gels and shells of PIP implants that had ruptured *in vivo* and medical-grade silicone control implants that had not ruptured (Fig. 9.3). All spectra showed significant peaks at  $786.8\text{ cm}^{-1}$ , which corresponded to Si-C bond vibrations. The peak at  $1009.6\text{ cm}^{-1}$  is generated by the stretching vibrations of Si-O-Si bonds, corresponding to the polymer backbone (Kaali et al., 2010). Bending vibrations at  $1257.4\text{ cm}^{-1}$  correspond to Si-CH<sub>3</sub> bonds. Compared with the unexposed control, the peak intensities of the PIP gel at  $786.8$  and  $1009.6\text{ cm}^{-1}$  were decreased significantly, whereas a new broad peak was detected between  $3200$  and  $3600\text{ cm}^{-1}$  (Fig. 9.3 (B)). This broad peak corresponds to vibrations of the Si-OH bonds. Additionally, a new 'protein-like' (Kaali et al., 2010) peak between  $1525$  and  $1760\text{ cm}^{-1}$  was observed in gels from explanted prostheses. Silicones are generally considered to be resistant to degradation but exposure to a strongly acidic environment results in hydrolytic degradation of cross-links and chain scission of the polymeric backbone (Tan et al., 2007). Such changes were observed in the present investigation, resulting in the conversion of the Si-O-Si bond to a Si-OH bond, corresponding to the appearance of a peak between  $3200$  and  $3600\text{ cm}^{-1}$  on FTIR spectra of PIP gels. Kaali and colleagues (Kaali et al., 2010) demonstrated an association between bacterial biofilm formation on silicone surfaces and material degradation, leading to changes in mechanical stability and surface characteristics. Micro-organismal penetration of silicone implants exposes the gel to bacteria-derived toxins capable of gel breakdown. Peri-implant inflammation, as part of the foreign body response, and bacterial contamination during the implantation procedure further accelerate silicone degradation.



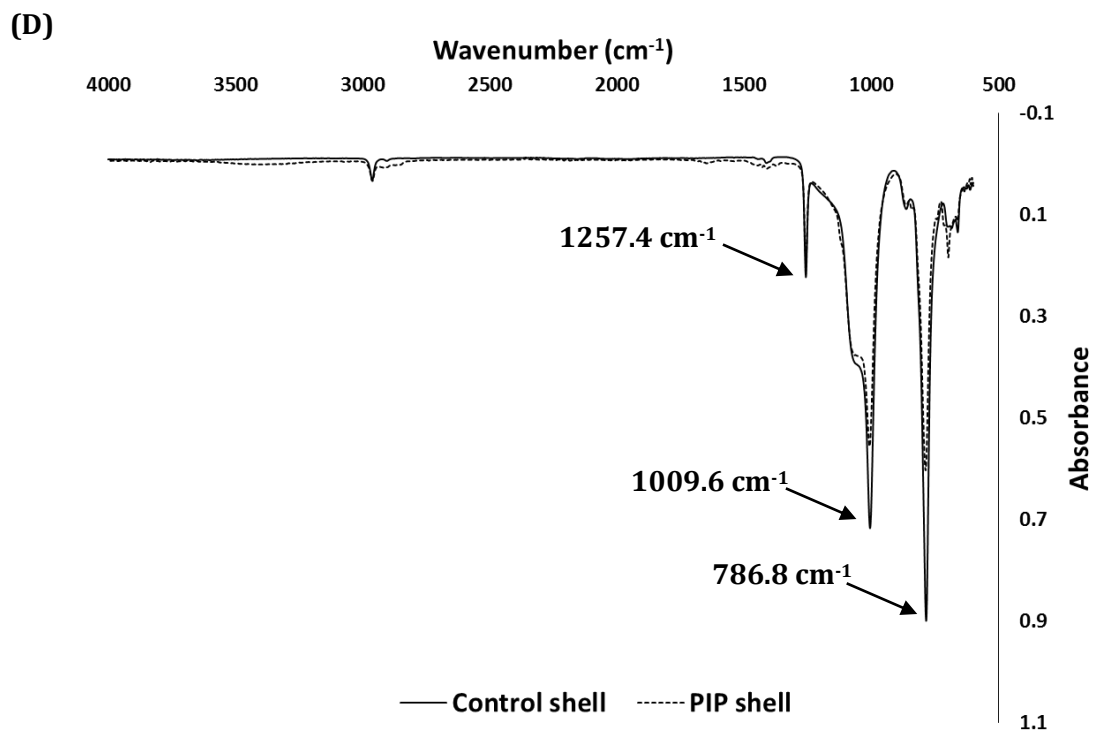
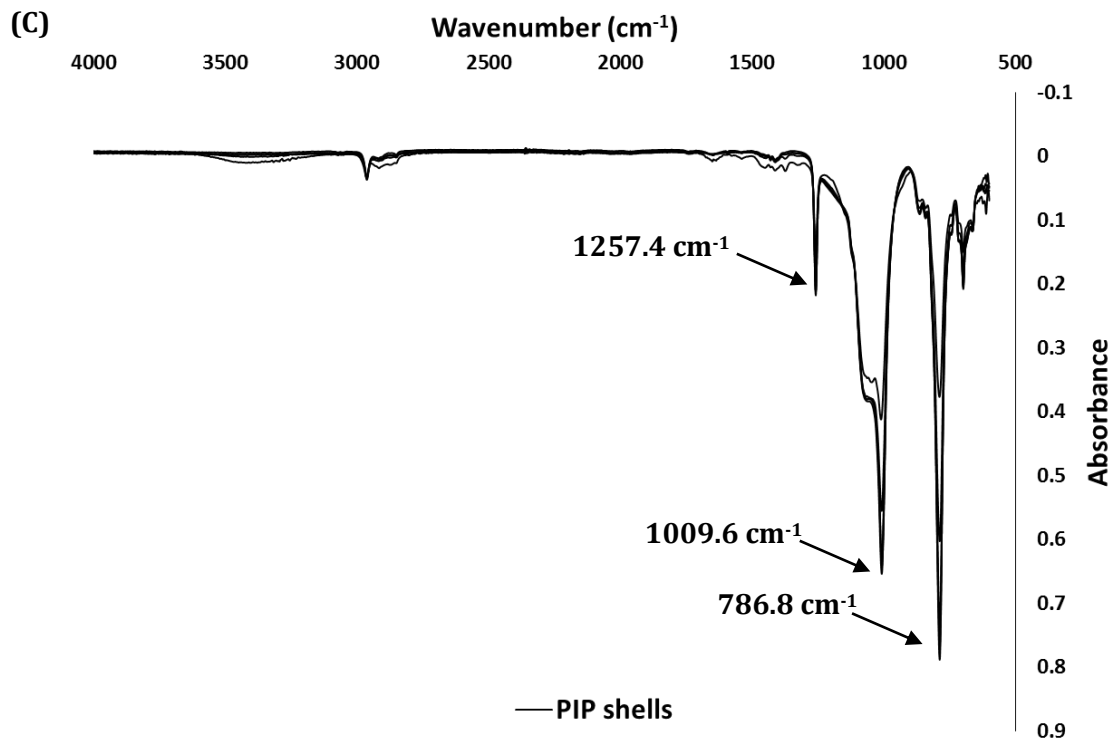


**Figure 9.3.** Overlaid attenuated total reflectance-Fourier transform infrared spectra of silicone gels and shells (6 per implant) from explanted Poly Implant Prosthèse (PIP) implants (A), (C) and comparison with medical-grade silicone control implants (B), (D). The peak at  $786.8 \text{ cm}^{-1}$  reflects Si-C bonds ( $800\text{-}760 \text{ cm}^{-1}$ ), the peak at  $1009.6 \text{ cm}^{-1}$  represents siloxane (Si-O-Si) bonds ( $1100\text{-}1000 \text{ cm}^{-1}$ ) and the peak at  $1257.4 \text{ cm}^{-1}$  corresponds to Si-CH<sub>3</sub> bonds ( $1280\text{-}1250 \text{ cm}^{-1}$ ) within the silicone compound. The spectra obtained from the PIP implant gels and shells have different peak intensities, most prominently shown within the marked areas, indicative of differing numbers

*of bonds within the material. This suggests material degradation, which cannot be seen in the spectrum of the control shells.*

The appearance of a 'protein-like' peak on infrared spectra of PIP gels that had ruptured *in vivo* (between 1525 and 1760  $\text{cm}^{-1}$ ) corresponds to the presence of a biofilm and bacterial cell wall material (Donlan et al., 2004, Bosch et al., 2008, Bosch et al., 2006). This finding is consistent with environmentally induced breakdown of gels. Scala and Hickman (Scala and Hickman, 1958) demonstrated a temporal association between exposure to bodily fluids with or without inflammatory surroundings and silicone degradation. Breast implants filled with medical-grade silicone have reported rupture rates of 2.1 % for primary augmentation and 1.5 % for primary reconstruction (Hammond et al., 2012).

3 of a total of 18 PIP implants were ruptured at explantation. Although this reflects the current opinion of PIP implant stability, the relatively small number of specimens analysed must be taken into account to avoid rash overestimation. However, this study corroborated correlations between the duration of implantation and PIP implant degeneration. Accelerated PIP implant degeneration was also reflected in the reasons for PIP removal, which included discomfort, nipple discharge and clinically diagnosed implant rupture. Control implants, however, were removed primarily for cosmetic reasons at relatively earlier time points compared with PIPs. This may skew results in favour of controls. Nevertheless, the present data demonstrated mechanical weakening of PIP shells compared with medical-grade shells and variability within the PIP cohort. Although differences between intact and ruptured PIP implants were not significant statistically, this trend should not be underestimated; a larger implant cohort may have resulted in a statistically significant difference, as demonstrated by Necchi and colleagues

(Necchi et al., 2011). Clinical observations have previously suggested the presence of two distinct subpopulations of PIP implants: those manufactured from suboptimal industrial silicone that are more susceptible to rupture and those containing 'normal' appearing silicones. The Agence Nationale de Sécurité du Médicament et des Produits de Santé has previously confirmed the heterogeneous nature of PIP implant quality (AFSSAPS, 2011). Although the SCENIHR has emphasized that silicone breast implants can fail regardless of manufacturer, several case reports have demonstrated the unreliability and unpredictability of PIP implants, resulting in symptomatic implant rupture and silicone leakage (Berry, 2007, O'Neill et al., 2008, Adams et al., 2007). This analysis of the material properties of substandard industrial silicones used in the manufacture of PIP silicone breast implants has demonstrated statistically significant negative correlations between PIP shell strength and implantation times.

## **9.5 CONCLUSION**

The present investigation demonstrated significant correlations between duration of implantation and structural deterioration. Combined with the propensity of PIP implants to rupture prematurely, implant carriers are exposed to unknown substances with potentially serious long-term effects. Although a final decision for or against prophylactic removal of such implants must take into account the clinical picture, the data presented in this study strongly suggest that there is a direct relationship between duration of implantation of PIP breast implants and a weakening of shell mechanical strength, which is an independent risk factor for implant rupture and subsequent complications. This study therefore supports the argument for prophylactic removal of PIP silicone breast implants.

## References

- ADAMS, T. S., CROOK, T. & CADIER, M. A. 2007. A late complication following the insertion of hydrogel breast implants. *J Plast.Reconstr.Aesthet.Surg.*, 60, 210-2.
- AFSSAPS 2011. Breast implants with silicone based gel filling from Poly Implant Prothèse Company : Update of tests results.
- BERRY, R. B. 2007. Rupture of PIP breast implants. *J Plast.Reconstr.Aesthet.Surg.*, 60, 967-8.
- BOSCH, A., MIÑÁN, A., VESCINA, C., DEGROSSI, J., GATTI, B., MONTANARO, P., MESSINA, M., FRANCO, M., VAY, C., SCHMITT, J., NAUMANN, D. & YANTORNO, O. 2008. Fourier transform infrared spectroscopy for rapid identification of nonfermenting gram-negative bacteria isolated from sputum samples from cystic fibrosis patients. *Journal of clinical microbiology*, 46, 2535-46.
- BOSCH, A., SERRA, D., PRIETO, C., SCHMITT, J., NAUMANN, D. & YANTORNO, O. 2006. Characterization of Bordetella pertussis growing as biofilm by chemical analysis and FT-IR spectroscopy. *Applied microbiology and biotechnology*, 71, 736-47.
- CHOICES, N. H. S. 2012. *RE: Breast implants*.
- DONLAN, R. M., PIEDE, J. A., HEYES, C. D., SANII, L., MURGA, R., EDMONDS, P., EL-SAYED, I. & EL-SAYED, M. A. 2004. Model system for growing and quantifying Streptococcus pneumoniae biofilms in situ and in real time. *Applied and environmental microbiology*, 70, 4980-8.
- FDA 2011. FDA Update on the Safety of Silicone Gel-Filled Breast Implants.
- GOVERNMENT, A. 2012. *RE: Australian Government Department of Health and Ageing Therapeutic Goods Administration*.
- HAMMOND, D. C., MIGLIORI, M. M., CAPLIN, D. A., GARCIA, M. E. & PHILLIPS, C. A. 2012. Mentor Contour Profile® Gel Implants: Clinical Outcomes at 6 Years. *Plastic and reconstructive surgery*.
- KAALI, P., MOMCILOVIC, D., MARKSTRÖM, A., AUNE, R., CZEL, G. & KARLSSON, S. 2010. Degradation of biomedical polydimethylsiloxanes during exposure to in vivo biofilm environment monitored by FE-SEM, ATR-FTIR, and MALDI-TOF MS. *J Appl Polymer Science*, 115, 802-10.
- KEOGH, B. 2012. Poly implant Prothese (Pip) Breast Implants: Final report of the Expert Group.
- NECCHI, S., MOLINA, D., TURRI, S., ROSSETTO, F., RIETJENS, M. & PENNATI, G. 2011. Failure of silicone gel breast implants: is the mechanical weakening due to shell swelling a significant cause of prostheses rupture? *J Mech.Behav.Biomed.Mater*, 4, 2002-8.
- NHS 2012. PIP breast implants - latest from the NHS.
- O'NEILL, J. K., RIGBY, H. & KENEALY, J. M. 2008. Leakage and osmotic shifts in PIP Hydrogel implants. A case demonstrating increase and decrease of implant volume in the same patient. *J Plast.Reconstr.Aesthet.Surg.*, 61, 1122-3.
- SCALA, L. & HICKMAN, W. 1958. Thermal and Oxidative Degradation of Silicones. *Industrial & Engineering Chemistry*, 50, 1583-4.
- SCENIHR 2012. The Safety of PIP Silicone Breast Implants.
- TAN, J., CHAO, Y. J., LI, X. & VAN ZEE, J. W. 2007. Degradation of silicone rubber under compression in a simulated PEM fuel cell environment. *J Power Sources*, 172, 782-9.